

Expanded Porphyrins: Ideal Models to Probe Conformational topology, Möbius and Hückel Aromaticity

By

SYAMASRIT DASH

CHEM11201604031

**National Institute of Science Education and Research,
Bhubaneswar, Odisha**

*A thesis submitted to the
Board of Studies in Chemical Sciences
In partial fulfillment of requirements
for the Degree of*

DOCTOR OF PHILOSOPHY

Of

HOMI BHABHA NATIONAL INSTITUTE



December, 2020

Homi Bhabha National Institute

Recommendations of the Viva Voce Committee

As members of the Viva Voce Committee, we certify that we have read the dissertation prepared by **Syamasrit Dash** entitled **“Expanded Porphyrins: Ideal Models to Probe Conformational Topology, Möbius and Hückel Aromaticity”** and recommend that it may be accepted as fulfilling the thesis requirement for the award of Degree of Doctor of Philosophy.

Chairman – Dr. Moloy Sarkar

Date: 30.12.2020

Moloy Sarkar

Guide / Convener – Prof. T. K. Chandrashekar

Date: 30.12.2020

T.K. Chandrashekar

Co-Guide – Prof. A. Srinivasan

Date: 30.12.2020

Prof. A. Srinivasan

Examiner – Prof. G. Sekar

Date: 30.12.2020

G. Sekar

Member 1 – Dr. V. Krishnan

Date:

30/12/2020

V. Krishnan

Member 2 – Dr. C. Gunanathan

Date: 30/12/2020

C. Gunanathan

Member 3 – Dr. Debasmita Pankaj Alone

Date: 30/12/2020

Debasmita Alone

Final approval and acceptance of this thesis is contingent upon the candidate's submission of the final copies of the thesis to HBNI.

We hereby certify that we have read this thesis prepared under my/our direction and recommend that it may be accepted as fulfilling the thesis requirement.

Prof. A. Srinivasan
30.12.2020

T.K. Chandrashekar
30.12.2020

Date: 30th December 2020

(Prof. A. Srinivasan)

(Prof. T. K. Chandrashekar)

Place: Bhubaneswar

(Co-Guide)

(Guide)

Homi Bhabha National Institute

Recommendations of the Viva Voce Committee

As members of the Viva Voce Committee, we certify that we have read the dissertation prepared by **Syamasrit Dash** entitled **“Expanded Porphyrins: Ideal Models to Probe Conformational Topology, Möbius and Hückel Aromaticity”** and recommend that it may be accepted as fulfilling the thesis requirement for the award of Degree of Doctor of Philosophy.

Chairman – Dr. Moloy Sarkar

Date: 30.12.2020

Moloy Sarkar

Guide / Convener – Prof. T. K. Chandrashekar

Date: 30.12.2020

T.K. Chandrashekar

Co-Guide – Prof. A. Srinivasan

Date: 30.12.2020

Prof. A. Srinivasan

Examiner – Prof. G. Sekar

Date: 30.12.2020

G. Sekar

Member 1 – Dr. V. Krishnan

Date:

30/12/2020

V. Krishnan

Member 2 – Dr. C. Gunanathan

Date: 30/12/2020

C. Gunanathan

Member 3 – Dr. Debasmita Pankaj Alone

Date: 30/12/2020

Debasmita Alone

Final approval and acceptance of this thesis is contingent upon the candidate's submission of the final copies of the thesis to HBNI.

We hereby certify that we have read this thesis prepared under my/our direction and recommend that it may be accepted as fulfilling the thesis requirement.

Prof. A. Srinivasan
30.12.2020

T.K. Chandrashekar
30.12.2020

Date: 30th December 2020

(Prof. A. Srinivasan)

(Prof. T. K. Chandrashekar)

Place: Bhubaneswar

(Co-Guide)

(Guide)

STATEMENT BY AUTHOR

This dissertation has been submitted in partial fulfillment of requirements for an advanced degree at Homi Bhabha National Institute (HBNI) and is deposited in the Library to be made available to borrowers under rules of the HBNI.

Brief quotations from this dissertation are allowable without special permission, provided that accurate acknowledgement of source is made. Requests for permission for extended quotation from or reproduction of this manuscript in whole or in part may be granted by the Competent Authority of HBNI when in his or her judgment the proposed use of the material is in the interests of scholarship. In all other instances, however, permission must be obtained from the author.

Syamasrit Dash

Syamasrit Dash

DECLARATION

I, hereby declare that the investigation presented in the thesis has been carried out by me. The work is original and has not been submitted earlier as a whole or in part for a degree / diploma at this or any other Institution / University.

Syamasrit Dash
Syamasrit Dash

LIST OF PUBLICATIONS

Published

#1. "Protonation-Triggered Hückel and Möbius Aromatic Transformations in Nonaromatic Core-Modified [30]Hexaphyrin(2.1.1.2.1.1) and Annulated [28]Hexaphyrin(2.1.1.0.1.1)," **Syamasrit Dash**, A. Ghosh, A. Srinivasan, C. H. Suresh and T. K. Chandrashekar,* *Org. Lett.* **2019**, *21*, 9637-9641.

#2. "Dithienothiophene fused 30π heptaphyrin and 34π octaphyrins: Syntheses, characterization and spectral properties," **Syamasrit Dash**, A. Ghosh and T. K. Chandrashekar,* *J. Porphyrins Phthalocyanines*. **2019**, *23*, 2-7.

#3. "Two non-identical twins in one unit cell: characterization of 34π aromatic core-modified octaphyrins, their structural isomers and anion bound complexes," A. Ghosh†, **Syamasrit Dash**†, A. Srinivasan, C. H. Suresh and T. K. Chandrashekar,* *Chem. Sci.* **2019**, *10*, 5911-5919. (†equally contributed).

#4. "Core-modified 48π and 42π decaphyrins: syntheses, properties and structures," A. Ghosh†, **Syamasrit Dash**†, A. Srinivasan, C. H. Suresh, S. Peruncheralathan and T. K. Chandrashekar,* *Org. Chem. Front.* **2019**, *6*, 3746-3753. (†equally contributed).

5. " 24π Core-Modified Nonfused Pentaphyrin with Möbius Aromaticity," A Ghosh, **Syamasrit Dash**, C. H. Suresh, A. Srinivasan and T. K. Chandrashekar,* *Chem. Eur. J.* **2018**, *24*, 17997-18002.

Manuscript Underpreparation

#1. “Core-Modified Homoporphyrins and its Phenyl bridged derivatives.” **Syamasrit Dash**, A Ghosh, A. Srinivasan and T. K. Chandrashekar*.

2. “A New Class of stable Decaphyrin Radical.” **Syamasrit Dash**, A. Ghosh, A. Srinivasan and T. K. Chandrashekar*.

#3. “Isomer and Hückel-Möbius Aromatic Transformations in Nonaromatic Core-Modified Annulated [28]Hexaphyrin(2.1.1.0.1.1) via protonation.” **Syamasrit Dash**, A. Ghosh, A. Srinivasan, C. H. Suresh and T. K. Chandrashekar*.

#pertaining to this thesis

Syamasrit Dash

Syamasrit Dash

Conferences

1. “A Nonaromatic-Möbius aromatic Switch in a 28π Expanded Porphyrin triggered by proton”, **Syamasrit Dash**, Arindam Ghosh, A. Srinivasan, Tavarekere K. Chandrashekar* in ACS on campus, July 23rd, 2018, organized by NISER Bhubaneswar (**Poster Presentation**).
2. “A Nonaromatic-Möbius aromatic Switch in a 28π Expanded Porphyrin triggered by proton”, **Syamasrit Dash**, Arindam Ghosh, A. Srinivasan, Tavarekere K. Chandrashekar* in MMM, October 28-31st, 2018, Organized by Department of Chemistry, IISc Bangalore (**Poster Presentation**).
3. “Non-Identical Vs. Identical Octaphyrin Twins: New emerging Structural Isomers, **Syamasrit Dash** and T. K. Chandrashekar* in International Symposium on Modern Trends in Inorganic Chemistry-XVIII (MTIC-XVIII), December 11-14th, 2019 organized by Department of Chemistry, IIT Guwahati, Guwahati University and Tezpur University at Guwahati(**Poster Presentation**).

Syamasrit Dash
Syamasrit Dash

Dedicated to....

My Family

&

Professor T. K. Chandrashekar

ACKNOWLEDGEMENTS

I may humbly be allowed to show my gratitude and thank each and every person who stood as a great companion throughout this journey.

I am grateful to the **Almighty** and **my grandparents** whose values and morals have been a blessing to me in every step of my life.

I am grateful to my **parents** helping me to grow and choose the right path. The blessings, inspiration and unconditional love from my **family** have strengthened me. It has nurtured me to become a better person in life and overcome all the challenges with confidence.

I would like to express my gratitude and respect to my supervisor, **Prof. T. K. Chandrashekar**, NISER, for his continuous support and kindness. He allowed me to think freely and gave me the opportunity to solve my research problems. His constant support throughout the entire phase of my Ph.D. will be always admired and remembered.

I would like to express my sincere gratitude to my Co-supervisor, **Prof. A. Srinivasan**, NISER, for constant guidance and help whenever needed.

I thank to the Director, **Prof. S. Panda**, NISER, for providing the laboratory facilities, which help me to complete my research work.

I thank my Doctoral committee members, Chairman **Dr. M. Sarkar**, **Dr. V. Krishnan**, **Dr. C. Gunanathan**, **Dr. Debasmita. P. Alone** and all other faculties of SCS NISER, for their useful suggestions and help. I thank **Dr. Arun Kumar**, scientific officer for his support on numerous occasions.

I owe my sincere thanks to collaborator of my research work, **Dr. C. H. Suresh**, NIIST-Trivandrum, for his valuable assistance regarding theoretical studies described in the thesis.

I sincerely thank **Mr. Deepak**, **Mr. Sanjaya**, **Mr. Amit**, **Mr. Prakash**, **Dr. Mriganka** and **Mrs. Anuradha**, NISER for performing characterization of my samples.

I am immensely obliged to **all my teachers** of school, graduation and post-graduation who inculcated knowledge and discipline in me.

It gives me immense pleasure to thank all my seniors, friends and juniors who made my life easy, gratifying and memorable at NISER. I would like to thank my labmates **Mahaprasad**, **Deepak**, **Subhashree**, **Sourav**, **Rampal**, **Prakhar**, **Manas**, **Suritra**

and especially thank my seniors **Dr. Arindam. Ghosh, Dr. B. Adinarayana, Dr. M. Murugavel, Dr. Narasingha Rao, Dr. Mainak Das, Mrs. Sangya Chitranshi** and **Dr. Pankaj** for their help and guidance. Dr. Arindam Ghosh proved to be best senior I could ever wish, thank you very much. I also thank my best friends **Bhagyashree** and **Pragnya** for their colossal support in various stages of my life. I also thank all my Ph.D. batchmates, especially **Sagarika, Kasturi** and **Sruti** for their help. My sincere thanks to all my hostelmates, for their love and endurance. My special thanks to **Mr. Subhayan** and **Ms. Shalini** who helped me in solving the NMR problems. I would like to thank the whole NISER family.

I am blessed to be strongly bonded to my beloved cousins **Sreeja Misra** and **Sakti Prasad Misra**, who cared for me and stood by me forever.

Last but not the least I would like to express my earnest gratitude to everyone who contributed for the accomplishment of my course.

Syamasrit Dash
Syamasrit Dash

CONTENTS

	Page No
Summary	xi
List of Tables	xii
List of Schemes	xiii
List of Figures	xv
List of Abbreviations	xxiv
Chapter 1	1
Chapter 2	36
Chapter 3	60
Chapter 4	95
Chapter 5	115
Chapter 6	166

List of Tables

1	Table 1.1	Table showing NICS and Δ values of aromatic and antiaromatic compounds	12
2	Table 2.1	Crystal data for 16 , 16.H⁺	50
3	Table 2.2	Crystal data for 17 and 18	51
4	Table 3.1	Crystallographic data for 6 and 6.2H⁺	76
5	Table 3.2	Crystallographic data for 8 and 8.2H⁺	77
6	Table 3.3	Crystallographic data for 10 and 10.2H⁺	78
7	Table 4.1	Crystal data for 7a	106
8	Table 5.1	$\Delta\delta$ values of octaphyrin isomers	136
9	Table 5.2	Crystallographic data for 16 and 16.2H⁺	140
10	Table 5.3	Crystallographic data for 19A and 19A.2H⁺	143
11	Table 5.4	Total energy in a.u. and relative energy (E_{rel}) of 'B' configuration with respect to 'A' in kcal/mol	151
12	Table 6.1	Formation of 8 , 9 and 10 with different concentration of TFA	172
13	Table 6.2	Crystal data for 10	184
14	Table 6.3	Crystal data for 13	187

List of Schemes

1	Scheme 1.1	Synthesis of di-cyano methyl subporphyrins radicals	7
2	Scheme 1.2	Synthesis of Hückel antiaromatic molecule 20	11
3	Scheme 1.3	Synthesis of Möbius aromatic molecules	13
4	Scheme 1.4	Möbius antiaromatic 24 and synthesis of 26	14
5	Scheme 1.5	24π , 25π , and 26π redox active pentathiaphyrins	15
6	Scheme 1.6	Protonation triggered Hückel-Möbius switchover	16
7	Scheme 1.7	Expanded porphyrins with various structural diversity	19
8	Scheme 1.8	Synthesis of heptaphyrin isomers	20
9	Scheme 2.1	Synthesis of azahomoporphyrin 2 and its decomposition to corresponding metallated porphyrin derivatives	39
10	Scheme 2.2	Synthesis of core-modified homoporphyrin 16	41
11	Scheme 2.3	Synthesis of phenyl bridged core-modified homoporphyrin dimer 17 and 18	41
12	Scheme 2.4	Precursor synthesis	55
13	Scheme 2.5	Precursor synthesis	56
14	Scheme 3.1	Synthesis of hexaphyrin 6	64
15	Scheme 3.2	Synthesis of hexaphyrin 8	64
16	Scheme 3.3	Synthesis of hexaphyrin 10	65
17	Scheme 3.4	Precursor syntheses	89
18	Scheme 3.5	Precursor syntheses	89
19	Scheme 4.1	Synthesis of 6	99
20	Scheme 4.2	Synthesis of octaphyrin 7	100
21	Scheme 4.3	Syntheses of 8 , 9 , 4b	110
22	Scheme 5.1	Synthesis of figure-eight octaphyrin	117
23	Scheme 5.2	Synthesis of octaphyrin 2	117
24	Scheme 5.3	Synthesis of octaphyrin 16 , 17(A and B)	122
25	Scheme 5.4	Synthesis of octaphyrin 18(A and B)	123
26	Scheme 5.5	Synthesis of octaphyrin 19(A)	123
27	Scheme 5.6	Precursor synthesis	158
28	Scheme 5.7	Precursor synthesis	159

29	Scheme 6.1	Formation of 8 , 9 and decaphyrin 10	172
30	Scheme 6.2	Synthesis of cyano complex 13 and decaphyrin 12	173
31	Scheme 6.3	Precursor syntheses	196

List of Figures

1	Figure 1.1	Applications of expanded porphyrins	4
2	Figure 1.2	Corrole and subporphyrins	6
3	Figure 1.3	Examples of tetravinyllogous expanded porphyrins	7
4	Figure 1.4	Examples of expanded porphyrins with various structural diversity	7
5	Figure 1.5	Expanded porphyrins with various structural diversity	8
6	Figure 1.6	Examples of N-confused porphyrins	9
7	Figure 1.7	Examples of N-confused porphyrin and other porphyrin isomers	9
8	Figure 1.8	Criteria for aromaticity in expanded porphyrins	10
9	Figure 1.9	[18]Annulene and [18]Annulene dianion	11
10	Figure 1.10	Current density maps of (a) diatropic and (b) paratropic expanded porphyrins	13
11	Figure 1.11	Different types of aromaticity in expanded porphyrins	13
12	Figure 1.12	Example of Hückel aromatic hexaphyrin	14
13	Figure 1.13	Möbius aromaticity in expanded porphyrins	16
14	Figure 1.14	Linear, Hückel and Möbius strips	16
15	Figure 1.15	Möbius aromaticities in expanded porphyrins upon lowering temperature	17
16	Figure 1.16	Hückel-Möbius aromaticity switch in expanded porphyrins	17
17	Figure 1.17	Examples of Möbius aromatic molecules	18

18	Figure 1.18	Möbius antiaromatic 32π heptaphyrin 27	20
19	Figure 1.19	Baird aromaticity in expanded porphyrins	21
20	Figure 1.20	Expanded porphyrins with Baird aromaticity	21
21	Figure 1.21	Electrochemical oxidation in expanded porphyrins	22
22	Figure 1.22	EPR of $2e^-$ oxidized Baird aromatic molecule	23
23	Figure 1.23	NICS values of Baird aromatic molecules	23
24	Figure 1.24	Bridged expanded porphyrins; models for Baird aromaticity	23
25	Figure 2.1	First stable core-modified homoporphyrins	39
26	Figure 2.2	Structure of nonaromatic carba-homoporphyrins and Möbius aromatic homoporphyrin	40
27	Figure 2.3	ESI-MS spectrum of 16 .	42
28	Figure 2.4	ESI-MS spectrum of 17	42
29	Figure 2.5	ESI-MS spectrum of 18	42
30	Figure 2.6	$^1\text{H-NMR}$ spectra of a) 16 b) 16.2H^+ in CD_2Cl_2	43
31	Figure 2.7	$^1\text{H-NMR}$ spectra of titration of 16	44
32	Figure 2.8	$^1\text{H-NMR}$ spectra of a) 17 b) 17.2H^+ in CD_2Cl_2	45
33	Figure 2.9	$^1\text{H-}^1\text{H}$ COSY correlation spectroscopy of a) 17 and b) 17.2H^+ in CD_2Cl_2 .	45
34	Figure 2.10	$^1\text{H-NMR}$ spectra of 18 in CD_2Cl_2	46
35	Figure 2.11	X-ray crystal structure 16 a) front view b) Side view.	46
36	Figure 2.12	Bond lengths in 16	47
37	Figure 2.13	X-ray crystal structure 16.2H^+ a) front view b) side view	47
38	Figure 2.14	X-ray crystal structure 17 a) front view b) side view	48

39	Figure 2.15	X-ray crystal structure 17 a) deviation of S1 from mean plane b) deviation of phenyl ring from mean plane	49
40	Figure 2.16	Bond lengths in 17	49
41	Figure 2.17	X-ray crystal structure 18	49
42	Figure 2.18	The electronic absorption spectra of 16 and 16.2H⁺ in CH ₂ Cl ₂	52
43	Figure 2.19	The electronic absorption spectra of 17 and 17.2H⁺ in CH ₂ Cl ₂	53
44	Figure 3.1	Möbius aromatic molecules upon external trigger	62
45	Figure 3.2	Aromatic molecules on external trigger	63
46	Figure 3.3	HRMS of hexaphyrin 6	65
47	Figure 3.4	HRMS of hexaphyrin 8	66
48	Figure 3.5	ESI-Mass of hexaphyrin 10	66
49	Figure 3.6	¹ H NMR Spectra of a) 6 and b) 6.2H⁺ at 298 K	67
50	Figure 3.7	¹ H COSY and 2D NOESY correlation spectroscopy of 6 (aromatic region) in CD ₂ Cl ₂	67
51	Figure 3.8	Low temperature ¹ H NMR spectroscopy of 6	68
52	Figure 3.9	¹ H COSY correlation spectroscopy of 6	69
53	Figure 3.10	¹ H NMR spectra of a) 8 at 273K and b) 8.2H⁺ at 298 K in CD ₂ Cl ₂	69
54	Figure 3.11	¹ H NMR low temperature studies of 8 in CD ₂ Cl ₂	70
55	Figure 3.12	¹ H NMR spectra titration studies with TFA	70
56	Figure 3.13	¹ H- ¹ H COSY correlation spectroscopy of 8 (273K) and 8.2H⁺ (298K) in CD ₂ Cl ₂	70
57	Figure 3.14	¹ H NMR spectra of 10 (193K) CD ₂ Cl ₂	71

58	Figure 3.15	^1H - ^1H COSY correlation spectroscopy of 10	71
59	Figure 3.16	Low temperature ^1H NMR spectroscopy of 10	72
60	Figure 3.17	^1H NMR Spectra of 10.2H⁺ (298K) in CD_2Cl_2	72
61	Figure 3.18	Single crystal X-ray structures of a) 6 and b) 6.2H⁺	74
62	Figure 3.19	Single crystal X-ray structures of a) 8 and b) 8.2H⁺	75
63	Figure 3.20	Single crystal X-ray structures of a) 10 and b) 10.2H⁺	76
64	Figure 3.21	NICS (0) values at M06L/6-31G** level of 6	79
65	Figure 3.22	ACID plots for 6 with current density vectors plotted on to isosurface of value 0.026	79
66	Figure 3.23	NICS (0) values at M06L/6-31G** level 8	80
67	Figure 3.24	ACID plots for 8 with current density vectors plotted on to isosurface of value 0.026	80
68	Figure 3.25	NICS (0) values at M06L/6-31G** level 8.2H⁺	81
69	Figure 3.26	ACID plots for 8.2H⁺ with current density vectors plotted on to isosurface of value 0.026	81
70	Figure 3.27	NICS (0) values at M06L/6-31G** level 10	82
71	Figure 3.28	ACID plots for 10 with current density vectors plotted on to isosurface of value 0.026	82
72	Figure 3.29	NICS (0) values at M06L/6-31G** level 10.2H⁺	83
73	Figure 3.30	ACID plots for 10.2H⁺ with current density vectors plotted on to isosurface of value 0.026	83
74	Figure 3.31	The electronic absorption spectra of 6 and 6.2H⁺	84
75	Figure 3.32	The electronic absorption spectra of 8 and 8.2H⁺	84
76	Figure 3.33	The electronic absorption spectra of 10 and 10.2H⁺ in CH_2Cl_2	85

77	Figure 4.1	Structure of fused expanded porphyrins 1, 2	97
78	Figure 4.2	Structure of heptaphyrin 6 and octaphyrin 7	98
79	Figure 4.3	ESI Mass spectrum of heptaphyrin 6	100
80	Figure 4.4	ESI Mass spectrum of octaphyrin 7a	100
81	Figure 4.5	ESI Mass spectrum of octaphyrin 7b	101
82	Figure 4.6	^1H NMR spectroscopy of 6 (a) and 6.2H⁺ (b)	102
83	Figure 4.7	^1H - ^1H COSY correlation spectroscopy of 6.2H⁺	102
84	Figure 4.8	^1H NMR spectroscopy of 7a (a) and 7b.2H⁺ (b)	103
85	Figure 4.9	Single crystal X-ray structure of 7a (a) top view and (b) side view	104
86	Figure 4.10	Self assembled dimer structure of 7a	105
87	Figure 4.11	One dimension array of 7a	105
88	Figure 4.12	Bond distances of 7a	105
89	Figure 4.13	Absorption spectra of 6 and 6.2H⁺ (10^{-2} M TFA)	107
90	Figure 4.14	Absorption spectra of 7a and 7a.2H⁺ (10^{-2} M TFA)	108
91	Figure 5.1	Structure of bridged octaphyrins 3 and 4	118
92	Figure 5.2	Structure of isomers of pentaphyrin	118
93	Figure 5.3	Structure of N-confused hexaphyrin	119
94	Figure 5.4	Structure of conformers of heptaphyrin	120
95	Figure 5.5	Structure of isomers A and B of octaphyrin 16, 17, 18, 19	121
96	Figure 5.6	ESI-Mass of octaphyrin 16	124
97	Figure 5.7	ESI-Mass of octaphyrin 17	124

98	Figure 5.8	ESI-Mass of octaphyrin 18	124
99	Figure 5.9	ESI-Mass of octaphyrin 19	125
100	Figure 5.10	^1H NMR spectrum of 16 in toluene- D_8 at 298K	126
101	Figure 5.11	^1H - ^1H COSY correlation spectrum of 16 at 213K	126
102	Figure 5.12	Low temperature (298K-193K) ^1H NMR spectrum of 16 in toluene- D_8	127
103	Figure 5.13	High temperature (298K-343K) ^1H NMR spectrum of 16 in toluene- D_8	127
104	Figure 5.14	^1H NMR Spectrum of 17 in toluene- D_8 at 298K	128
105	Figure 5.15	^1H NMR spectra of 16 with varying concentration of TFA in CH_2Cl_2 at 298K	129
106	Figure 5.16	^1H NMR spectrum of 16.2H⁺ in toluene- D_8 at 298K	129
107	Figure 5.17	^1H - ^1H COSY correlation spectrum of 16.2H⁺ at 298K in toluene- D_8	130
108	Figure 5.18	^1H NMR spectrum of 17.2H⁺ in toluene- D_8 at 298K	130
109	Figure 5.19	^1H - ^1H COSY spectrum of 18 at 298K in toluene- D_8	131
110	Figure 5.20	^1H NMR spectrum of 18 in toluene- D_8 at 298K	131
111	Figure 5.21	Low temperature (298K-193K) ^1H NMR spectrum of 18 in toluene- D_8	132
112	Figure 5.22	^1H NMR spectrum of 18.2H⁺ in toluene- D_8 at 298K	133
113	Figure 5.23	^1H - ^1H COSY spectrum of 18 at 298K in toluene- D_8	133
114	Figure 5.24	^1H NMR spectrum of 19 in toluene- D_8 at 298K	134
115	Figure 5.25	^1H - ^1H COSY spectrum of 19 at 213K in toluene- D_8	134
116	Figure 5.26	^1H NMR spectrum of 19.2H⁺ in toluene- D_8 at 298K	135
117	Figure 5.27	^1H - ^1H COSY spectrum of 19.2H⁺ at 213K in toluene- D_8	135

118	Figure 5.28	Single crystal X-ray structure of 16 . a) top view and b) side view	138
119	Figure 5.29	Single crystal X-ray structure a) top view and b) side view of 16B.2H⁺(2ClO₄⁻)	139
120	Figure 5.30	Single crystal X-ray structure of 19A (front View)	141
121	Figure 5.31	Single crystal X-ray structure a) top view and b) side view of 19A.2H⁺(2ClO₄⁻)	142
122	Figure 5.32	Electronic absorption spectra of 16 in various solvents	152
123	Figure 5.33	Electronic absorption spectra of 17 in various solvents	152
124	Figure 5.34	Electronic absorption spectra of 16 and 16.2H⁺ in CH ₂ Cl ₂	153
125	Figure 5.35	Electronic absorption Spectra of 18 and 18.2H⁺ in CH ₂ Cl ₂	153
126	Figure 5.36	Electronic absorption Spectra of 19 and 19.2H⁺ in CH ₂ Cl ₂	153
127	Figure 6.1	Structure of turcasarin 1 and its di-oxa complex 2	168
128	Figure 6.2	Structure of decaphyrin 3 and 4	169
129	Figure 6.3	Structure of dibenzidecaphyrin 5	170
130	Figure 6.4	Structure of decaphyrins 10 and 12	171
131	Figure 6.5	HRMS of decaphyrin 10	174
132	Figure 6.6	HRMS of cyano complex 13	174
133	Figure 6.7	HRMS of decaphyrin 12	174
134	Figure 6.8	¹ H NMR Spectrum (a) 10 (298K) and (b) 10.4H⁺ (298K) in CD ₂ Cl ₂	175
135	Figure 6.9	¹ H- ¹ H COSY spectrum of 10 with correlation in pyrrole and thiophene rings	176
136	Figure 6.10	Low temperature ¹ H NMR spectrum of 10 in CD ₂ Cl ₂	176

	(aromatic region)	
137	Figure 6.11	^1H - ^1H COSY spectrum of 10.4H⁺ 177
138	Figure 6.12	2D NMR NOESY spectrum of 10.4H⁺ in CD_2Cl_2 178
139	Figure 6.13	Titration spectrum of 10.4H⁺ in CD_2Cl_2 178
140	Figure 6.14	^1H NMR spectrum; (a) 12 (298K) and (b) 12.2H⁺ (298K) in CD_2Cl_2 179
141	Figure 6.15	^1H - ^1H COSY spectrum of 12 with correlation in pyrrole and thiophene rings 179
142	Figure 6.16	Low temperature ^1H NMR spectrum of 12 in CD_2Cl_2 180
143	Figure 6.17	Low temperature ^1H NMR spectrum of 12.2H⁺ in CD_2Cl_2 180
144	Figure 6.18	^1H NMR spectrum of 13 in CD_2Cl_2 180
145	Figure 6.19	^1H - ^1H COSY spectrum of 13 181
146	Figure 6.20	Crystal structure of 10 (a) top view and (b) side view 182
147	Figure 6.21	Self-assembled dimer of 10 183
148	Figure 6.22	One dimensional array structure of 10 183
149	Figure 6.23	Two dimensional arrays of 10 183
150	Figure 6.24	Crystal structure of 13 (a) top view and (b) side view 185
151	Figure 6.25	Intermolecular hydrogen bonding in 13 186
152	Figure 6.26	Two dimensional array of 13 186
153	Figure 6.27	Optimized structure of 10 and 10.4H⁺ 188
154	Figure 6.28	Optimized structure of 10 and 10.4H⁺ 189
155	Figure 6.29	Energy and relative energy of the two configurations of 10.4H⁺ 189
156	Figure 6.30	Optimized structure of (a) 12 and (b) 12.2H⁺ 190

157	Figure 6.31	Optimized structure of (a) 12 and (b) 12.2H⁺	190
158	Figure 6.32	Absorption spectra of decaphyrin 10 and 10.4H⁺ in CH_2Cl_2	191
159	Figure 6.33	Titration with dilute solution of TFA in CH_2Cl_2 on decaphyrin 10 with concentration	192
160	Figure 6.34	Absorption spectra of decaphyrin 12 and 12.4H⁺ in CH_2Cl_2	192
161	Figure 6.35	Titration with dilute solution of TFA in CH_2Cl_2 on decaphyrin 12 with concentration	193

List of Abbreviations

^1H NMR	Proton Nuclear Magnetic Resonance
^{13}C NMR	Carbon-13 Nuclear Magnetic Resonance
^{11}B NMR	Boron-11 Nuclear Magnetic Resonance
^{19}F NMR	Fluorine-19 Nuclear Magnetic Resonance
^{31}P NMR	Phosphorus-31 Nuclear Magnetic Resonance
EPR	Electron Paramagnetic Resonance
UV-Vis	Ultraviolet–Visible
ESI	Electrospray Ionization
GOF	Goodness of Fit
CCDC	Cambridge Crystallographic Data Centre
DFT	Density Functional Theory
DDQ	2,3-Dichloro-5,6-dicyano-1,4-benzoquinone
CH_2Cl_2	Dichloromethane
CHCl_3	Chloroform
EtOAc	Ethyl acetate
CH_3CN	Acetonitrile
CH_3OH	Methanol
THF	Tetrahydrofuran
$\text{ClCH}_2\text{CH}_2\text{Cl}$	1,2-Dichloroethane
DMF	Dimethylformamide
$\text{C}_6\text{F}_5\text{COCl}$	Benzoyl chloride
$\text{CH}_3\text{SO}_2\text{Cl}$	Methanesulfonyl chloride
NaBH_4	Sodium borohydride
$\text{C}_6\text{F}_5\text{CHO}$	Pentafluorobenzaldehyde
POCl_3	Phosphorus oxychloride
PhMgBr	Phenylmagnesium bromide
PhBCl_2	Dichlorophenyl borane
TEA	Triethylamine
DMAP	4-Dimethylaminopyridine
TMP	Tetramethylpiperidine
NCP	N-confused porphyrin

CO	Carbon monoxide
HCl	Hydrogen chloride
TFA	Trifluoroacetic acid
BF ₃ .Et ₂ O	Boron trifluoride diethyl etherate
<i>p</i> -TSA	<i>para</i> -toluenesulfonic acid
TMS	Tetramethylsilane
CDCl ₃	Deuterated chloroform
CD ₂ Cl ₂	Dideuteromethylenechloride
CD ₃ CN	Deuterated acetonitrile
CD ₃ OD	Deuterated methanol
Toluene- <i>d</i> ₈	Deuterated toluene
DMSO- <i>d</i> ₆	Hexadeuterodimethyl sulfoxide
FB	Free-Base
TLC	Thin Layer Chromatography
Na ₂ SO ₄	Sodium sulphate
Zn(OAc) ₂	Zinc acetate
Cu(OAc) ₂	Copper acetate
Pd(OAc) ₂	Palladium acetate
Zn(ClO ₄) ₂	Zinc perchlorate
Ag(PF ₆)	Silver hexafluorophosphate
Ag(OTf)	Silver triflate
[Rh(CO) ₂ Cl] ₂	Di- μ -chloro-tetracarbonyldirhodium(I)
NaBF ₄	Sodium tetrafluoroborate
FeCl ₃	Iron(III) chloride

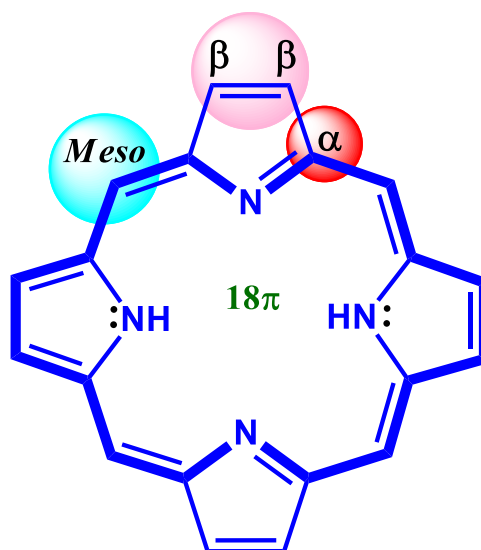
CHAPTER 1

Evolution of Core-Modified Expanded Porphyrins and its Molecular Topology

1.1	Porphyrins	3
1.2	Modifications	4
1.2.1	Contracted Porphyrins	5
1.2.2	Expanded Porphyrins	6
1.2.3	N-confused Porphyrins	8
1.3	Aromaticity	10
1.3.1	NICS(Nucleus Independent Chemical Shift)	10
1.3.2	AICD(Anistropy Induced Current Density)	12
1.3.3	Hückel Aromaticity	14
1.3.4	Hückel Anti-aromaticity	14
1.3.5	Möbius Aromaticity	15
1.3.6	Möbius Anti-aromaticity	19
1.3.7	Baird Aromaticity	20
1.4	Aromaticity and Structural Switchover	23
1.4.1	Redox Initiator	24
1.4.2	Protonation and Deprotonation	25
1.4.3	Isomerization	26
1.5	Scope and Objective of the present thesis	27
1.6	References	29

1.1 Porphyrins

Porphyrins are naturally occurring tetrapyrrolic macrocycles which are termed as “Pigments of Life.”¹ The tetrapyrrolic moiety consists of two amine and two imine nitrogens connected by four methine/*meso* carbon bridges and the inner core contains 16 atoms in the macrocyclic framework with 18π conjugated electrons exhibiting aromatic features. It plays an important role in several biological functions such as oxygen transport and storage in the form of Hemoglobin and Myoglobin,^{2,3} electron transport in cytochromes,^{4,5} harvesting the light energy in the form of chlorophyll^{6,7} and peroxide breakdown by catalase and peroxidase enzymes.^{8,9} Indeed, several biological processes are performed or catalyzed by heme-containing proteins. More recently, they have been used as efficient sensitizers for photodynamic therapy (PDT) for cancer treatment.^{10,11}



The word “Porphyrin” comes from “Porphine”. The name is derived from the Greek word “porphura” which means purple and is named because of the highly intense purple color of porphyrins and its derivatives. As a consequence of highly close conjugated π system it gives well defined electronic absorption spectra. The electronic spectral analysis exhibits an intense absorption band around 400 nm and called as “Soret band” and four weak Q-like bands between 450 to 700 nm range. NMR

spectral analyses reveals the diamagnetic ring current which is reflected from the deshielding of the pyrrolic β -CH protons and *meso* protons, while the inner NH protons are in the shielded region conforming its aromatic nature. The dianionic tetradentate square planar ligand contains two imine and two amine nitrogens thus it can act as a coordination site to bind metal ions in the cavity. The richness of porphyrin chemistry and its diverse applications has inspired researchers to synthesize new derivatives of porphyrins and their analogues since past three decades.

1.2 Modifications

Several modifications such as; contraction of the porphyrin ring by decreasing methine carbon atom or pyrrole ring,¹²⁻¹⁴ expansion of the ring by adding more pyrrole rings in conjugation, replacement of one or more pyrrole rings by other heterocyclic ring^{15,16} such as thiophene and selenophene and new isomers of porphyrins have been done to exploit their rich chemistry as well as their diverse functional applications. Some of the applications of expanded porphyrins are depicted in the following Figure 1.1.

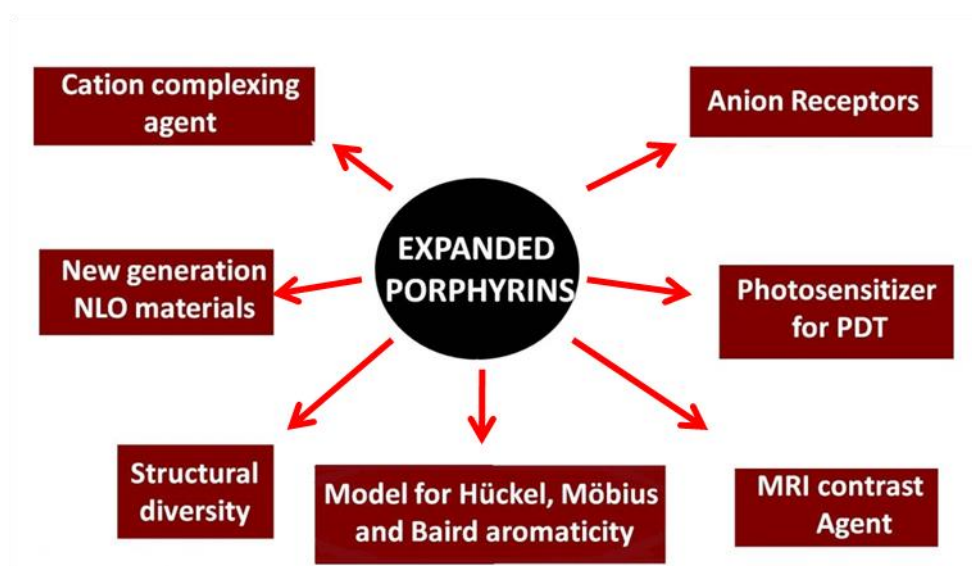


Figure 1.1: Applications of expanded porphyrins

1.2.1 Contracted Porphyrins

Contracted porphyrins are formed by reducing the number of pyrrole and / or *meso*-carbon units in the porphyrin skeleton, which leads to reduction in the size of the porphyrin skeleton. Several contracted porphyrins have been studied though they are not structurally diverse as expanded porphyrins, some of them are corroles, subphthalocyanines, subporphyrins, norcorroles, isocorroles etc. based on the number of pyrrole ring and position of *meso* carbons. Corrole is a tetrapyrrolic moiety which has 19 atoms in general and found in cobalamin.^{17,18} The structure is oxidized form of corrin ring and was synthesized by Jonson and Kay in the year 1965.^{19,20} The eminent difference between porphyrins and corrole **1** is one *meso* carbon less than porphyrins and has direct bond between two pyrrolic rings. It is also an 18π aromatic system like porphyrins and the presence of three NH protons makes it a trianionic ligand for coordination with metals with higher oxidation state. Subporphyrins are another class of contracted porphyrins which contains three pyrrole rings and three *meso* carbons. In 2006, Osuka and coworkers²¹ synthesized first tribenzosubporphyrin **2** and synthesized by using (3-oxo-2,3-dihydro1*H*-isoindol-1-yl)acetic acid, boric acid grinded then heated up to 350 °C for over 3.5 h. The yield of **2** is 1.4% compound after repeated chromatographic purification shown in Figure 1.2. Boron (III) coordinating subporphyrins are extensively studied due to their applications such as radical stabilizing units due to their spin delocalization. Recently Osuka and coworkers²² have synthesized stable B(III)- subporphyrin **3** substituted dicyano-methyl radicals by S_NAr reaction with *meso*-bromosubporphyrins with malanonitrile followed by oxidation with PbO_2 shown in Scheme 1.1. In solid state this molecule showed weak π -dimers with antiferromagnetic interactions but in solution it existed as stable dicyano-methyl radical even at low temperatures.

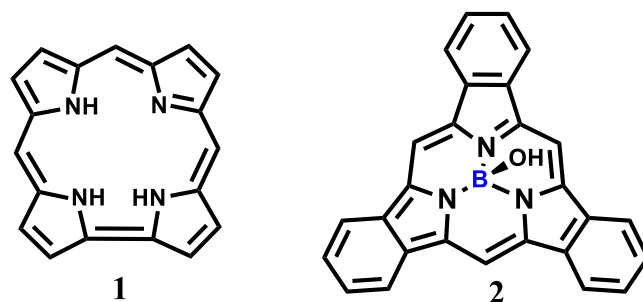
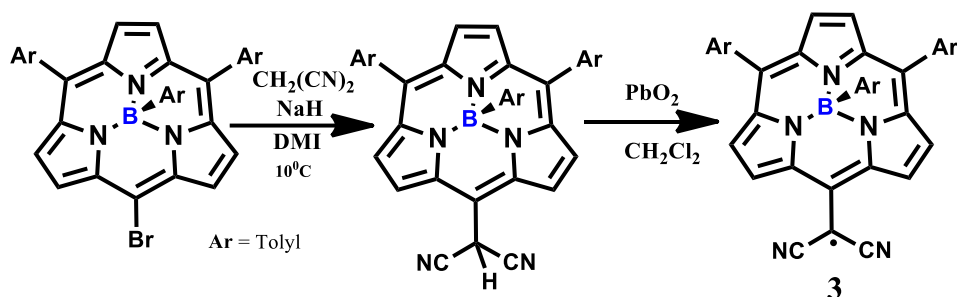


Figure 1.2: Corrole and benzosubporphyrins.



Scheme 1.1: Synthesis of di-cyano methyl subporphyrin radicals.

1.2.2 Expanded Porphyrins

Expanded porphyrins are formed by increasing one or more pyrrolic units or number of *meso* carbon units in the porphyrin framework which leads to increase in the π electron conjugation. Sessler and Seidel in 2003 defined the expanded porphyrins as “*Macrocyclic that contains pyrrole, furan, thiophene and other heterocyclic subunits linked either directly or through spacer atoms in such manner that the internal ring pathway contains a minimum of 17 atoms*”.²³ Depending on increase in the meso carbons expanded porphyrins are categorized as tetravinyllogous expanded porphyrins where there is only increase in *meso* carbons and pyrrolic units remain constant as shown in Figure 1.3.²⁴ The early work on the other side where *meso* carbons remains constant with increase in heterocyclic rings on expanded porphyrins was started by Woodward and coworkers²⁵ where they reported the formation of sapphyrin as the first expanded porphyrins with five pyrrole rings. However, due to synthetic

difficulties and availability of precursors, the chemistry of expanded porphyrins picked up momentum only in late eighties and early nineties. Expanded porphyrins such Pentaphyrins,^{26,27} Hexaphyrins,^{28,29} Heptaphyrins,^{30,31} Octaphyrins,^{32,33} Nonaphyrins,³⁴ Decaphyrins,³⁵ Undecaphyrins, Dodecaphyrin³⁶ and so on depending on the number of heterocyclic rings in the core of the macrocycle have been synthesized so far as shown in Figure 1.4.

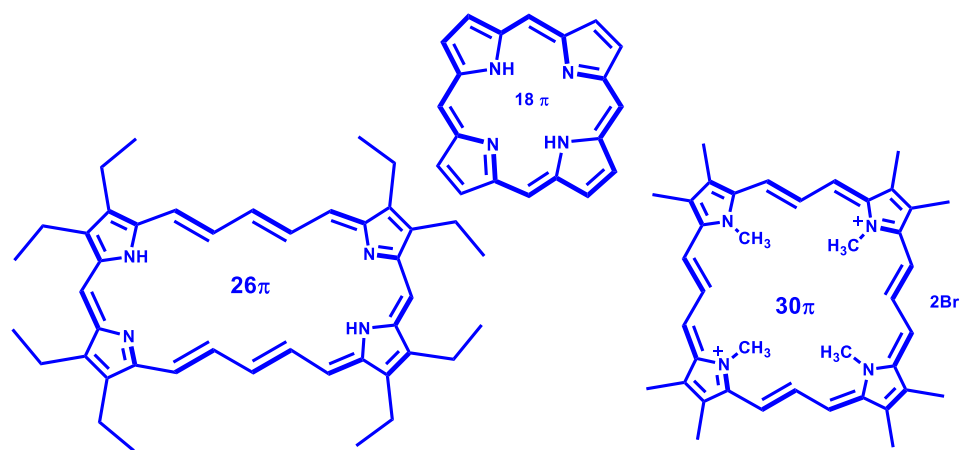


Figure 1.3: Examples of tetravinyllogous expanded porphyrins.²⁴

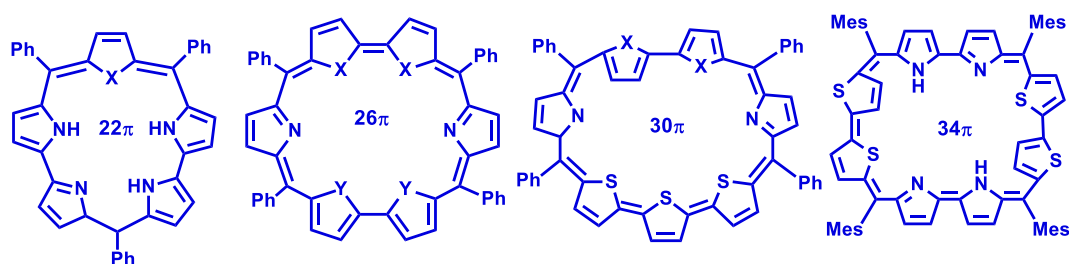


Figure 1.4: Examples of expanded porphyrins with various structural diversity.³⁷

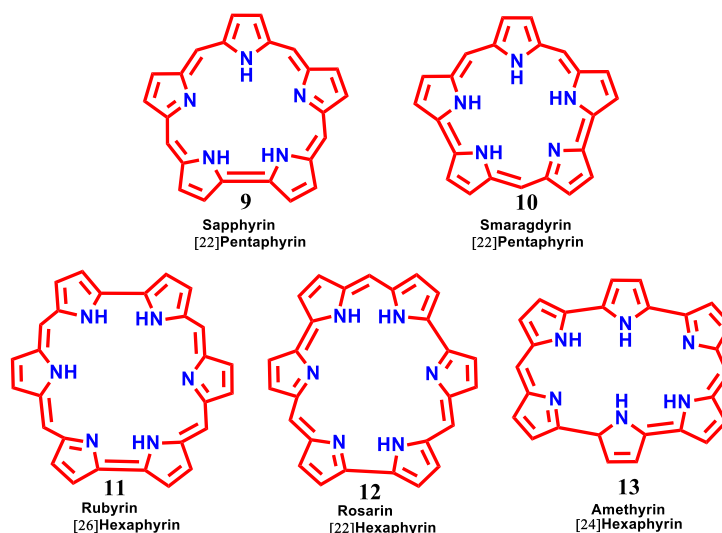


Figure 1.5: Expanded porphyrins with various structural diversity.

However change in the number of *meso* linking pyrrole rings generates new macrocycle with altered electronic structures such as *sapphyrins* **9**, *smaragdyrins* **10**, *rubyrin* **11**, *rosarian* **12**, *amethyrin* **13** shown in Figure 1.5 which indeed changes the π - electronic conjugation of the macrocyclic core showing structural diversity and properties.³⁸⁻⁴³

The study of expanded porphyrins are motivated by several factors such as to study the nature of aromaticity and the large core size can accommodate more than one metal ions to produce multi-metallic complexes and it also binds with anionic and neutral substrates.⁴⁴⁻⁵⁰ It also serves as an objective to understand Möbius aromatic and even antiaromatic systems, which is indeed hard with any other class of macrocycles.⁵¹⁻⁶⁰

1.2.3 N-confused Porphyrins

In normal porphyrins, the pyrrole rings are connected through α , α' -linkage but in the N-confused porphyrinoid the position of one or more pyrrole (α and β') units are connected to the *meso*-carbon bridges, where the pyrrole nitrogen is pointed outside

the macrocyclic framework;^{61,62} They are achieved by changing the bonding mode of heterocyclic rings in the normal porphyrins. Their hetero-analogues are further classified according to their heterocyclic counterparts, such as N-confused porphyrins, O-confused porphyrins, S-confused porphyrins, Se-confused porphyrins.⁶³⁻⁶⁶ Among the confused porphyrins, N-confused porphyrins (NCP) are of particular research interest in many fields. The first N-confused porphyrin **14** and **15** was independently synthesized in 1994 by Furuta⁶⁷ and Latos-Grażyński research groups respectively.⁶⁸ Since then, a series of several confused derivatives and porphyrin isomers have been developed and exploited for their coordination properties shown in Figure 1.6 and 1.7.

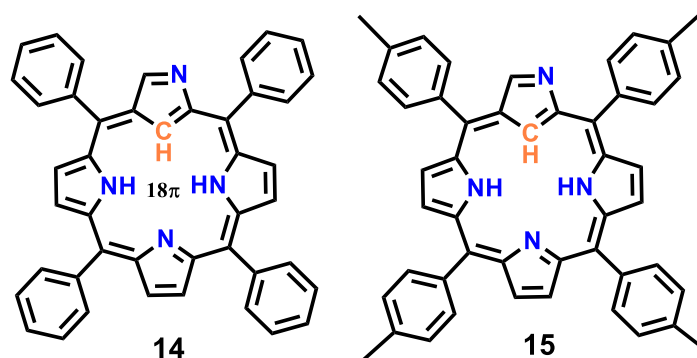


Figure 1.6: Examples of N-confused porphyrins.

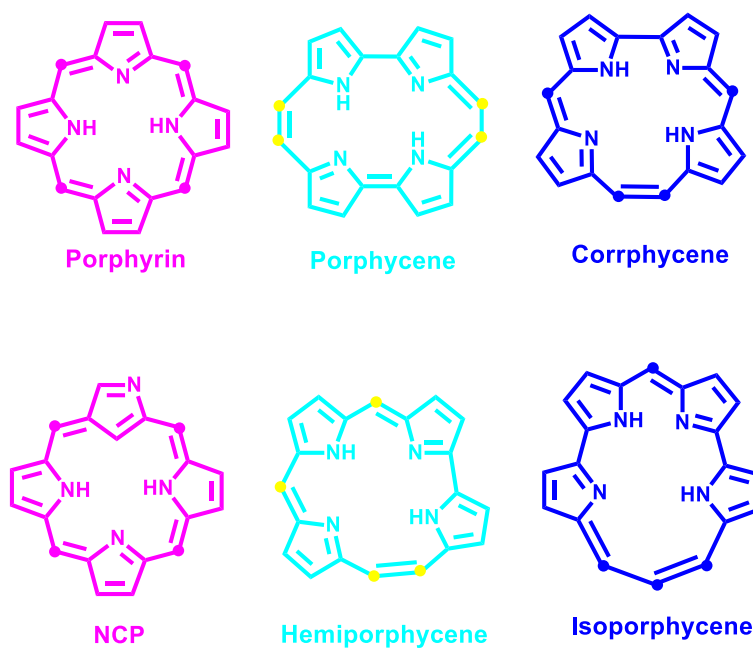


Figure 1.7: Examples of N-confused porphyrin and other porphyrin isomers.

1.3 Aromaticity

Aromaticity can be defined by the ability of a molecule to sustain a ring current when placed inside a magnetic field. It is an important fundamental that governs the electronic properties of π -conjugated molecules. A structural change from planar to a twisted molecule or rigid half twisted or both in the same molecule leads to situations of aromaticity change. The main standard for characterizing aromaticity involves four main groups. Each group has its own disadvantages: **Structural** property for bond length equalization and planarity. **Energy** increased stabilization. **Reactivity** lowered reactivity, electrophilic aromatic substitution. **Magnetic properties** proton chemical shift, magnetic susceptibility exaltation, NICS, ring current chemical shift plots shown in Figure 1.8.

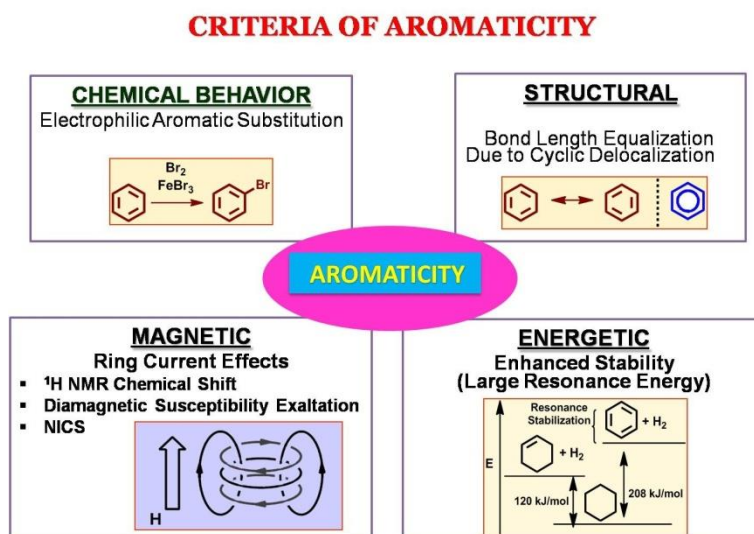


Figure 1.8: Criteria for aromaticity in expanded porphyrins.

1.3.1. NICS (Nucleus Independent Chemical Shift)

Apart from the structure elucidation by planarity, aromaticity can also be characterized on the basis of magnetic properties such as ^1H NMR chemical shift, magnetic susceptibility and NICS. ^1H NMR chemical shifts are often the most useful

criteria for analyzing aromaticity i.e, for cyclic $[18\pi]$ annulene **16** aromatic systems due to the diatropic ring current effect the inner protons are more shielded and resonates at -3.0 ppm and outer protons are deshielded and resonates at 9.28 ppm whereas in contrary to an dianion of cyclic $[18\pi]$ annulene **17** shown in Figure 1.9 the outer protons are shielded and resonates at -1.13 ppm and inner protons are deshielded and resonates at 28.1 ppm due to paratropic ring current showing its anti-aromaticity.⁶⁹ NICS has become one of the most widely used parameters to judge aromaticity. Before NICS came into account magnetic susceptibilities (Λ) were first magnetic criteria which were employed which resulted from the cyclic delocalization of electrons.

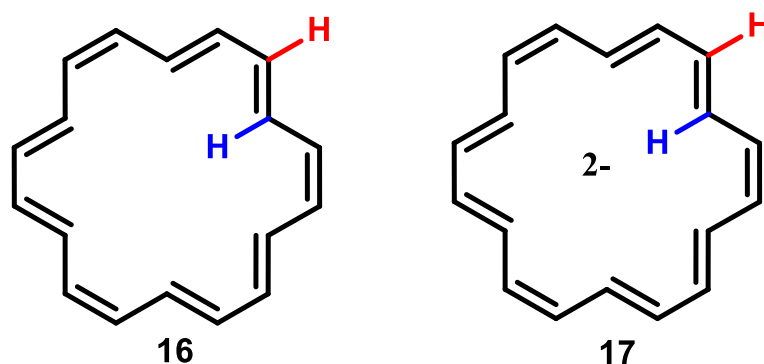


Figure 1.9: [18]Annulene and [18]Annulene dianion.

The magnetic susceptibility depends on the ring size and is defined as the difference between the bulk magnetic susceptibility and the susceptibility evaluated on the basis of an increment system. Computation of the total chemical shielding of a nucleus to explore aromaticity leads to the (NICS) nucleus-independent chemical shift which was first shown by Schleyer, Maerker, Dransfeld, Jiao, and Hommes in the year 1996.⁷⁰ NICS is nothing but the absolute magnetic shieldings computed at the ring centers; where $\text{NICS} < 0$ tends to aromatic behaviour and $\text{NICS} > 0$ tends to antiaromaticity shown in Table 1.1.

Table 1.1: Table showing NICS and Λ values of aromatic and antiaromatic compounds.

COMPOUND	$\Lambda(10^{-6}\text{cm}^3\text{mol}^{-1})$	NICS(ppm)
	0.0	-2.2
	-13.7	-9.7
	-6.5	-3.2
	32.6	54.2

1.3.2 ACID (Anisotropy Current Induced Density)

It is a general method to quantify and visualize electronic delocalization. On the grounds of the ACID calculations, molecules give a set of base which is used to foresee the aromaticity and antiaromaticity. Anisotropy current induced density plots (ACID plots) calculated on to isosurface when suggests a clockwise orientation of current density vectors indicate presence of diatropic ring current and an anticlockwise orientation of current density vectors indicate presence of paratropic current density. The -ve and +ve NICS values of the aromatic compounds and antiaromatic species respectively shows diatropic and paratropic induced ring currents in the systems, shown in Figure 1.10.⁷¹ Furthermore, the NICS and ACID results are in relation with the small transition energies of the lowest E.S in comparison with the energy gaps between the HOMO and LUMO.

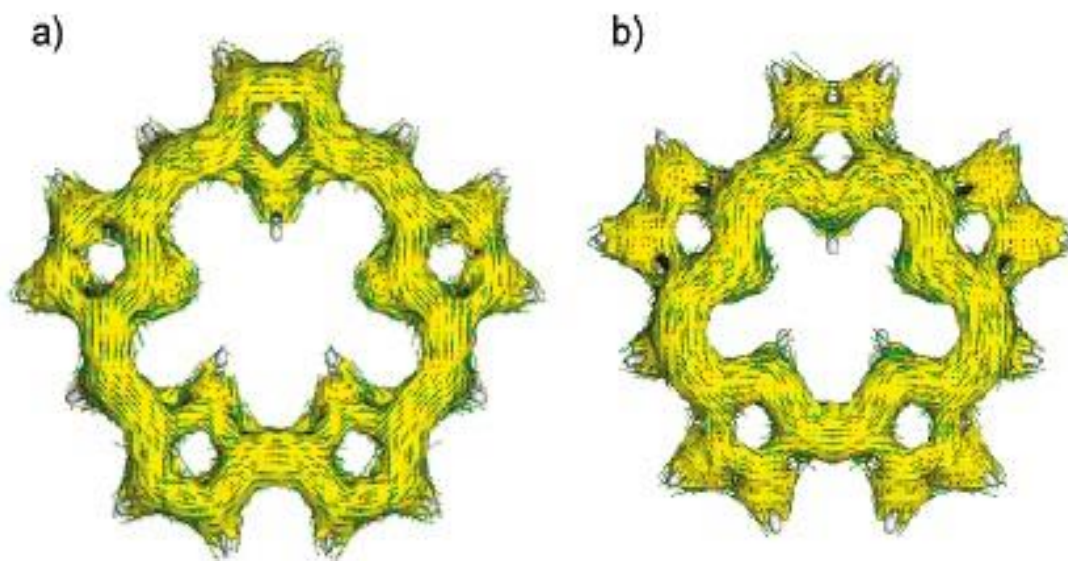


Figure 1.10: Current Density maps of (a) diatropic and (b) paratropic expanded porphyrins.

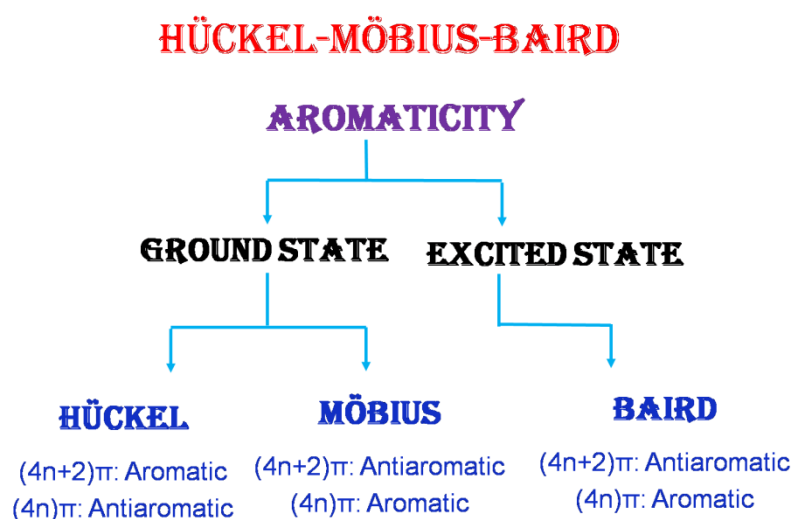


Figure 1.11: Different types of aromaticity in expanded porphyrins.

The aromatic character of porphyrin systems is well known and is one of the most important and basic concept to judge aromaticity of organic molecules in chemistry. Basically classified into two categories till date i) Ground state aromatics (This type of aromaticity is governed by two types that are “Hückel and Möbius concept”. ii) Excited state aromatics “Baird aromaticity” shown in Figure 1.11.

1.3.3 Hückel Aromaticity

The concept of “Hückel Aromaticity” is well known in the porphyrinoid chemistry.⁶⁰ According to Hückel concept, molecules that possess $(4n+2)\pi$ electrons in conjugation pathway with planar structure are said to Hückel aromatic. Recently, continuous trials to show the amount of aromaticity by various methods, such as structuralal and spectroscopic studies have been made.^{74,23} The first 26π Hückel aromatic hexaphyrin **18** with β -substituted derivative was reported by Gossauer and coworkers in 1983 shown in Figure 1.12.⁷³ The presence of β -substitution prevents the pyrrolic ring inversion and also exhibit cis-trans Isomerization.

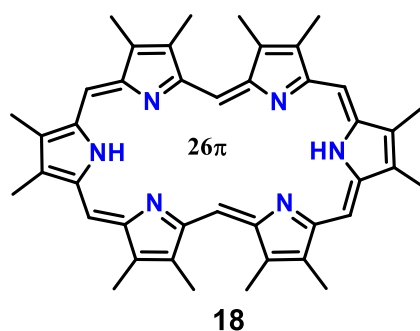
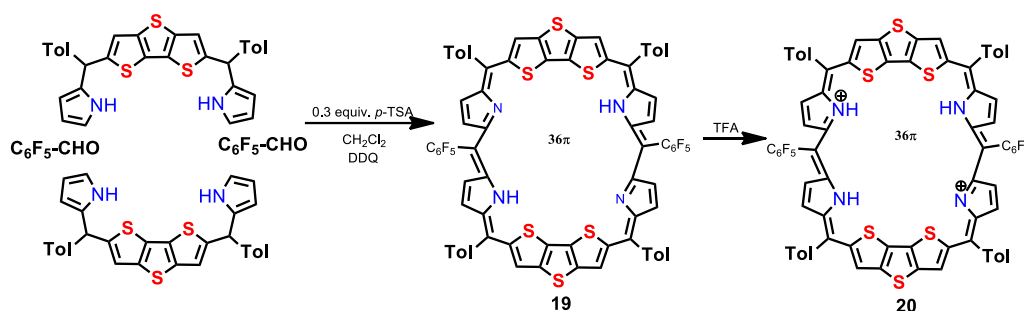


Figure 1.12: Example of Hückel aromatic Hexaphyrin.

1.3.4 Hückel Antiaromaticity

The concept of “Hückel Antiaromaticity” in the porphyrinoid chemistry is molecule that contains $4n\pi$ conjugative pathway. Sessler research group gave a very early example of amethyrin as an antiaromatic porphyrinoid.⁷⁴ Doubly fused 36π octaphyrins that shows a conformational and structural changes from a perverted figure-eight nonaromatic **19** to an open antiaromatic **20** structure caused by protonation shown by Chandrashekar and co-workers shown in Scheme 1.2.⁷⁵ Here two broad NH signals were observed at $\delta=18.7$ and 0.1 ppm and two sets of β -CH pyrrole signals shown as a doublet of doublet at $\delta=15.91$ ppm and $\delta=4.36$ ppm

suggested a major structural change upon protonation and was confirmed to be antiaromatic in nature.



Scheme 1.2: Synthesis of Hückel antiaromatic molecule **20**.

1.3.5 Möbius Aromaticity

Expansion in the porphyrin core by adding of substituent the free movement of the ring is restricted and angular strain also increases which leads to change in the conformation of the molecule like π surface twisting or a subunit inversion. Due to the π surface twisting there is attainment of Möbius Aromaticity. Unlike Hückel rule, the $(4n+2)\pi$ electronic conjugation are Möbius antiaromatic whereas the $4n\pi$ systems are Möbius aromatic in nature. Relationship between conformation and aromaticity in expanded Porphyrin systems is basically our area of interest. The concept of “Möbius aromaticity” in a closed shell configuration with $[4n]\pi$ -electron conjugation in molecular systems was proposed as early as 1964 by Heilbronner.⁵¹ A molecule can gain Möbius aromatic stabilization if the nuclear frame work were twisted so that the p-orbitals composing the π -system would contain an odd no. of nodes. To introduce a node in the orbitals, a series of p-orbitals could itself be twisted by contorting the nuclear frame work. The twisted p-orbitals would then form a C_2 - symmetric π -system that lies on the surface of the Möbius strip shown in Figure 1.13 and Figure 1.14.

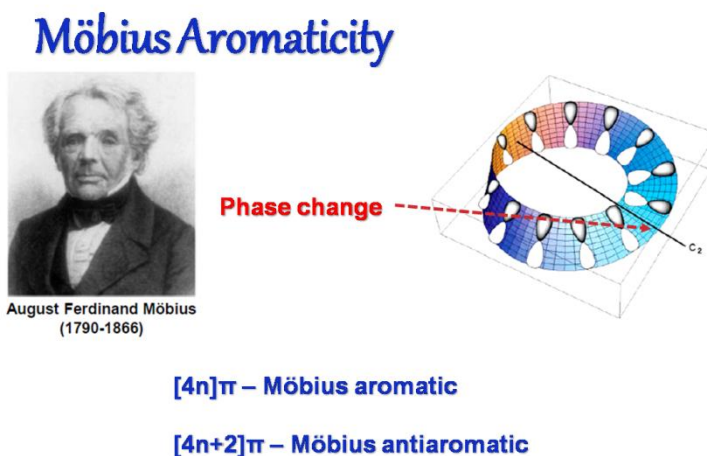


Figure 1.13: Möbius aromaticity in expanded porphyrins.

However, the first real example of a Möbius aromatic hydrocarbon was realized only in 2003 by Herges and coworkers.⁵² Since then, several reports have appeared in literature on molecules which exhibit $[4n]\pi$ Möbius aromaticity especially in cyclic annulenes and its derivatives.

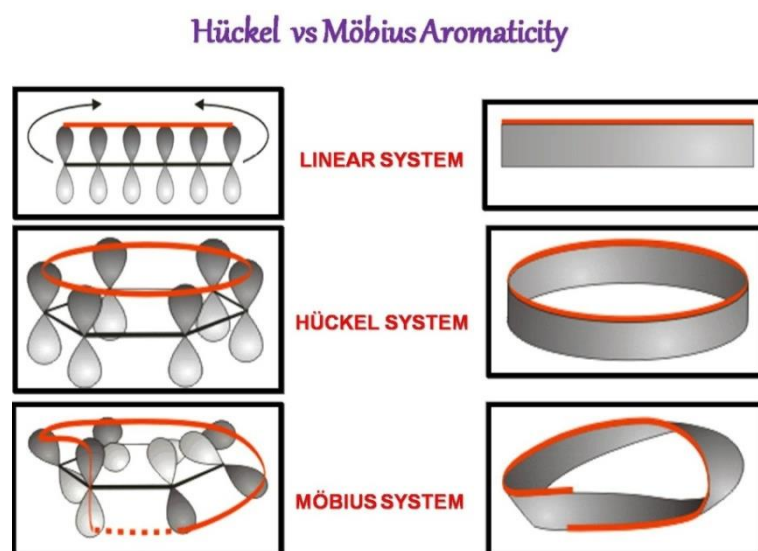


Figure 1.14: Linear, Hückel and Möbius strips.

The first example of expanded porphyrin analogue such as di-*p*-benzi[28 π] Hexaphyrin **21** which exhibits Möbius aromaticity was reported in 2007 by Latos-

Grażyński and coworkers.⁵⁵ Here the hexaphyrin is shuttling between Hückel and Möbius topology upon lowering temperature and changing polarity of the solvents, at room temperature, **21** exhibited Hückel $4n\pi$ non-aromatic character, however upon lowering temperature the pyrrolic NH and phenylene CH protons at 16.51 ppm and 8.16 ppm were shifted upfield and resonated at 10.31 ppm shown in Figure 1.15 and 1.16.

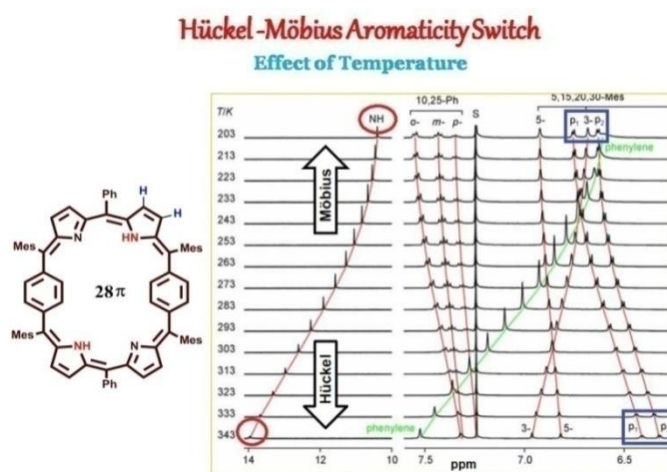


Figure 1.15: Möbius aromaticities in expanded porphyrins upon lowering temperature.

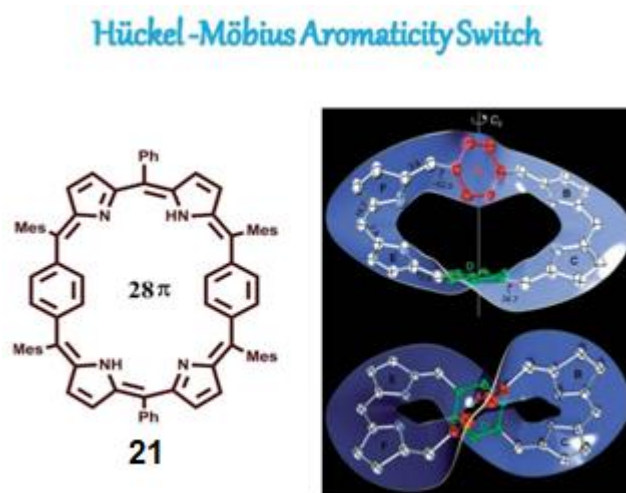


Figure 1.16: Hückel-Möbius aromaticity switch in expanded porphyrins.

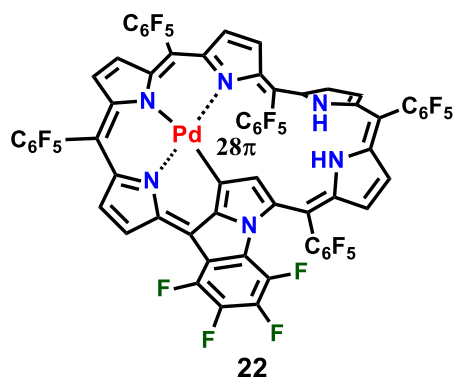
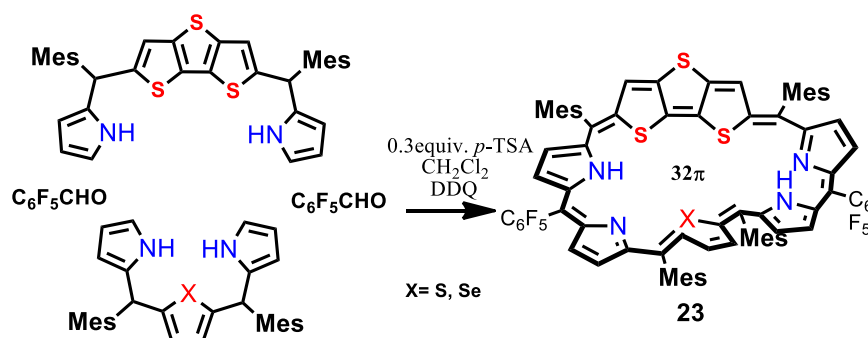


Figure 1.17: Example of Möbius aromatic molecule.

In 2010, Osuka and coworkers have synthesized first N-fused 28π hexaphyrin **22** which exhibits Möbius aromaticity upon Pd metal coordination shown in Figure 1.17.^{59,76} Later in the year 2015, Osuka and coworkers rare examples of Möbius aromatic thiophene-fused [28]hexaphyrin⁵⁷ in freebases reaction of [26]hexaphyrin with triethylamine in the presence of $\text{BF}_3 \cdot \text{OEt}_2$ and O_2 . Later Chandrashekar and group in 2016 also reported Möbius aromatic 32π core-modified Heptaphyrin **23**⁷⁷ which showed Möbius aromaticity in freebase form upon lowering temperature shown in Scheme 1.3.

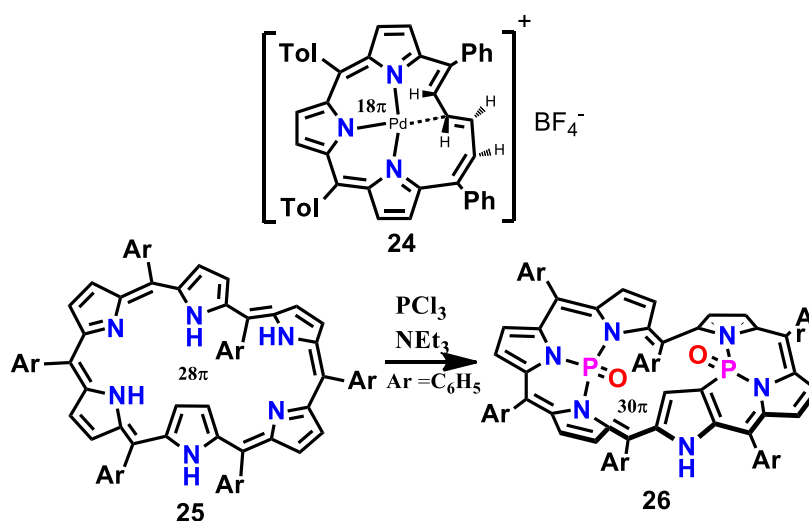


Scheme 1.3: Synthesis of Möbius aromatic molecules.

1.3.6 Möbius Anti-aromaticity

Till date $(4n+2)\pi$ Möbius anti-aromatic molecules are quite rare as the molecules suffer structural distortion and electronic destabilization. The first Möbius anti-

aromatic molecule a cationic Palladium (II) vacataporphyrin **24**⁷⁸, was explored by Latos-Grażyński in the year 2008, it was found to have weak paratropic ring current and the crystal structures were not available. The description of conformers were studied using proton NMR and by DFT calculations and synthetically identified the first example of Möbius antiaromatic molecule in case of porphyrins. Later in the year 2010, bis-phosphorous 30 π Hexaphyrin **26**⁷⁹ complex was synthesized shown in Scheme 1.4 from 28 π Hexaphyrin **25** with phosphorous trichloride and triethylamine by Osuka which indicated a strong paratropic current through deshielded inner β -protons and shielded outer β -protons with $\Delta\delta$ value of 5.60 ppm and gave the first crystal structure of Möbius anti-aromatic molecule. NICS values calculated were consistent with Möbius antiaromatic character that is $\delta = +3.65$ ppm and the AICD plots also illustrated paramagnetic terms of current density. Later in the year 2012, Osuka synthesized a 32 π monophosphorus inserted Heptaphyrin **27**⁸⁰ complex shown in Figure 1.18 which was found to be Möbius anti-aromatic has been confirmed on the basis of its twisted Möbius X-ray structure, a weak paratropic ring current, ill-defined absorption characteristics in the UV-Visible spectra, fast excited-state decay, and a relatively small TPA cross section, highly reduced HOMO-LUMO gap.



Scheme 1.4: Möbius antiaromatic **24** and synthesis of **26**.

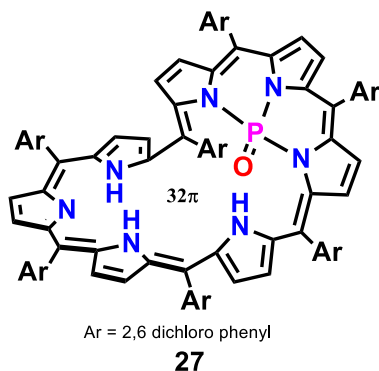


Figure 1.18: Möbius antiaromatic 32π Heptaphyrin **27**.

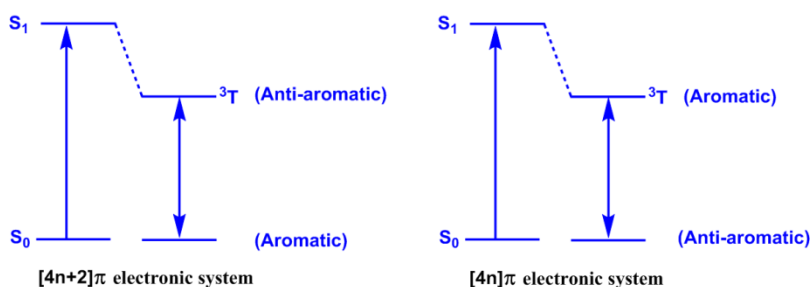
1.3.7 Baird Aromaticity

According to Baird's prediction aromatic molecules which have $[4n+2]\pi$ configuration in ground state are anti-aromatic in the lowest triplet excited state and anti-aromatic molecules which have $[4n]\pi$ configuration in ground state are aromatic in the lowest triplet excited state. This reversal of aromaticity upon going from ground state to excited triplet state was predicted by Baird in 1971.⁸¹

Baird's rule (aromaticity in lowest triplet state)

Prediction: (1972)

"Hückel aromaticity $(4n + 2)\pi$ observed in the ground state systems would be reversed in the lowest triplet state"



Baird's rule prediction:

- **Baird's prediction is supported by theoretical calculations such as NICS, HOMA.**

Figure 1.19: Baird aromaticity in expanded porphyrins.

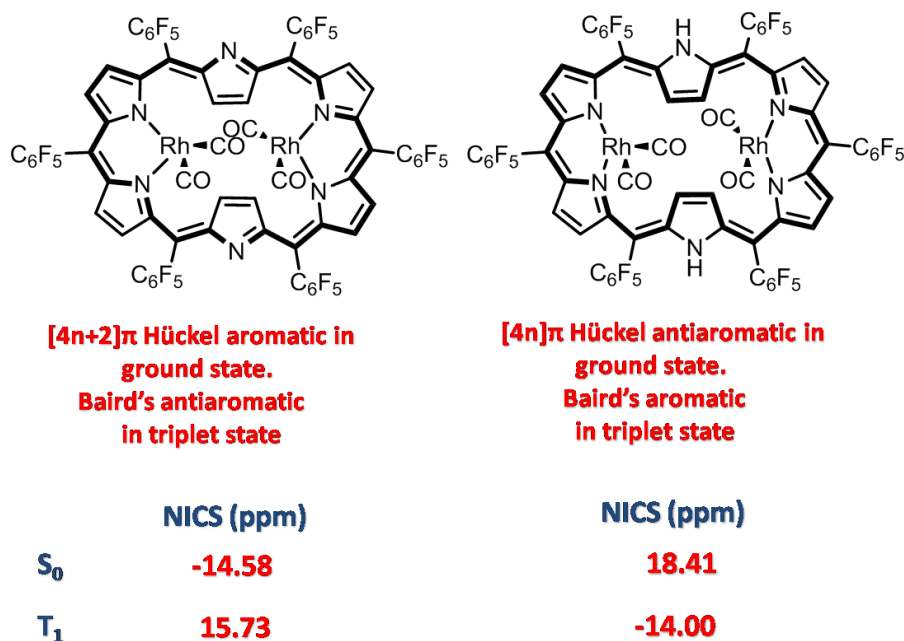


Figure 1.20: Expanded porphyrins with Baird aromaticity

Experimentally, Baird's rule has been verified by using following molecules in 2015 by Osuka $[4n+2]\pi$ Hückel aromatic in ground state Baird's antiaromatic in triplet state $[4n]\pi$ Hückel antiaromatic in ground state, Baird's aromatic in triplet state shown in Figure 1.19. At singlet ground state (S_0), $[26]\pi$, **28** and $[28]\pi$ **29** hexaphyrins were aromatic and antiaromatic and its reversal aromaticity was reflected from the transient absorption spectra at triplet excited state (T_1), where the Soret band in **28** was turned into broad absorption bands, whereas, in **29** the broad bands were changed into sharp Soret like band. The result was further supported by theoretical calculations.⁸² In order to test the Baird's prediction for porphyrinoid systems our group used octaphyrins **30** and **31**,⁸³ which contain 42π electrons shown in Figure 1.24 which exhibit Hückel aromaticity in ground state as the second example in literature which proves the Baird's prediction. Upon oxidation of this molecule by $2e^-$ a 40π electronic system $[4n\pi]$, which according to Baird's rule should exhibit aromaticity in the lowest excited triplet state shown in Figure 1.22. Verification this by recording triplet state

ESR spectra of the oxidised species of (30^{++}) and evaluated the zero field splitting parameters D and E. The D and E values are 256G and 33G shown in Figure 1.22.

The NICS values also support Baird aromaticity shown in Figure 1.23.

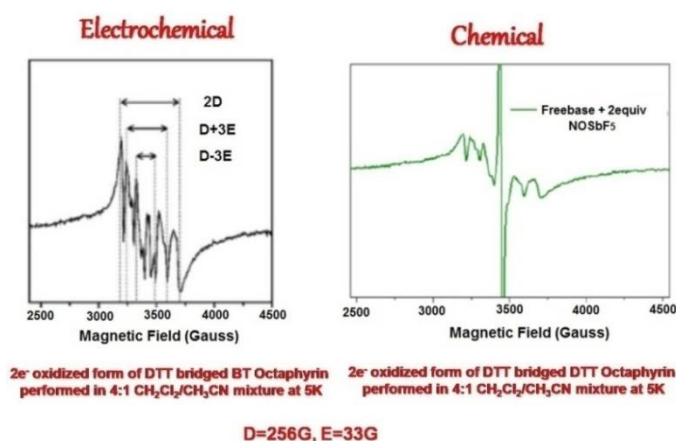


Figure 1.21: Electrochemical oxidation in expanded porphyrins.

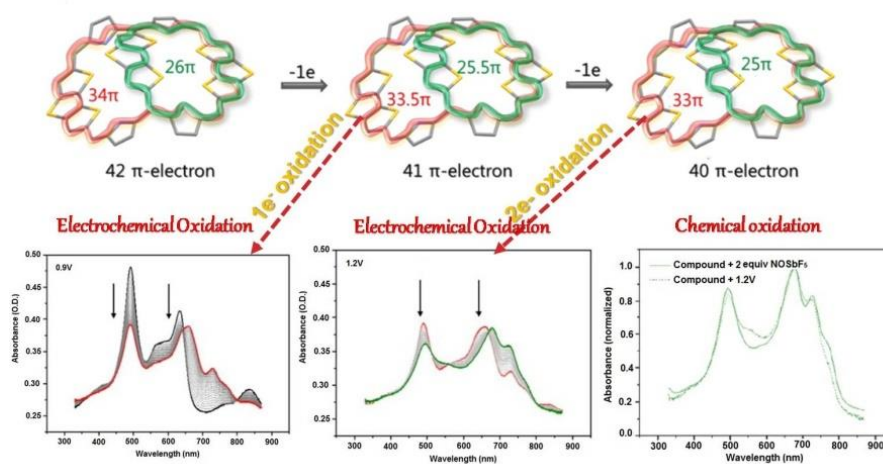


Figure 1.22: EPR of $2e^-$ oxidized Baird aromatic molecule.

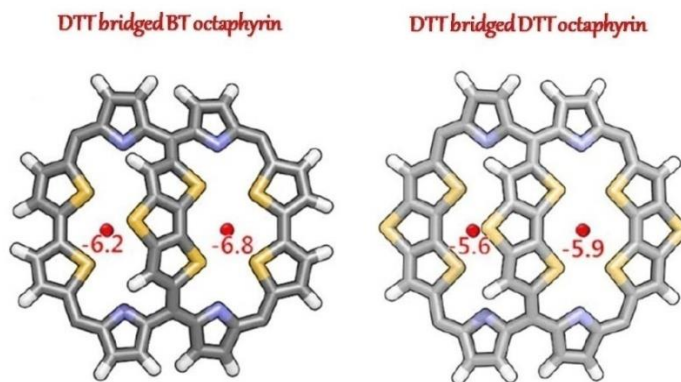


Figure 1.23: NICS values of Baird aromatic molecules.

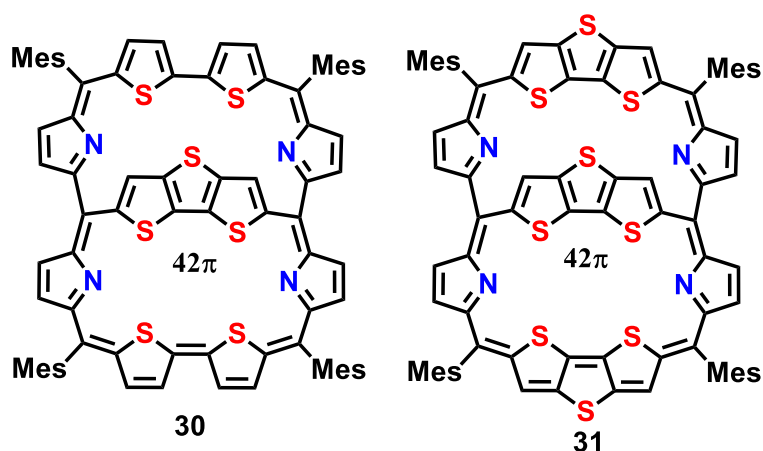


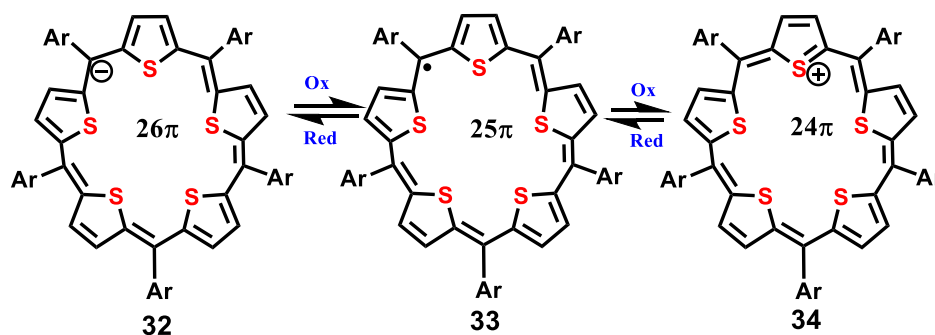
Figure 1.24: Bridged expanded porphyrins; models for Baird aromaticity

1.4 Aromaticity and Structural Switchover

Expanded porphyrin exhibits various structures, aromaticities, electronic properties. However facile interconversion of aromaticity through modifications is possible through modulators. Several modulators can be used for switchover of aromaticity in expanded Porphyrins. These modulators can be 1) Redox switching, 2) Protonation and deprotonation, 3) Temperature variation, 4) Isomerization, 5) Chemical modifications.

1.4.1 Redox Initiator

Expanded Porphyrins aromaticity is controlled by increased number of π -electrons and its size in the system which determines its aromatic character. So, two electron oxidation or reduction would favor reversible change in the structure. Recently, Anand and coworkers⁸⁴ showed a [25]Pentathiaphyrins(1.1.1.1.1) radical **33** which could be transformed through readily available redox agent into aromatic [26]Pentathiaphyrins(1.1.1.1.1) anion **32** and antiaromatic [24]Pentathiaphyrins(1.1.1.1.1) cation **34** shown in Scheme 1.5. The diatropic and paratropic nature was confirmed through ¹H-NMR studies. Proton NMR spectrum of **34** resonated a signal at $\delta = 6.7$ ppm in 293 K, and again shielded and shifted to 7.8 ppm. The large shielded ring current effect expected for a 24π antiaromatic cation showed the one-electron oxidation. Proton NMR spectrum obtained by adding KO₂ and 18-crown-6 to **33**, shows a singlet at 11.15 ppm for **32**. Such a deshielding effect shows that the diatropic ring current of the 26π aromatic anion.

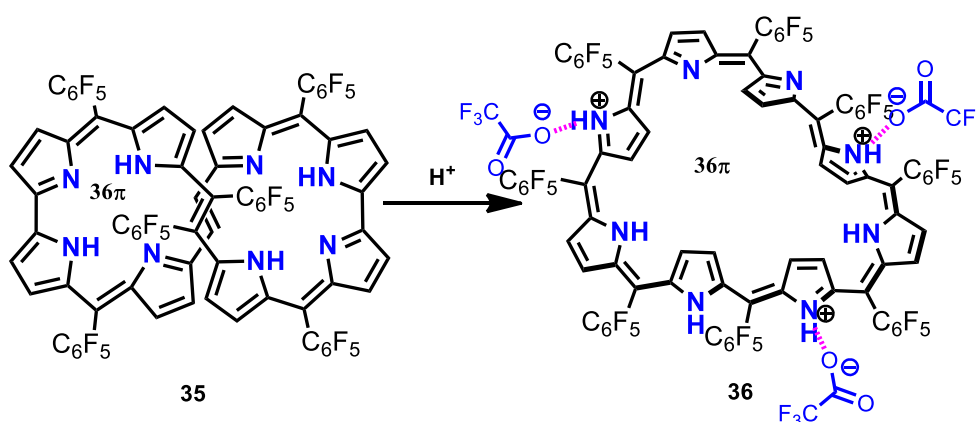


Scheme 1.5: 24π , 25π , and 26π redox active pentathiaphyrins.

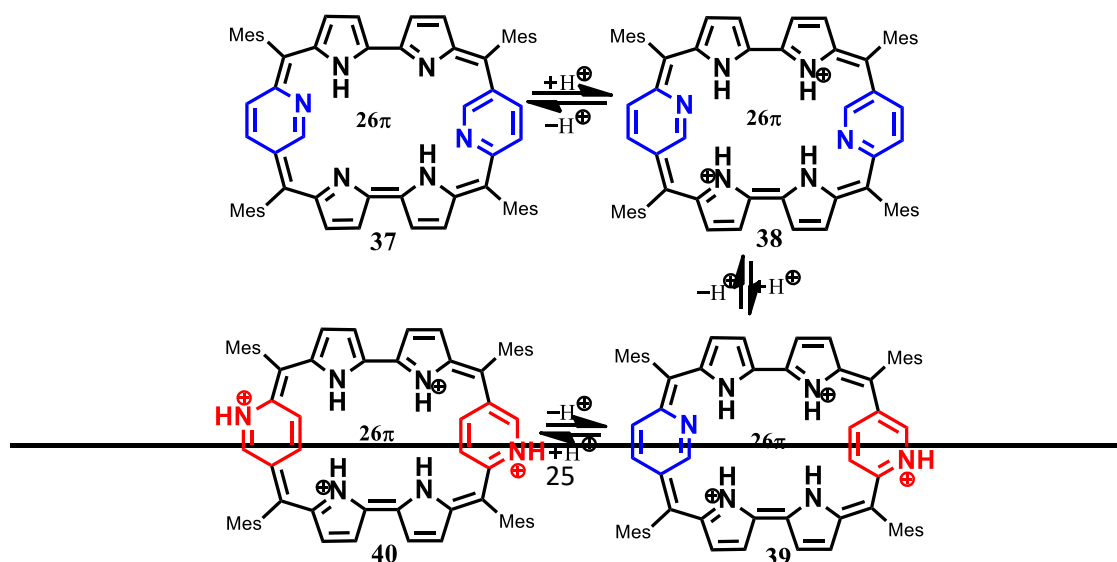
1.4.2 Protonation and Deprotonation

Protonation triggered aromaticity is well defined where the confirmation of the molecule change by changing the molecular topology. In 2010 Osuka and coworkers synthesized a diprotonated [36]Octaphyrin **36**⁵⁹ where protonation-triggered

conformational changes in conversion of its molecular topology figure-eight in its freebase to Möbius aromatic upon Protonation shown in Scheme 1.6. This was proved through $^1\text{H-NMR}$ studies in which the protonated molecules gave several signals in the range of -1.0 to -2.0 ppm and -3.0 to -5.0 ppm respectively, because of the inner protons showing their aromaticity. Spectrophotometric titration processes of **35** with MSA, the spectral changes show two-step processes. Titration in the range of MSA of concentration of 0×10^{-4} - 2.72×10^{-4} M, a drastic change was seen having the two isobestic points at 426 and 667 nm. The broadband at 637 nm was found to have bathochromic shift to 731 nm with increase in intensity while small and broad bands were seen at 1020, 1075, 1185, and 1254 nm. These characteristics are seen to that of typical aromatic systems with intense Soret-like and distinct Q-like bands. Single crystal X-ray structures also reflect Möbius aromaticity of the protonated form.



Scheme 1.6: Protonation triggered Hückel-Möbius switchover



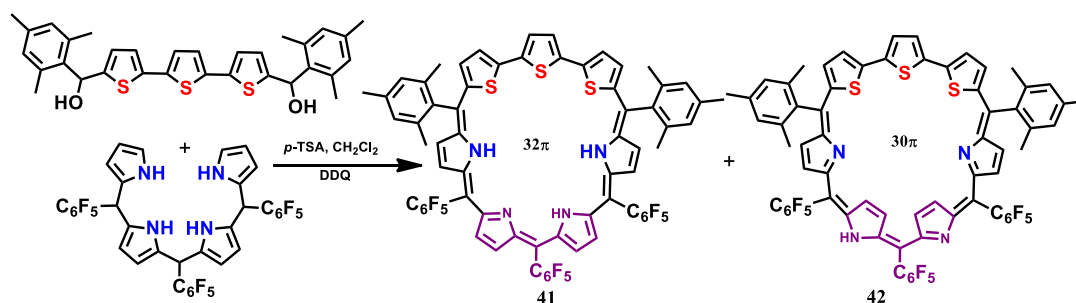
Scheme 1.7: Expanded porphyrin with various structural diversity

Recently, Latos-Grażyński and co-workers have synthesized the α , β' -pyridine inserted rubyrin macrocycle **37**⁸⁵ and its protonation process was observed by titration with tetrafluoroboric acid diethyl ether complex. Eventually, formed dicationic, tricationic and tetracationic forms. The singly N-inverted tricationic by inversion of one protonated pyridine ring and tetracationic form was formed by inversion of both the protonated pyridine rings. Three fundamental conformers were synthesized regular **38**, singly N-confused **39** and doubly N-confused conforms **40** shown in Scheme 1.7.

1.4.3 Isomerization

Chandrashekar and co-workers synthesized oxidized and reduced heptaphyrins **41** and **42** in a one pot and are two examples of isomer where both show different aromatic behaviour shown in Scheme 1.8.⁸⁶ The UV-Vis spectrum of **41** and **42** shows nonaromatic and aromatic molecules respectively. Proton NMR spectrum of **41** show deshielding in (5-8.75 ppm) region and 11.71, 8.50, and 6.01 ppm were assigned to three pyrrolic -NH protons. All other β -CHs resonate as seven doublets in the range of 5.6-7.6 ppm, hence **41** was a 32π nonaromatic molecule. Proton NMR of **42** in shows aromatic nature. Doublets in the range of 8.49-9.50 ppm were seen for six different β -CHs. The β -CH signal of the inverted pyrrole ring comes under ring current area and is in shielded range of 2.44-3.85 ppm. A broadened singlet at 9.37 ppm appeared for

the NH proton of inverted Pyrrole. These data shows that **42** is 30π Aromatic molecule.



Scheme 1.8: Synthesis of Heptaphyrin isomers.

1.5 Scope and objectives of the present thesis

In a concise way, this thesis is focused to address the questions on Hückel-Möbius aromaticity/antiaromaticity using expanded porphyrins as models. Many reports in the literature suggest that an external trigger such as solvent polarity, temperature variation or metal coordination are required to attain the Möbius aromatic and antiaromatic topologies. In this thesis I have self questioned that; (a) Can a molecule which exhibit Möbius aromaticity be synthesized in freebase without any external trigger. (b) Is it possible to transform a nonaromatic topology to a Hückel aromatic topology by an external trigger. (c) Is it possible to transform a nonaromatic molecule to a Möbius aromatic topology by an external trigger. Some of these questions have been well addressed in this thesis. We were successful in designing synthetic strategy to synthesize a twisted S-shaped 30π hexaphyrin which exhibit nonaromatic features in freebase form. This $(4n+2)\pi$ nonaromatic hexaphyrin changes over to $(4n+2)\pi$ Hückel aromatic planar topology upon protonation. The authors have also shown that

it is possible to transform a 28π nonaromatic to a Möbius aromatic topology triggered by addition of proton. Structural evidence has been provided for all these hexaphyrins in the freebase as well as protonated forms.

The second aspect addressed in this thesis is on the structural isomerization of expanded porphyrins. A normal 18π porphyrin exhibit rich structural diversity and over the years several structural isomers of porphyrins such as N-confused porphyrins, porphycene, etc have been reported Figure 1.7, such structural isomers in expanded porphyrins are not common.

In this thesis, I have examined the structural isomers exhibited by modified Octaphyrins. In modified Octaphyrins, we have characterized two types of isomers. The isomer A, where the middle thiophene ring is inverted while in the other isomer B, the terminal thiophene ring of the terthiophene moiety is inverted. These structural isomers were not separable and spectroscopic and structural studies indicate the presence of both the isomers in solution as well as solid state. We have also shown that it is possible one to other by protonation of pyrrole nitrogens. Change of hetero atom in the heterocyclic rings from S to Se, stabilizes a particular isomer in comparison of other isomers. Energy optimized structures and calculation of energies of these isomers reveal only small differences in energies and any external perturbation can tilt one with respect to other.

The third aspect addressed in this thesis is the synthesis of higher order expanded porphyrins. Specially, synthesis of two decaphyrins; a ten pyrrole containing macrocycle. The 48π decaphyrin is flexible and exhibit figure-eight conformation in solid state with loss of aromaticity. The 48π decaphyrin changes over to an open planar confirmation on protonation and spectral studies indicating it has antiaromatic

features. We have also prepared a rigid 42π decaphyrin. The synthetic methodology used here is rare and successfully synthesized 42π decaphyrin in 30% yield without acid catalyst. This 42π decaphyrin remains nonaromatic in freebase as well as in protonated form. In conclusion, in this thesis we have synthesized homoporphyrins, hexaphyrins, heptaphyrins, octaphyrins and decaphyrins and examined their 1) aromatic/nonaromatic properties and their interconversion, 2) characterized nonidentical structural isomers and 3) designed and developed synthetic methods to synthesize decaphyrins and their properties have been studied.

1.6 References

1. A. R. Battersby, C. J. Fookes, G. W. Matcham, E. McDonald, *Nature* **1980**, 285, 17-21.
2. J. M. Vanderkooi, M. Erecinska, *Eur. J. Biochem.* **1975**, 60, 199-207.
3. J. L. R. Anderson, C. T. Armstrong, G. Kodali, B. R. Lichtenstein, D. W. Watkins, J. A. Mancini, A. L. Boyle, T. A. Farid, M. P. Crump, C. C. Moser, P. L. Dutton, *Chem. Sci.* **2014**, 5, 507-514.
4. L. A. Lewis, M. -H. Sung, M. Gipson, K. Hartman, D. W. Dyer, *J. Bacterio.* **1998**, 22, 6043-6047.
5. F. Basolo, B. M. Hoffman, J. A. Ibers, *Syn. Oxy. Carr.* **1975**, 8, 384-392.
6. A. Osuka, K. Maruyama, *Chem. Lett.* **1987**, 16, 825-828.
7. A. Kaplan, E. Korin, A. Bettelheim, *Eur. J. Inorg. Chem.* **2014**, 2288-2295.
8. M. Heidari-Golafzani, M. Rabbani, R. Rahimi, A. Azad, *RSC Adv.* **2015**, 5, 99640-99645.
9. S. M. Adam, I. Garcia-Bosch, A. W. Schaefer, S. K. Sharma, M. A. Siegler, E. I. Solomon, K. D. Karlin, *J. Am. Chem. Soc.* **2017**, 139, 472-481.

-
10. J. Tian, L. Ding, H. -J. Xu, Z. Shen, H. Ju, L. Jia, L. Bao, J. -S. Yu, *J. Am. Chem. Soc.* **2013**, *135*, 18850-18858.
 11. T. Wang, D. Zhu, G. Liu, W. Tao, W. Cao, L. Zhang, L. Wang, H. Chen, L. Mei, L. Huang, X. Zeng, *RSC Adv.* **2015**, *5*, 50617-50627.
 12. A. Johnson, A. Todd, *Vitamins & Hormone.* **1957**, *15*, 1-30.
 13. A. Johnson, R. Price, *J. Chem. Soc.* **1960**, 1649-1653.
 14. Z. Gross, N. Galili, I. Saltsman, *Angew. Chem. Int. Ed.* **1999**, *38*, 1427-1429.
 15. S. Saito, A. Osuka, *Angew. Chem. Int. Ed.* **2011**, *50*, 4342-4373.
 16. M. Stępień, N. Sprutta, L. Latos-Grażyński, *Angew. Chem. Int. Ed.* **2011**, *50*, 4288-4340.
 17. D. C. Hodgkin, J. Kamper, J. Lindsey, M. MacKay, J. Pickworth, J. Robertson, C. B. Shoemaker, J. White, R. Prosen, K. Trueblood, In *The Structure of Vitamin B12. An Outline of the Crystallographic Investigation of Vitamin B12*, Proceedings of the Royal Society of London A: Mathematical, Physical and Engineering Sciences, The Royal Society: **1957**, 228-263.
 18. A. Johnson, A. Todd, *Vitamins & Hormones.* **1957**, *15*, 1-30.
 19. A. Johnson, R. J. Price, *Chem. Soc.* **1960**, 1649-1653.
 20. A. Johnson, I. J. Kay, *Chem. Soc.* **1965**, 1620-1629.
 21. Y. Inokuma, J. H. Kwon, T. K. Ahn, M. C. Yoo, D. Kim, A. Osuka, *Angew. Chem. Int. Ed.* **2006**, *45*, 961-964.
 22. B. Adinaryana, D. Shimizu, A. Osuka *Chem. Eur. J.* **2019**, *25*, 1706–1710.
 23. J. L. Sessler, D. Seidel, *Angew. Chem. Int. Ed.* **2003**, *42*, 5134-5175.
 24. A. Jasat, D. Dolphin, *Chem. Rev.* **1997**, *97*, 2267 -2334.
-

-
25. V. J. Bauer, D. L. J. Clive, D. Dolphin, J. B. Paine, F. L. Harris, M. M. King, J. Loder, S. W. C. Wang, R. B. Woodward, *J. Am. Chem. Soc.* **1983**, *105*, 6429-6436.
26. H. Rexhausen, A. Gossauer, *J. Chem. Soc., Chem. Commun.* **1983**, 275.
27. S. Gokulnath, T. K. Chandrashekar, *Org. Lett.* **2008**, *10*, 637-640.
28. M. G. P. M. S. Neves, R. M. Martins, A. C. Tome, A. J. D. Silvestre, A. M. S. Silva, V. Felix, J. A. S. Cavaleiro, M. G. B. Drew, *Chem. Commun.* **1999**, 385-386.
29. J. L. Sessler, D. Seidel, A. E. Vivian, V. Lynch, B. L. Scott, D. W. Keogh, *Angew. Chem. Int. Ed.* **2001**, *40*, 591-594.
30. S. Saito, A. Osuka, *Chem. Eur. J.* **2006**, *12*, 9095-9102.
31. V. G. Anand, S. K. Pushpan, S. Venkatraman, S. J. Narayanan, A. Dey, T. K. Chandrashekar, R. Roy, B. S. Joshi, S. Deepa, G. N. Sastry, *J. Org. Chem.* **2002**, *67*, 6309-6319.
32. M. Bröring, J. Jendry, L. Zander, H. Schmickler, J. Lex, Y.-D. Wu, M. Nendel, J. Chen, D. A. Plattner, K. N. Houk, E. Vogel, *Angew. Chem. Int. Ed. Engl.* **1995**, *34*, 2515-2517.
33. N. Sprutta, L. Latos-Grażyński, *Chem. Eur. J.* **2001**, *7*, 5099-5112.
34. S. Shimizu, R. Taniguchi, A. Osuka, *Angew. Chem. Int. Ed.* **2005**, *44*, 2225-2229.
35. J. L. Sessler, S. J. Weghorn, V. Lynch, M. R. Johnson, *Angew. Chem., Int. Ed. Engl.* **1994**, *33*, 1509-1512.
36. T. Soya, W. Kim, D. Kim, A. Osuka, *Chem. Eur. J.* **2015**, *21*, 8341-8346.
37. A) R. Misra, T. K. Chandrashekar, *Acc. Chem. Res.* **2003**, *36*, 676 – 691.
-

-
38. G. Karthik, A. Srinivasan, T. K. Chandrashekar, *Org. Lett.* **2014**, *16*, 3472-3475.
39. M. J. Broadhurst, R. Grigg, A. W. Johnson, *J. Chem. Soc., Perkin Trans. 1.* **1972**, 2111–2116.
40. S. J. Narayanan, B. Sridevi, T. K. Chandrashekar, U. Englich, K. Ruhlandt-Senge, *Org. Lett.* **1999**, *1*, 587-590.
41. J. -i. Setsune, M. Toda, T. Yoshida, K. Imamura, K. Watanabe, *Chem. Eur. J.* **2015**, *21*, 12715-12727.
42. S. Fukuzumi, K. Ohkubo, M. Ishida, C. Preihs, B. Chen, W. T. Borden, D. Kim, J. L. Sessler, *J. Am. Chem. Soc.* **2015**, *137*, 9780-9783.
43. Z. Zhou, Y. Chang, S. Shimizu, J. Mack, C. Schütt, R. Herges, Z. Shen, N. Kobayashi, *Angew. Chem. Int. Ed.* **2014**, *53*, 6563-6567.
44. M. Shionoya, H. Furuta, V. Lynch, A. Harriman, J. L. Sessler, *J. Am. Chem. Soc.* **1992**, *114*, 5714-5722.
45. V. Král, H. Furuta, K. Shreder, V. Lynch, J. L. Sessler, *J. Am. Chem. Soc.* **1996**, *118*, 1595-1607.
46. J. L. Sessler, S. Camiolo, P. A. Gale, *Coordin. Chem. Rev.* **2003**, *240*, 17-55.
47. J. L. Sessler, T. Morishima, V. Lynch, *Angew. Chem. Int. Ed. Engl.* **1991**, *30*, 977-980.
48. J. L. Sessler, D. Seidel, V. Lynch, *J. Am. Chem. Soc.* **1999**, *121*, 11257-11258.
49. D. Seidel, V. Lynch, J. L. Sessler, *Angew. Chem. Int. Ed.* **2002**, *41*, 1422-1425.
50. V. G. Anand, S. Venkatraman, H. Rath, T. K. Chandrashekar, W. Teng, K. Ruhlandt-Senge, *Chem. Eur. J.* **2003**, *9*, 2282-2290.
51. E. Heilbronner, *Tetrahedron Lett.* **1964**, *29*, 1923-1928.
-

-
52. D. Ajami, O. Oeckler, A. Simon, R. Herges, *Nature*. **2003**, 426, 819-821.
53. M. Mauksch, S. B. Tsogoeva, *Chem. Eur. J.* **2010**, 16, 7843-7851.
54. C. Castro, W. L. Karney, *J. Phys. Org. Chem.* **2012**, 25, 612-619.
55. M. Stępień, L. Latos-Grażyński, N. Sprutta, P. Chwalisz, L. Szterenber, *Angew. Chem. Int. Ed.* **2007**, 46, 7869-7873.
56. J. K. Park, Z. S. Yoon, M. -C. Yoon, K. S. Kim, S. Mori, J. -Y. Shin, A. Osuka, D. Kim, *J. Am. Chem. Soc.* **2008**, 130, 1824-1825.
57. S. Tokuji, J. -Y. Shin, K. S. Kim, J. M. Lim, K. Youfu, S. Saito, D. Kim, A. Osuka, *J. Am. Chem. Soc.* **2009**, 131, 7240-7241.
58. S. Saito, J. -Y. Shin, J. M. Lim, K. S. Kim, D. Kim, A. Osuka, *Angew. Chem. Int. Ed.* **2008**, 47, 9657-9660.
59. J. M. Lim, J. -Y. Shin, Y. Tanaka, S. Saito, A. Osuka, D. Kim, *J. Am. Chem. Soc.* **2010**, 132, 3105-3114.
60. T. Soya, H. Mori, Y. Hong, Y. H. Koo, D. Kim, A. Osuka, *Angew. Chem. Int. Ed.* **2017**, 56, 3232-3236.
61. S. J. Weghorn, V. Lynch, J. L. Sessler, *Tetrahedron Lett.* **1995**, 36, 4713-4716.
62. C. Brückner, E. D. Sternberg, R. W. Boyle, D. Dolphin, *Chem. Commun.* **1997**, 1689-1690.
63. T. D. Lash, *Chem. Asian J.* **2014**, 9, 682-705.
64. K. Berlin, C. Steinbeck, E. Breitmaier, *Synthesis*. **1996**, 1996, 336-340.
65. D. A. Colby, T. D. Lash, *Chem. Eur. J.* **2002**, 8, 5397-5402.
66. M. Pawlicki, L. Latos-Grażyński, *Chem. Rec.* **2006**, 6, 64-78.
67. H. Furuta, T. Asano, T. Ogawa, *J. Am. Chem. Soc.* **1994**, 116, 767-768.
68. P. J. Chmielewski, L. Latos-Grażyński, K. Rachlewicz, T. Glowiak, *Angew.*
-

-
- Chem., Int. Ed. Engl.* **1994**, *33*, 779-781.
69. J. F. M. Oth, E. P. Woo, F. Sondheimer, *J. Am. Chem. Soc.* **1973**, *95*, 7337.
70. P. v. R. Schleyer, C. Maeker, A. Dransfeld, H. Jiao, N. J. R. v. Eikema Hommes, *J. Am. Chem. Soc.* **1996**, *26*, 6317.
71. S. Cho, Z. S. Yoon, K. S. Kim, M. -C. Yoon, D. -G. Cho, J. L. Sessler, D. Kim, *J. Phys. Chem. Lett.* **2010**, *1*, 895-900.
72. M. Stępień, L. Latos-Grażyński, Aromaticity and Tautomerism in porphyrins and porphyrinoids, Aromaticity in heterocyclic compounds, T. M. Krygowski, M. K. Cyranski, (Eds.), Springer, **2009**.
73. R. Charriere, T. A. Jenny, H. Rexhausen, A. Gossauer, *Heterocycles.* **1993**, *36*, 1561.
74. J. L. Sessler, S. J. Weghorn, Y. Hisaeda, V. Lynch, *Chem. Eur. J.* **1995**, *1*, 56-67.
75. G. Karthik, J. M. Lim, A. Srinivasan, C. H. Suresh, D. Kim, T. K. Chandrashekar, *Chem. Eur. J.* **2013**, *19*, 17011-17020.
76. T. Higashino, M. Inoue, A. Osuka, *J. Org. Chem.* **2010**, *75*, 7958.
77. A. Ghosh, A. Chaudhary, A. Srinivasan, C. H. Suresh, T. K. Chandrashekar, *Chem. Eur. J.* **2016**, *22*, 3942-3946.
78. E. Pacholska-Dudziak, J. Skonieczny, M. Pawlicki, L. Szterenber, Z. Ciunik, L. Latos-Grażyński, *J. Am. Chem. Soc.* **2008**, *130*, 6182 – 6195.
79. T. Higashino, J. M. Lim, T. Miura, S. Saito, J. -Y. Shin, D. Kim, A. Osuka, *Angew. Chem. Int. Ed.* **2010**, *49*, 4950-4954.
80. T. Higashino, B. S. Lee, J. M. Lim, D. Kim, A. Osuka, *Angew. Chem. Int. Ed.* **2012**, *51*, 13105-13108.
81. N. C. Baird, *J. Am. Chem. Soc.* **1972**, *94*, 4941-4948.
-

82. Y. M. Sung, M. -C. Yoon, J. M. Lim, H. Rath, K. Naoda, A. Osuka, D. Kim, *Nat. Chem.* **2015**, *7*, 418-422.
83. W. -Y. Cha, T. Kim, A. Ghosh, Z. Zhang, X. -S. Ke, R. Ali, V. M. Lynch, J. Jung, W. Kim, S. Lee, S. Fukuzumi, J. S. Park, J. L. Sessler, T. K. Chandrashekar, D. Kim, Bicyclic Baird-Type Aromaticity. *Nat. Chem.* **2017**, *9*, 1243–1248.
84. T. Y. Gopalakrishna, S. Reddy, V. G. Anand, *Angew. Chem. Int. Ed.* **2014**, *53*, 10984 –10987.
85. R. Myśliborski, K. Hurej, M. Pawlicki, L. Latos-Grażyński, *Angew. Chem. Int. Ed.* **2018**, *7*, 16866– 16870.
86. S. Gokulnath, V. Prabhuraja, T. K. Chandrashekar, *Org. Lett.* **2007**, *9*, 3355-3357.

CHAPTER 2

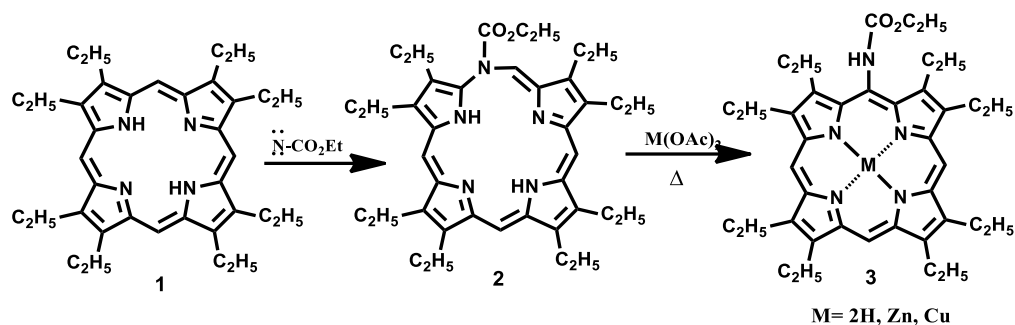
Core-Modified Homoporphyrin and its Phenyl bridged derivatives

2.1	Introduction	38
2.2	Objective	40
2.3	Results and discussions	40
2.3.1	Syntheses	40
2.3.2	Spectral characterization	41
2.3.2.1	Mass spectrometric analysis	41
2.3.2.2	NMR Analysis	43
2.3.2.3	Single crystal X-ray structure and analysis	46
2.3.2.4	Electronic spectral analysis	52
2.4	Conclusion	53
2.5	Experimental Procedure	53
2.5.1	synthesis of 16	53
2.5.2	synthesis of 17	54
2.5.3	precursor Syntheses	55
2.5.3.1	synthesis of 20	56
2.5.3.2	synthesis of 19	57
2.5.3.3	synthesis of 13	57
2.5.3.4	synthesis of 15	57
2.6	References	58

2.1 Introduction

Expanded porphyrins are porphyrin analogues, which have more than 18π electrons in their conjugative pathway tending to either an increased in the number of heterocyclic rings or *meso* carbon bridges. According to Sessler, this is the minimum number of atoms required for the fulfilment of expanded category, hence homoporphyrins are designated as the simplest expanded porphyrin.¹ Expanded porphyrins are extensively studied due to their potential applications in various fields, such as; i) cationic and anionic receptors; ii) MRI contrasting agents; iii) (NLO) non-linear optical materials and iv) photodynamic therapeutic agents (PDT).²⁻⁵ 22π sapphyrins by Woodward and co-workers in 1966⁶ was the first expanded porphyrin synthesized and due to its applications received much attention. However, homoporphyrins being the smallest expanded 20π porphyrin remain unleashed for a long time due to their synthetic difficulties as well as stability factors. In porphyrins, four pyrrole rings are connected with four *meso* carbons in (1.1.1.1) fashion. In homoporphyrin, four pyrrole rings are linked with five *meso* carbon in (2.1.1.1) fashion.⁷ Due to this special structural arrangement; it captivates 17 atoms in the macrocyclic core.

The first N-*meso*-azahomoporphyrin **2** was reported by Grigg *et al.* in 1967.⁸ The compound **2** was synthesized by reaction of freebase β -ethyl substituted **1** with nitrene and exhibited the non-aromatic character (Scheme 2.1).⁹ The compound **2** was unstable and decomposed to corresponding metallated porphyrin derivatives **3**, when the reaction was performed with Zn and Cu salts.



Scheme 2.1: Synthesis of azahomoporphyrin **2** and its decomposition to corresponding metallated porphyrin derivatives.

The first stable core modified homoporphyrins were reported by Ravikanth and co-workers. The corresponding homoporphyrins, [20]dithiahomoporphyrin(2.1.1.1) **9** and [20]dioxahomoporphyrin(2.1.1.1) **10** were synthesized by [2+2] acid-catalyzed condensation of *meso*-aryldipyrromethanes with dithia or dioxo-ethenediol derivatives by *p*-TSA catalyzed condensation followed by oxidation with DDQ (Figure 2.1). The structural analyzes of **9** and **10** showed significant distortion, thus revealed nonaromatic characteristics.¹⁰⁻¹¹

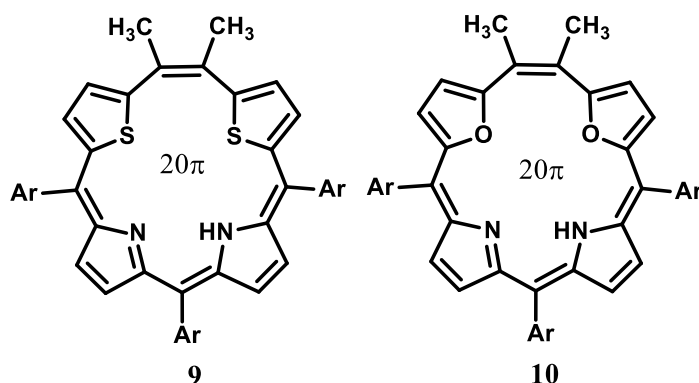


Figure 2.1: The first stable core-modified homoporphyrins.

Recently, terphenyl based homocarbaporphyrinoids **11** are reported by Srinivasan and coworkers (Figure 2.2).¹² Carba analogue of homoporphyrin was also found to be nonaromatic in nature. In 2017, Srinivasan and coworkers

again formed all aza analogue homoporphyrin **12** which is Möbius aromatic in nature.

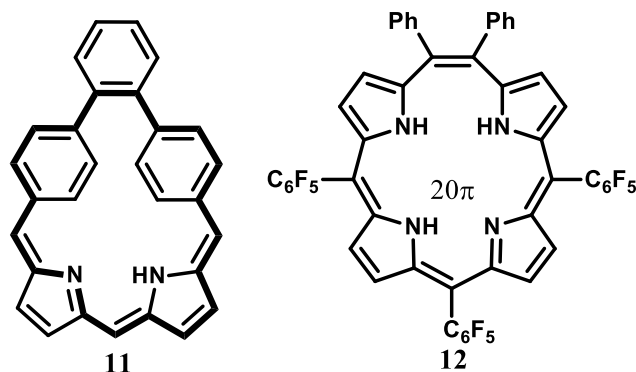


Figure 2.2: Structure of nonaromatic carba-homoporphyrins and Möbius aromatic homoporphyrin.

2.2 Objective

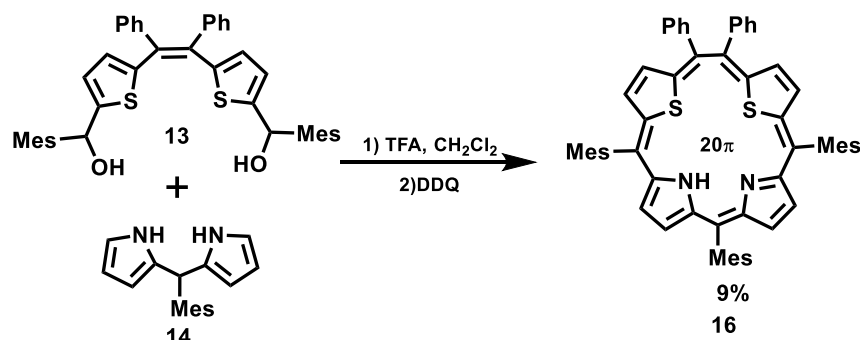
In continuation to our efforts towards understanding aromatic/nonaromatic properties of core-modified homoporphyrinoid and its topology change on bridging it with a phenyl ring constructing its phenyl bridged dimer. In this chapter the author wish to report syntheses and characterization of core-modified 20π homoporphyrin and its phenylene bridged derivative Though the stable core-modified homoporphyrinoid are known till date, its extensive study and its extended phenylene bridged dimer analogue is hitherto unknown in the literature.

2.3 Results and discussions

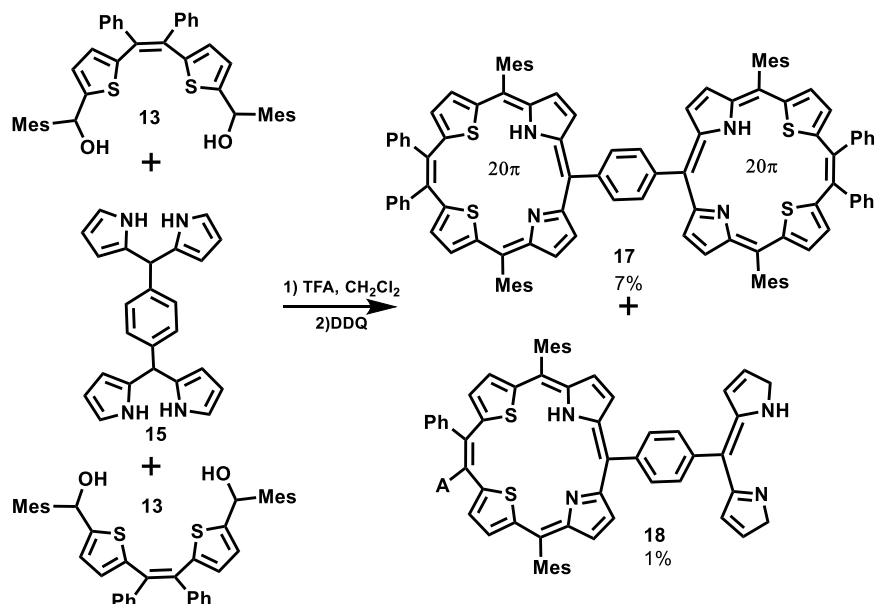
2.3.1 Syntheses

In this chapter, the simplest core-modified homoporphyrin **16** and its extended *p*-phenylene bridged dimer **17** have been synthesized and their structure and properties have been described. The trifluoroacetic acid (TFA) catalysed condensation of (5,5'-(1,2-diphenylethene-1,2-diyl)bis(thiophene-5,2-diyl))bis(mesitylmethanol) **13** with 2,2'-(mesitylmethylene)bis(1H-pyrrole) **14**

in CH_2Cl_2 and follows oxidation with 2,3-dichloro-5,6-dicyano-1,4-benzoquinone (DDQ) producing homoporphyrin **16** with 9% yield (Scheme 2.2). The TFA acid catalysed condensation of **13** with 1,4-bis(di(1H-pyrrol-2-yl)methyl)benzene **15** in dry CH_2Cl_2 with DDQ gave **17** and 1% yield of **18** (Scheme 2.3)



Scheme 2.2: Synthesis of core-modified homoporphyrin **16**.



Scheme 2.3: Synthesis of *p*-Phenylene bridged core-modified homoporphyrin dimer **17** and half dimer **18**.

2.3.2 Spectral Characterization

2.3.2.1 Mass spectrometric analysis

The mass spectrum of homoporphyrin **16** gave molecular ion peak at m/z 865.16 confirming the exact composition of **16** (Figure 2.3). The molecular ion peak of

homoporphyrin *p*-phenylene bridged dimer **17** was found to be m/z 1568.10 (Figure 2.4) and the molecular ion peak of the product **18** was found to be m/z 965.2598.

From the mass spectrometric analysis confirms exact composition of the macrocycle shown in Figure 2.5 was confirmed.

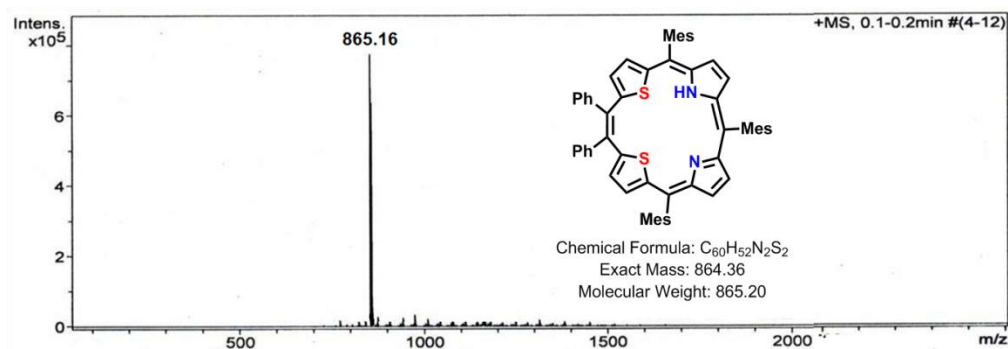


Figure 2.3: ESI-MS spectrum of **16**.

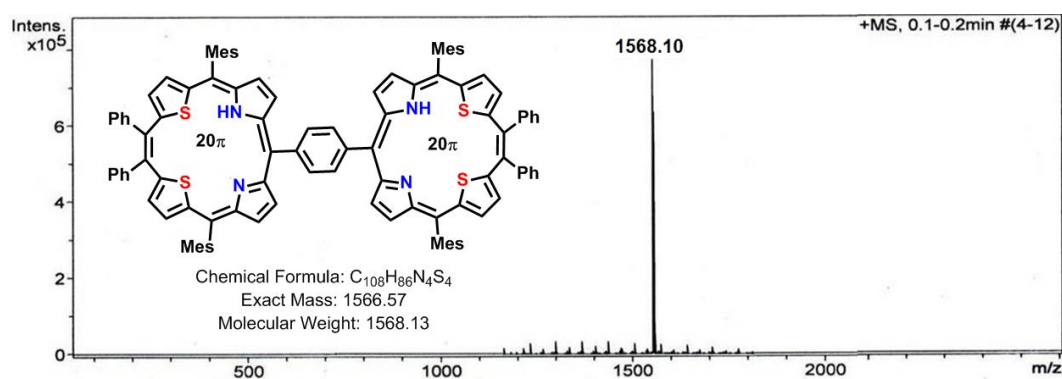


Figure 2.4: ESI-MS spectrum of **17**.

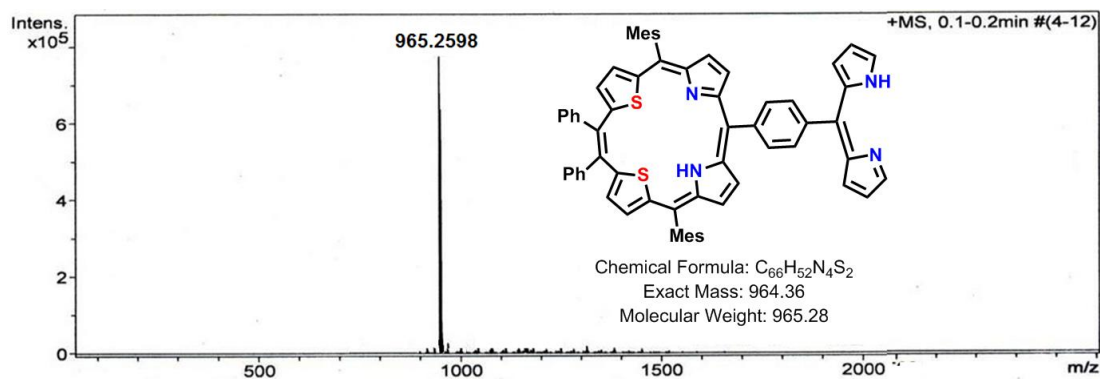


Figure 2.5: ESI-MS spectrum of **18**.

2.3.2.2 NMR Analysis

The ^1H NMR spectral analyses of **16** in CD_2Cl_2 at room temperature are shown in Figure 2.6. The compound **16** with C_2 symmetry exhibits the signals exactly for half of the molecule (Figure 2.6a). All the β -CH (*a*, *b*, *c*, *d*) protons resonated between 5.7-7.0 ppm. The thiophene protons (*c*, *d*) are in local aromatic region but NH signal in freebase states resonated at 11.8 ppm, owing to $4n\pi$ nonaromatic behavior. All the *meso* aryl phenyl and mesityl CH protons resonated at nonaromatic region. Titration of TFA also the ^1H NMR spectra of **16** in CD_2Cl_2 at room temperature (Figure 2.7) and shows C_2 symmetry where all the β -CH (*a*, *b*, *c*, *d*) protons are little deshielded and resonate between 6.2-7.3 ppm pertaining its $4n\pi$ nonaromatic behavior (Figure 2.6b). The NH signal in the protonated states resonated at 9.7 ppm confirming its nonaromatic character in protonated state.

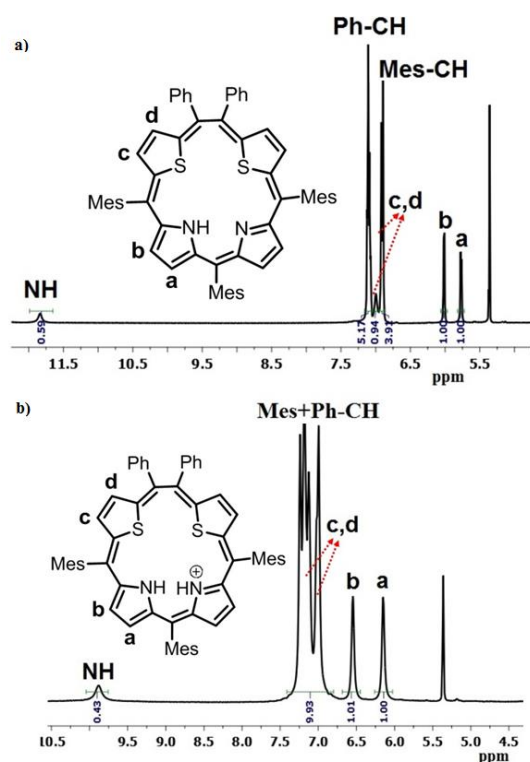


Figure 2.6: ^1H -NMR spectra of a) **16** b) **16.2H⁺** in CD_2Cl_2 .

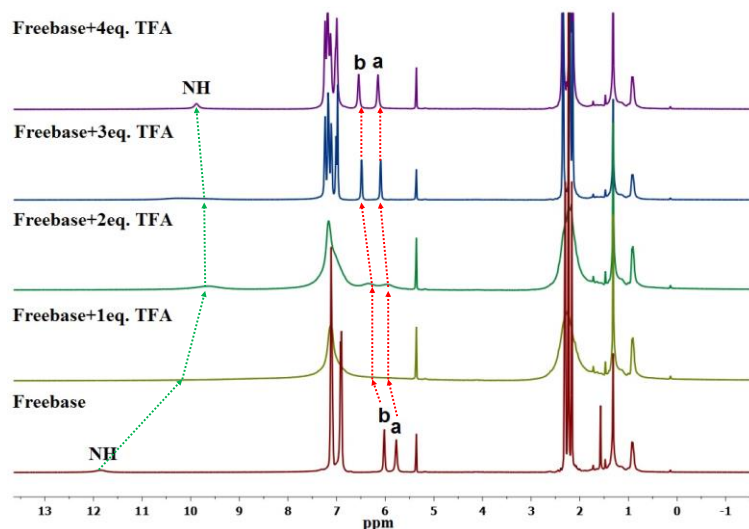


Figure 2.7: ^1H -NMR spectra of titration of **16** with various equiv. of TFA.

The ^1H NMR spectra analyses of **17** in CD_2Cl_2 at room temperature are shown in Figure 2.8 has a similar pattern to that of **16**. In compound **17** both the homoporphyrin rings besides the phenyl bridge exhibits C_2 symmetry; the signals exactly for half of the molecule and all the assignments are made by ^1H - ^1H COSY spectra (Figure 2.9). The NH signal in the freebase states resonated at 11.8 ppm and all the β -CH (*a*, *b*, *c*, *d*, *e*) protons resonated between 6.0-7.3 ppm owing to $4n\pi$ nonaromatic behavior. All the *meso* aryl phenyl and mesityl CH protons resonated at nonaromatic region. Upon protonation also the ^1H NMR spectra of **17** in CD_2Cl_2 at room temperature Figure 2.8b shows C_2 symmetry where all the β -CH (*a*, *b*, *c*, *d*, *e*) protons are little deshielded and resonate between 6.5-7.5 ppm pertaining its $4n\pi$ nonaromatic behavior. The NH signal in the protonated states resonated at 9.13 ppm confirming its nonaromatic character in protonated state.

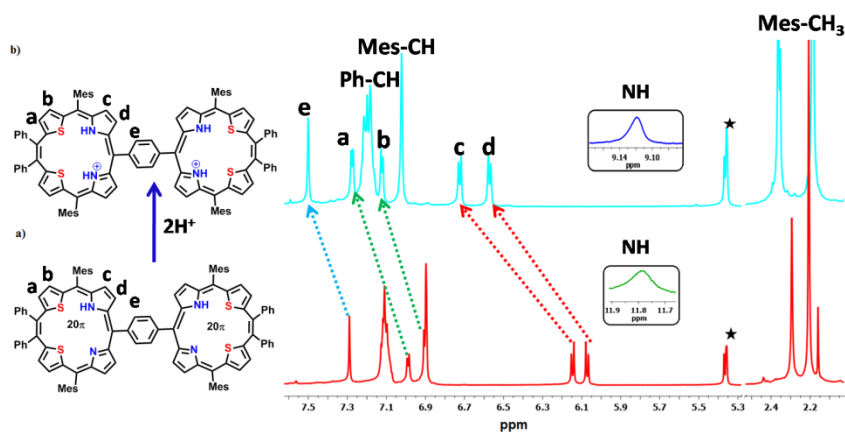


Figure 2.8: ^1H -NMR spectra of a) **17** b) 17.2H^+ in CD_2Cl_2 .

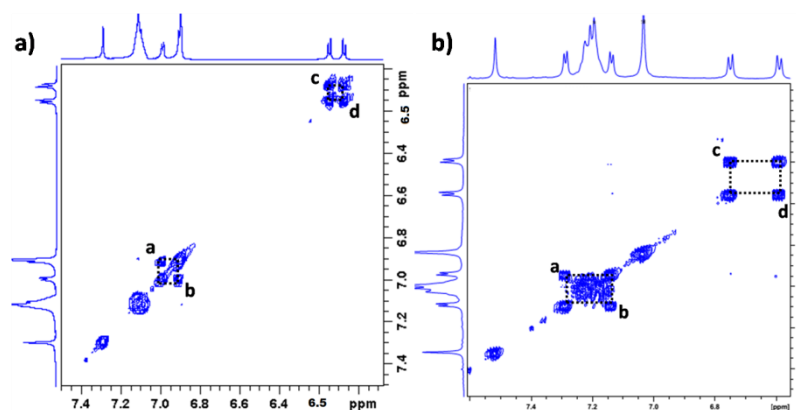


Figure 2.9: ^1H - ^1H COSY correlation spectroscopy of a) **17** and b) 17.2H^+ in CD_2Cl_2 .

The ^1H NMR spectral analyses of the side product **18** in CD_2Cl_2 at room temperature are shown in Figure 2.10. The compound **18** exhibits all the β -CH (*a, b, c, d, g, h, i*) protons signals between 6-7.8 ppm. The NH signal in freebase states resonated at 11.8 ppm. All the *meso* aryl phenyl and mesityl CH protons resonated at nonaromatic region.

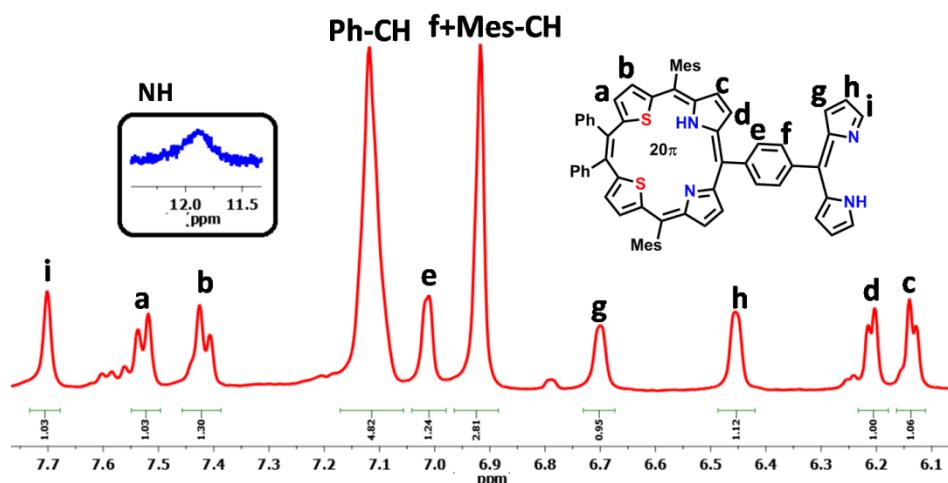


Figure 2.10: ^1H -NMR spectrum of **18** in CD_2Cl_2 .

2.3.2.3 Single crystal X-ray structure

The molecular form of **16** was confirmed by X-ray structural analyses and shown in Figure 2.11. The crystal data are in Table 2.1. All the crystals were grown in CH_2Cl_2 over CH_3CN by diffusion method. The bond lengths in **16** are shown in Figure 2.12. The anticipated nonaromatic character of **16** from ^1H NMR spectral analysis is further reflected from the crystal analyses. The compound crystallizes in monoclinic crystal lattice with $I2/a$ space group. The observation in ^1H NMR spectra, that the molecule attains almost planar conformation in which all thiophene rings and pyrrole units are in plane except the S1 thiophene unit which is 85.63° deviated from the mean macrocyclic plane containing *meso* carbon atoms (C2, C3, C8, C13, C18) is shown also by X-ray data.

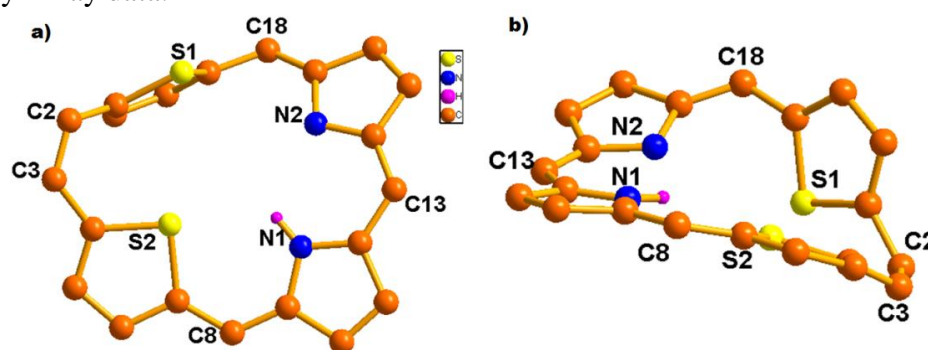


Figure 2.11: Structure of **16** a) front view b) side view. The hydrogen and *meso* substituents are omitted for clarity.

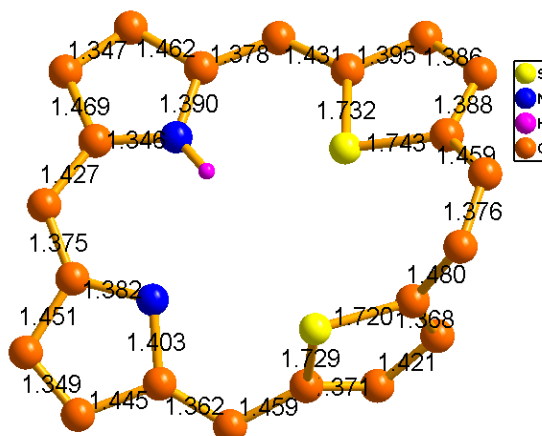


Figure 2.12: Bond lengths in **16**.

The molecular structures of **16.H⁺** was unambiguously confirmed by single crystal X-ray analyses and shown in Figure 2.13. The crystal data are in Table 2.1. All the crystals were grown in CH₂Cl₂ and toluene mixture. The compound crystallized in monoclinic crystal lattice with $P2_1/n$ space group.¹³ The imine nitrogens are protonated and are in intermolecular hydrogen bonding with one perchlorate anion and located above the mean macrocyclic plane. The bond distance and angle of N1-H1...O1 and N2-H2...O1 are 2.11 Å & 132.55° and 2.43 Å & 143.72°. The crystal structure shows both the thiophene rings S1 and S2 thiophene unit are 62.28° and 31.84° respectively deviated from the mean macrocyclic plane containing *meso* carbon atoms (C2, C3, C8, C13, C18). Overall retains the nonaromatic character.

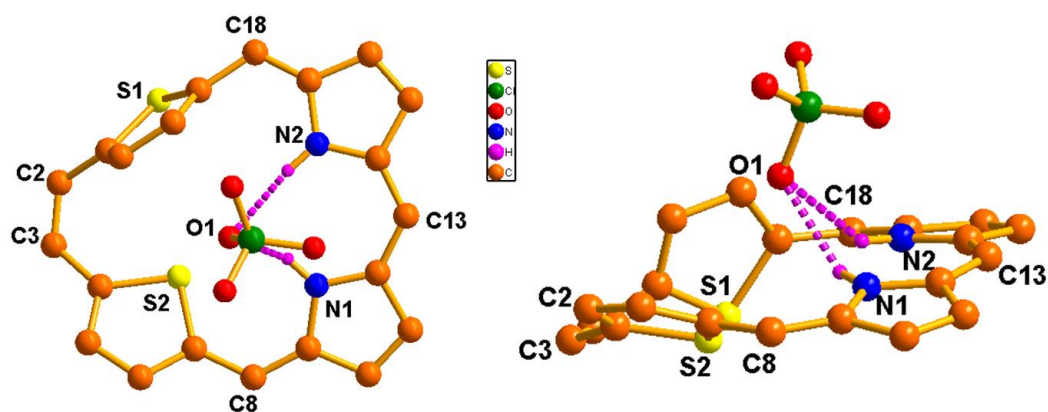


Figure 2.13: X-ray crystal structure **16.H⁺** a) front view b) side view. The hydrogen atoms and *meso*-aryl substituents are omitted for clarity.

The molecular structures of **17** was unambiguously confirmed by single crystal X-ray analyses and shown in Figure 2.14 the crystal data are in Table 2.2. All the crystals were grown in CH₂Cl₂ over CH₃CN by diffusion method. The homoporphyrin on both sides of the phenyl ring are equivalent which is seen by bond length equalization on both sides (Figure 2.16). The molecule crystallizes in triclinic lattice with *P*-1 spacial group.¹⁴ The crystal shows thiophene rings and pyrrole units are in plane except the S1 thiophene unit which is 70.33° deviated from the mean macrocyclic plane containing *meso* carbon atoms (C2, C3, C8, C13, C18). Both the hmoporphyrin rings are almost perpendicular to the mean plane of phenylene by 76.08° (Figure 2.15). The anticipated nonaromatic character of **17** from ¹H NMR spectral analysis is further reflected from the crystal analyses. The structure of the product **18** was also confirmed by single crystal X-ray analyses and shown in Figure 2.17 the crystal data are in Table 2.2. All the crystals were grown in CH₂Cl₂ over CH₃CN by diffusion method. The compound crystallized in triclinic crystal lattice with *P*-1 space group.

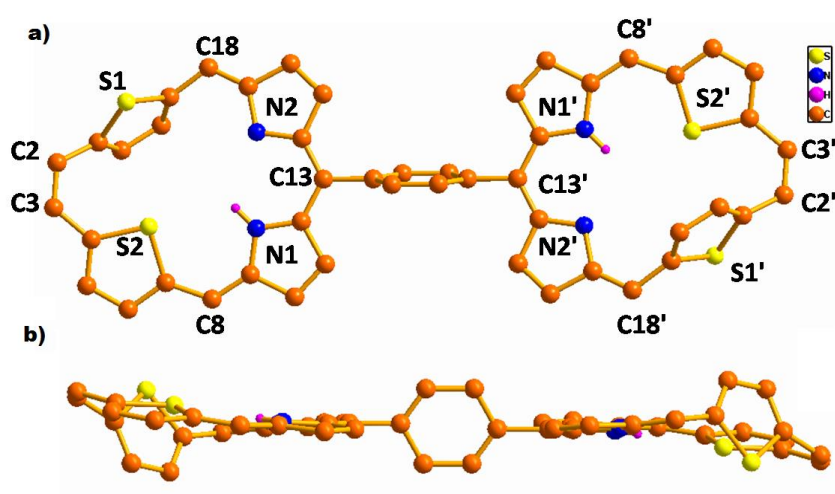


Figure 2.14: X-ray crystal structure of **17** a) front view b) side view.

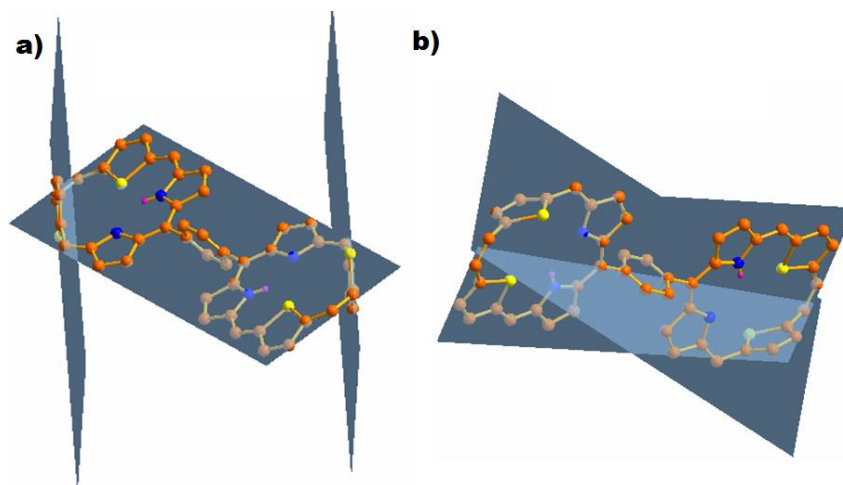


Figure 2.15: X-ray crystal structure of **17** a) deviation of S1 from mean plane b) deviation of phenyl ring from mean plane. The hydrogen atoms and *meso*-aryl substituents are omitted for clarity.

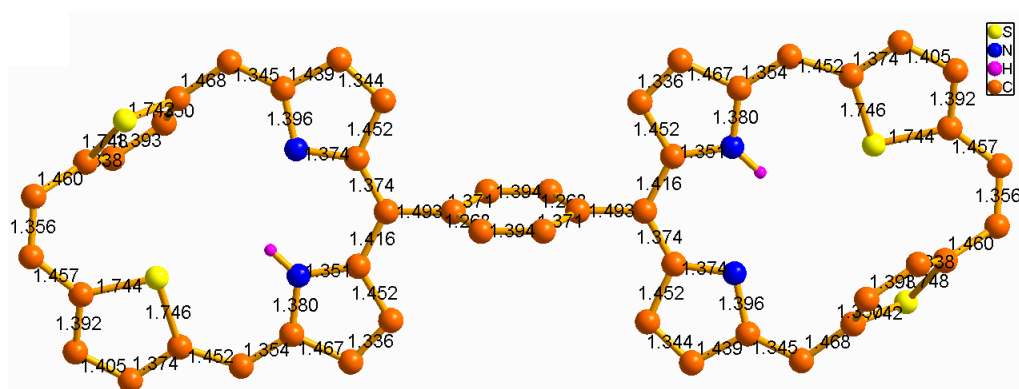


Figure 2.16: Bond lengths in **17**.

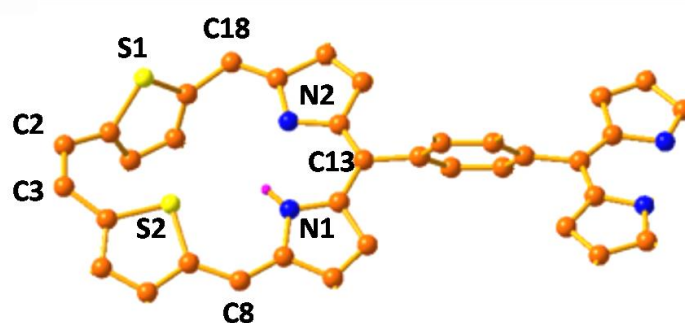


Figure 2.17: X-ray crystal structure of **18**. The hydrogen atoms and *meso*-aryl substituents are omitted for clarity.

Table 2.1: Crystal data for **16**, **16.H⁺**

Identification code	16	16.H⁺
Empirical formula	$C_{65}H_{60}N_6S_2$	$C_{67}H_{79}Cl_4N_2O_4S_2$
Formula weight	993.73	1233.97
Temperature/K	117(4)	112.7(4)
Crystal system	monoclinic	Monoclinic
Space group	$I2/a$	$P2_1/n$
$a/\text{\AA}$	32.6215(5)	14.4979(2)
$b/\text{\AA}$	14.4899(2)	25.8117(4)
$c/\text{\AA}$	24.9048(3)	17.4872(2)
α°	90	90
β°	106.617(2)	94.0940(10)
γ°	90	90
Volume/ \AA^3	11280.4(3)	6527.28(15)
Z	8	4
$\rho_{\text{calc}}/\text{cm}^3$	1.170	1.256
μ/mm^{-1}	1.251	1.592
$F(000)$	4209.0	2620.0
Crystal size/ mm^3	$0.25 \times 0.23 \times 0.19$	$0.25 \times 0.25 \times 0.21$
Radiation	CuK α ($\lambda = 1.54184$)	CuK α ($\lambda = 1.54184$)
2θ range for data collection/ $^\circ$	6.724 to 153.632	6.85 to 151.706
Index ranges	$-41 \leq h \leq 39, -18 \leq k \leq 18, -23 \leq l \leq 31$	$-18 \leq h \leq 16, -32 \leq k \leq 28, -21 \leq l \leq 21$
Reflections collected	86148	97920
Independent reflections	11746 [$R_{\text{int}} = 0.0849, R_{\text{sigma}} = 0.0309$]	13355 [$R_{\text{int}} = 0.1223, R_{\text{sigma}} = 0.0458$]
Data/restraints/parameters	11746/0/586	13355/0/695
Goodness-of-fit on F^2	1.071	1.054
Final R indexes [$I > 2\sigma(I)$]	$R_1 = 0.0653, wR_2 = 0.1655$	$R_1 = 0.0768, wR_2 = 0.2006$
Final R indexes [all data]	$R_1 = 0.0670, wR_2 = 0.1666$	$R_1 = 0.0837, wR_2 = 0.2061$
Largest diff. peak/hole / $e \text{\AA}^{-3}$	0.40/-0.58	0.84/-0.52

Table 2.2: Crystal data for 17, 18.

Identification code	17	18
Empirical formula	$C_{107}H_{58}N_4S_4$	$C_{65}H_{51}N_4S_2$
Formula weight	1403.01	965.30
Temperature/K	293(2)	239.98(10)
Crystal system	triclinic	triclinic
Space group	<i>P</i> -1	<i>P</i> -1
<i>a</i> /Å	11.1348(16)	13.2574(8)
<i>b</i> /Å	14.843(2)	13.5257(5)
<i>c</i> /Å	19.781(2)	15.7700(6)
α °	84.585(10)	83.745(3)
β °	88.894(11)	71.350(5)
γ °	69.406(14)	77.722(4)
Volume/Å ³	3046.5(7)	2615.5(2)
<i>Z</i>	1	2
$\rho_{\text{calc}}/\text{cm}^3$	0.855	1.226
μ/mm^{-1}	0.115	0.148
<i>F</i> (000)	826.0	1016.0
Crystal size/mm ³	0.25 × 0.21 × 0.20	0.25 × 0.202 × 0.108
Radiation	MoK α ($\lambda = 0.71073$)	MoK α ($\lambda = 0.71073$)
2 θ range for data collection/°	6.814 to 61.898	5.448 to 57.942
Index ranges	$-14 \leq h \leq 15, -17 \leq k \leq 20, -27 \leq l \leq 26$	$-17 \leq h \leq 17, -14 \leq k \leq 17, -21 \leq l \leq 20$
Reflections collected	37976	44627
Independent reflections	13731 [$R_{\text{int}} = 0.1773, R_{\text{sigma}} = 0.2152$]	12048 [$R_{\text{int}} = 0.0474, R_{\text{sigma}} = 0.0528$]
Data/restraints/parameters	13731/0/529	12048/0/655
Goodness-of-fit on F^2	1.043	1.116
Final <i>R</i> indexes [$I > 2\sigma(I)$]	$R_1 = 0.1334, wR_2 = 0.3258$	$R_1 = 0.0804, wR_2 = 0.2300$
Final <i>R</i> indexes [all data]	$R_1 = 0.2006, wR_2 = 0.3737$	$R_1 = 0.1122, wR_2 = 0.2449$
Largest diff. peak/hole / e Å ⁻³	1.00/-0.67	0.59/-0.78

2.3.2.4 Electronic spectral analysis

The nonaromatic property of **16** in freebase form is also seen in the absorption spectra analysis where broad band absorption at 389 nm and at 707 nm were observed in CH_2Cl_2 (Figure 2.18). Addition of proton in **16** was followed by a consecutive addition of dilute solution of TFA in CH_2Cl_2 . Absorption spectrum the band for $\mathbf{16.H^+}$ shifts to 383 nm, 479 nm, 638 nm and 796 nm but the bands still remain broad. The broadening of absorption bands upon protonated form suggest macrocycle to be nonaromatic.

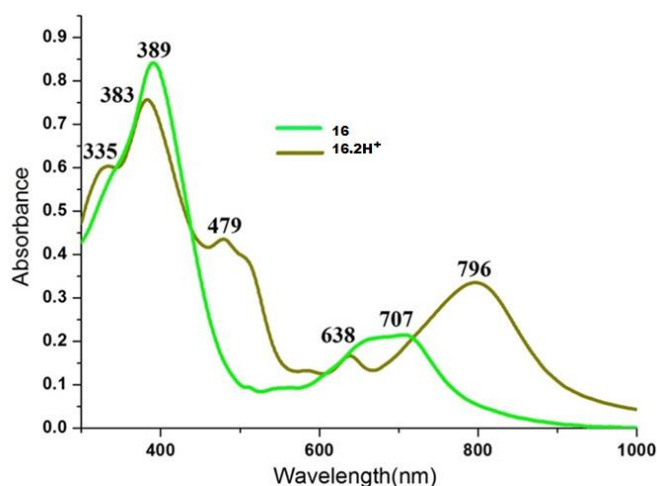


Figure 2.18: The electronic absorption spectra of **16** and $\mathbf{16.H^+}$ in CH_2Cl_2

The nonaromatic feature of **17** is also shown in the UV-Vis spectra where band absorption is similar to that of **16** and the bands are at 402 nm and at 707 nm was observed in CH_2Cl_2 (Figure 2.19). Addition of proton to **17** was also followed by a consecutive addition of solution of TFA in dichloromethane by UV-Visible spectrum the band for $\mathbf{17.2H^+}$ shifts to 393 nm, 508 nm, and 806 nm but the bands still remain broad. The broadening of absorption bands both in freebase and protonated form suggests nonaromaticity of macrocycle.

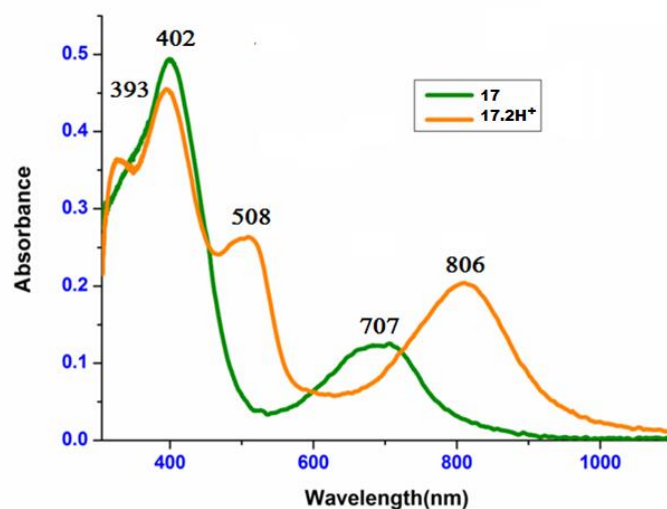


Figure 2.19: The electronic absorption spectra of **17** and **17.2H⁺** in CH₂Cl₂

2.4 Conclusion

In summary, we have successfully demonstrated the synthesis, spectral and structural characterization of core-modified homoporphyrin. The core-modified homoporphyrin was found to be nonaromatic in its freebase and its protonated state. The phenyl bridged dimer of core-modified homoporphyrin was also synthesized and its spectral and structural characterization. The spectral analyses revealed the nonaromatic characteristic owing to its $4n\pi$ conjugation in all the compounds and further confirmed by crystal analyses. Finally, further spectral properties are yet on progress by making its BODIPY complex.

2.5 Experimental Procedure

2.5.1 Synthesis of 16

A mixture of 5,5'-(1,2-diphenylethene-1,2-diyl)bis(thiophene-5,2-diyl)bis(mesitylmethanol (**13**) (200 mg, 0.31 mmol), 2,2'-(mesitylmethylene)bis(1H-pyrrole) (**14**) (82 mg, 0.31 mmol) were dissolved in 200 ml of dry dichloromethane and the resulting solution was allowed stirring for 15 mins under nitrogen atmosphere.

Trifluoroacetic acid (24 μ L, 0.31 mmol) was added and the solution was stirred under nitrogen atmosphere for one hour and further DDQ (212 mg, 0.93 mmol) was added and the mixture was stirred for another one hour in open air condition. After evaporation of solvent compound was purified by column chromatography. A green color band eluted with 20% CH₂Cl₂ considered as desire homoporphyrin (16) with 9% yield.

Compound 16:

¹H NMR (400 MHz, CD₂Cl₂, 298K): δ (in ppm) = 11.83 (br, NH), 7.10 (ddt, $J = 9.9, 6.6, 3.3$ Hz, 10H), 7.00 (s, 2H), 6.95 – 6.88 (m, 8H), 6.02 (d, $J = 5.1$ Hz, 2H), 5.77 (d, $J = 5.0$ Hz, 2H), 2.30 (d, $J = 6.7$ Hz, 9H), 2.23 (s, 12H), 2.16 (s, 6H).

¹³C NMR (101 MHz, CD₂Cl₂, 298K) δ (in ppm) 141.65, 138.69, 137.23, 136.77, 131.43, 130.59, 129.26, 128.14, 127.99, 127.71, 126.98, 53.96, 53.69, 53.42, 53.15, 52.88, 29.69, 20.75, 20.72, 20.22, 20.07.

16·H⁺: ¹H NMR (400 MHz, CDCl₃) δ (in ppm) = 9.88 (br, NH), 7.14 (dd, $J = 60.1, 37.1$ Hz, 20H), 6.55 (s, 2H), 6.15 (s, 2H), 2.35 (s, 9H), 2.17 (d, $J = 22.5$ Hz, 18H).

16: UV/Vis (CH₂Cl₂): λ_{max} in nm (ϵ in dm³mol⁻¹cm⁻¹) = 389 (6.9 $\times 10^4$), 707 (3.1 $\times 10^4$);

16·H⁺ (TFA/CH₂Cl₂): λ_{max} in nm (ϵ in dm³mol⁻¹cm⁻¹) = 335 (5.2 $\times 10^4$), 383 (6.4 $\times 10^4$), 479 (4.6 $\times 10^4$), 638 (1.2 $\times 10^4$), 796 (4.4 $\times 10^4$).

2.5.2 Synthesis of 17

A mixture of 5,5'-(1,2-diphenylethene-1,2-diyl)bis(thiophene-5,2-diyl)bis(mesitylmethanol (13) (700 mg, 1.09 mmol), 1,4-bis(di(1H-pyrrol-2-yl)methyl)benzene (15) (200 mg, 0.54 mmol) were dissolved in 200 ml of dry dichloromethane and the resulting solution was allowed stirring for 15 mins under

nitrogen atmosphere. Trifluoroacetic acid (41 μ L, 0.54 mmol) was added and the solution was stirred under nitrogen atmosphere for one hour and further DDQ (372 mg, 1.63 mmol) was added and the mixture was stirred for another one hour in open air condition. After evaporation of solvent compound was purified by column chromatography. A green color band eluted with CH_2Cl_2 and hexane considered as desire homoporphyrin (17) with 7% yield and with CH_2Cl_2 and hexane (18) was collected with 1% yield.

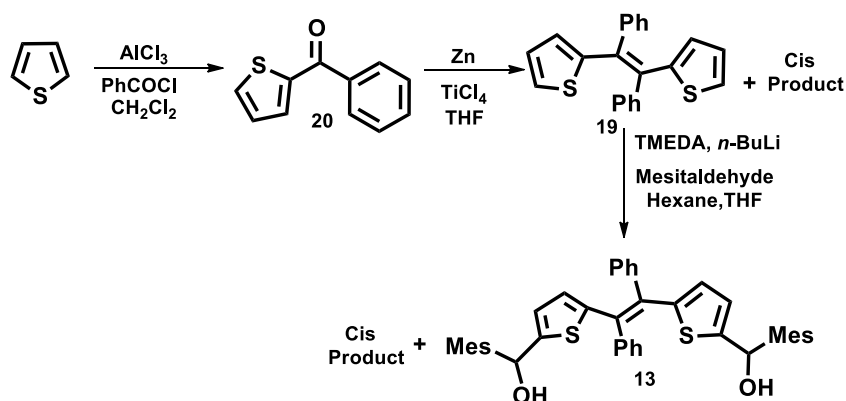
Compound 17: ^1H NMR (400 MHz, CD_2Cl_2 , 298K): δ (in ppm) 11.8 (NH, br), 7.29 (s, 4H), 7.14 – 7.07 (m, 20H), 6.99 (d, $J = 3.8$ Hz, 4H), 6.90 (d, $J = 4.3$ Hz, 12H), 6.15 (d, $J = 5.2$ Hz, 4H), 6.07 (d, $J = 5.2$ Hz, 4H), 2.29 (s, 12H), 2.21 (s, 24H).

17·2H⁺: ^1H NMR (400 MHz, CDCl_3) δ (in ppm) = 7.49 (s, 4H), 7.26 (t, $J = 6.6$ Hz, 4H), 7.20 (dd, $J = 8.4, 4.8$ Hz, 20H), 7.12 (d, $J = 3.9$ Hz, 4H), 7.02 (s, 8H), 6.71 (d, $J = 5.1$ Hz, 4H), 6.56 (d, $J = 5.1$ Hz, 4H), 2.36 (s, 12H), 2.18 (s, 24H), 9.28 (br, NH).

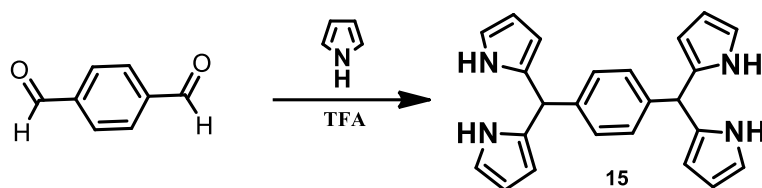
17: UV/Vis (CH_2Cl_2): λ_{max} in nm (ϵ in $\text{dm}^3\text{mol}^{-1}\text{cm}^{-1}$) = 398 (6.9×10^4), 707 (3.1×10^4);

17·2H⁺ (TFA/ CH_2Cl_2): λ_{max} in nm (ϵ in $\text{dm}^3\text{mol}^{-1}\text{cm}^{-1}$) = 326 (5.2×10^4), 391 (6.4×10^4), 508 (4.6×10^4), 806 (4.4×10^4).

2.5.3 Precursor Syntheses



Scheme 2.4: Precursor Synthesis.



Scheme 2.5: Precursor Synthesis.

2.5.3.1 Synthesis of **20**

In a 250 ml two-necked round bottom flask, anhydrous AlCl_3 (10 g, 75 mmol) was mixed with 30 ml of dry CH_2Cl_2 and the resultant suspension was stirred for 15 min. A solution of thiophene (6 g, 71 mmol) and benzoyl chloride (10 g, 75 mmol) with 25 ml dry CH_2Cl_2 was added slowly with syringe, over a period of 3.5 h. The resultant solution was stirred for overnight. The mixture was refluxed for 2 h, cooled and poured on cold water and organic layer was separated with diethyl ether. The residue layer was treated with Na_2CO_3 water and anhydrous Na_2SO_4 was added to remove moisture. Solvent evaporation and recrystallized over petroleum ether led to the formation of 6.3 g product **20** with 80% yield.

^1H NMR (400 MHz, CDCl_3 , 298K): δ (ppm): 7.85-7.83 (m, 2H), 7.69-7.43 (m, 5H) 7.09 (d, 1H).

2.5.3.2 Synthesis of **19**

In a 250 ml two-necked round bottom flask under nitrogen atmosphere, mixture of activated Zn powder (3.0 g, 46 mmol) in dry THF (80 ml) was stirred for 20 min. TiCl_4 (2.52 ml, 23 mmol) was added slowly in ice cool condition. The resultant solution was stirred at room temperature for 30 mins and refluxed for 3h. The mixture was cooled in ice condition and 2-benzoyl thiophene (**20**) (1 ml, 5.3 mmol) in dry THF (25 ml) was added slowly and the resultant solution was refluxed for another

12h. The reaction was monitored by TLC analysis and was quenched with 10% aqueous NaHCO₃ solution and extracted with diethyl ether. The crude product was purified by silica gel (100-200 mesh) column chromatography. A pale yellow color band was eluted with hexane and identified as 2.6 g of cis product of **19** with yield of 56%.

¹H NMR (400 MHz, CDCl₃, 298K): δ (ppm): 7.40-7.41 (m, 10H), 7.06 (d, *J*=5.8 Hz, 2H), 6.71(t, *J*=5.8 Hz, 2H), 6.37 (d, *J*=5.8 Hz, 2H).

2.5.3.3 Synthesis of **13**

In a 100 ml two necked round bottom flask, 1,2-diphenyl-1,2-dithienylethene (**19**) (1 g, 2.9 mmol) in dry hexane (30 ml) was added and the resulting solution was stirred for 15 min under nitrogen atmosphere. N,N,N',N'-tetramethylethylene diamine (1.3 ml, 7.8 mmol) solution was added and stirred for another 5 min. *n*-Butyllithium (10 ml, 1.6 M in hexane, 29 mmol) solution was added and the resultant solution was stirred at room temperature for 1h. The mixture was refluxed for 1h. The mesitaldehyde (1.32 ml, 7.8 mmol) with dry Tetrahydrofuran (10 ml) was added to resulting mixture at RT. Solution was stirred for 12h at RT. After workup with diethyl ether and water, the crude product was purified through silica gel column chromatography (100-200 mesh). A pale yellow color solution was eluted with ethyl acetate/hexane (20:80, V/V) and identified as 0.54 g of **13** with 60% yield.

¹H NMR (400 MHz, CDCl₃, 298K): δ (ppm): 7.35-7.30 (m, 6H), 7.07 (s, 2H), 6.88-6.78 (m, 12H), 2.51 (s, 1H), 2.28 (s, 6H), 2.25 (s, 6H), 2.21 (s, 6H).

2.5.3.4 Synthesis of **15**

To a 100 ml single necked round bottom flask terephthalaldehyde (10 g, 74 mmol) and pyrrole (2mL, 298 mmol) was stirred under nitrogen atmosphere for 5min. To this

mixture trifluoroacetic acid (0.58 mL, 7.4 mmol) was added and it was stirred for 30 mins. The reaction was quenched with 30ml of CH₂Cl₂ and 20ml of 0.1N NaOH. The organic layer was extracted. The residue was purified through silica gel column chromatography (100-200 mesh) with ethyl acetate/hexane (8:92, V/V) and identified as **15** with 81% yield.

¹H NMR (400 MHz, CDCl₃, 298 K), δ(ppm): 7.68 (br, 4H), 6.89 (d, 4H), 6.78 (m, 4H), 6.34 (m, 4H) 6.22 (m, 4H), 7.23 (d, 4H).

2.6 References

1. J. L. Sessler, D. Seidel, *Angew. Chem. Int. Ed.* **2003**, *42*, 5134-5175.
2. T. Tanaka, A. Osuka, *Chem. Rev.* **2017**, *117*, 2584-2640.
3. Y. M. Sung, J. Oh, W.-Y. Cha, W. Kim, J. M. Lim, M.-C. Yoon, D. Kim, *Chem. Rev.* **2017**, *117*, 2257-2312.
4. Y. Ding, W.-H. Zhu, Y. Xie, *Chem. Rev.* **2017**, *117*, 2203-2256.
5. S. Saito, A. Osuka, *Angew. Chem. Int. Ed.* **2011**, *50*, 4342-4373.
6. R. B. Woodward, Aromaticity Conference, Sheffield, UK, 1966.
7. A. Jasat, D. Dolphin, *Chem. Rev.* **1997**, *97*, 2267-2287.
8. R. Grigg, *J. Chem. Commun.* **1967**, 1238-1239.
9. R. Grigg, *J. Chem. Soc. C* **1971**, 3664-3668.
10. E. Ganapathi, W.-Z. Lee, M. Ravikanth, *J. Org. Chem.* **2014**, *79*, 9603-9612.
11. E. Ganapathi, S. Kuilya, T. Chatterjee, M. Ravikanth, *Eur. J. Org. Chem.* **2016**, 282-290.
12. B. Adinarayana, M. Das, C. H. Suresh, A. Srinivasan, *Chem. Eur. J.* **2019**, *25*, 4683-4687.
13. V. G. Anand, S. Venkatraman, H. Rath, T. K. Chandrashekar, W. Teng, K. Ruhlandt-Senge, *Chem. Eur. J.* **2003**, *9*, 2282-2290.

14. T. K. Chandrashekar, V. Prabhuraja, S. Gokulnath, R. Sabarinathan, A. Srinivasan, *Chem. Commun.* **2010**, 46, 5915-5917.

CHAPTER 3

Protonation triggered Hückel and Möbius aromatic transformations in nonaromatic core-modified [30]hexaphyrin(2.1.1.2.1.1) and annulated [28]hexaphyrin(2.1.1.0.1.1)

3.1	Introduction	62
3.2	Objective	63
3.3	Results and discussions	63
3.3.1	Syntheses	63
3.3.2	Spectral Characterization	65
3.3.2.1	Mass spectrometric analysis	65
3.3.2.2	NMR Analysis	66
3.3.2.3	Single crystal X-ray analysis	73
3.3.2.4	NICS(0) calculations and AICD plots	79
3.3.2.5	Electronic spectral analysis	84
3.4	Conclusion	85
3.5	Experimental Section	86
3.5.1	Synthesis of 6	86
3.5.2	Synthetic of 8	87
3.5.3	Synthesis of 10	88
3.5.4	Precursor Syntheses	89
3.5.4.1	Synthesis of 11	89
3.5.4.2	Synthesis of 7	90
3.5.4.3	Synthesis of 12	90
3.5.4.4	Synthesis of 9	91
3.6	References	92

3.1 Introduction

Expanded porphyrins with large π -electronic conjugation exhibit significant conformational flexibility.¹ This has been exploited to understand the intricacies involved in Hückel, Möbius² and Baird aromaticity.³ Synthesis of $4n\pi$ Möbius aromatic molecules are complicated because of requirement of cyclic π -conjugation and singly twisted topology within a single molecular framework.⁴ Herges and co-workers were the first to synthesize a hybrid molecule containing planar conjugated cyclooctatetraene and bianthraquinodimethane exhibiting distinct Möbius aromaticity.⁵ Latos-Grażyński and co-workers reported solvent, temperature and protonation dependent conformational switch between Hückel-Möbius topologies using di-*p*-benzi [28]hexaphyrins **1** and **2** shown in Figure 3.1.⁶⁻⁸

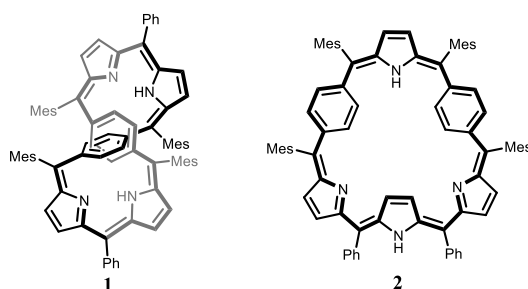


Figure 3.1: Möbius aromatic molecules upon external trigger.

Osuka, Kim and co-workers have reported formation of Möbius aromatic topology in a range of *meso* aryl expanded porphyrins triggered by metalation, fusion, protonation, deprotonation and solvent control.⁹ For example 32π heptaphyrin **3** undergoes conformational change to Möbius topology upon protonation.¹⁰ Recently, we have reported 32π core-modified heptaphyrin which exhibit Möbius aromaticity both in freebase and protonated form.¹¹ Very recently, Yamada and co-workers have shown that insertion of Cu(II) to vinylene bridged hexaphyrins(2.1.2.1.2.1) **4** induces aromaticity in metal complexes (Figure 3.2).¹²

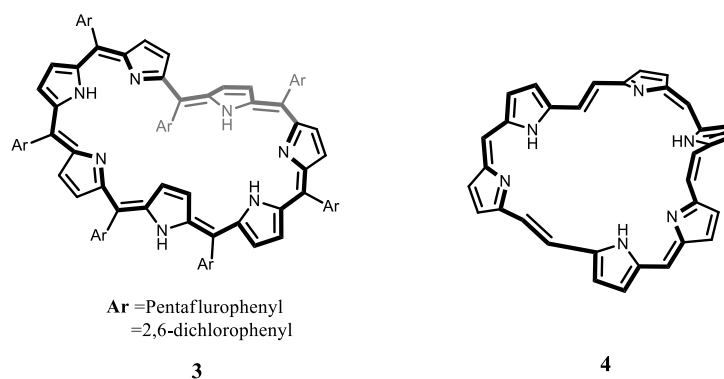


Figure 3.2: Aromatic molecules on external trigger.

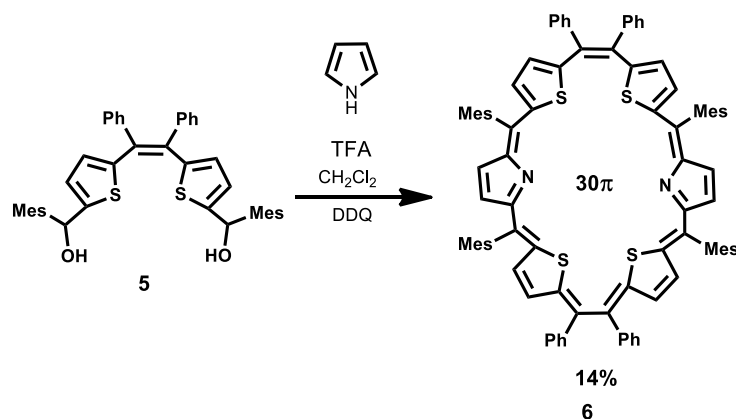
3.2 Objective

In continuation to our efforts towards understanding different aromatic transformations triggered by an external stimulant, in this thesis the author wish to report syntheses and characterization of three hexaphyrins; 28π and 30π hexaphyrins which on protonation transforms to a Möbius aromatic and Hückel aromatic topologies respectively. These transformations are accompanied by change in conformation from figure-eight structure to open extended structure.

3.3 Results and discussions

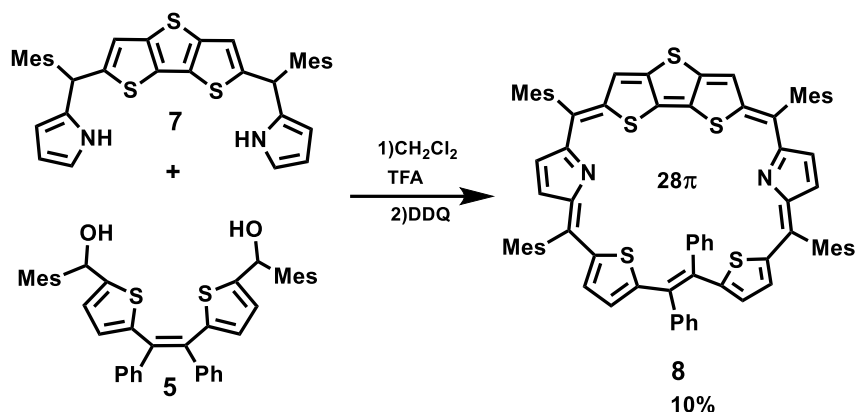
3.3.1 Syntheses

Our synthetic strategy included, incorporation of flexible 1,2-diphenyl-1,2-dithienyl ethene groups on either side of the expanded porphyrin skeleton so that the anticipated twist^{2d} upon protonation can be achieved. Keeping this in mind, the precursor 5,5'-bis(mesitylhydroxymethyl)-1,2-diphenyl-1,2-di(thiophene-2-yl)ethene **5** was synthesized.¹³ The trifluoroacetic acid (TFA) catalysed condensation of **5** with pyrrole in dry CH_2Cl_2 followed by oxidation with 2,3-dichloro-5,6-dicyano-1,4-benzoquinone (DDQ) afforded **6** in 14% yield (Scheme 3.1).



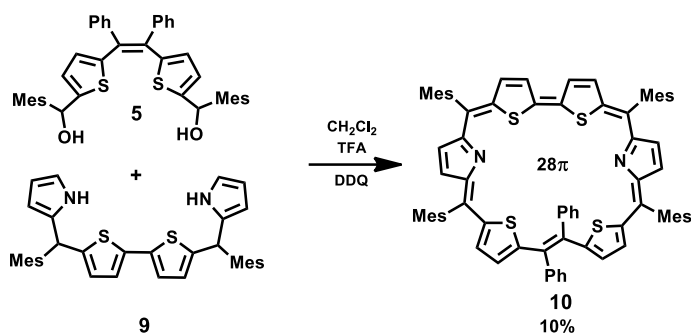
Scheme 3.1: Synthesis of hexaphyrin **6**.

We further examined the effect of replacement of 1,2-diphenyl-1,2-dithienyl ethene moiety by rigid dithieno[3,2-b:2',3'-d]thiophene (DTT) on the molecular topology of hexaphyrin. This was achieved by synthesizing the rigid precursor 2,6-bis(mesityl(1H-pyrrol-2-yl)methyl)dithieno[3,2-b:2',3'-d]thiophene **7**¹⁴ which on reaction with **5** under TFA acid catalysed condition followed by DDQ oxidation gave **8** in 10% yield (Scheme 3.2).



Scheme 3.2: Synthesis of hexaphyrin **8**.

The 2,2'-bithiophene (BT) was achieved by synthesizing the rigid precursor 5,5'-bis(mesityl(1H-pyrrol-2-yl)methyl)-2,2'-bithiophene (**9**) which on reaction with **5** under TFA acid catalysed condition followed by DDQ oxidation gave **10** in 10% yield (Scheme 3.3).



Scheme 3.3: Synthesis of hexaphyrin **10**.

3.3.2 Spectral Characterization

3.3.2.1 Mass Spectroscopic analysis

The mass spectrum of **6**, **8** and **10** gave molecular ion peak at m/z 1337.4960 m/z 1189.3777 m/z 1159.4174 respectively from the HRMS and ESI mass spectrometric analysis confirms exact composition of the macrocycle shown in Figure 3.3-3.5.

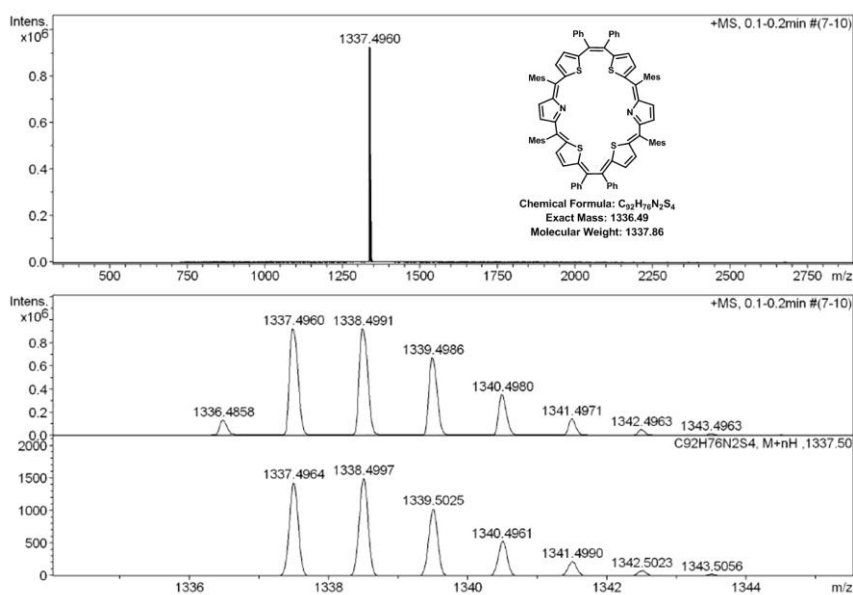


Figure 3.3: HRMS of hexaphyrin **6**.

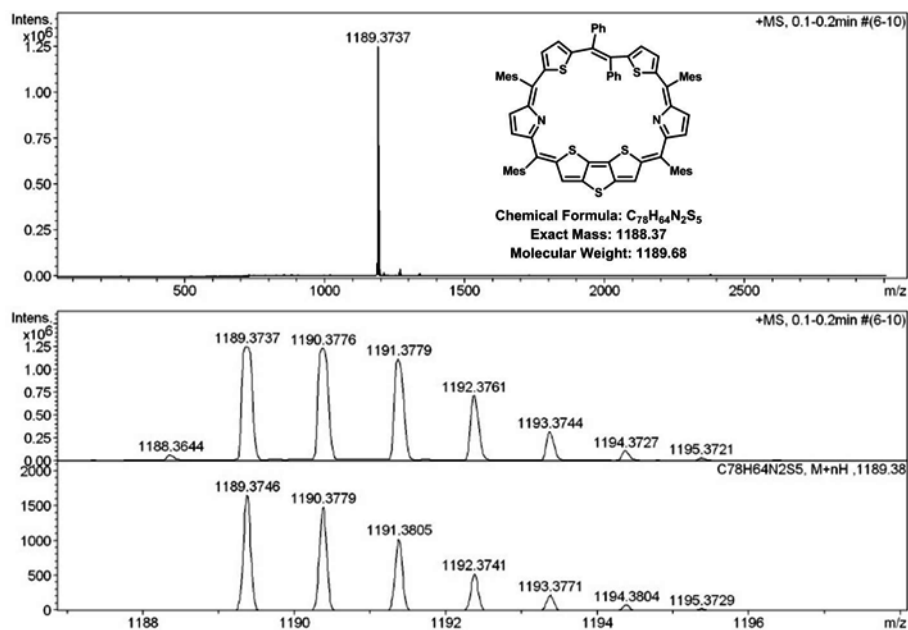


Figure 3.4: HRMS of hexaphyrin **8**.

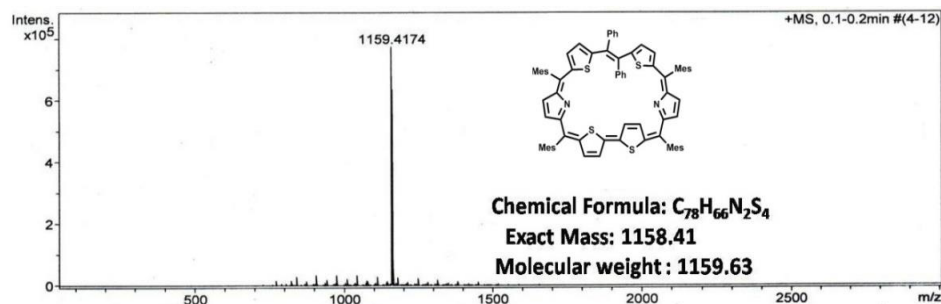


Figure 3.5: ESI-Mass of hexaphyrin **10**.

3.3.2.2 NMR Analysis

The hexaphyrin **6** with 30π electrons in its conjugation pathway is expected to show Hückel aromatic behaviour. However, the ^1H NMR spectra of **6** (Figure 3.6) shows that outer β -CH protons of pyrrole rings (*c*, *d*) and thiophene rings (*a*, *b*) appear in the region 6.1 – 6.9 ppm. The inner β -CH protons of two inverted thiophene rings (*e*, *f*) experience deshielding and appeared at 6.31 and 8.35 ppm respectively.

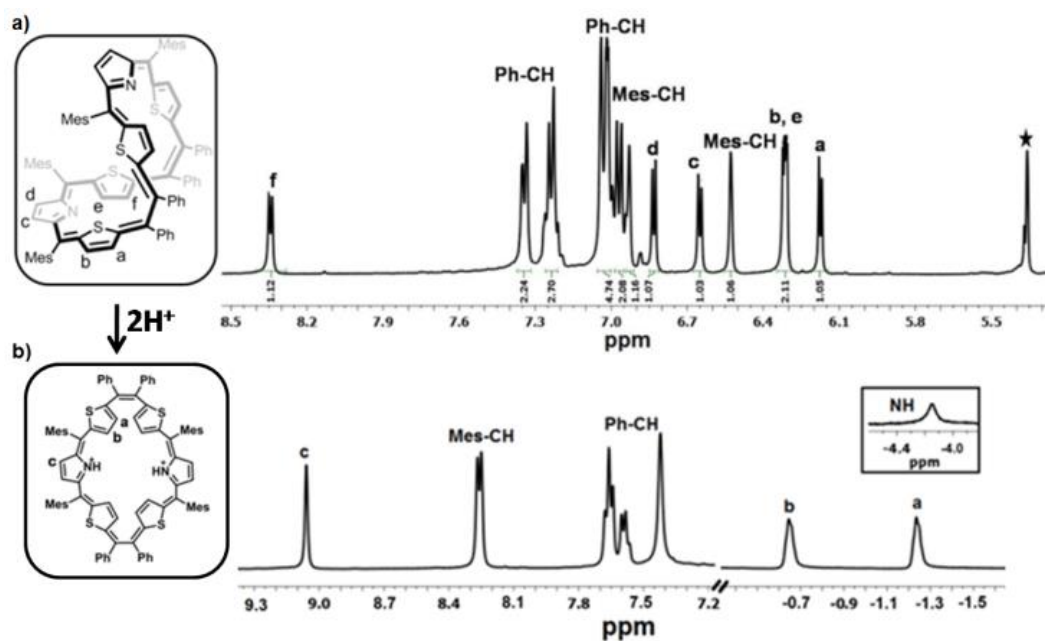


Figure 3.6: ^1H NMR Spectra of a) **6** and b) $\mathbf{6.2H^+}$ at 298 K in CD_2Cl_2 .

These assignments were based on ^1H - ^1H COSY correlation experiment (Figure 3.7) and NOESY experiment. Variable temperature studies from 298 K to 193 K did not significantly change the spectrum but for small shielding of '*f*' protons (0.39 ppm) (Figure 3.8) suggesting the conformational rigidity in the temperature range studied.

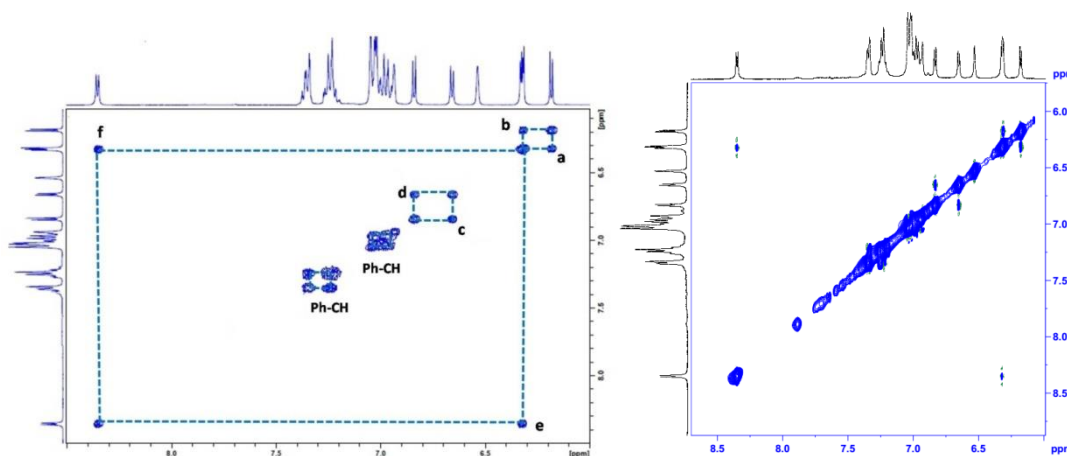


Figure 3.7: ^1H COSY and 2D NOESY correlation spectroscopy of **6** (aromatic region) in CD_2Cl_2 .

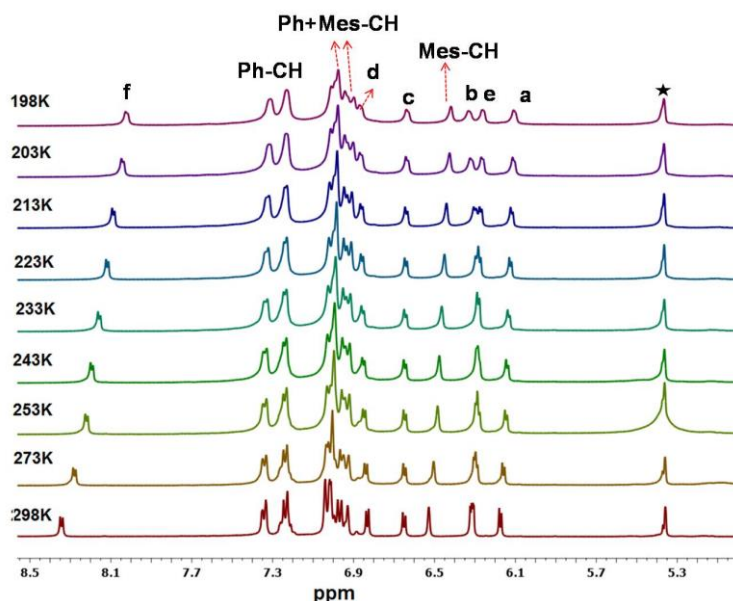


Figure 3.8: Low temperature ^1H NMR spectroscopy of **6** (aromatic region) in CD_2Cl_2 . Upon protonation of pyrrole nitrogens in **6** with TFA, there is drastic change in the ^1H NMR spectrum (Figure 3.6). The β -CH protons of thiophene rings (*a* and *b*) resonate as two doublets at -0.65 and -1.24 ppm suggesting that the thiophene rings are inverted and are experiencing the diatropic ring current of the macrocycle.¹⁵ The pyrrole NH protons resonate as a broad singlet at -4.21 ppm. On the other hand, the pyrrole β -CH protons (*c*) experience significant deshielding (~ 2.4 ppm) and the mesityl CH protons are also deshielded (~ 1.5 ppm) with respect to freebase. These observations suggest a major structural change on protonation and the chemical shift values indicate the aromatic nature of $\mathbf{6.2H}^+$ with complete restoration of π -electronic conjugation. The difference in chemical shift ($\Delta\delta$) between inner NH and outer (*c*) protons value about 13.2 ppm justifies $(4n+2)\pi$ Hückel aromatic nature of $\mathbf{6.2H}^+$. These assignments were based on ^1H - ^1H COSY correlation experiment (Figure 3.9)

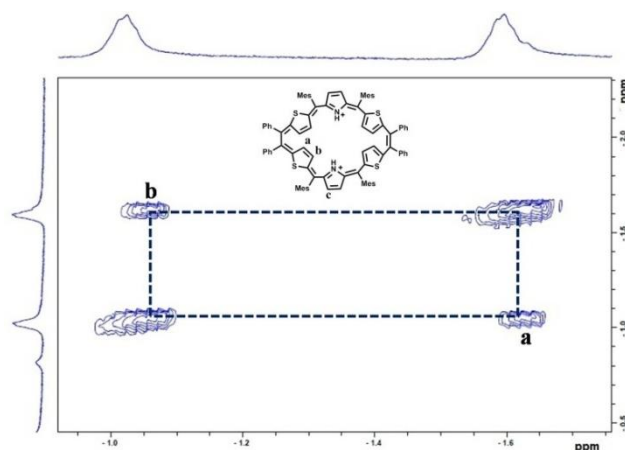


Figure 3.9: ^1H COSY correlation spectroscopy of **6** (aromatic region) in CD_2Cl_2 .

^1H NMR analysis of **8** (Figure 3.10) where the β -CH protons of pyrrole (*b,c*), thiophene (*d,e*) and DTT (*a*) resonate between 6.66 ppm and 7.50 ppm. These assignments were based on ^1H - ^1H COSY correlation experiment (Figure 3.13).

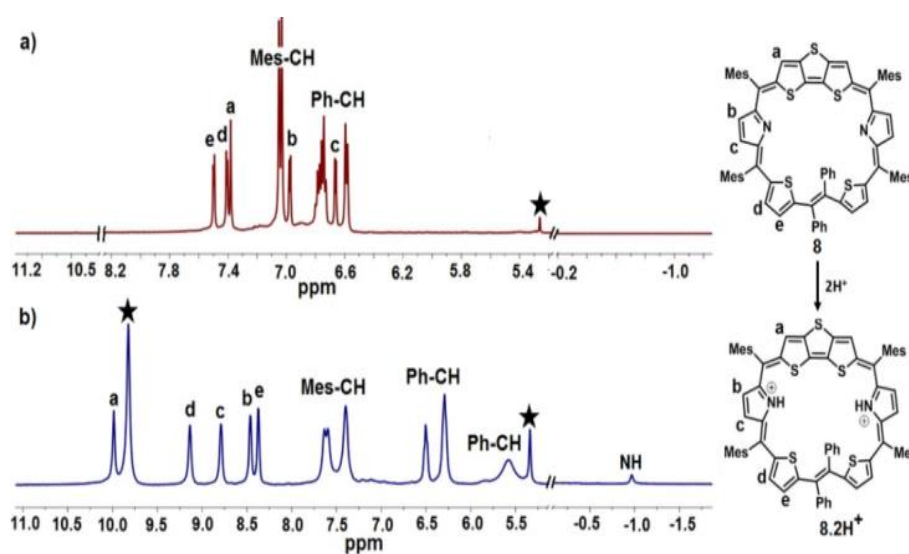


Figure 3.10: ^1H NMR Spectra of a) **8** at 273K and b) **8.2H⁺** at 298 K in CD_2Cl_2

Temperature variation from 298 K to 193 K did not show any major changes indicating conformational stability of **8** in the temperature range (Figure 3.11). However, upon protonation of pyrrole nitrogens, the β -CH protons are significantly deshielded and the DTT protons (*a*) resonate at 9.98 ppm suggesting the presence of diatropic ring current (Figure 3.10-3.13). The inner pyrrole NH protons resonate as a

broad singlet at -0.94 ppm. The $\Delta\delta$ value of ~ 10.0 ppm between the inner NH and outer (*a*) protons, clearly suggest the Möbius aromatic nature of $\mathbf{8.2H}^+$

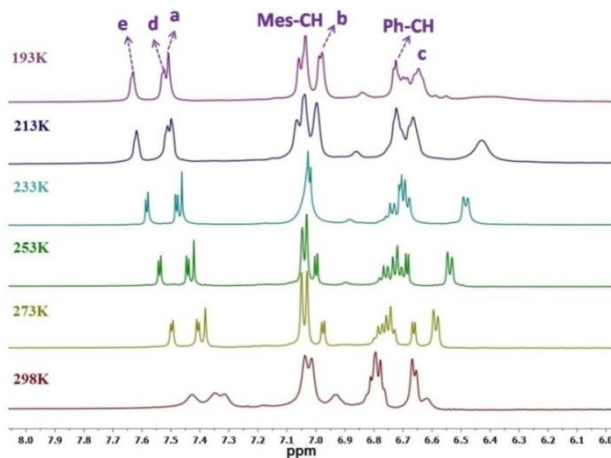


Figure 3.11: ^1H NMR low temperature studies of $\mathbf{8}$ in CD_2Cl_2 .

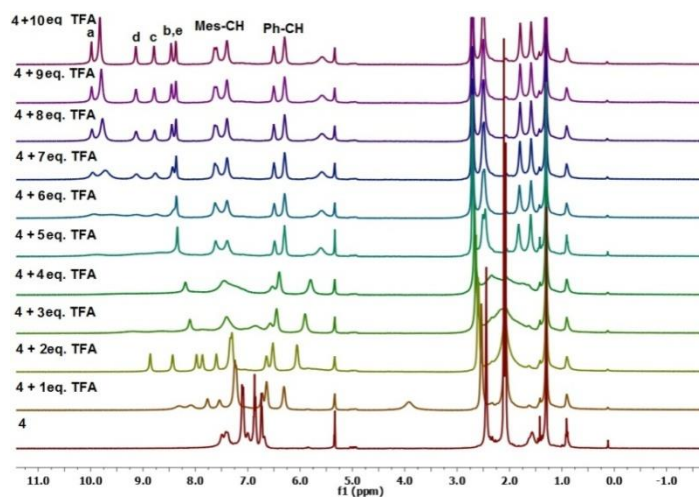


Figure 3.12: ^1H NMR Spectra titration studies with TFA.

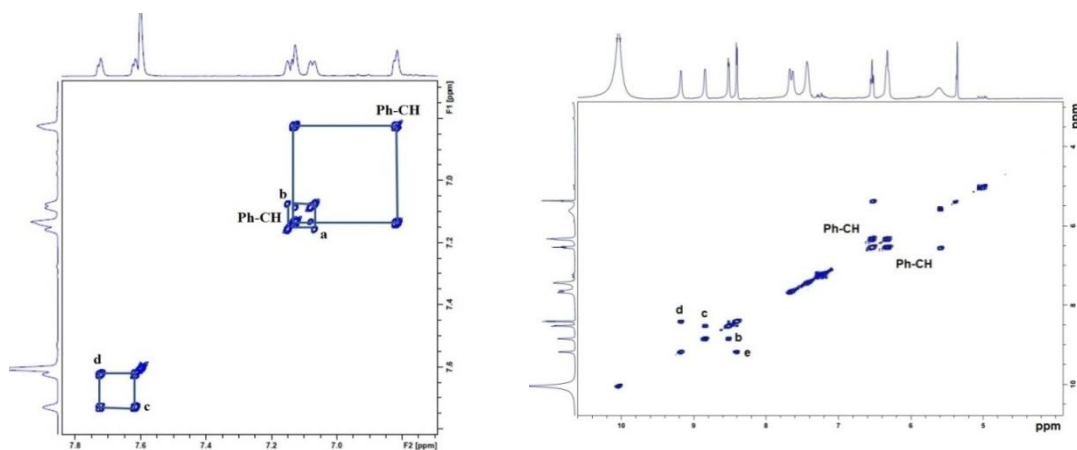


Figure 3.13: ^1H - ^1H COSY correlation spectroscopy of $\mathbf{8}$ (273K) and $\mathbf{8.2H}^+$ (298K) in CD_2Cl_2 .

Hexaphyrin **10** with $4n\pi$ configuration in freebase form is also characterized by ^1H NMR analysis at 193K shown in Figure 3.14. All the protons resonated individually because of nonsymmetry of the macrocycle. All assignments were based on ^1H - ^1H COSY experiments (Figure 3.15). Here the β -CH protons of inverted thiophene (*a*, *b*) resonated at 5.27 ppm and 4.85 ppm respectively and the normal thiophene β -CH protons (*c*, *d*, *g*, *h*, *i*, *j*) and pyrrole β -CH protons (*e*, *f*, *k*, *l*) resonated between 6.60 ppm to 7.83 ppm but still peaks were broad and temperature variation from 298K to 193K did not show any major changes (Figure 3.16).

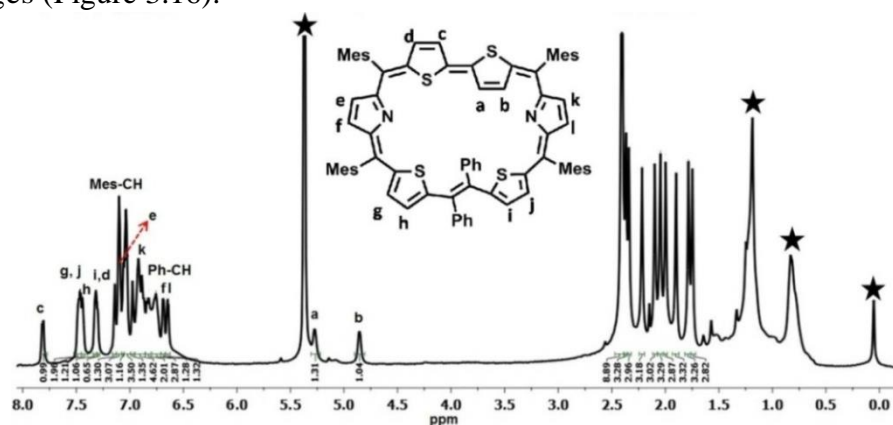


Figure 3.14: ^1H NMR Spectra of **10** (193K) CD_2Cl_2 (* symbols are solvents and acid impurities).

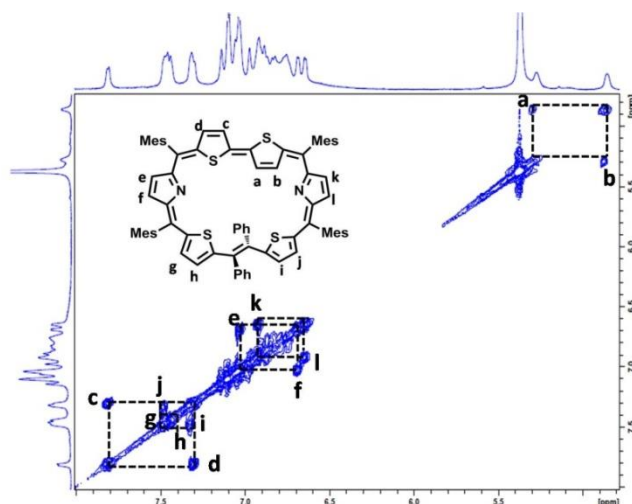


Figure 3.15: ^1H - ^1H COSY correlation spectroscopy of **10** (aromatic region) in CD_2Cl_2 at 193K.

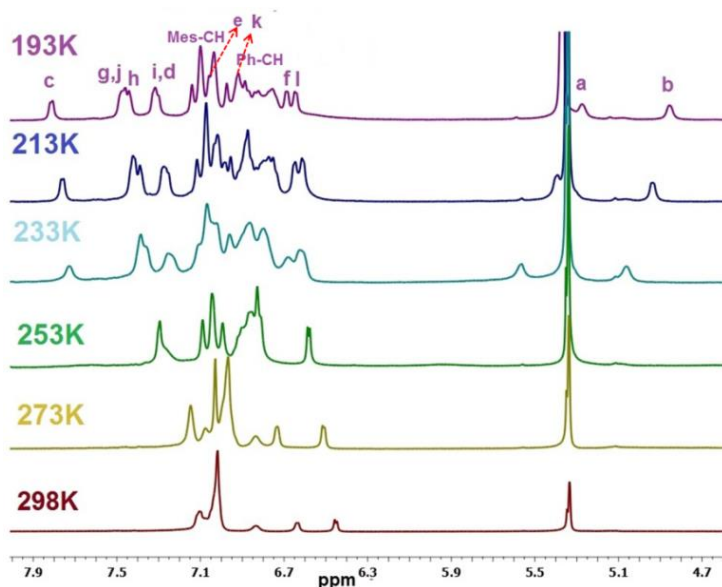


Figure 3.16: Low temperature ^1H NMR spectroscopy of **10** (aromatic region) in CD_2Cl_2 .

However upon protonation also the peaks were still broad and the thiophene protons (*c, d, g, h, i, j*) further are deshielded to 8.22-7.74 ppm and the β -CH protons of pyrrole rings, are also deshielded and the inverted thiophene protons (*a, b*) are deshielded and resonate at 6.69 ppm shown in Figure 3.17. But still peaks were broad and temperature variation from 298K to 193K did not show any major changes.

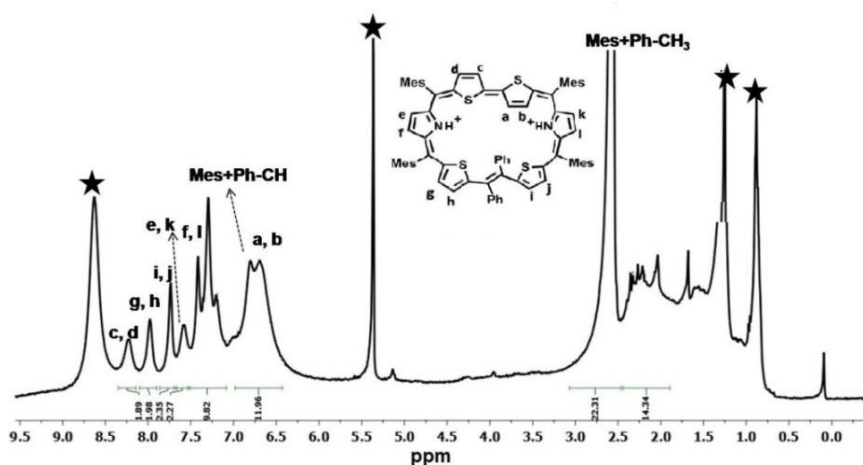


Figure 3.17: ^1H NMR Spectra of $\mathbf{10.2H}^+$ (298K) in CD_2Cl_2 (* symbols are solvents and acid impurities).

3.3.2.3 Single Crystal X-ray analysis

The figure-eight conformation of **6** was confirmed by single crystal X-ray structure (Figure 3.18 and Table 3.1). The two 1,2-diphenyl-1,2-dithienyl ethene groups are connected to two pyrrole moieties by four *meso* carbon bridges to generate a 30π electronic macrocyclic framework. The crystal analysis shows that both the phenyl rings on 1,2-diphenyl-1,2-dithienyl ethene moieties are in *cis*-orientation and one thiophene ring in each moiety is inverted and the 'S' atoms (S1 and S4) are pointed outside the macrocyclic core. The torsion angle at the maximum twisted ethene moiety is 53.66° (C14-C15-C16-C17). The bond length data within the macrocyclic ring suggests that thiophene rings (A and B) have localised double bonds while (C and D) have effective π -delocalization. The figure-eight conformation completely blocks effective π -delocalization in the macrocyclic skeleton. The structure of **6.2H⁺** was confirmed through single crystal X-ray analysis (Figure 3.18). The compound crystallized in triclinic crystal lattice with *I2/a* space group. As observed in ¹H NMR spectroscopy, the molecule attains almost planar conformation where all the thiophene rings are inverted and the inverted thiophene units are 25° and pyrrolic units are 3.09° deviated from the mean macrocyclic plane containing *meso* carbon atoms (C6, C6', C6'', C6'''). The crystal analysis reveals that the two units of perchlorate anions are located above and below the macrocycle with intermolecular hydrogen bonding interaction with the protonated imine NH (N1- H1) and inverted thiophene β -CH (C3H3) with distances and angles of N1-H1...O1 is 2.13 Å and 141.01° and C3-H3...O3 is 2.54 Å and 162.53° respectively. This confirms structural transformation from a twisted topology to almost planar Hückel aromatic topology of **6.2H⁺**.¹⁶

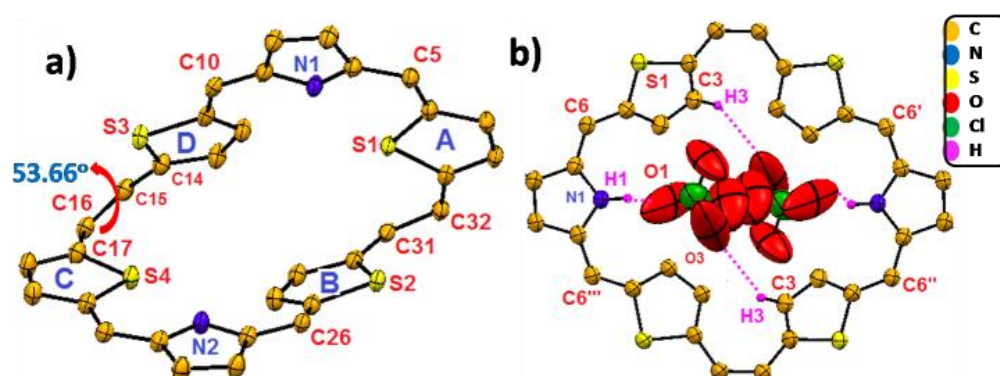


Figure 3.18: Single crystal X-ray structures of **a) 6** and **b) 6.2H⁺**. The *meso*-aryl groups are omitted for clarity.

The molecular structure of **8** is shown in Figure 3.19 and Table 3.2. The DTT (6.91°), pyrrole (14.84°, 9.48°) and thiophene rings (S4, 9.26°) show small deviation from the mean plane of the macrocycle while the thiophene ring S5 is highly deviated by an angle of 26.29°, thus disrupting the π -conjugation. The two phenyl rings on ethene-bridge are in *trans*-orientation. The structure of **8.2H⁺** (Figure 3.19) reveals substantial distortion of the individual rings relative to the freebase form. The distortion of the macrocycle triggers the molecule to attain Möbius topology with distinct aromatic character.¹⁷ The tilt angles of DTT, pyrrole and thiophene units from the mean macrocyclic (C9, C14, C25, C30) plane are 9.03° (DTT), 32.33° (N1), 14.43° (N2), 36.02° (S4) and 35.58° (S5) respectively. The major twist observed in the S4 and S5 thiophene units due to the steric congestion induced by *meso* phenyl substituent of 1,2-diphenyl-1,2-dithienyl ethene moiety. Thus, allows the π -electron delocalization required for the Möbius conformation. Furthermore, the torsion angles at the maximum twisted 1,2-diphenyl-1,2-dithienyl ethene moiety are 53.9° (S4, C18, C19, C20), 125.23° (C17, C18, C19, C20) and 44° (C19, C20, C21, S5), 139.89° (C19, C20, C21, C22) respectively and these values are comparable with the Möbius systems reported till date.¹⁸ The crystal analysis reveals that two units of ClO₄⁻ anions

are located above and below the macrocyclic plane with intermolecular hydrogen bonding interactions with protonated imine nitrogens (N1-H1 and N2-H2). The bond distances and angles of N1-H1...O1 and N2-H2...O2 are 2.53 Å & 108.44° and 2.37 Å & 110.52° respectively.

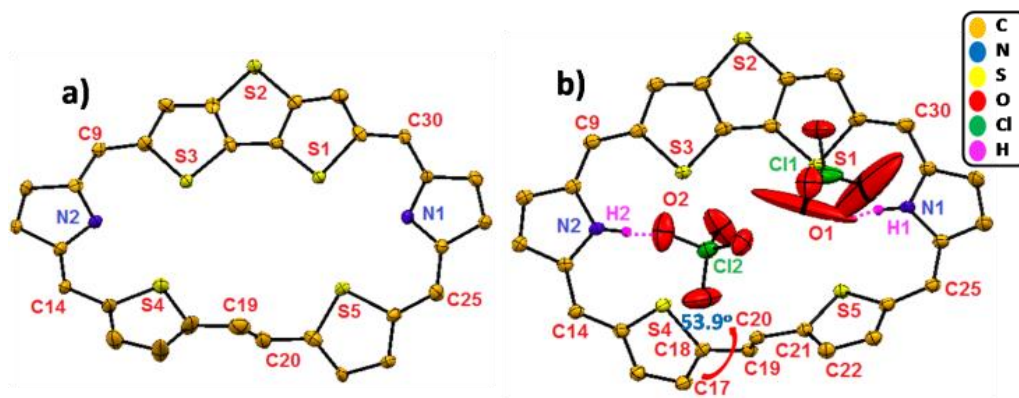


Figure 3.19: Single crystal X-ray structures of a) **8** and b) **8.2H⁺**. The *meso*-aryl groups are omitted for clarity.

The molecular structure of **10** is shown in Figure 3.20 and Table 3.3 is confirmed by single crystal X-ray analysis. The S4 thiophene ring is inverted into the macrocyclic unit. The tilt angles from plane (C8, C13, C22, C27) are 12.10° (S3), 13.23° (S4), 15.79° (N2), 16.48° (N1), 32.48° (S1) and 38.70° (S2) respectively. The major twist observed in the S1 and S2 thiophene units due to the steric congestion induced by *meso* phenyl substituent of 1,2-diphenyl-1,2-dithienyl ethene moiety. Thus, allows the π -electron delocalization required for the Möbius conformation. Furthermore, the torsion angles at the maximum twisted 1,2-diphenyl-1,2-dithienyl ethene moiety is 63.99° (S2, C4, C3, C2) and this values are comparable with the Möbius systems reported till date. The structure of **10.2H⁺** (Figure 3.20) was also confirmed by single crystal X-ray analysis. The distortion of the macrocycle triggers the molecule to attain Möbius topology with distinct aromatic character. The tilt angles from the mean macrocyclic (C8, C13, C22, C27) plane are 13.34° (S3), 9.00° (S4), 16.13° (N2), 28.01° (N1), 49.49° (S1) and 38.22° (S2) respectively and S4 is still inverted. The

major twist observed in the S1 and S2 thiophene units due to the steric congestion induced by *meso* phenyl substituent of 1,2-diphenyl-1,2-dithienyl ethene moiety. Thus, allows the π -electron delocalization required for the Möbius conformation. Furthermore, the torsion angles at the maximum twisted 1,2-diphenyl-1,2-dithienyl ethene moiety is 60.94° (C3, C2, C1, S1) and this values are comparable with the Möbius systems reported till date.

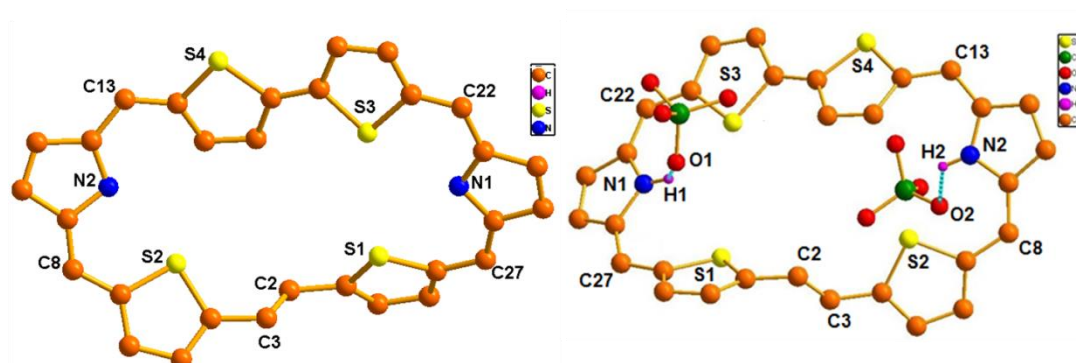


Figure 3.20: Single crystal X-ray structures of a) **10** and b) **10.2H⁺**. The *meso*-aryl groups are omitted for clarity.

Table 3.1: Crystallographic data for **6** and **6.2H⁺**

	6	6.2H⁺
<i>T</i>, K	120 K	120K
Formula	C ₉₂ H ₇₆ N ₂ S ₄	C ₉₂ H ₇₈ N ₂ S ₆ Cl ₂ O ₈
Formula weight	1429.91	1538.70
Color and Habit	Dark brown	Golden
Crystal system	Monoclinic	Monoclinic
Space group	<i>P</i> 2 ₁ / <i>c</i>	<i>I</i> 2/ <i>a</i>
<i>a</i>, Å	25.4648(2)	20.6244(4)
<i>b</i>, Å	13.16930(10)	19.9862(3)
<i>c</i>, Å	27.9437(3)	24.8524(4)
α, deg	90	90
β, deg	105.3870(10)	104.931(2)
γ, deg	90	90
<i>V</i>, Å³	9035.12(14)	9898.4(3)
Radiation (λ, Å)	Cu K α (1.54184)	Cu K α (1.54184)
<i>Z</i>	4	4
d_{calcd}, g•cm⁻³	1.051	1.033

μ , mm ⁻¹	1.292	1.756
$F(000)$	3024	3224
No. of unique reflns	13559	87401
No. of params. refined	8644	10176
GOF on F ²	1.015	1.067
$R1a$ [$I > 2\sigma(I)$]	0.0593	0.0832
$R1^a$ (all data)	0.0628	0.0865
$wR2b$ (all data)	0.1512	0.2500

Table 3.2: Crystallographic data for **8** and **8.2H⁺**

	8	8.2H⁺
T , K	296 K	120K
Formula	C ₇₉ H ₆₅ Cl ₃ N ₂ S ₅	C ₉₂ H ₈₂ N ₂ S ₅ Cl ₂ O ₈
Formula weight	2617.95	3149.58
Color and Habit	Dark green	Golden
Crystal system	Monoclinic	Monoclinic
Space group	$I2/a$	$P2_1/c$
a , Å	13.0469(9)	25.0052(2)
b , Å	17.3726(12)	23.2365(2)
c , Å	65.878(5)	16.8002(2)
α , deg	90	90
β , deg	91.658(6)	96.3690(10)
γ , deg	90	90
V , Å ³	14925.6(19)	9701.23(16)
Radiation (λ , Å)	Cu K α (1.54184)	Cu K α (1.54184)
Z	8	4
dcalcd, g•cm ⁻³	1.165	1.078
μ , mm ⁻¹	0.305	1.997
$F(000)$	5472	3304
No. of unique reflns	40956	143821
No. of params. refined	14161	20163
GOF on F ²	1.054	1.039
$R1a$ [$I > 2\sigma(I)$]	0.1564	0.0725
$R1^a$ (all data)	0.1857	0.0784
$wR2b$ (all data)	0.4006	0.2050

Table 3.3: Crystallographic data for **10** and **10.2H⁺**

Identification code	10	10.2H⁺
Empirical formula	C ₇₈ H ₆₆ N ₂ S ₄	C ₇₈ H ₆₈ Cl ₈ N ₂ O ₈ S ₄
Formula weight	1158.41	1350.56
Temperature/K	116(20)	112
Crystal system	triclinic	Monoclinic
Space group	<i>P</i> -1	<i>P</i> 2 ₁ / <i>c</i>
<i>a</i> , Å	13.4993(6)	24.8648(2)
<i>b</i> , Å	16.3947(7)	21.8967(2)
<i>c</i> , Å	20.1716(10)	18.12740(2)
α , deg	67.817(4)	90
β , deg	72.672(5)	92.2230(10)
γ , deg	87.064(4)	90
<i>V</i> , Å ³	3936.8(3)	9862.16(13)
<i>Z</i>	2	4
ρ_{calc} /cm ³	2.193	(1.040)
μ /mm ⁻¹	16.029	1.763
<i>F</i> (000)	2585.0	3248.0
Crystal size/mm ³	0.25 × 0.25 × 0.21	0.25 × 0.25 × 0.21
Radiation	CuK α (λ = 1.54184)	CuK α (λ = 1.54184)
2 Θ range for data collection/°	7.166 to 171.278	6.332 to 154.15
Index ranges	-16 ≤ <i>h</i> ≤ 15, -20 ≤ <i>k</i> ≤ 20, -25 ≤ <i>l</i> ≤ 25	-31 ≤ <i>h</i> ≤ 31, -21 ≤ <i>k</i> ≤ 27, -22 ≤ <i>l</i> ≤ 15
Reflections collected	68288	147391
Independent reflections	16176 [<i>R</i> _{int} = 0.1882, <i>R</i> _{sigma} = 0.1036]	20546 [<i>R</i> _{int} = 0.1053, <i>R</i> _{sigma} = 0.0466]
Data/restraints/parameters	16176/0/823	20546/0/987
GOF on <i>F</i> ²	1.575	1.080
Final <i>R</i> indexes [<i>I</i> >= 2 σ (<i>I</i>)]	<i>R</i> ₁ = 0.1494, <i>wR</i> ₂ = 0.4130	<i>R</i> ₁ = 0.0740, <i>wR</i> ₂ = 0.2096
Final <i>R</i> indexes [all data]	<i>R</i> ₁ = 0.1799, <i>wR</i> ₂ = 0.4431	<i>R</i> ₁ = 0.0808, <i>wR</i> ₂ = 0.2170
Largest diff. peak/hole / e Å ⁻³	1.48/-1.26	1.26/-1.31

3.3.2.4 NICS (0) Calculations and ACID Plots

The NICS (0) values¹⁹ calculated for **6** the individual rings show significant variation depending on the nature of the heterocyclic rings. The two thiophene rings show values of -10.2 and -10.0 ppm (rings A and B), while the other two thiophene rings show values of -4.0 and -4.2 ppm (ring C and D) (Figure 3.21). The two pyrrole rings show value of -1.4 and -1.2 ppm. The NICS (0) values at the centre of the ring is -2.8 ppm. The ACID²⁰ plots show an anticlockwise and clockwise orientation of current density towards top twist region characterized by ethene C-C bond distance of 1.49Å and 1.37Å respectively (Figure 3.22).

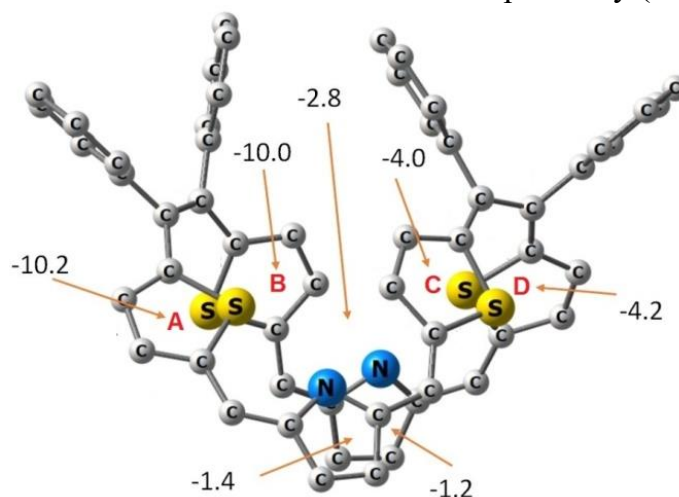


Figure 3.21: NICS (0) values at M06L/6-31G** level of **6**.

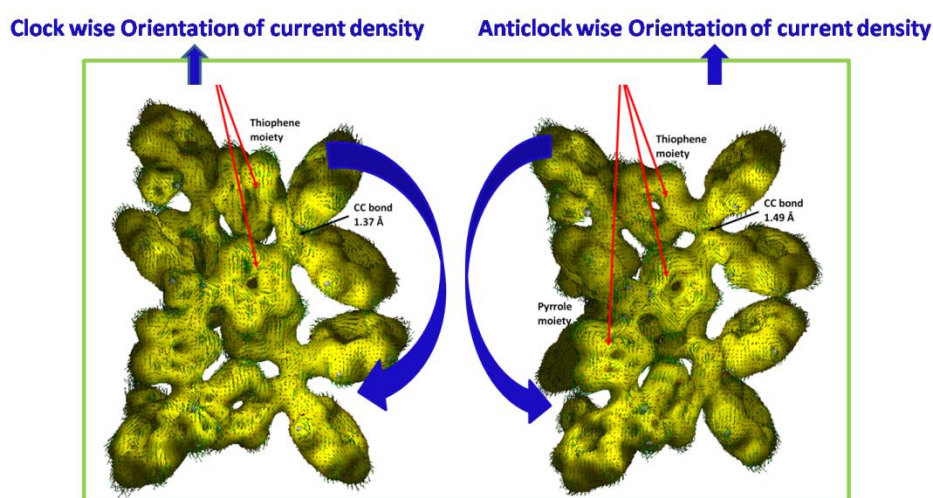


Figure 3.22: ACID plots for **6** with current density vectors plotted on to isosurface of value 0.026.

The NICS (0) values of **8** calculated for the individual rings show significant variation depending on the nature of the heterocyclic rings. The two pyrrole rings show values of -1.1 ppm in the freebase form, while the other heterocyclic rings showed higher negative ppm values shown in Figure 3.23. The NICS (0) values at the centre of the ring is -2.0 ppm. The ACID plots show a clockwise orientation of current vectors plotted on to isosurface of value 0.026 shown in Figure 3.24.

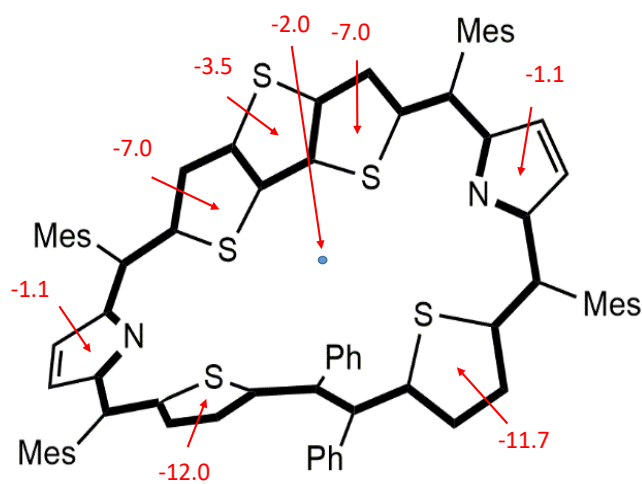


Figure 3.23: NICS (0) values at M06L/6-31G** level **8**.

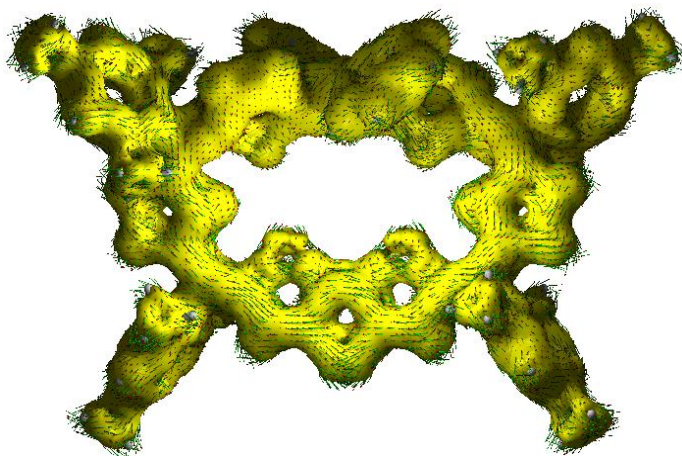


Figure 3.24: ACID plots for **8** with current density vectors plotted on to isosurface of value 0.026.

The NICS (0) values of $\mathbf{8.2H}^+$ upon protonation calculated for the individual rings show significant variation in the nature of the heterocyclic rings. The two pyrrole rings which showed values of -1.1 ppm in the freebase form, upon protonation the two pyrrole rings showed values of -9.7 ppm while the other heterocyclic rings further shifted to higher negative ppm values shown in Figure 3.25. The NICS (0) values at the centre of the ring is -5.5 ppm. The AICD plots show a clockwise orientation of current vectors plotted on to isosurface of value 0.026 shown in Figure 3.26.

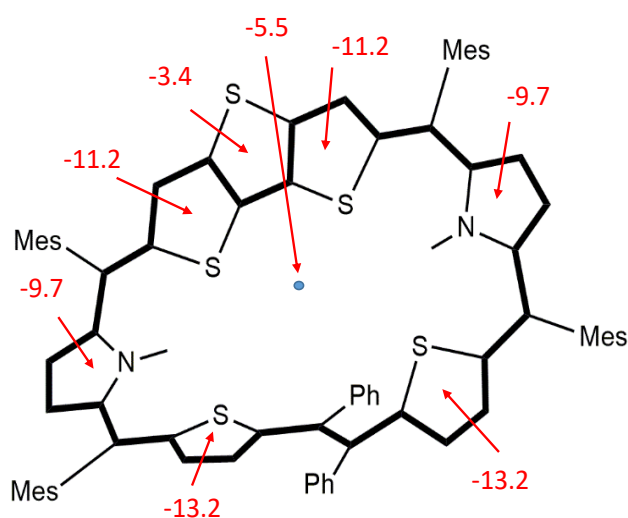


Figure 3.25: NICS (0) values at M06L/6-31G** level $\mathbf{8.2H}^+$.

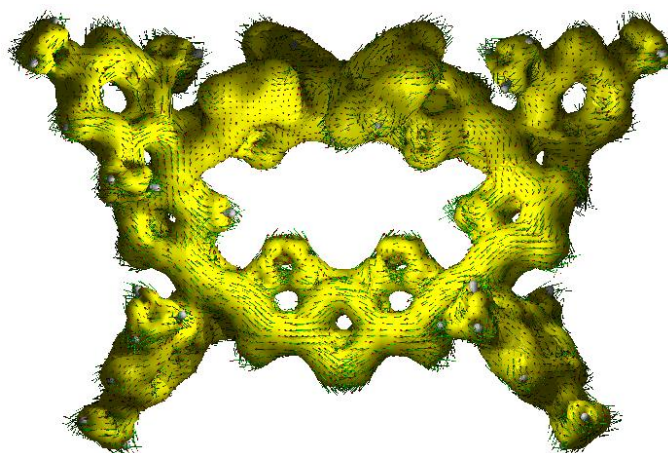


Figure 3.26: AICD plots for $\mathbf{8.2H}^+$ with current density vectors plotted on to isosurface of value 0.026.

The NICS (0) values of **10** calculated for the individual rings show significant variation depending on the nature of the heterocyclic rings. The two pyrrole rings show values of -1.1 ppm and -0.8 ppm in the freebase form, while the other heterocyclic rings showed higher negative ppm values shown in Figure 3.27. The NICS (0) values at the centre of the ring is -2.0 ppm. The AICD plots show a clockwise orientation of current vectors plotted on to isosurface of value 0.026 shown in Figure 3.28.

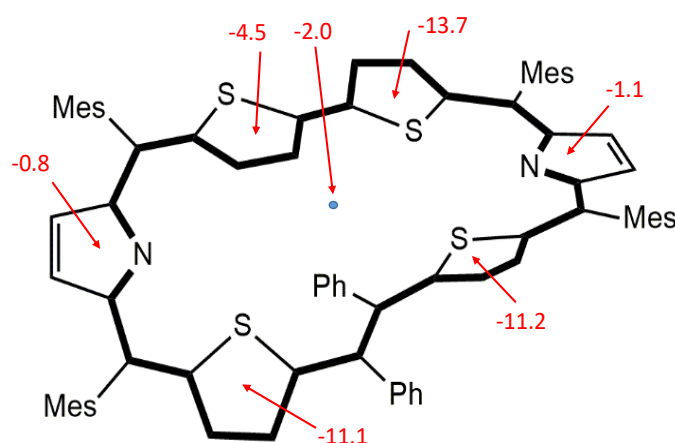


Figure 3.27: NICS (0) values at M06L/6-31G** level **10**.

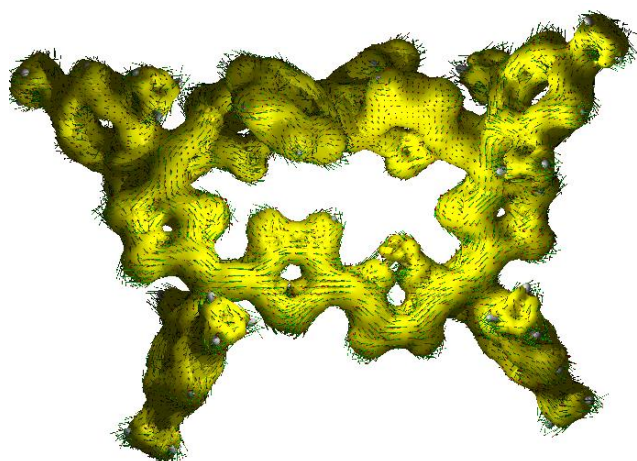


Figure 3.28: AICD plots for **10** with current density vectors plotted on to isosurface of value 0.026.

The NICS (0) values of 10.2H^+ upon protonation calculated for the individual rings show significant variation in the nature of the heterocyclic rings. The two pyrrole rings which showed values of -1.1 ppm and -0.8 ppm in the freebase form, upon protonation the two pyrrole rings showed values of -9.3 ppm and -8.9 ppm while the other heterocyclic rings further shifted to higher negative ppm values shown in Figure 3.29. The NICS (0) values at the centre of the ring is -5.6 ppm. The ACID plots show a clockwise orientation of current vectors plotted on to isosurface of value 0.026 shown in Figure 3.30.

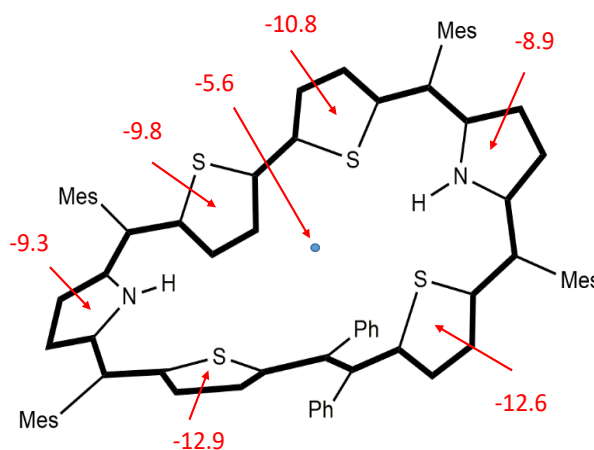


Figure 3.29: NICS (0) values at M06L/6-31G** level 10.2H^+ .

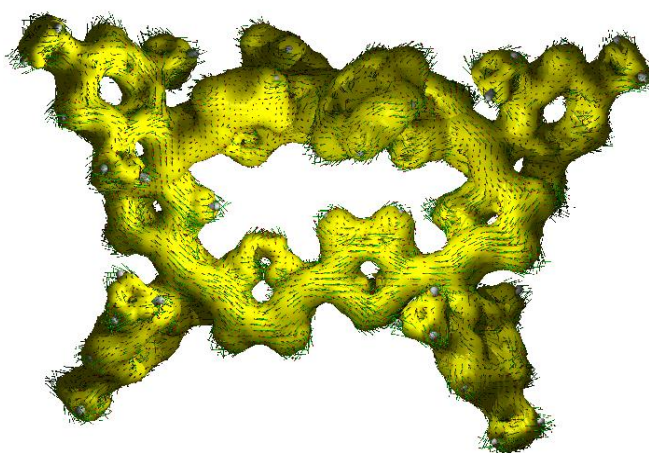


Figure 3.30: ACID plots for 10.2H^+ with current density vectors plotted on to isosurface of value 0.026.

3.3.2.5 Electronic spectral analysis

The UV–Vis spectrum of **6** (Figure 3.31) shows weak broad bands in the region 365–575 nm. The observation of sharp intense absorption band in the UV-visible spectrum of $\mathbf{6.2H^+}$ also justifies aromatic nature of the protonated species with four fold increase in the ϵ values.

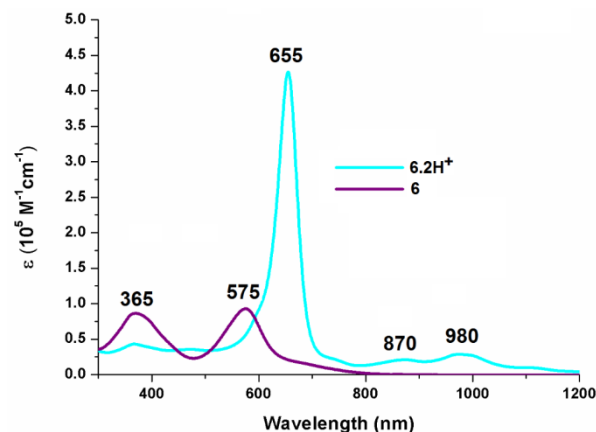


Figure 3.31: The electronic absorption spectra of **6** and $\mathbf{6.2H^+}$ in CH_2Cl_2 .

The UV–Vis spectrum of **8** (Figure 3.32) shows Soret-like broad bands at 542 nm and a split Q-like band at 796 nm. However, upon protonation $\mathbf{8.2H^+}$ there is large red shift of sharp intense Soret-like broad bands at 595 nm and a split Q-like band at 991 nm. The ϵ values also increased almost 1.5 times and sharp bands are indicative of aromatic nature.

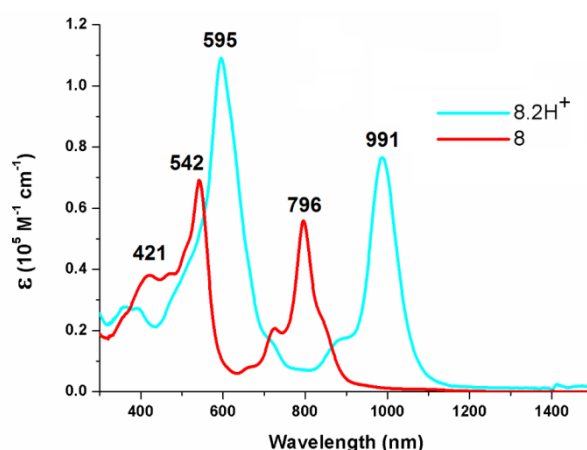


Figure 3.32: The electronic absorption spectra of **8** and $\mathbf{8.2H^+}$ in CH_2Cl_2 .

The UV–Vis spectrum of **10** (Figure 3.33) shows absorption bands where in the Soret-like bands absorb at 554 nm and a split Q-like band at 812 nm. However, upon protonation $10.2H^+$ there is a large red shift of sharp intense Soret-like broad bands at 607 nm and a split Q-like band at 1009 nm. The ϵ values also increased almost 1.5 times and sharp bands are indicative of aromatic nature.

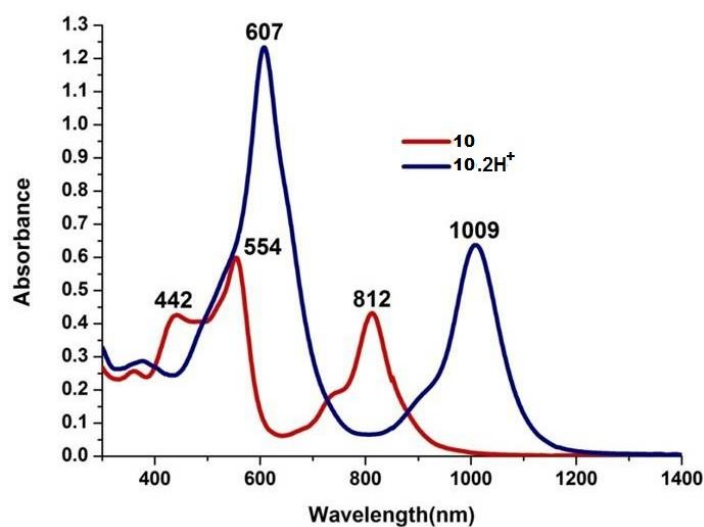


Figure 3.33: The electronic absorption spectra of **10** and $10.2H^+$ in CH_2Cl_2 .

3.4 Conclusion

In conclusion, this study suggests that from a careful design strategy, it is possible to synthesize expanded porphyrin derivatives where their molecular topology can be controlled by choosing appropriate flexible groups in the molecular skeleton. A proton triggers transformation of **6** from a nonaromatic to Hückel aromatic molecule; in **8** nonaromatic to Möbius aromatic; and in **10** moderately to a Möbius aromatic molecule. Understanding intricacies involved in such transformations are important to use them in molecular devices. Studies are in progress in this direction.

3.5 Experimental Procedure

3.5.1 Synthesis of 6

A mixture of 1,2-diphenyl 1,2-dithienyl ethene diol (5) (200 mg, 0.31 mmol) and Pyrrole (21 μ L, 0.31 mmol) were dissolved in 200 ml of dry dichloromethane and the resulting solution was allowed stirring for 15 mins under nitrogen atmosphere. Trifluoroacetic acid (23 μ L, 0.31 mmol) was added and the solution was stirred under nitrogen atmosphere for one hour and further DDQ (210 mg, 1.02 mmol) was added and the mixture was stirred for another one hour in open air condition. After evaporation of solvent compound was purified by column chromatography. A red color band eluted with 42% CH_2Cl_2 :58% hexane considered as desired hexaphyrin (6) with 14% yield.

Compound 6:

^1H NMR (400 MHz, CD_2Cl_2 , 298K): δ (in ppm) = 8.34 (d, 1H, $J=5.0$), 7.34 (d, 2H, $J=6.5$), 7.24 (d, 3H, $J=7.5$), 7.04-7.01 (m, 5H), 6.97 (s, 2H), 6.93 (s, 1H), 6.83 (d, 1H $J=5.0$), 6.65 (d, 1H $J=5.0$), 6.53 (s, 1H), 6.31(d, 2H $J=7.0$), 6.17 (d, 1H $J=4.5$), 2.39 (s, 3H), 2.31 (s, 3H), 2.29 (s, 3H), 2.26 (s, 3H), 2.04 (s, 3H), 1.28 (s, 3H).

^{13}C NMR (101 MHz, CD_2Cl_2 , 298K) δ (in ppm) 206.30, 160.42, 159.91, 153.02, 150.02, 147.10, 145.03, 141.16, 141.12, 140.56, 137.60, 137.53, 137.50, 137.43, 137.09, 136.54, 136.49, 136.31, 135.34, 134.97, 133.23, 132.05, 131.69, 131.24, 131.04, 130.24, 128.75, 127.99, 127.93, 127.67, 127.55, 127.47, 127.27, 127.03, 126.96, 37.08, 31.95, 30.59, 30.04, 29.71, 29.38, 27.07, 22.71, 20.87, 20.38, 20.23, 19.81, 18.55, 13.89.

6·2H⁺: ¹H NMR (400 MHz, CDCl₃) δ (in ppm) = 9.06 (d, 1H), 8.26 (s, 2H), 7.66 (t, J = 7.2 Hz, 2H), 7.59 (d, J = 7.2 Hz, 1H), 7.42 (s, 2H), 2.67 (s, 3H), 2.02 (s, 6H), -0.65 (s, 1H), -1.24 (s, 1H), -4.21(br, NH)

6: UV/Vis (CH₂Cl₂): λ_{\max} in nm (ϵ in dm³mol⁻¹cm⁻¹) = 365 (8.6×10⁴), 575 (9.3×10⁴);
2·2H⁺ (TFA/CH₂Cl₂): λ_{\max} in nm (ϵ in dm³mol⁻¹cm⁻¹) = 655 (4.26×10⁵), 870 (2.8×10⁴), 980 (3.3×10⁴).

3.5.2 Synthesis of **8**

A mixture of DTT-tetrapyrane (**7**) (200 mg, 0.34 mmol) and 1,2-diphenyl 1,2-dithienyl ethene diol (**5**) (216 mg, 0.34 mmol) were dissolved in 200 ml of dry dichloromethane and the resulting solution was allowed stirring for 15 mins under nitrogen atmosphere. Trifluoroacetic acid (26 μ L, 0.34 mmol) was added and the solution was stirred under nitrogen atmosphere for one hour and further DDQ (230 mg, 1.02 mmol) was added and the mixture was stirred for another one hour in open air condition. After evaporation of solvent compound was purified through column chromatography. A red color band eluted with 32% CH₂Cl₂: 68% hexane considered as desire hexaphyrin (**8**) with 10% yield.

Compound 8: ¹H NMR (400 MHz, CD₂Cl₂, 298K): δ (in ppm) 7.50 (d, J = 3.9 Hz, 1H), 7.41 (d, J = 3.9 Hz, 1H), 7.38 (s, 1H), 7.05 (s, 2H), 7.03 (s, 2H), 6.98 (d, J = 4.5 Hz, 1H), 6.76 (m, 3H), 6.66 (d, J = 4.5 Hz, 1H), 6.59 (d, J = 7.3 Hz, 2H), 2.38 (s, 6H), 2.05 (s, 12H).

¹³C NMR (101 MHz, CD₂Cl₂, 298K) δ (in ppm) 163.55, 160.15, 145.86, 143.39, 137.89, 137.79, 137.56, 136.10, 134.53, 130.33, 129.02, 128.25, 127.97, 127.45,

127.09, 122.06, 33.81, 31.93, 31.59, 29.69, 29.50, 29.36, 29.16, 29.00, 22.69, 22.65, 20.94, 20.26, 20.06, 13.88.

8·2H⁺: ¹H NMR (400 MHz, CDCl₃) δ (in ppm) = 9.98 (d, 1H), 9.82 (d, 2H), 9.14 (d, 1H), 8.79 (d, 2H), 8.46 (s, 1H), 8.37 (s, 1H), 7.63 (s, 2H), 7.40 (s, 2H), 6.50 (d, 1H), 6.29 (d, 2H), 2.72 (s, 3H), 2.70 (s, 3H), 2.50 (s, 6H), 1.79 (s, 3H), 1.58 (s, 3H), -0.94 (br, NH). **8**: UV/Vis (CH₂Cl₂): λ_{max} in nm (ε in dm³mol⁻¹cm⁻¹) = 421 (3.8×10⁴), 542 (6.9×10⁴), 796 (5.6×10⁴); **8·2H⁺** (TFA/CH₂Cl₂): λ_{max} in nm (ε in dm³mol⁻¹cm⁻¹) = 595 (1.1×10⁵), 991 (7.6×10⁴).

3.5.3 Synthesis of 10

A mixture of BT-tetrapyrane **9** (200 mg, 0.36 mmol) and 1,2-diphenyl 1,2-dithienyl ethene diol **5** (227 mg, 0.36 mmol) were dissolved in 200 ml of dry dichloromethane and the resulting solution was allowed stirring for 15 mins under nitrogen atmosphere. Trifluoroacetic acid (27 μL, 0.36 mmol) was added and the solution was stirred under nitrogen atmosphere for one hour and further DDQ (242 mg, 1.06 mmol) was added and the mixture was stirred for another one hour in open air condition. After evaporation of solvent compound was purified through column chromatography. A red color band eluted with 30% CH₂Cl₂: 70% hexane considered as desire hexaphyrin (**10**) with 10% yield.

Compound 10: ¹H NMR (400 MHz, CD₂Cl₂, 298K): δ (in ppm) 7.50 (d, *J* = 3.9 Hz, 1H), 7.41 (d, *J* = 3.9 Hz, 1H), 7.38 (s, 1H), 7.05 (s, 2H), 7.03 (s, 2H), 6.98 (d, *J* = 4.5 Hz, 1H), 6.76 (m, 3H), 6.66 (d, *J* = 4.5 Hz, 1H), 6.59 (d, *J* = 7.3 Hz, 2H), 2.38 (s, 6H), 2.05 (s, 12H).

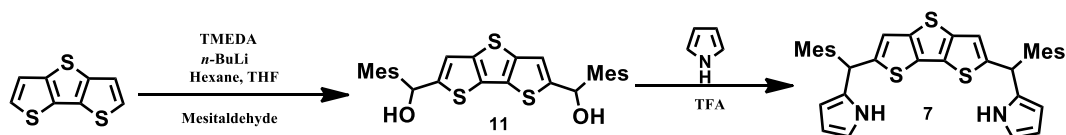
¹³C NMR (101 MHz, CD₂Cl₂, 298K) δ(in ppm) 163.55, 160.15, 145.86, 143.39, 137.89, 137.79, 137.56, 136.10, 134.53, 130.33, 129.02, 128.25, 127.97, 127.45,

127.09, 122.06, 33.81, 31.93, 31.59, 29.69, 29.50, 29.36, 29.16, 29.00, 22.69, 22.65, 20.94, 20.26, 20.06, 13.88.

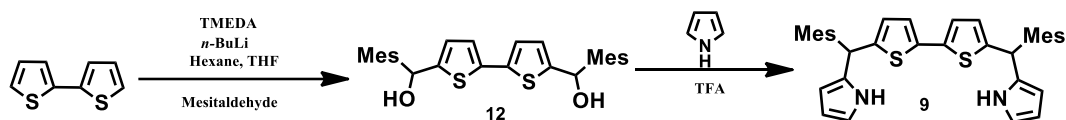
10·2H⁺: ¹H NMR (400 MHz, CDCl₃) δ (in ppm) = 8.22 (d, 2H), 7.98 (d, 2H), 7.74 (d, 2H), 7.58 (d, 2H), 7.42-7.19 (m, 10H), 6.81-6.69 (m, 12H), 2.55 (s, 22H), 2.35 – 2.04 (s, 14H).

10: UV/Vis (CH₂Cl₂): λ_{\max} in nm (ϵ in dm³mol⁻¹cm⁻¹) = 442 (2.5×10⁴), 554 (3.5×10⁴), 812 (2.3×10⁴); **10·2H⁺** (TFA/CH₂Cl₂): λ_{\max} in nm (ϵ in dm³mol⁻¹cm⁻¹) = 607 (7.2×10⁴), 1009 (3.7×10⁴).

3.5.4 Precursor Syntheses



Scheme 3.4: Precursor Syntheses.



Scheme 3.5: Precursor Syntheses.

3.5.4.1 Synthesis of 11

To a solution of N,N,N',N'-tetramethylethylenediamine (TMEDA) (2.3 ml, 15 mmol) in dry THF (40 ml), *n*-butyllithium (10 ml, 1.6 M in hexane, 0.9 mmol) was added followed by dithienothiophene (1 g, 5 mmol) under nitrogen atmosphere. The reaction mixture was stirred at room temperature for 45 min and heated under reflux for another 1h. The reaction mixture was then allowed to attain room temperature slowly. Mesitaldehyde (1.8 ml, 15 mmol) in dry THF was added dropwise to the reaction mixture at 0 °C. The resulting mixture was allowed to stir at room temperature for overnight. The reaction was quenched by using saturated NH₄Cl (100 ml) solution

and extracted with diethyl ether. The crude product was purified by silica gel column chromatography (100-200 mesh). A yellow band was eluted with ethyl acetate/hexane (22:78, V/V) afforded desired diol (**11**) 5,5'-Bis-(mesitylhydroxymethyl)-dithienothiophene as pale yellow color solid with yield of 65%.

^1H NMR (400 MHz, CDCl_3 , 298K): δ (ppm): 6.83 (s, 4H), 6.74 (s, 2H), 6.45 (s, 2H), 2.47 (s, 1H), 2.32(s, 12H), 2.26(s, 6H).

3.5.4.2 Synthesis of **7**

To the diol **11** (0.5 g, 1.01 mmol), pyrrole (3.66 ml, 56.5 mmol) was added. The mixture was degassed by bubbling with nitrogen gas. To this mixture, TFA (0.03 ml 0.38 mmol) was added and the resulting mixture was stirred in dark condition for 30 min in room temperature. After completion of reaction, 100 ml of CH_2Cl_2 was added in open air condition and the mixture was neutralized with 100 ml of 0.1 M NaOH solution. Organic layer was separated, twice washed with water and dried over anhydrous Na_2SO_4 . The solvent and excess pyrrole was removed by vacuum. The crude product was purified by silica gel column chromatography (100-200 mesh) with ethyl acetate/hexane (8:92, V/V) and identified as 5,5'-Bismesityl-2,2'-dithienothiophenetetrapyrane (**7**). Yield: 0.43 g, 90%.

^1H (400 MHz, CDCl_3 , 298K): δ (ppm): 7.85 (br, 2H), 6.85 (s, 4H), 6.65 (d, $J=3.7$ Hz, 2H), 6.62 (s, 2H), 6.16 (d, $J=3.7$ Hz, 2H), 6.03 (d, $J=3.7$ Hz, 2H), 5.99 (s, 2H), 2.27 (s, 12H); 2.12 (s, 6H).

3.5.4.3 Synthesis of **12**

To a solution of N,N,N',N'-tetramethylethylenediamine (TMEDA) (2.7 ml, 18 mmol) in dry THF (40 ml), *n*-butyllithium (11 ml, 1.6 M in hexane, 1 mmol) was added followed by 2,2'-bithiophene (1 g, 6 mmol) under nitrogen atmosphere. The reaction mixture was stirred at room temperature for 45 min and heated under reflux for

another 1h. The reaction mixture was then allowed to attain room temperature slowly. Mesitaldehyde (2.2 ml, 15 mmol) in dry THF was added dropwise to the reaction mixture at 0 °C. The resulting mixture was allowed to stir at room temperature for overnight. The reaction was quenched by using saturated NH₄Cl (100 ml) solution and extracted with diethyl ether. The crude product was purified by silica gel column chromatography (100-200 mesh). A yellow band was eluted with ethyl acetate/hexane (20:80, V/V) afforded desired diol 5,5'-bis-(mesitylhydroxymethyl)-2,2'-bithiophene (**12**) as pale yellow color solid. Yield: 0.74 g, 54%.

¹H NMR (400 MHz, CDCl₃, 298K): δ (ppm): 6.92 (d, *J*=3.7 Hz, 2H), 6.87 (s, 4H), 6.52 (d, 2H), 6.46 (d, *J*=3.7 Hz, 2H), 2.34 (s, 12H), 2.29 (s, 6H).

3.5.4.4 Synthesis of **9**

To diol **12** (0.5 g, 1mmol), pyrrole (3 ml, 43 mmol) and TFA (0.008 ml, 0.1 mmol) under same reaction condition as mentioned for the synthesis of **7**. The crude product was purified by using silica gel column chromatography (100-200 mesh) with ethyl acetate/ hexane (8:92, V/V) and identified as 5,5'-Bismesityl-2,2'-bithiophenetetrapyrane (**9**). Yield: 0.46 g, 94% yield. The synthesis of precursor **5** has been shown in the previous chapter **2**.

¹H NMR (400 MHz, CDCl₃, 298K): δ (ppm): 7.88 (br, 2H), 6.93 (d, 2H), 6.88 (s, 4H), 6.74 (d, 2H), 6.67 (d, 2H), 6.18 (d, 2H), 6.11 (d, 2H), 6.03 (s, 2H), 2.20 (s, 6H), 2.08 (s, 12H).

3.6 References

-
1. (a) T. Tanaka, A. Osuka, *Chem. Rev.* **2017**, *117*, 2584–2640; (b) B. Szyszko, M. J. Białek, E. Pacholska-Dudziak, L. Latos-Grażyński, *Chem. Rev.* **2017**, *117*, 2839-2909; (c) N. Shivran, S. C. Gadekar, V. G. Anand, *Chem. Asian J.* **2017**, *12*, 6-20.
 2. (a) M. Pawlicki, L. Latos-Grażyński, *Chem. Asian J.* **2015**, *10*, 1438–1451; (b) M. Stępień, N. Sprutta, L. Latos-Grażyński, *Angew. Chem. Int. Ed.* **2011**, *50*, 4288-4340; (c) A. Osuka, S. Saito, *Chem. Commun.* **2011**, *47*, 4330-4339; (d) P. M. J. Warner, *Org. Chem.* **2006**, *71*, 9271–9282; (e) E. Pacholska-Dudziak, J. Skonieczny, M. Pawlicki, L. Szterenberg, Z. Ciunik, L. Latos-Grażyński, *J. Am. Chem. Soc.* **2008**, *130*, 6182 – 6195; (f) T. Higashino, J. M. Lim, T. Miura, S. Saito, J. -Y. Shin, D. Kim, A. Osuka, *Angew. Chem. Int. Ed.* **2010**, *49*, 4950-4954; (g) T. Higashino, B. S. Lee, J. M. Lim, D. Kim, A. Osuka, *Angew. Chem. Int. Ed.* **2012**, *51*, 13105-13108.
 3. (a) Y. M. Sung, M. -C. Yoon, J. M. Lim, H. Rath, K. Naoda, A. Osuka, D. Kim, *Nat. Chem.* **2015**, *7*, 418-422; (b) W. -Y. Cha, T. Kim, A. Ghosh, Z. Zhang, X. -S. Ke, R. Ali, V. M. Lynch, J. Jung, W. Kim, S. Lee, S. Fukuzumi, J. S. Park, J. L. Sessler, T. K. Chandrashekar, D. Kim, *Nat. Chem.* **2017**, *9*, 1243-1248.
 4. H. S. Rzepa, *Chem. Rev.* **2005**, *105*, 3697-3715.
 5. (a) D. Ajami, O. Oeckler, A. Simon, R. Herges, *Nature.* **2003**, *426*, 819-821; (b) C. Castro, Z. Chen, C. S. Wannere, H. Jiao, W. L. Karney, M. Mauksch, R. Puchta, N. J. R. v. E. Hommes, P. v. R. Schleyer, *J. Am. Chem. Soc.* **2005**, *127*, 2425-2432; (c) D. Ajami, K. Hess, F. Köhler, C. Näther, O. Oeckler, A. Simon, C. Yamamoto, Y. Okamoto, R. Herges, *Chem. Eur. J.* **2006**, *12*, 5434-5445.
 6. M. Stępień, L. Latos-Grażyński, N. Sprutta, P. Chwalisz, L. Szterenberg, *Angew. Chem. Int. Ed.* **2007**, *46*, 7869-7873.
 7. M. Stępień, B. Szyszko, L. Latos-Grażyński, *J. Am. Chem. Soc.* **2010**, *132*, 3140-3152.
-

-
8. B. Szyszko, N. Sprutta, P. Chwalisz, M. Stępień, L. Latos- Grażyński, *Chem. Eur. J.* **2014**, *20*, 1985-1997.
9. (a) Y. Tanaka, S. Saito, S. Mori, N. Aratani, H. Shinokubo, N. Shibata, Y. Higuchi, Z. S. Yoon, K. S. Kim, S. B. Noh, J. K. Park, D. Kim, A. Osuka, *Angew. Chem. Int. Ed.* **2008**, *47*, 681-684; (b) J. K. Park, Z. S. Yoon, M. -C. Yoon, K. S. Kim, S. Mori, J. -Y. Shin, A. Osuka, D. Kim, *J. Am. Chem. Soc.* **2008**, *130*, 1824-1825; (c) M. Inoue, K. S. Kim, K. S. Suzuki, J. M. Lim, J. -Y. Shin, D. Kim, A. Osuka, *Angew. Chem. Int. Ed.* **2009**, *48*, 6687-6690.
10. S. Saito, J. -Y. Shin, J. M. Lim, K. S. Kim, D. Kim, A. Osuka, *Angew. Chem. Int. Ed.* **2008**, *47*, 9657-9660.
11. A. Ghosh, A. Chaudhary, A. Srinivasan, C. H. Suresh, T. K. Chandrashekar, *Chem. Eur. J.* **2016**, *22*, 3942-3946.
12. S. Xue, D. Kuzuhara, N. Aratani, H. Yamada, *Angew. Chem. Int. Ed.* **2019**, *58*, 12524-12528.
13. (a) E. Ganapathi, W. -Z. Lee, M. Ravikanth, *J. Org. Chem.* **2014**, *79*, 9603-9612; (b) E. Ganapathi, S. Kuilya, T. Chatterjee, M. Ravikanth, *Eur. J. Org. Chem.* **2016**, 282-290.
14. T. K. Chandrashekar, V. Prabhuraja, S. Gokulnath, R. Sabarinathan, A. Srinivasan, *Chem. Commun.* **2010**, *46*, 5915-5917.
15. A. Ghosh, S. Dash, A. Srinivasan, C. H. Suresh, T. K. Chandrashekar, *Chem. Sci.* **2019**, *10*, 5911-5919.
16. J. M. Lim, J. -Y. Shin, Y. Tanaka, S. Saito, A. Osuka, D. Kim, *J. Am. Chem. Soc.* **2010**, *132*, 3105-3114.
17. A. Ghosh, S. Dash, A. Srinivasan, M. S. R. Sahu, C. H. Suresh, T. K. Chandrashekar, *Chem. Eur. J.* **2018**, *24*, 17997-18002.
-

18. (a) T. Higashino, T. Soya, W. Kim, D. Kim, A. Osuka, *Angew. Chem. Int. Ed.* **2015**, *54*, 5456-5459; (b) T. Soya, H. Mori, Y. Hong, Y. H. Koo, D. Kim, A. Osuka, *Angew. Chem. Int. Ed.* **2017**, *56*, 3232-3236.
19. (a) P. v. R. Schleyer, C. Maerker, A. Dransfeld, H. Jiao, N. J. R. van Eikema Hommes, *J. Am. Chem. Soc.* **1996**, *118*, 6317-6318; (b) K. Wolinski, J. F. Hilton, P. Pulay, *J. Am. Chem. Soc.* **1990**, *112*, 8251-8260.
20. R. Herges, D. J. Geuenich, *Phys. Chem.* **2001**, *105*, 3214-3220.

CHAPTER 4

Dithienothiophene fused 30π Heptaphyrin and 34π Octaphyrins: Syntheses, Characterization and Spectral Properties

4.1	Introduction	97
4.2	Objective	98
4.3	Results and Discussion	99
	4.3.1 Syntheses	99
	4.3.2 Spectral characterization	100
	4.3.2.1 Mass spectrometric analysis	100
	4.3.2.2 NMR Analysis	101
	4.3.2.3 Single crystal X-ray analysis	104
	4.3.2.4 Electronic spectral analyses	107
4.4	Conclusion	108
4.5	Experimental Procedure	108
	4.5.1 Synthetic procedure of 10	108
	4.5.2 Synthetic procedure of 12	108
	4.5.3 Precursor Syntheses	111
4.6	References	112

4.1 Introduction

Synthesis of expanded porphyrins¹⁻³ with large π -conjugation is increasingly becoming important because of their potential applications. The applications include; (a) Optoelectronic devices and sensors,^{4,5} (b) Non-linear optical materials,⁶⁻⁸ (c) Sensitizers for PDT^{9,10} and (d) Models for Hückel,^{11,12} Möbius¹³⁻¹⁶ and Baird¹⁷⁻¹⁹ aromaticity. Fusion of one or more pyrrole rings in expanded porphyrins lead to fused macrocycle with altered electronic structure. Such a fusion, not only imparts stability to the macrocycle but also avoids twisting of macrocycle promoting π -electron conjugation.^{20,21} The first report on N-fused Pentaphyrin **1**²² (Figure 4.1) came from Osuka's group introducing the fusion of pyrrole ring through its nitrogen. Later many reports appeared in the literature on N-fused expanded porphyrins.²³⁻²⁵ The fusion without involving pyrrolic nitrogens was reported in a Sapphyrin **2** by C. H. Lee and co-workers.²⁶ We used a rational approach to synthesize singly and doubly fused Rubyrins **3** using DTT (Dithienothiophene) as the fused precursor.²⁷ Our strategy was to induce fusion in the precursor itself before condensation of the macrocycle. The DTT was chosen because of its electron rich rigid core, makes the macrocycle planar thus promoting strong π -electronic conjugation which is required for the optoelectronic applications.^{28,29}

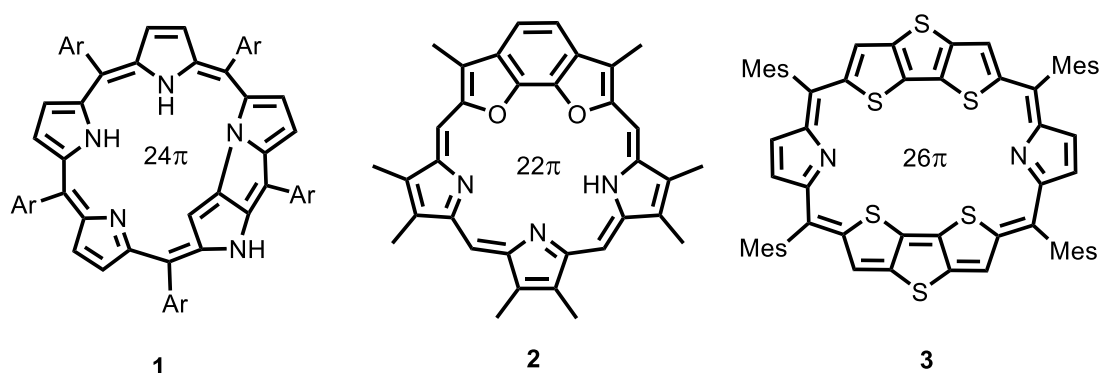


Figure 4.1: Structures of fused expanded porphyrins **1**, **2**, **3**.

4.2 Objective

In this chapter we wish to report syntheses and characterization of two fused expanded porphyrins containing 30π and 34π electrons in conjugation shown in Figure 4.2. It has been shown that 30π Heptaphyrin **6** which has one fused DTT unit, exhibit aromatic characteristics with the selenophene ring opposite to the DTT unit undergoing a 180° ring inversion. The 34π Octaphyrin **7** is completely planar exhibiting large aromaticity in the freebase form. Interestingly upon protonation one of the DTT ring experiences a ring inversion. Eventhough, the ring inversion of small heterocyclic rings like pyrrole, thiophene are well known in the literature,^{30,31} the inversion of a rigid DTT ring is unprecedented in the literature. The easy synthetic methods to prepare expanded porphyrins with large π -electronic conjugation reported here allow one to exploit their rich chemistry and potential applications.

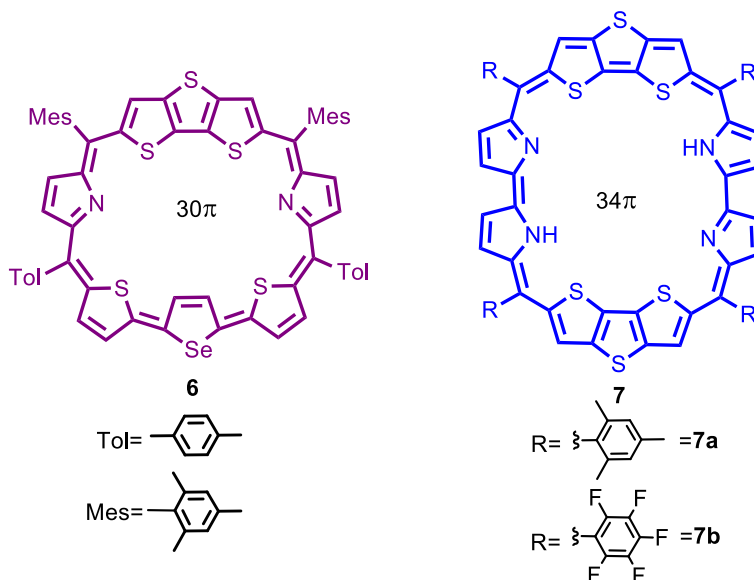
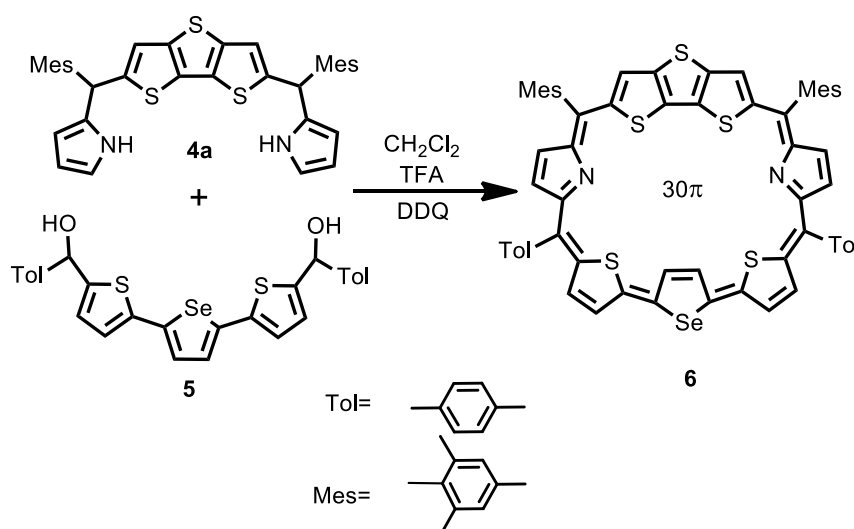


Figure 4.2: Structures of heptaphyrin **6** and octaphyrin **7**.

4.3 Results and Discussion

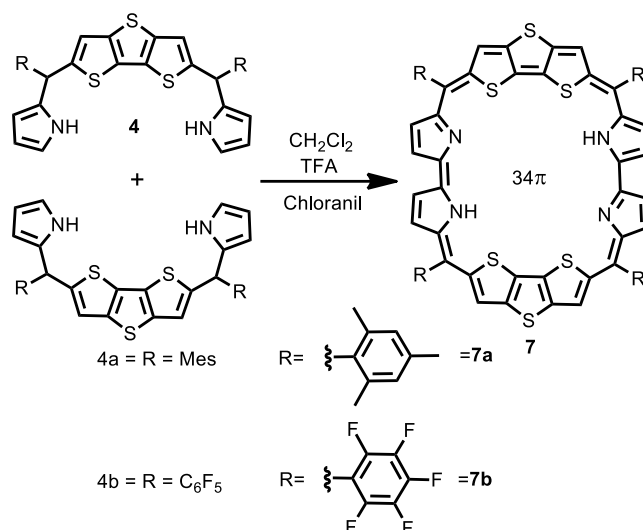
4.3.1 Syntheses

The 30π monofused heptaphyrin **6** was synthesized by the Macdonald type condensation of precursors **4a** (2,6-bis(mesityl(1H-pyrrol-2-yl)methyl)dithieno[3,2-b:2',3'-d]thiophene) with **5** (5,5'-(selenophene-2,5-diyl)bis(thiophene-5,2-diyl))bis(p-tolylmethanol) catalysed by TFA in CH_2Cl_2 . Further oxidation with DDQ gave the expected **6** in 30% yield (Scheme 4.1). The precursors **4a** and **5** were synthesized following the earlier reported procedures.^{32,33}



Scheme 4.1: Synthesis of **6**.

The 34π doubly fused octaphyrin **7a** was synthesized by an oxidative coupling reaction of **4a** (2,6-bis(mesityl(1H-pyrrol-2-yl)methyl)dithieno[3,2-b:2',3'-d]thiophene) with TFA in CH_2Cl_2 followed by DDQ oxidation. **7a** was isolated as bronze colored solid in 3% yield (Scheme 2). For the synthesis of **7b**, we needed the precursor **4b** (2,6-bis((perfluorophenyl)(1H-pyrrol-2-yl)methyl)dithieno[3,2-b:2',3'-d]thiophene) which was synthesized. Subsequently **4b** under oxidative coupling reaction conditions followed by DDQ oxidation gave **7b** in 7% yield (Scheme 4.2)



Scheme 4.2: Synthesis of octaphyrin **7**.

4.3.2 Spectral Characterization

4.3.2.1 Mass Spectroscopic analysis

The composition of **6** was confirmed by ESI mass spectrum which gave a molecular ion peak at m/z 1085.1691 and the composition of **7a** ($m/z = 1171.2836$) and **7b** ($m/z = 1312.1271$) were also confirmed by ESI mass spectrometry shown in Figure 4.3-4.5.

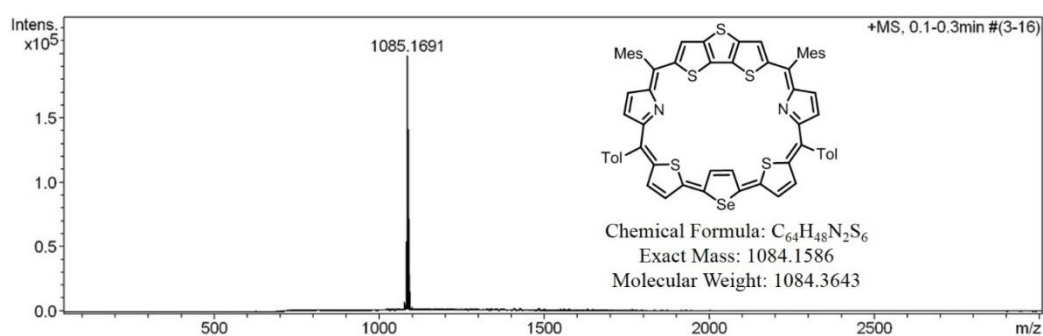


Figure 4.3: ESI Mass spectrum of heptaphyrin **6**.

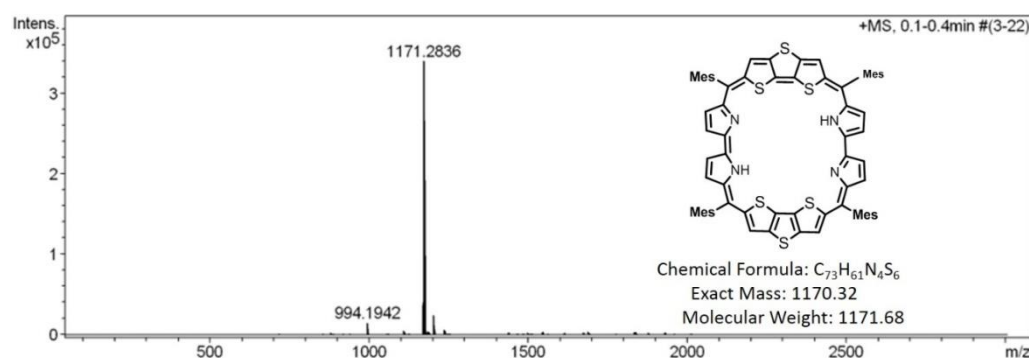


Figure 4.4: ESI Mass spectrum of octaphyrin **7a**.

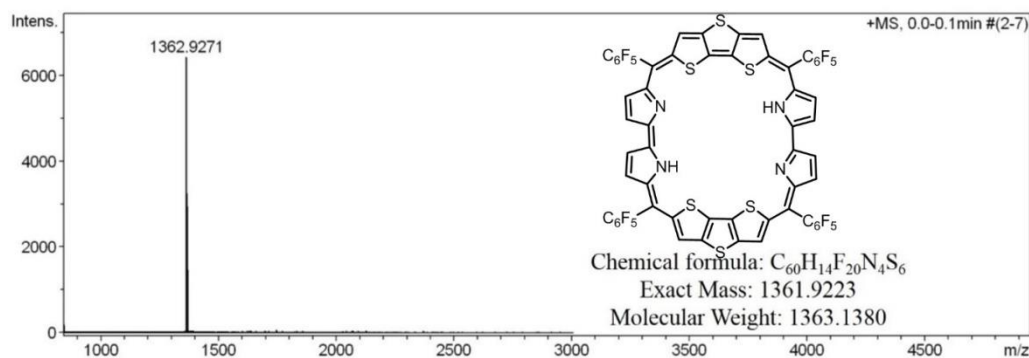


Figure 4.5: ESI Mass spectrum of octaphyrin **7b**.

4.3.2.2 NMR analysis

The ^1H NMR spectra of **6** and its protonated form 6.2H^+ are shown in Figure 4.6a. The DTT proton (*f*) appears as a sharp singlet around 10.70 ppm while the β -CH protons of thiophene ring (*b* and *c*) appear in the region 9.78-10.40 ppm. The pyrrolic β -CH protons (*d* and *e*) resonate in the region 8.80-8.93 ppm. The mesityl and tolyl -CH protons and CH_3 protons appear in their respective region. The chemical shift positions of these ring protons clearly indicate the aromatic nature of **6** in its freebase form. The selenophene ring opposite to the DTT unit in **6** is inverted and the β -CH proton of the inverted selenophene ring (*a*) appears at -0.65 ppm confirming that these protons are experiencing the diatropic ring current of the macrocycle. Protonation of pyrrolic nitrogens leads to small deshielding of ring protons (Figure 4.6b). However, the (*a*) protons of the inverted selenophene ring are highly shielded and appear as a singlet at -3.98 ppm suggesting that the selenophene ring comes in to the plane of the macrocycle upon protonation, exposing the (*a*) protons to the ring current of the macrocycle. The NH protons of the pyrrole rings appear as a broad signal at -6.21 ppm. The assignments marked were based on ^1H - ^1H COSY correlation experiments (Figure 4.7). The large $\Delta\delta$ (difference between the chemical shift of most shielded and

desielded ring protons) value of 15.5 ppm clearly indicate the strong aromaticity of $6.2H^+$.

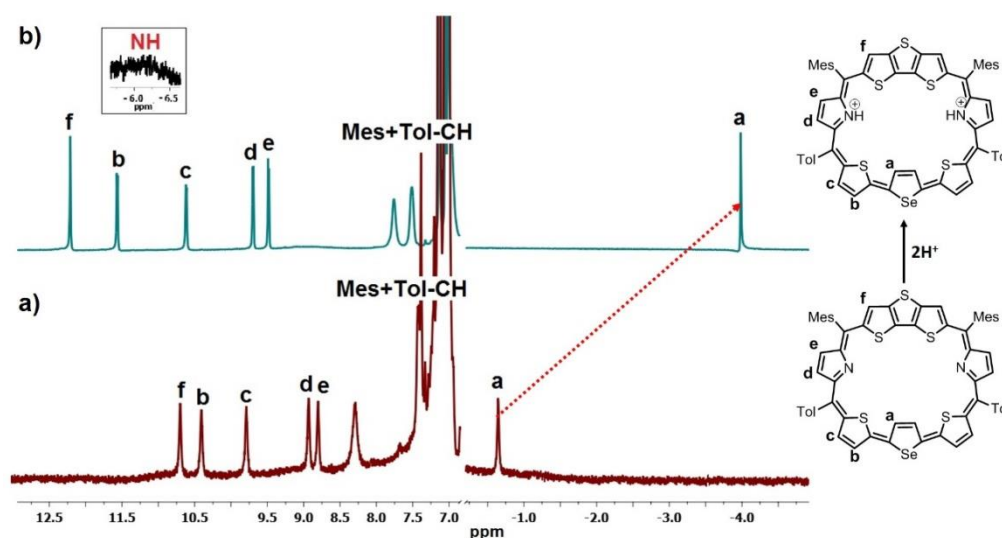


Figure 4.6: 1H NMR spectroscopy of **6(a)** and $6.2H^+$ (**b**) in Toluene d_8 at 298K (Titration with 10^{-1} M TFA solution).

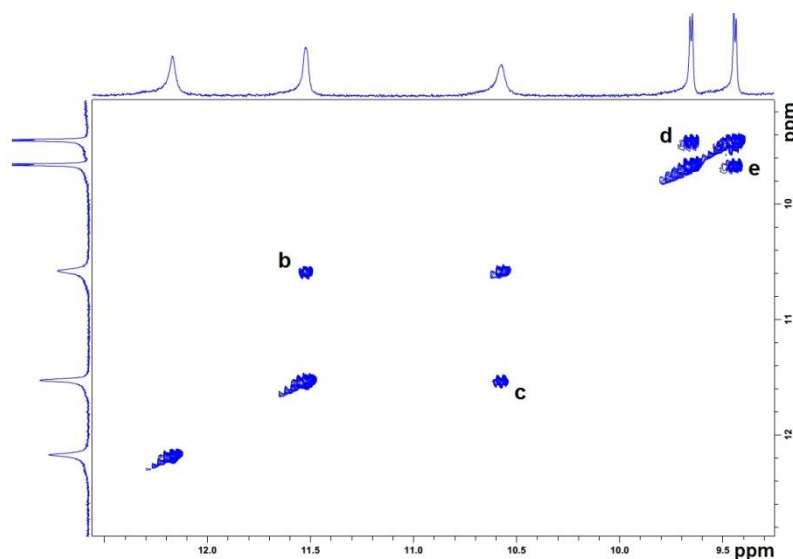


Figure 4.7: 1H - 1H COSY correlation spectroscopy of $6.2H^+$.

The 1H NMR spectra of **7a** and $7b.2H^+$ are shown in Figure 4.8. The symmetric nature of **7a** permits easy interpretation of the spectrum. The protons of two DTT rings are equivalent (**a**) and appear as a singlet at 12.87 ppm. The eight pyrrolic protons (**b** and **c**) appear in the region 11.00-12.00 ppm and mesityl -CH protons

appear as a sharp singlet at 8.21 ppm. The inner pyrrolic NH proton resonates as a broad signal at -1.62 ppm. The $\Delta\delta$ value of 13 ppm clearly suggests the aromatic nature of **7a**. The equivalence of DTT ring protons is indicative of planar nature of the macrocycle. Protonation of pyrrolic nitrogens in **7b** leads to major changes (Figure 4.8b) in the ^1H NMR spectrum. One of the DTT rings experience a ring inversion and the ring protons (**f**) appear at -10.5 ppm as a sharp singlet. On the other hand, the other DTT ring protons which is not inverted (**a**) appear at 12.34 ppm as a sharp singlet. This large difference in the chemical shift of DTT protons clearly reflect the inversion of one of the rings and the protons of inverted rings are exposed to the ring current of the macrocycle, thus experiencing a large shielding. The pyrrole protons (**b** and **c**) appear in the region 10.57-10.55 ppm and (**d** and **e**) at 9.75-10.25 ppm. There are two type of -NH protons and they appear as sharp singlets at -8.12 ppm and -8.27 ppm. The large $\Delta\delta$ value of 18.0 ppm is clearly indicative of the strong π -electron conjugation and hence strong aromaticity of **7b.2H⁺**.

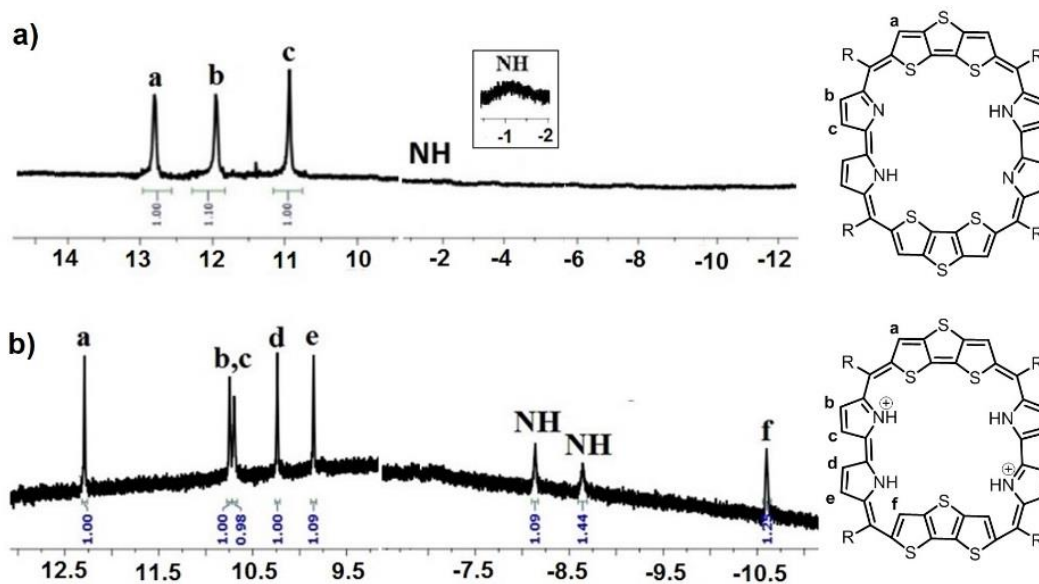


Figure 4.8: ^1H NMR spectroscopy of **7a** (a) and **7b.2H⁺** (b) in CDCl_3 at 298K

(Titration with 10-1 M TFA solution).

4.3.2.3 Single Crystal X-ray analysis

The structure of **7a** was unambiguously confirmed through single crystal X-ray structural analysis (Figure 4.9). The mountable quality crystals were grown by slow diffusion of CH₃CN over CHCl₃ solution at room temperature and were diffracted by using X-rays of Mo source. The compound crystallizes in monoclinic crystal lattice with *P*2₁/*c* space group (Table 4.1). As reflected from the NMR analysis, two units of dithienothiophene (DTT) moieties are connected with four pyrrolic units via four *meso* carbon bridges. The structure is found to be highly planar and with minimal heterocyclic ring deviation. The tilt angles for the corresponding heterocyclic moieties are found to be 2.64° (DTT), 4.47° (imino pyrroles) and 7.10° (amino pyrroles) respectively with respect to the mean macrocyclic plane (C5, C14, C5' and C14'). The *meso* mesityl substituents are nearly perpendicular (87.93°, 77.71°, 87.93° and 77.71) with the mean macrocyclic plane which resembles to the *meso* aryl expanded porphyrinoids. The structural analysis reveals two different type of weak intermolecular hydrogen bonding interaction between i) S3(π) and H30-C30, ii) Mes (π) and H27-C27, generates self assembled dimer and 1D array with distances and angles of i) 3.02Å, 149.78° and ii) 3.04Å, 137.86° (Figure 4.10-4.12).

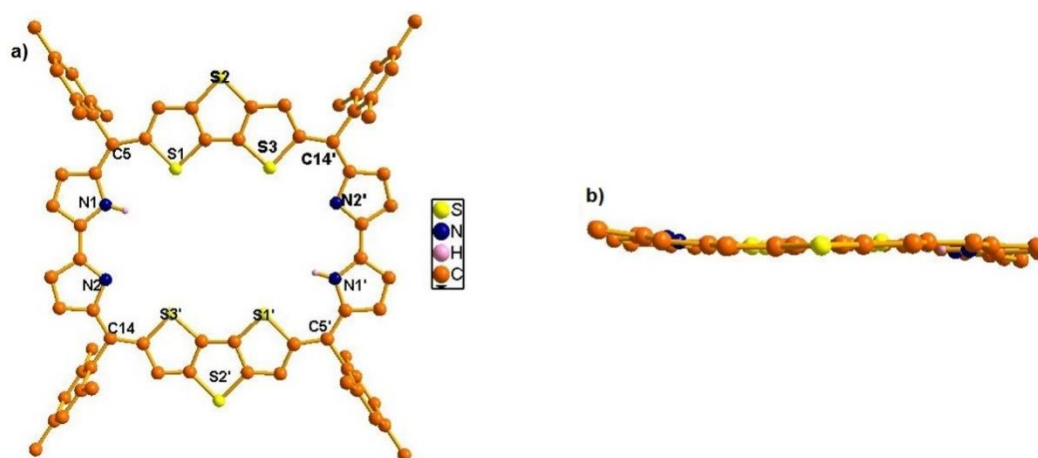


Figure 4.9: Single crystal X-ray structure of **7a** (a) Top View and (b) Side View; hydrogen atoms (a) and *meso* mesityl substituents (b) are omitted for clarity.

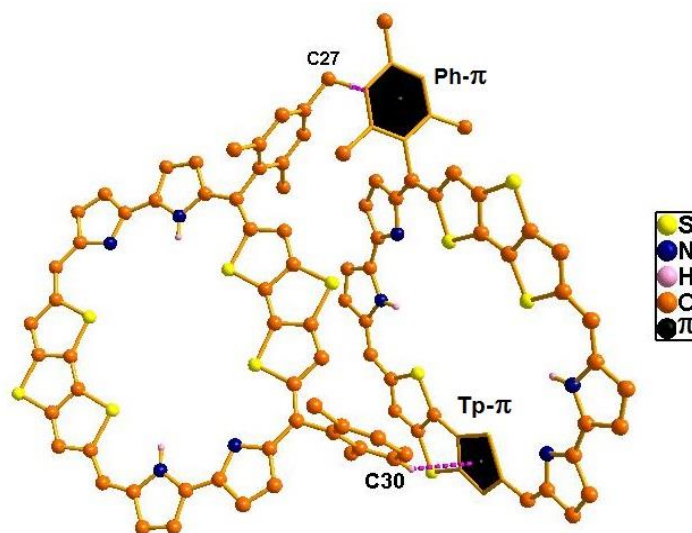


Figure 4.10: Self assembled dimer structure of 7a.

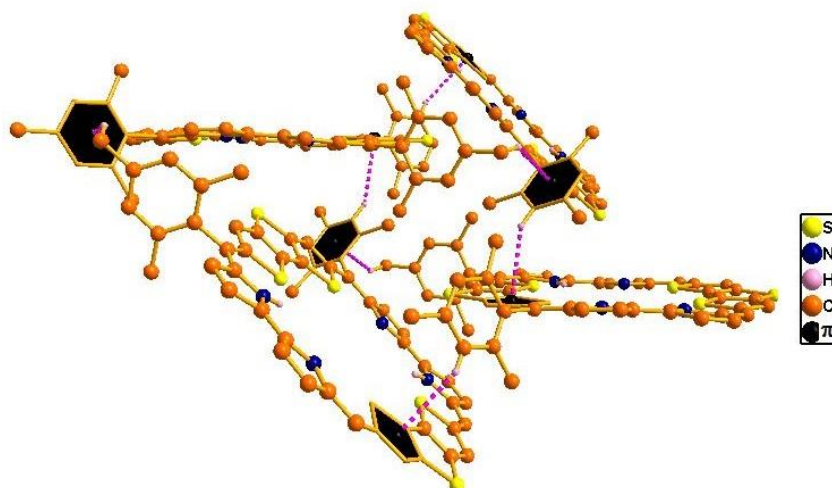


Figure 4.11: One dimension array of 7a.

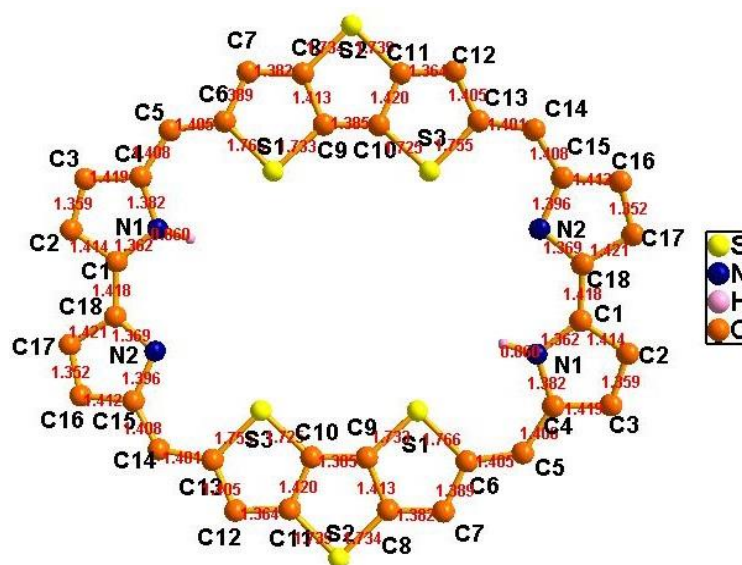


Figure 4.12: Bond distances of 7a.

Table 4.1: Crystal data for **7a**

Crystal code	7a
<i>T</i> , K	100 K
Formula	$C_{72}H_{58}Cl_2N_4S_6$
Formula weight	1171.58
Color and Habit	Dark brown
Crystal system	Monoclinic
Space group	$P2_1/c$
<i>a</i> , Å	13.929(5)
<i>b</i> , Å	16.036(5)
<i>c</i> , Å	16.308(5)
α , deg	90
β , deg	109.199(5)
γ , deg	90
<i>V</i> , Å ³	3440.0(19)
Radiation (λ , Å)	MoK α ($\lambda = 0.71073$)
<i>Z</i>	2
d_{calcd} , g•cm ⁻³	1.131
μ , mm ⁻¹	0.240
<i>F</i> (000)	1228.0
No. of unique reflns	37485
No. of params. refined	6559
GOF on F^2	0.873
<i>R</i> 1 [$I > 2\sigma(I)$]	0.0608
<i>R</i> 1 (all data)	0.1308
$wR2$ (all data)	0.1258

4.3.2.4 Electronic spectral analyses

The UV-Visible spectrum of **6** and its protonated derivative **6.2H⁺** in CH₂Cl₂ (Figure 4.13) shows a split intense Soret type band at 576 nm ($\epsilon = 1.05 \times 10^5 \text{ dm}^3 \text{ mol}^{-1} \text{ cm}^{-1}$) and 613 nm ($\epsilon = 6.58 \times 10^4 \text{ dm}^3 \text{ mol}^{-1} \text{ cm}^{-1}$) followed by a broad Q-like band at 840 nm ($\epsilon = 3.05 \times 10^4 \text{ dm}^3 \text{ mol}^{-1} \text{ cm}^{-1}$). Protonation of **6** leads to red shift of all the bands and the Q-band experience a shift of 178 nm and absorbs at 1018 nm. The red shift observed in the absorption bands is typical of *meso*-aryl expanded porphyrins.²⁷ The high ϵ -values suggest the aromatic nature of **6** and **6.2H⁺**. **7** also exhibits a split Soret type band at 584 nm ($\epsilon = 9.74 \times 10^4 \text{ dm}^3 \text{ mol}^{-1} \text{ cm}^{-1}$) and 624 nm ($\epsilon = 9.63 \times 10^4 \text{ dm}^3 \text{ mol}^{-1} \text{ cm}^{-1}$) for **7a** (Figure 4.14). Upon protonation, the Soret like band became sharper and absorbs at 616 nm ($\epsilon = 1.41 \times 10^5 \text{ dm}^3 \text{ mol}^{-1} \text{ cm}^{-1}$). The sharpening of the Soret type band and intensity increase clearly suggests that the macrocycle is planar and highly aromatic in nature. **7b** also exhibits similar changes upon protonation. Thus, the UV-Visible spectra of both **6** and **7** confirms porphyrinic as well as their aromatic nature.³⁴⁻³⁵

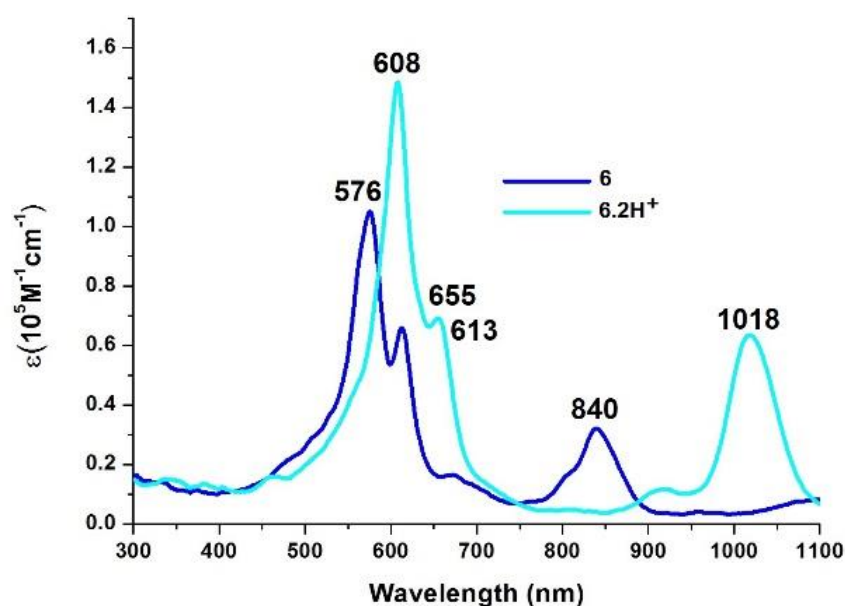


Figure 4.13: Absorption spectra of **6** and **6.2H⁺** (10⁻² M TFA) in CH₂Cl₂.

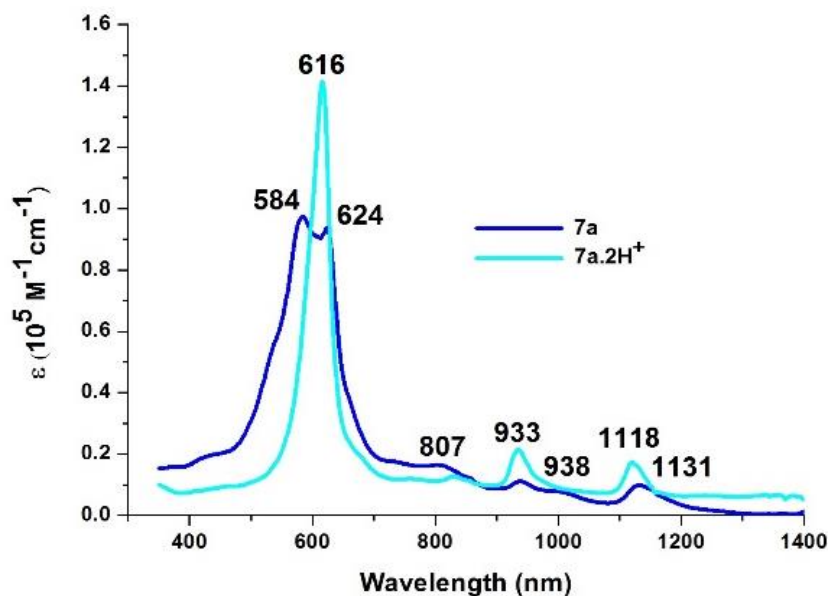


Figure 4.14: Absorption spectra of **7a** and **7a.2H⁺** (10^{-2} M TFA) in CH_2Cl_2 .

4.4 Conclusions

The syntheses of two new fused core-modified expanded porphyrins containing 30π and 34π electrons by an easy and efficient synthetic methodology are reported and are characterized by spectroscopic and single crystal X-ray crystallography. Both 30π heptaphyrin and 34π octaphyrin display aromatic characteristics in freebase and protonated form. This methodology can be applied to synthesize larger expanded porphyrins using appropriate precursors. Studies are in progress to exploit their NLO and Optoelectronic properties.

4.5 Experimental Procedure

4.5.1 Synthesis of **6**:

The precursors **4a** (2,6-Bis(mesityl(1H-pyrrol-2-yl)methyl)dithieno[3,2-b:2',3'-d]thiophene) (200 mg, 0.33 mmol) and **5** (5,5'-(Selenophene-2,5-diyl)bis(thiophene-5,2-diyl))bis(p-tolylmethanol) (119 mg, 0.33 mmol) were dissolved in dry CH_2Cl_2 for 10 min. Excess TFA (26 μl , 0.33 mmol) was added and was stirred for 1 h. 2,3-dichloro-5,6-dicyano-*p*-benzoquinone (DDQ) (230 mg, 1.01 mmol) were added and

stirred in open air for more 1h. Progress of the reaction was monitored by TLC. Purification was done through basic alumina and then again by silica gel column chromatography. The second moving violet band was eluted with CH₂Cl₂/*n*-Hexane (32:68, V/V) and identified as heptaphyrin (**6**).

6: ¹H NMR (400 MHz, Tol-D8, 298K): δ (in ppm) = 10.70 (s, 1H), 10.40 (d, 1H, *J*=2.8), 9.78 (d, 1H, *J*=2.8), 8.93 (d, 1H, *J*=3.6), 8.80 (d, 1H, *J*=3.6), 8.28 (m, 2H), 7.42-7.39 (m, 5H), 2.65 (s, 3H), 2.43 (s, 3H), 2.24 (s, 6H), -0.67 (s, 1H).

6·2H⁺: ¹H NMR (400 MHz, Tol-D8) δ (in ppm) = 12.21 (s, 1H), 11.57 (d, 1H, *J*=2.8), 10.62 (d, 1H, *J*=2.8), 9.70 (d, 1H, *J*=3.2), 9.49 (d, 1H, *J*=3.2), 7.76-7.51 (m, 4H), 6.98 (m, 3H), -3.76 (s, 1H), 2.75 (s, 3H), 2.55 (s, 3H), 1.99 (s, 6H), -6.21 (br, NH).

6: UV/Vis (CH₂Cl₂): λ_{max} in nm (ε in dm³mol⁻¹cm⁻¹) = 576 (1.1×10⁵), 613 (0.7×10⁵), 840 (0.3×10⁵).

6·2H⁺ (TFA/CH₂Cl₂): λ_{max} in nm (ε in dm³mol⁻¹cm⁻¹) = 608 (1.5×10⁵), 655 (0.7×10⁵), 1018 (0.7×10⁵).

4.5.2 Synthesis of **7**:

The C-C oxidative coupling of **4a** (2,6-Bis(mesityl(1H-pyrrol-2-yl)methyl)dithieno[3,2-b:2',3'-d]thiophene) (200 mg, 0.33 mmol) was dissolved in dry CH₂Cl₂ for 10 min. TFA (26μl, 0.33 mmol) was added and stirred for 1h. 2,3-dichloro-5,6-dicyano-*p*-benzoquinone (DDQ) (230 mg, 1.01 mmol) was added and then was stirred for more 1h in open air. Reaction was monitored by TLC. Residue was purified by basic alumina further by silica gel column chromatography. The first moving bluish band with CH₂Cl₂/*n*-Hexane (40:60, V/V) and identified as cyanopentapyrrane (**7a**). After evaporation it gave bronze color solid. **7b** was made under same synthetic procedure with **4b**.

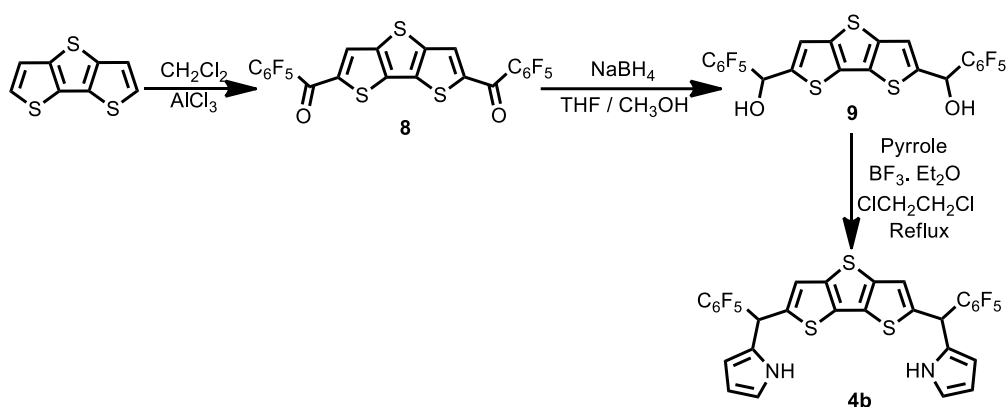
7a: ^1H NMR (400 MHz, CDCl_3 , 298K): δ (in ppm) = 12.87 (s, 1H), 11.98 (d, 1H, $J=2.8$), 11.01 (d, 1H, $J=2.8$), 8.17 (s, 2H), 3.51 (s, 3H), 2.45 (s, 6H), -1.62 (br, NH).

7b·2H $^+$: ^1H NMR (400 MHz, CDCl_3) δ (in ppm) = 12.27 (s, 1H), 10.78 (d, 1H, $J=2.2$), 10.62 (d, 1H, $J=2.2$), 10.23 (d, 1H, $J=3.2$), 9.82 (d, 1H, $J=3.2$), -8.27 (br, NH), -8.12 (br, NH), -10.43 (s, 1H).

7a: UV/Vis (CH_2Cl_2): λ_{max} in nm (ϵ in $\text{dm}^3\text{mol}^{-1}\text{cm}^{-1}$) = 584 (0.97×10^5), 624 (0.95×10^5), 807 (0.19×10^5), 938 (0.13×10^5), 1131 (0.12×10^5).

7a·2H $^+$ (TFA/ CH_2Cl_2): λ_{max} in nm (ϵ in $\text{dm}^3\text{mol}^{-1}\text{cm}^{-1}$) = 616 (1.46×10^5), 933 (0.27×10^5), 1118 (0.22×10^5).

4.5.3 Precursor synthesis



Scheme 4.3: Syntheses of **8**, **9**, **4b**.

Synthesis of 8:

To a 250 ml two-necked round bottom flask, anhydrous AlCl_3 (10 g, 75 mmol) was mixed with 30 ml of dry CH_2Cl_2 and the resultant suspension was stirred for 15 min. A solution of dithieno[3,2-b:2',3'-d]thiophene (6 g, 71 mmol) and pentafluorobenzoyl chloride (10 g, 75 mmol) with 25 ml dry CH_2Cl_2 was added slowly with syringe, over a period of 3.5 h. The resultant solution was stirred for overnight at ambient temperature. The mixture was refluxed for 2 h, cooled and extracted with diethyl ether. The layer was washed with Na_2CO_3 solution. Evaporation of the solvent, leads

to the product **8**. Yield: 6.3 g, 80%. ^1H NMR (400 MHz, CH_2Cl_2) δ (in ppm) = 8.09 (s, 1H).

Synthesis of **9**:

NaBH_4 (2.06 g, 54.6 mmol) was added in several portion to the solution of **8** (2 g, 5.5 mmol) in 50 ml (7:3) THF/ CH_3OH mixture under N_2 atmosphere in ice condition and was allowed to stirred for 2 h. Then the reaction mixture was quenched with water and the compound was extracted with CH_2Cl_2 , dried over Na_2SO_4 and concentrated by rotary evaporator. Compound was purified by recrystallization in $\text{CH}_2\text{Cl}_2/n$ -hexane to afford white crystalline compound **9** in 90% Yield. ^1H NMR (400 MHz, CH_2Cl_2) δ (in ppm) = 7.10 (s, 1H), 6.37 (s, 1H).

Synthesis of **4b**:

DTT Pentafluorobenzoyl-diol (**9**) (0.5 g, 0.85 mmol) pyrrole (2.94 ml, 42.5 mmol) were dissolved in 20 ml of dry $\text{C}_2\text{H}_4\text{Cl}_2$ and the resultant mixture was degassed by bubbling of nitrogen gas. To this solution $\text{BF}_3 \cdot \text{Et}_2\text{O}$ (0.45 ml 8.5 mmol) was added and the resulting mixture was refluxed under dark condition for about 4 h. After completion of reaction 100 ml dichloromethane was added in open air condition and the resulting solution was neutralized with 100 ml of 0.1 M NaOH solution. Organic layer was separated and washed with water two times. The solvent and the excess pyrrole were removed. Purification was done through silica gel with ethyl acetate/hexane (12:88 V/V) afforded desired tetrapyrane (**4b**) with 90% yield. ^1H NMR (400 MHz, CH_2Cl_2) δ (in ppm) = 8.32 (br, 1H, NH), 7.75 (s, 1H), 6.95 (d, 1H), 6.82 (d, 1H), 6.72 (d, 1H), 6.05 (s, 1H).

4.6 References

1. S. Saito, A. Osuka, *Angew. Chem. Int. Ed.* **2011**, *50*, 4342-4373.
2. J. L. Sessler, D. Seidel, *Angew. Chem. Int. Ed.* **2003**, *42*, 5134-5175.
3. M. Stępień, N. Sprutta, L. Latos-Grażyński, *Angew. Chem. Int. Ed.* **2011**, *50*, 4288-4340.
4. J. L. Sessler, A. Gebauer, S. J. Weghorn, in the *Porphyrin Handbook*, ed. K. M. Kadish, K. M. Smith, R. Guilard, vol. 2. Academic press: San Diego, **1999**, 55-124.
5. H. Rath, J. Sankar, V. Prabhuraja, T. K. Chandrashekar, A. Nag, D. Goswami, *J. Am. Chem. Soc.* **2005**, *127*, 11608-11609.
6. A. Chaudhary, A. Srinivasan, T. K. Chandrashekar, *The Handbook of Porphyrin Science*, K.M. Kadish, K.M. Smith R. Guilard vol. 32. World scientific Ltd: **2014**, 271-366.
7. J. -Y. Shin, K. S. Kim, M. -C. Yoon, J. M. Lim, Z. S. Yoon, A. Osuka, D. Kim, *Chem. Soc. Rev.* **2010**, *39*, 2751-2767.
8. J. M. Lim, Z. S. Yoon, J. -Y. Shin., K. S. Kim, M. -C. Yoon, D. Kim, *Chem. Commun.* **2009**, 261-273.
9. B. Marydasan, B. Madhuri, S. Cherukommu, J. Jose, M. Viji, S.C. Karunakaran, T. K. Chandrashekar, K. S. Rao, C. M. Rao, D. Ramaiah *J. Med. Chem.* **2018**, *61*, 5009-5019.
10. T. Wang, D. Zhu, G. Liu, W. Tao, W. Cao, L. Zhang, L. Wang, H. Chen, L. Mei, L. Huang, X. Zeng, *RSC Adv.* **2015**, *5*, 50617-50627.
11. Y. M. Sung, J. Oh, W. -Y. Cha, W. Kim, J. M. Lim, M. -C. Yoon, D. Kim, *Chem. Rev.* **2017**, *117*, 2257-2312.

-
12. M. Ménand, M. Sollogoub, B. Boitrel, S. Le Gac, *Angew. Chem. Int. Ed.* **2016**, *55*, 297-301.
13. A. Ghosh, S. Dash, A. Srinivasan, M. S. R. Sahu, C. H. Suresh, T. K. Chandrashekar, *Chem. Eur. J.* **2018**, *24*, 17997-18002.
14. A. Ghosh, A. Chaudhary, A. Srinivasan, C. H. Suresh, T. K. Chandrashekar, *Chem. Eur. J.* **2016**, *22*, 3942-3946.
15. S. Saito, J. –Y. Shin, J. M. Lim, K. S. Kim, D. Kim, A. Osuka, *Angew. Chem. Int. Ed.* **2008**, *47*, 9657-9660.
16. M. Stępień, L. Latos-Grażyński, N. Sprutta, P. Chwalisz, L. Szterenberga, *Angew. Chem. Int. Ed.* **2007**, *46*, 7869-7873.
17. N. C. Baird, *J. Am. Chem. Soc.* **1972**, *94*, 4941-4948.
18. Y. M. Sung, M. –C. Yoon, J. M. Lim, H. Rath, K. Naoda, A. Osuka, D. Kim, *Nat. Chem.* **2015**, *7*, 418-422.
19. W. –Y. Cha, T. Kim, A. Ghosh, Z. Zhang, X. –S. Ke, R. Ali, V. M. Lynch, J. Jung, W. Kim, S. Lee, S. Fukuzumi, J. S. Park, J. L. Sessler, T. K. Chandrashekar, D. Kim, *Nat. Chem.* **2017**, *9*, 1243-1248.
20. P. K. Panda, Y. –J. Kang, C. –H. Lee, *Angew. Chem. Int. Ed.* **2005**, *44*, 4053-4055.
21. D. Firmansyah, S. J. Hong, R. Dutta, Q. He, J. Bae, H. Jo, H. Kim, K. M. Ok, V. M. Lynch, H. R. Byon, J. L. Sessler, C. –H. Lee, *Chem. Eur. J.* **2019**, *25*, 3525-3531.
22. J. –Y. Shin, H. Furuta, A. Osuka, *Angew. Chem. Int. Ed.* **2001**, *40*, 619-621.
23. M. Suzuki, R. Taniguchi, A. Osuka, *Chem. Commun.* **2004**, 2682-2683.
24. H. Hata, Y. Kamimura, H. Shinokubo, A. Osuka, *Org. Lett.* **2006**, *8*, 1169-1172.
-

-
25. H. Mori, N. Aratani, A. Osuka, *Chem. Asian J.* **2012**, *7*, 1340-1346.
26. D. -G. Cho, P. Plitt, S. K. Kim, V. M. Lynch, S. -J. Hong, C. -H. Lee, J. L. Sessler, *J. Am. Chem. Soc.* **2008**, *130*, 10502-10503.
27. T. K. Chandrashekar, V. Prabhuraja, S. Gokulnath, R. Sabarinathan, A. Srinivasan, *Chem. Commun.* **2010**, *46*, 5915-5917.
28. J. Frey, A. D. Bond, A. B. Holmes, *Chem. Commun.* **2002**, 2424-2425.
29. R. P. Ortiz, M. C. R. Delgado, J. Casado, V. Hernandez, O. -K. Kim, H. Y. Woo, J. T. Lopez Navarrete, *J. Am. Chem. Soc.* **2004**, *126*, 13363-13376.
30. G. Karthik, A. Srinivasan, T. K. Chandrashekar, *Org. Lett.* **2014**, *16*, 3472-3475.
31. R. Kumar, R. Misra, T. K. Chandrashekar, *Org. Lett.* **2006**, *8*, 4847-4850.
32. G. Karthik, J. M. Lim, A. Srinivasan, D. Kim, T. K. Chandrashekar, *Chem. Eur. J.* **2013**, *19*, 17011-17020.
33. H. Rath, V. Prabhuraja, T. K. Chandrashekar, A. Nag, D. Goswami, B. S. Joshi, *Org. Lett.* **2006**, *8*, 2325-2328.
34. T. Sarma, G. Kim, S. Sen, W. -Y. Cha, Z. Duan, M. D. Moore, V. M. Lynch, Z. Zhang, D. Kim, J. L. Sessler, *J. Am. Chem. Soc.* **2018**, *140*, 12111-12119.
35. V. G. Anand, S. K. Pushpan, S. Venkatraman, A. Dey, T. K. Chandrashekar, B. S. Joshi, R. Roy, W. Teng, K. R. Senge, *J. Am. Chem. Soc.* **2001**, *123*, 8620-8621.

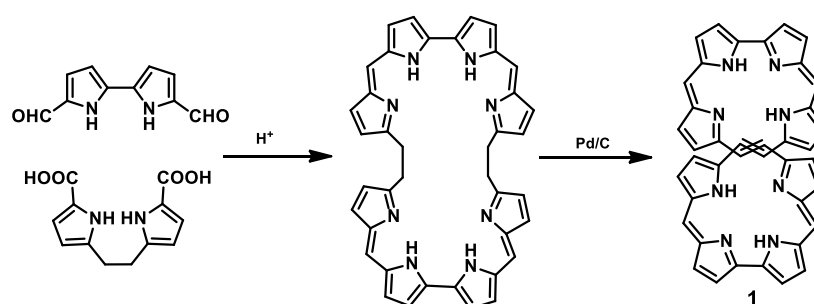
CHAPTER 5

Two non-identical twins in one unit cell: characterization of 34π aromatic core-modified octaphyrins, their structural isomers and anion bound complexes

5.1	Introduction	117
5.2	Objective	120
5.3	Results and Discussion	122
5.3.1	Syntheses	122
5.3.2	Spectral Characterization	123
5.3.2.1	Mass spectrometric analysis	123
5.3.2.2	NMR Analysis	125
5.3.2.3	Difference in Chemical shifts($\Delta\delta$)	136
5.3.2.4	Single crystal X-ray analysis	137
5.3.2.5	NICS(0) Calculation and ACID Plots	144
5.3.2.6	DFT Calculations	150
5.3.2.7	Electronic spectral analysis	151
5.4	Conclusion	154
5.5	Experimental Procedure	155
5.5.1	Synthesis of 16	155
5.5.2	Synthesis of 17	156
5.5.3	Synthesis of 18	157
5.5.4	Synthesis of 19	158
5.5.5	Precursor Synthesis	158
5.5.5.1	Synthesis of 20a	159
5.5.5.2	Synthesis of 21	159
5.5.5.3	Synthesis of 22	160
5.5.5.4	Synthesis of 23	160
5.5.5.5	Synthesis of 24	161
5.5.5.6	Synthesis of 25	161
5.6	Reference	162

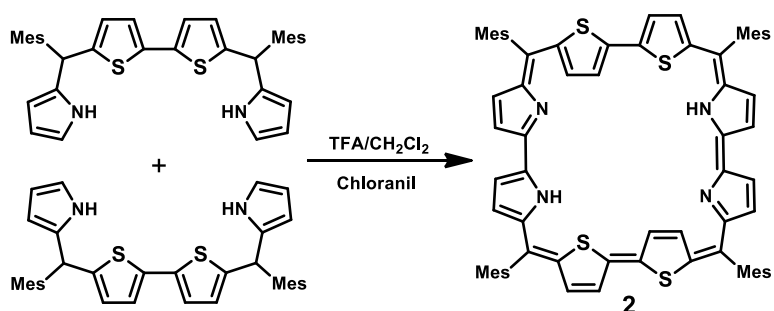
5.1 Introduction

Octaphyrin contains eight pyrrole rings and the pyrrole rings are connected in a cyclic fashion via *meso* carbon bridges and/ or with some direct pyrrole-pyrrole links.¹ Octaphyrins because of its larger size are known to be conformationally flexible and can to adopt twisted figure-eight,² dumbbell,³ aromatic planar,⁴ antiaromatic planar⁵ conformations. Attainment of figure-eight conformation shown in Scheme 5.1 in **1** results in loss of aromaticity.⁶



Scheme 5.1: Synthesis of figure-eight octaphyrin.

Various synthetic approaches have been adopted to synthesize planar aromatic octaphyrins. Perusal of an approach by substituting sterically bulkier mesityl groups at the *meso* positions to restrict twist of the macrocycle to synthesize **2**⁴ which is a 34π planar aromatic core-modified Octaphyrin shown in Scheme 5.2.



Scheme 5.2: Synthesis of Octaphyrin **2**.

Later Osuka and co-workers followed a bridging approach shown in Figure 5.1 to tie a bridge across the *meso* carbons to avoid twisting and were successful in

synthesizing **3** which turned out to be non-aromatic.⁷ Later, we used a similar bridging approach to synthesize 34π aromatic bridged octaphyrin **4**.⁸

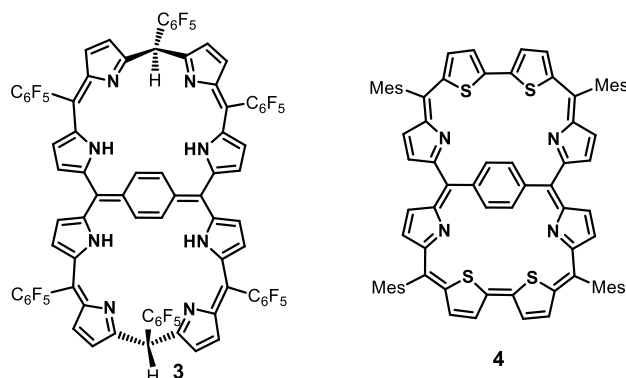


Figure 5.1: Structures of bridged octaphyrins **3** and **4**

Structural isomers of porphyrins such as porphycene,⁹ corphycene,¹⁰ hemiporphycene¹¹ and N-confused porphyrins¹² and their diverse chemistry have been well documented in literature.¹³⁻¹⁵ However, there are only limited reports on the structural isomers of expanded porphyrins in general and octaphyrins in particular.

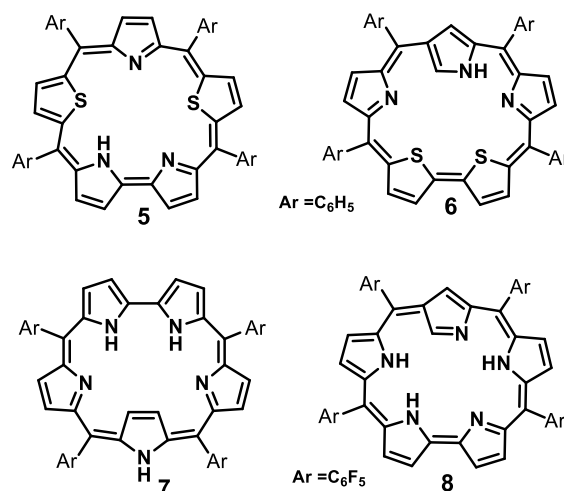


Figure 5.2: Structures of isomers of pentaphyrin.

Latos-Grażyński and co-workers reported the first synthesis of core-modified sapphyrin **5**.¹⁶ Later, Chandrashekar and coworkers reported synthesis of **5** and along with Furuta demonstrated the synthesis of its N-confused isomer **6**.¹⁷ In 2008, Furuta reported all aza N-confused sapphyrin **8**¹⁹ which is a structural isomer of **7**¹⁸ in

which one of the pyrrole ring has a β -connectivity as shown in Figure 5.2. The structural isomers of hexaphyrins singly, doubly and triply N-confused hexaphyrins **9**,²⁰ **10**²¹ and **11**²² respectively was reported by Furuta and Xie in 2009 shown in Figure 5.3.

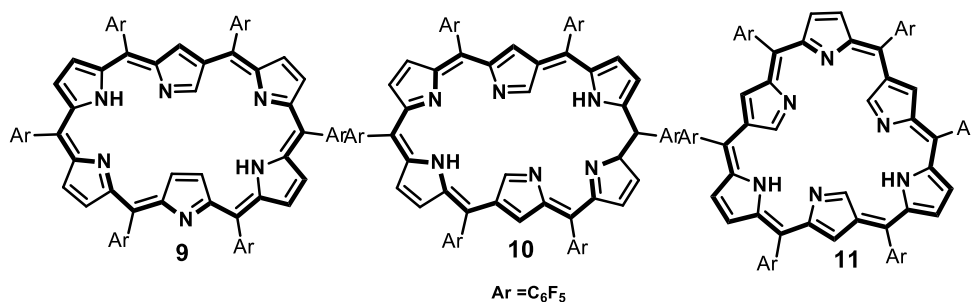


Figure 5.3: Structures of N-confused hexaphyrin.

We have characterized two conformers of heptaphyrin **12** and **13** shown in Figure 5.4.²³ Furthermore, existence of two tautomers of **12** where pyrrole NH proton is exchanging between imine and amine pyrrolic nitrogens were structurally characterized by our group.⁴ Recently, Furuta and Xie reported synthesis of neo-confused octaphyrin which is an isomer of all aza figure-eight octaphyrin.²⁴ More recently, Ishida and Furuta reported synthesis of doubly N-confused 36π octaphyrin which exhibit isomerization between figure-eight **14** and dumbbell **15** structures.³ However, upon bis-metallation only figure-eight structure is stabilized relative to dumbbell structure. In all the above examples the structural isomers have been independently synthesized by various synthetic routes and their chemistry has been reported. The brief literature survey, described above clearly reveal that the characterization of structural isomers of expanded porphyrins in general and octaphyrins in particular is in its infancy and more studies are needed to understand the structural diversity of expanded porphyrins to exploit their rich and diverse

chemistry.²⁵ Recently, we and others have shown that aromatic octaphyrins are good NLO materials²⁶ as well as they exhibit Bicyclic Baird type aromaticity.²⁷

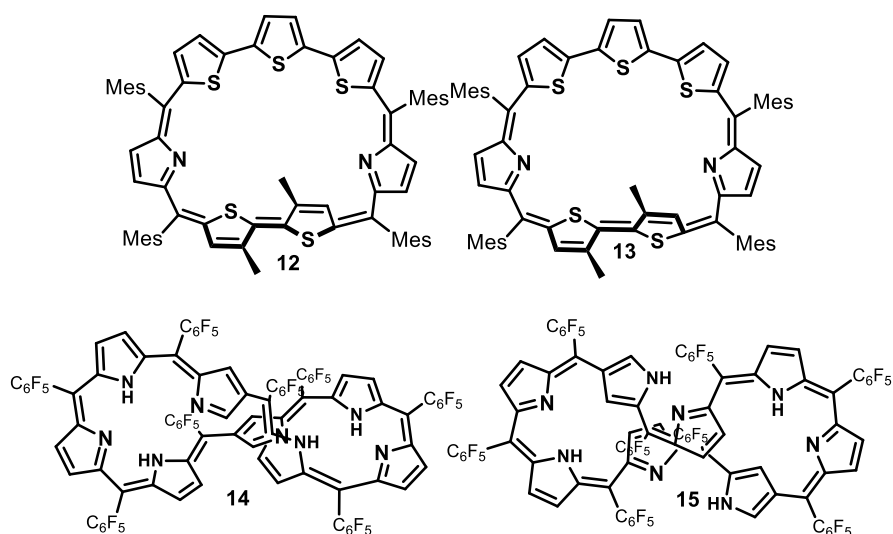


Figure 5.4: Structures of conformers of Heptaphyrin.

5.2 Objective

In this chapter we show new structural isomers of core-modified octaphyrins of 34π where rotational isomerism is shown through C-C bond rotation. Aromatic modified octaphyrins of 34π electrons in conjugation are synthesized by varying hetero atom present in the core shown in Figure 5.5. Four different core-modified planar 34π octaphyrins (**16**, **17**, **18**, **19**) which exhibit rotational isomerism have been synthesized and characterized both in solution and solid state. Octaphyrins; **16**, **17** and **18** show two inseparable isomers **A** and **B** which crystallize in the same unit cell. However, **19** forms one isomers of **A**. Structurally, the two isomers (**A** and **B**) are different only in the ring inversion of one of the thiophene or selenophene rings present in the terthiophene subunit of the macrocycle. In isomer **A**, the middle thiophene or selenophene rings are inverted while in isomer **B**, the terminal thiophene rings are inverted. ^1H NMR spectrum of these macrocycles shows peaks assignable to protons of both the isomers in toluene D_8 . The single crystal structure analysis of **16** reveals

the presence of both isomers **16A** and **16B** in a single unit cell with $P2_1/n$ space group. Both the isomers exhibit aromatic behaviour in the freebase forms. Protonation of pyrrole nitrogens leads to exclusive formation of isomer **B** for **16** and **17**. However, both the isomers are present upon protonation of **18** where the central heterocyclic ring of terthiophene subunits has thiophene and selenophene rings. Octaphyrin **19** crystallizes in $P2_1/c$ space group and exclusively isomer **A** was formed in the reaction. Protonation of pyrrole nitrogens leads to significant increases in aromaticity as revealed by ^1H NMR chemical shift data.

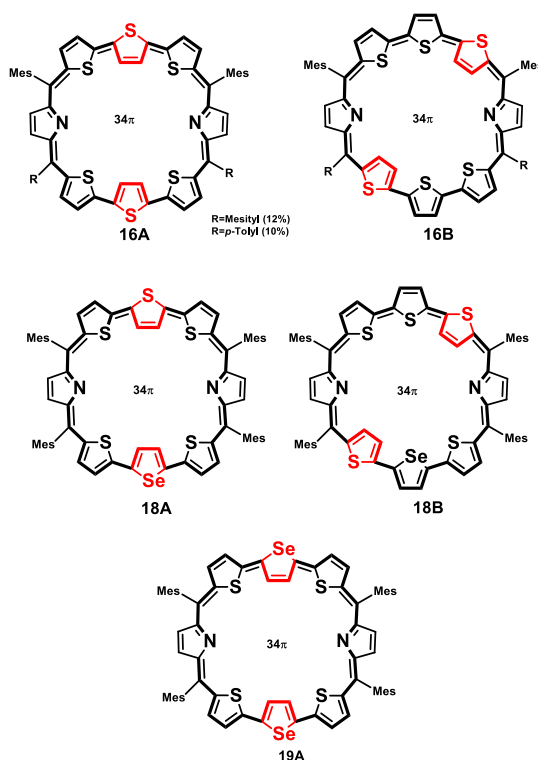


Figure 5.5: Structures of isomers **A** and **B** of octaphyrin **16**, **17**, **18**, **19**.

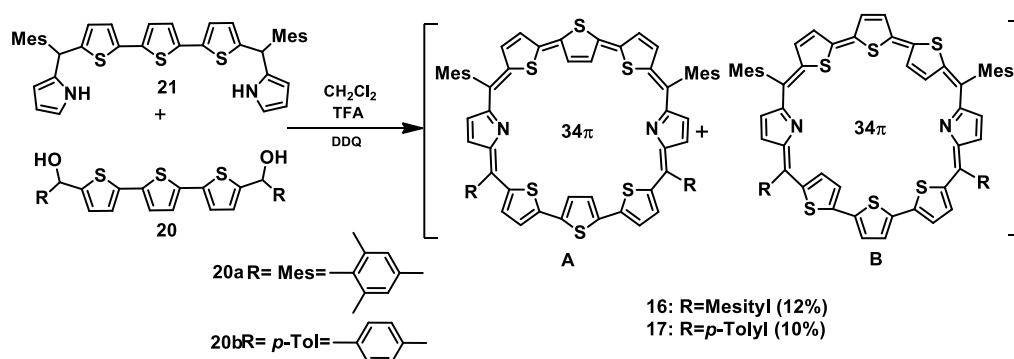
The NICS values calculation on the individual heterocyclic rings as well as the centre before and after proton addition justify such a conclusion. The AICD plots show diatropic or clock-wise orientation of current density vectors in the octaphyrins. Energy calculations were also done at M06L/CC-pVTZ//M06L/6-31G** level, which

concludes for only stability of a particular isomer relative to another on proton addition.

5.3 Results and discussions

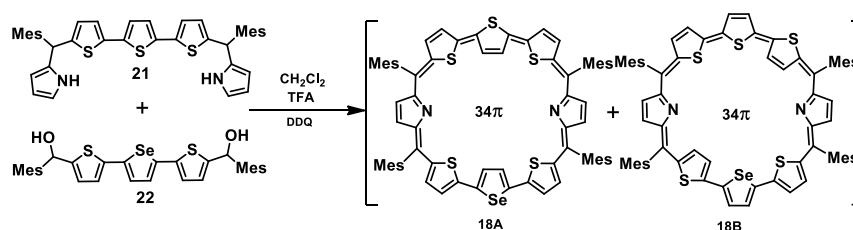
5.3.1 Syntheses

The syntheses of terthiophene based $[34]\pi$ octaphyrins **16** and **17** is outlined in Scheme 5.3. We have adopted $[5 + 3]$ acid-catalyzed Mac-Donald type condensation reaction. The required precursors 5,5''-bis(mesityl(1H-pyrrol-2-yl)methyl)-2,2':5',2''-terthiophene **21** and [2,2':5',2''-terthiophene]-5,5''-diylbis(arylmethanol) **20** were synthesized from our earlier reported procedures.²⁸ Thus the condensation of **20** and **21** in presence of 1 equiv. of trifluoroacetic acid (TFA) in dry CH_2Cl_2 followed by oxidation with 2,3-dichloro-5,6-dicyano-1,4-benzoquinone (DDQ) gave octaphyrin **16** and **17** with 10-12% yield.



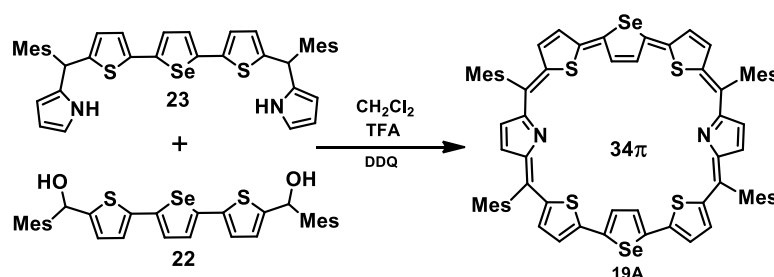
Scheme 5.3: Synthesis of Octaphyrin **16**, **17**(**A** and **B**).

The synthesis of **18** in which one of the central thiophene rings of terthiophene moiety is replaced by selenophene ring, the required precursor **22** was synthesized by reported procedure.²⁹ Thus, the condensation of **21** and **22** under acid-catalyzed condition in CH_2Cl_2 followed by DDQ oxidation shown in Scheme 5.4 gave **18**, a dark blue band on silica gel column (100-200 mesh) eluted with $\text{CH}_2\text{Cl}_2/n$ -hexane (58:42 v/v) in 9% yield. Here also isomers **18A** and **18B** were inseparable and **18A** was a major isomer while **18B** is minor.



Scheme 5.4: Synthesis of Octaphyrin **18(A and B)**.

The third octaphyrin **19** was synthesized by [5+3] approach outlined in Scheme 5.5. The required Precursor **23** was synthesized from our earlier reported procedure.²⁸ Upon acid-catalyzed condensation of **22** and **23** in CH₂Cl₂ followed by DDQ oxidation gave **15**. The compound was eluted with CH₂Cl₂ /*n*-hexane (52:48 v/v) in 10% yield. The reaction afforded isomer **A** exclusively whereas isomer **B** was not formed.



Scheme 5.5: Synthesis of Octaphyrin **19(A)**.

5.3.2 Spectral Characterization

5.3.2.1 Mass spectrometric analysis

The macrocycles **16**, **17**, **18** and **19** are stable and their composition were confirmed through ESI mass spectrometry (m/z 1145.3190 for **16** and m/z 1089.2703 for **17**), (m/z 1193.2602 for **18**) and (m/z , 1241.2308 for **19**) all show molecular ion signal shown in (Figure 5.6-5.9).

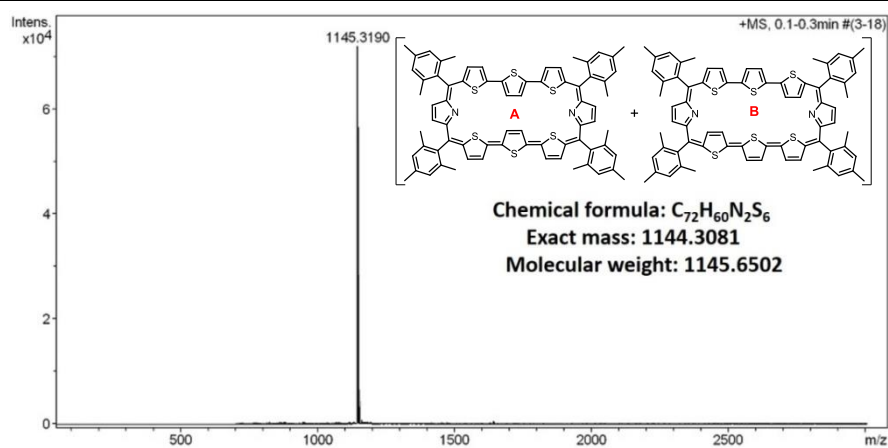


Figure 5.6: ESI-Mass of Octaphyrin 16.

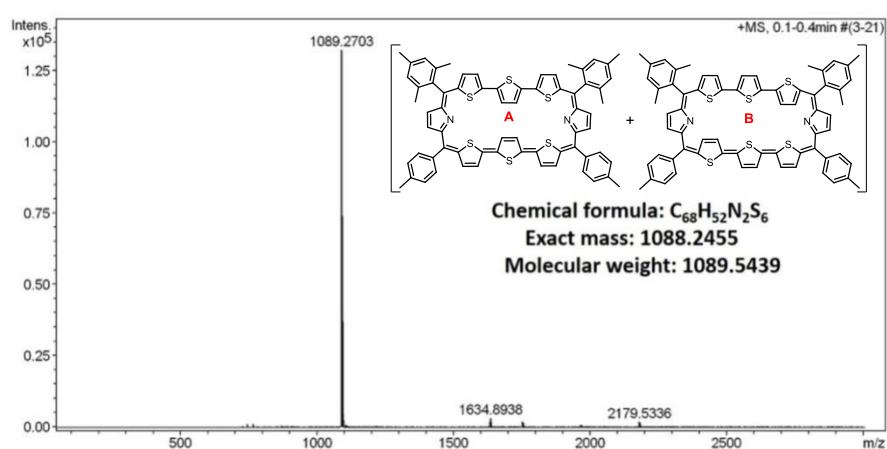


Figure 5.7: ESI-Mass of Octaphyrin 17.

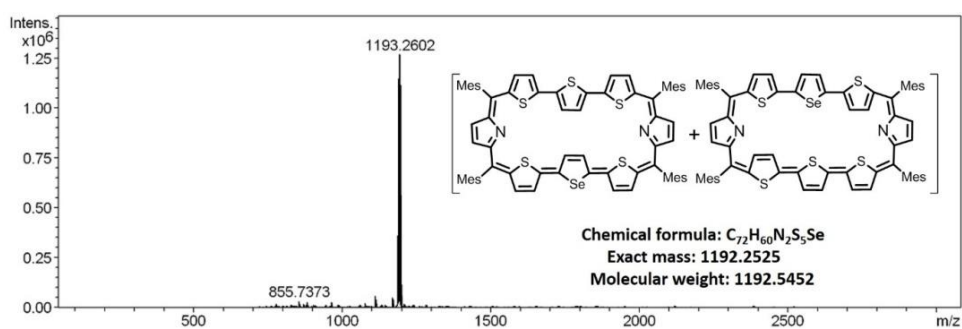


Figure 5.8: ESI-Mass of Octaphyrin 18.

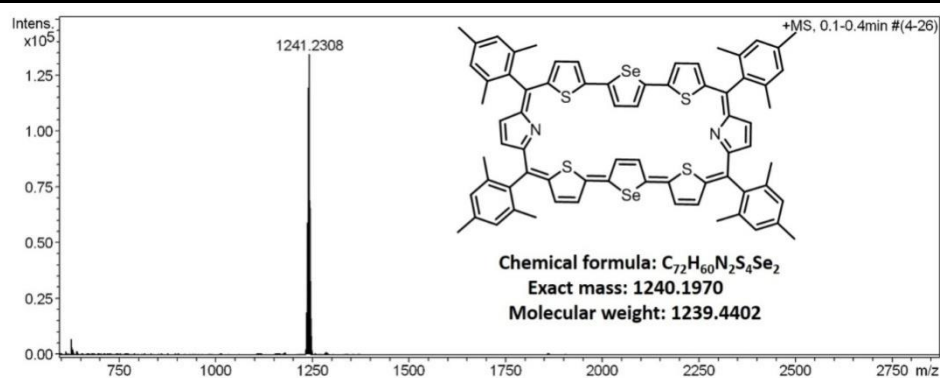


Figure 5.9: ESI-Mass of Octaphyrin **19**.

5.3.2.2 NMR analysis:

The solution structures of the various octaphyrins were proved by ^1H and 2D NMR studies. The ^1H NMR spectrum of **16** in toluene D_8 shown in Figure 5.10 shows signals more than needed showing that more than one isomer is present in solution. ^1H - ^1H COSY correlation experiments shows the correlations (Figure 5.11) and the NH protons confirmed by D_2O exchange experiments. The central inverted thiophene ring β -CH protons of **16A** appear at 0.37 ppm (a) while β -CH protons of terminally inverted thiophene rings of **16B** appear at 0.37 (1) and -1.26 (2) ppm at 298K. These chemical shifts suggest that the β -CH protons of inverted thiophene rings are experiencing the diatropic ring current of the macrocycle. The normal thiophene β -CH signals of **16A** (b, c) and **16B** (3, 4, 5, 6) and pyrrolic β -CH signals (d, 7, 8) appear in the region from 8.49 ppm to 9.85 ppm. The *meso* mesityl CH protons and CH_3 protons appear in the expected region.

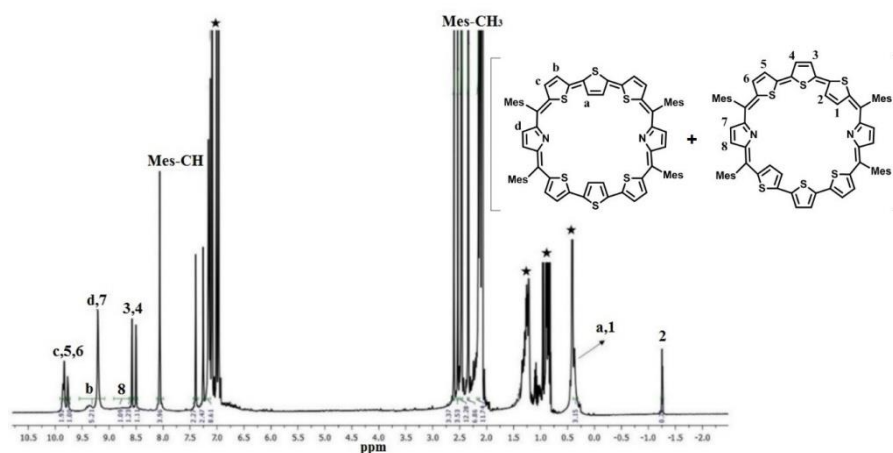


Figure 5.10: ^1H NMR Spectrum of **16** in Toluene- D_8 at 298K.

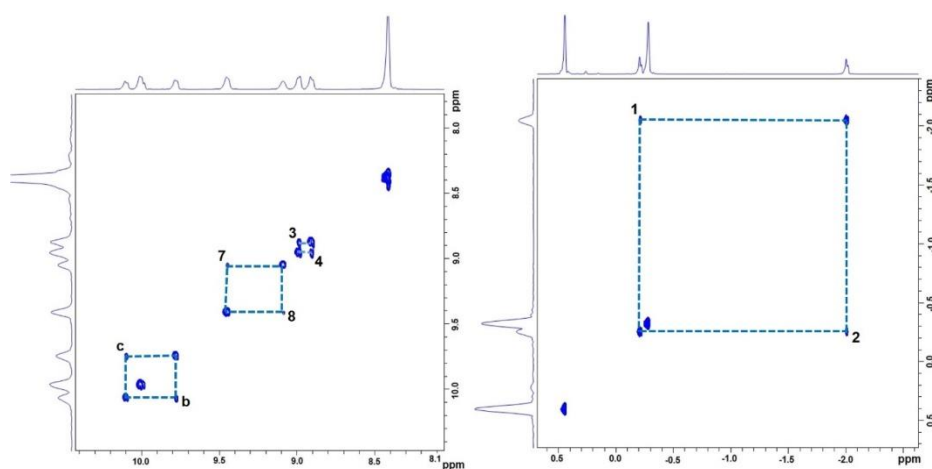


Figure 5.11: ^1H - ^1H COSY correlation spectrum of **16** at 213K in Toluene- D_8 .

Variation of temperature (343K to 193K) did not show any significant changes in the chemical shift of various protons (Figure 5.12, 5.13). The intensity could not be changed much when temperature was varied. There was no interconversion between the isomers and no change in conformation in various temperature range. ^1H NMR of **17** (Figure 5.14) also shows same behaviour and because of presence of two alike *meso* substituents, the symmetry lowers and this is seen by increase in signals. Overall the two isomers were observed in a ratio of 1:1.

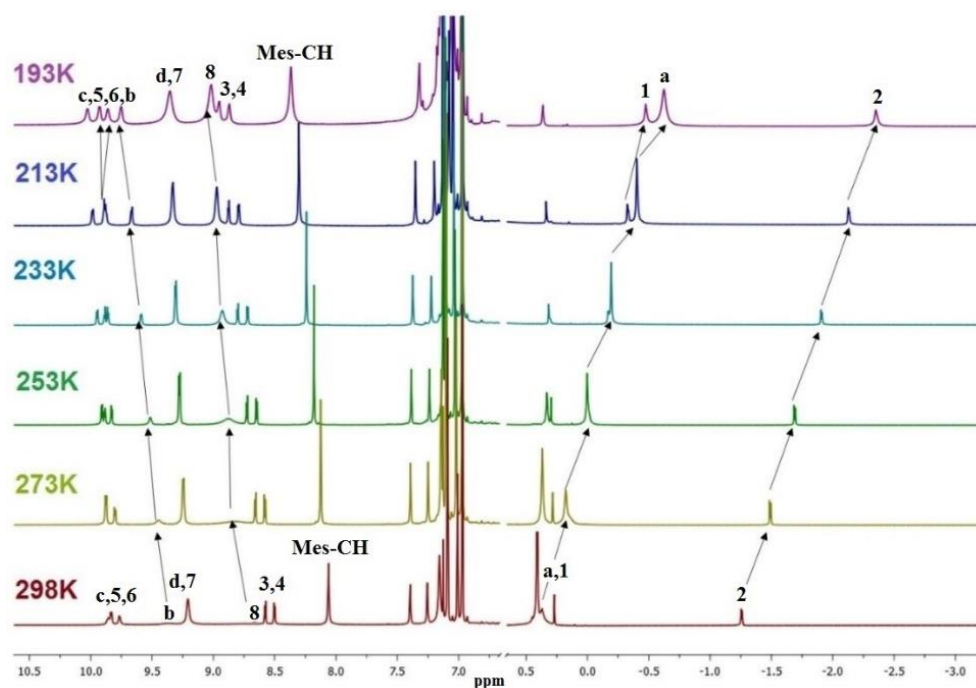


Figure 5.12: Low temperature (298K-193K) ^1H NMR spectrum of **16** in Toluene- D_8 .

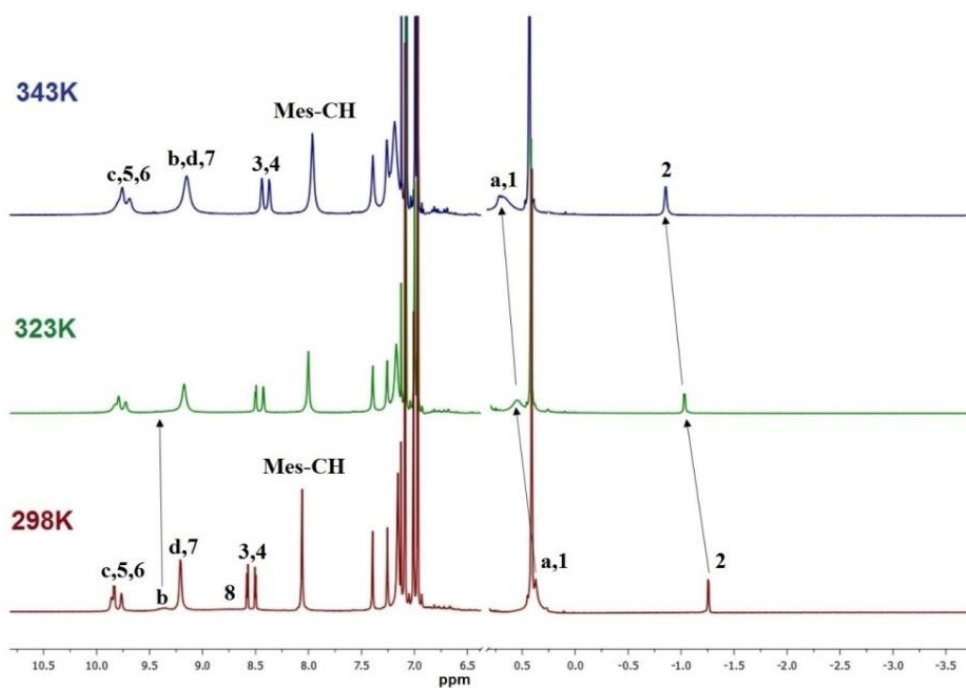


Figure 5.13: High temperature (298K-343K) ^1H NMR spectrum of **16** in Toluene- D_8 .

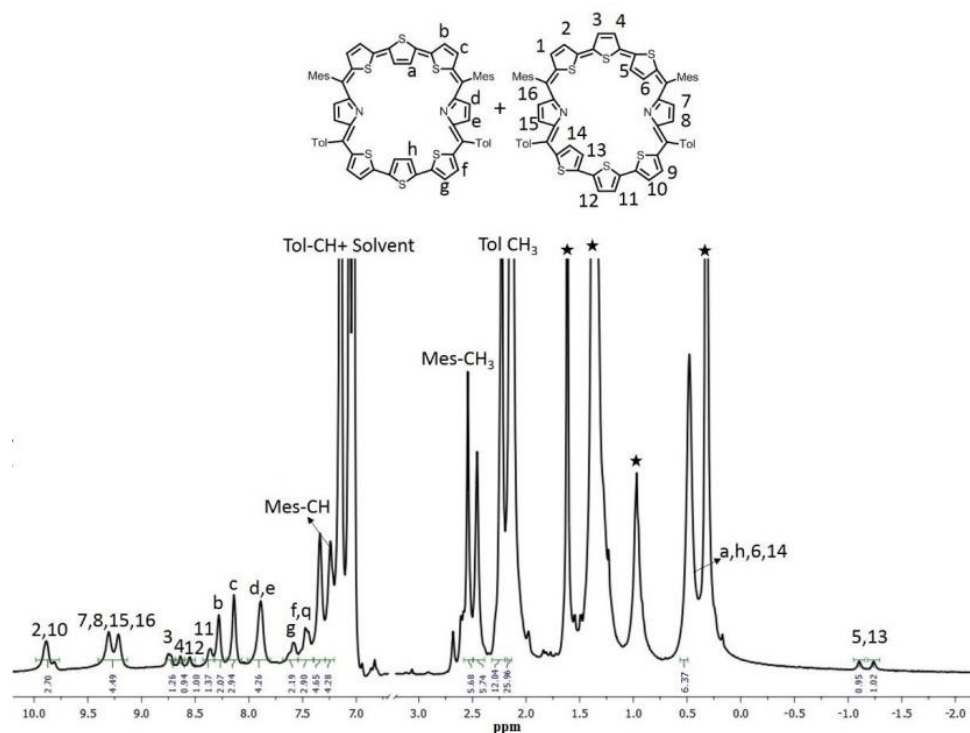


Figure 5.14: ^1H NMR Spectrum of **17** in Toluene- D_8 at 298K.

Protonation of pyrrolic nitrogens with dilute solution of TFA leads to stabilization of isomer **B** and the proton NMR spectrum of **16B**. 2H^+ shown in (Figure 5.15) confirms this observation. Specifically, the pyrrolic NH protons which are experiencing the diatropic ring current appear as broad signal at -2.76 ppm and a D_2O experiment confirm the assignment. The terminal inverted thiophene ring β -CH protons (**1**, **2**) are further shielded relative to freebase form and appear at -4.29 ppm and -4.70 ppm. The β -CH protons of normal thiophene rings (**3**, **4**, **5**, **6**) are further deshielded and appear between 10.47 ppm and 11.28 ppm. The β -CH protons of pyrrole ring (**7**, **8**) appear as doublet at 9.29 ppm and 9.34 ppm. The CH protons of mesityl rings appear between 7.45-7.61 ppm and methyl signals between 2.01-2.75 ppm. Thus, comparison of proton NMR of freebase and protonated form of **16** clearly suggests stabilization of **16B** upon protonation. **17** showed (Figure 5.18) same behaviour on proton addition

where lowered symmetry separate signals are seen for two inverted thiophene (Figure 5.14, 5.16).

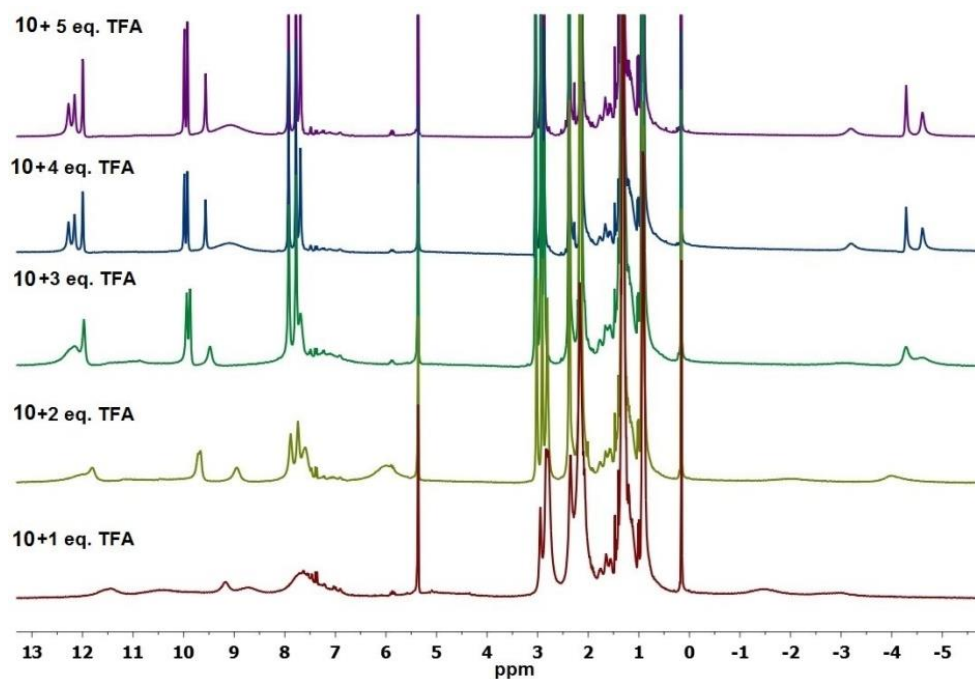


Figure 5.15: ^1H NMR spectra of **16** with varying concentration of TFA in CH_2Cl_2 at 298K.

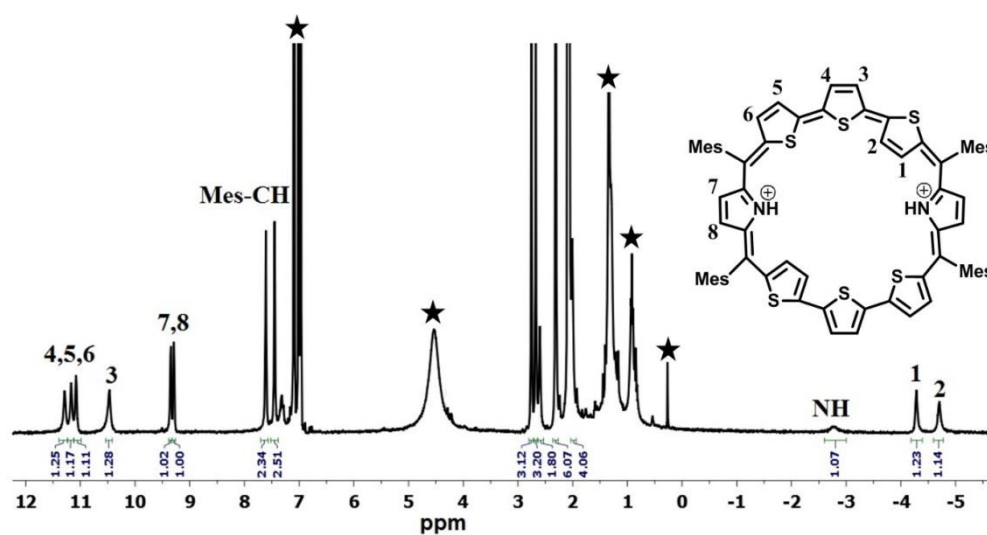


Figure 5.16: ^1H NMR Spectrum of **16B.2H⁺** in Toluene- D_8 at 298K.

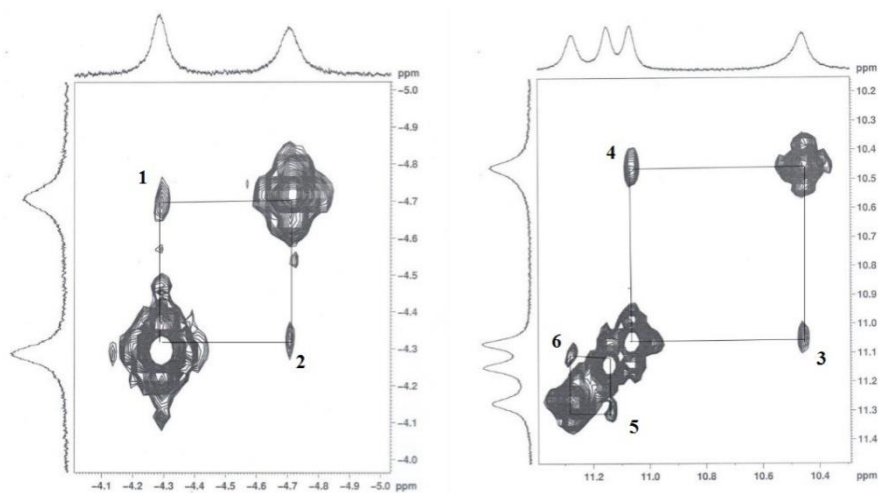


Figure 5.17: ^1H - ^1H COSY correlation spectrum of 16.2H^+ at 298K in Toluene- D_8 .

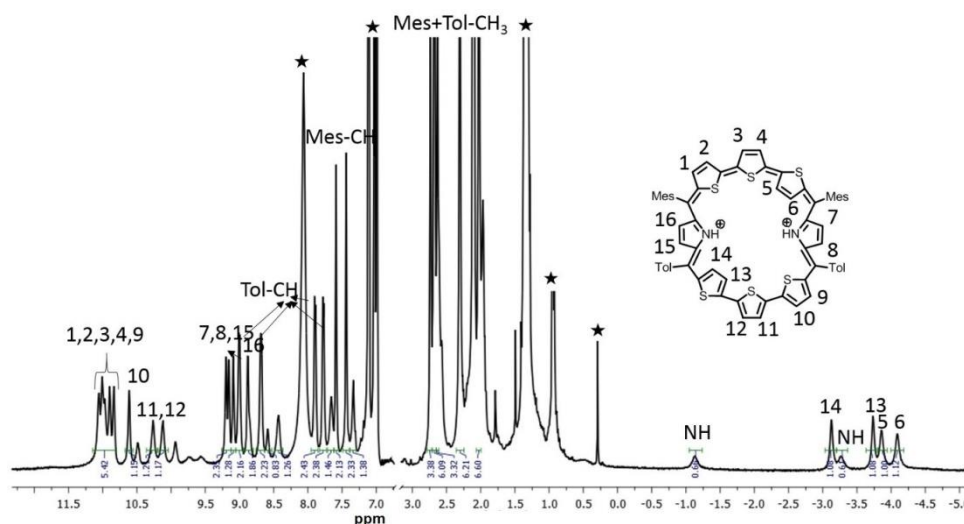


Figure 5.18: ^1H NMR Spectrum of 17.2H^+ in Toluene- D_8 at 298K.

The proton NMR spectra of freebase and protonated forms of **18** are shown in Figure 5.19 and Figure 5.20. Presence of two hetero atoms (S and Se), in the macrocycle shows own signals for the ring protons (Figure 5.20). For isomer **18A**, β -CH protons of inverted thiophene (**a**) and selenophene rings (**h**) appear at 0.14 ppm and 0.49 ppm respectively while for **13B**, the terminally inverted thiophene ring protons (**1**, **2**, **9** and **10**) appear at 0.49 (**10**), 0.14 (**9**), -1.01 (**2**) and -1.22 (**1**) suggesting that these protons are experiencing the diatropic ring current of the macrocycle. The β -CH protons of normal thiophene rings of **13A** (**c**, **b**, **f**, **g**) appear in the region 8.73-9.22 ppm while

that of isomer **18B** (**3**, **4**, **5**, **6**, **11**, **12**, **13** and **14**) appear between 9.4 ppm to 10.03 ppm. The pyrrole β -CH protons of **18A** (**d**, **e**) appear in the region 8.02-8.08 ppm while that of **18B** (**7**, **8**, **15** and **16**) are slightly deshielded and appear in the range 8.4 ppm to 8.5 ppm. Aspect on the spectral pattern shows both the isomers (**18A** and **18B**) are in ratio of 4:1. The addition of proton to pyrrole nitrogens leads to significant upfield and downfield effects gained for an aromatic molecule (Figure 5.22). However, both the isomers **18A** and **18B** retain their identity unlike in **16**. Variation in temperature did not show any major change as shown in Figure 5.21.

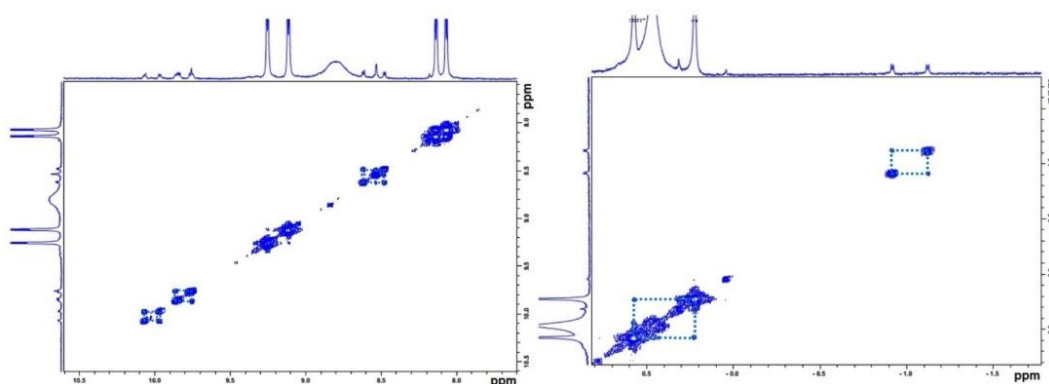


Figure 5.19: ^1H - ^1H COSY spectrum of **18** at 298K in Toluene- D_8 .

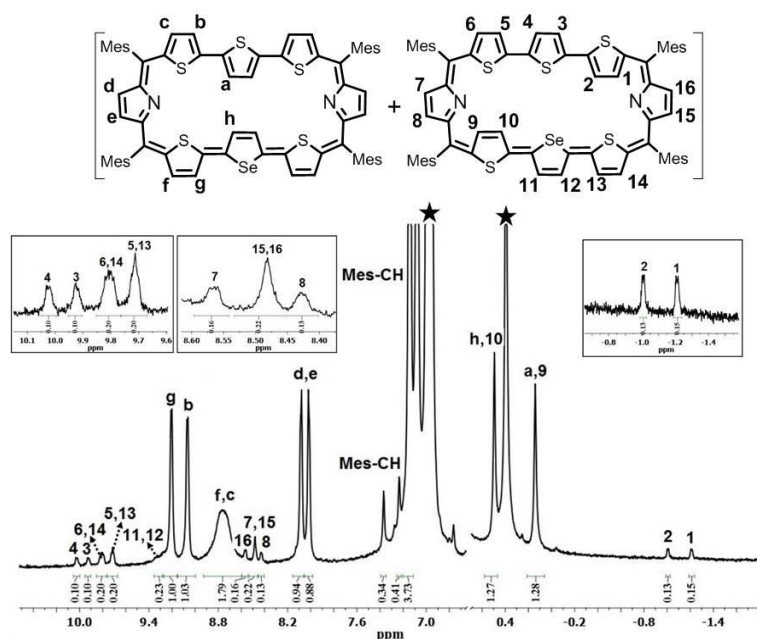


Figure 5.20: ^1H NMR spectrum of **18** in Toluene- D_8 at 298K.

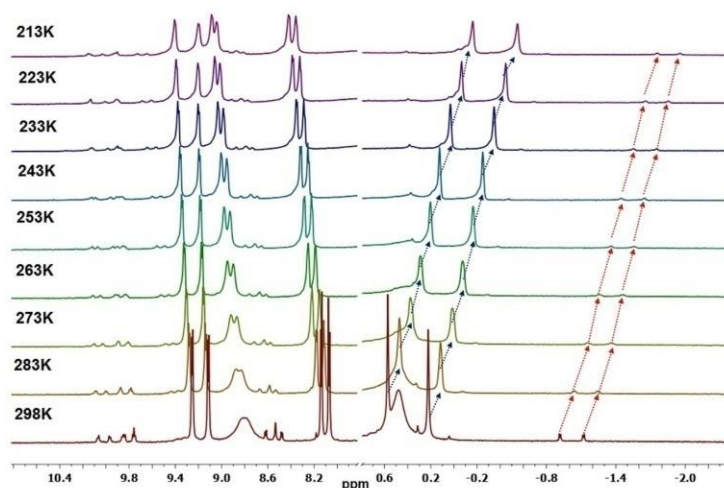


Figure 5.21: Low temperature (298K-193K) ^1H NMR spectrum of **18** in Toluene- D_8 .

The inverted thiophene (**a**) and selenophene (**h**) β -CH protons experience significant shielding upon protonation, and appear at -3.35 ppm (**h**) and -4.02 ppm (**a**). The terminally inverted β -CH protons of thiophene rings (**1**, **2**, **9** and **10**) of **18B.2H⁺** appear between -4.13 ppm and -4.92 ppm. The normal thiophene protons of **18B.2H⁺** also experience deshielding effect and appear between 10.47 and 11.6 ppm as eight doublets. The pyrrole β -CH protons of **18A.2H⁺** (**d**, **e**) appear at 8.99-9.02 ppm as two doublets while that of **18B.2H⁺** (**7**, **8**, **15** and **16**) appear in the region 9.28-9.4 ppm. The pyrrole NH protons of **13.2H⁺** appear as a broad signal at -6.5 ppm (**18A.2H⁺**) and -7.5 ppm (**18B.2H⁺**). The shielding and deshielding of different protons suggest aromatic nature of the macrocycles (Figure 5.22, 5.23).

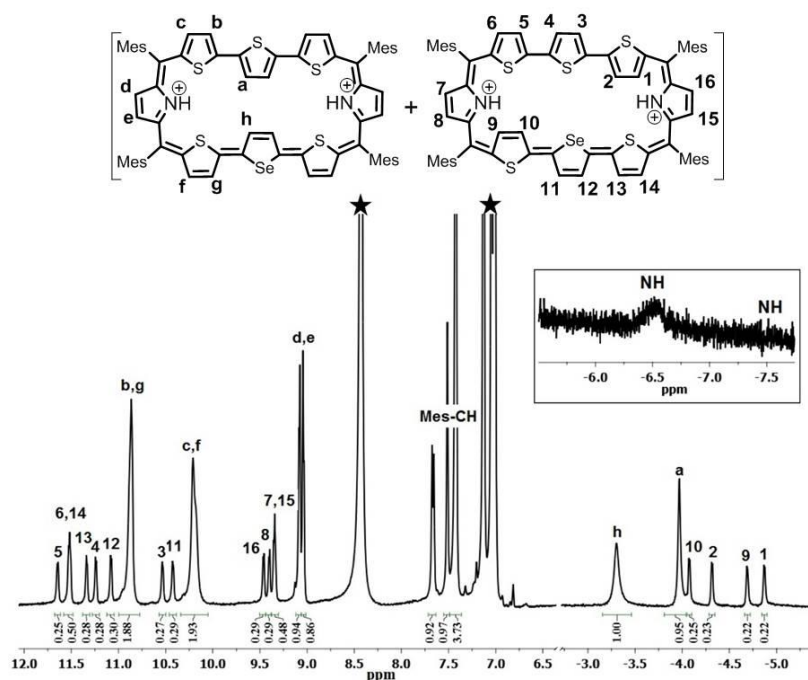


Figure 5.22: 1H NMR spectrum of $18.2H^+$ in Toluene- D_8 at 298K.

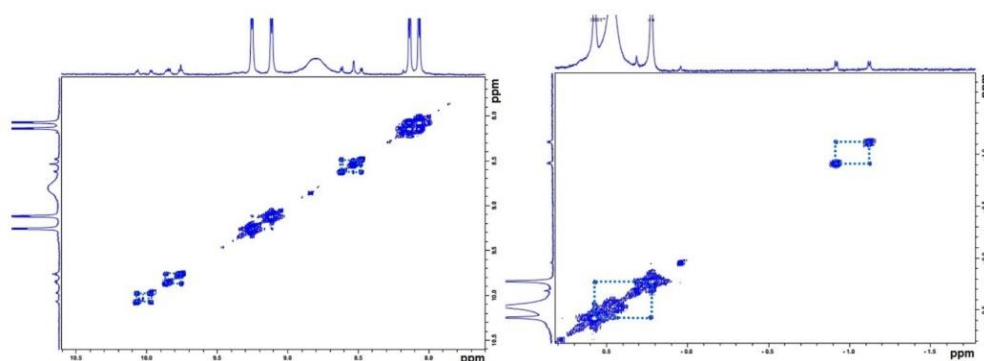


Figure 5.23: 1H - 1H COSY spectrum of 18 at 298K in Toluene- D_8 .

In case of 19 , since only one isomer, i.e the centrally inverted symmetric isomer **A** was formed, the 1H NMR spectrum was simple to interpret shown in Figure 5.24, 5.25 depicts 1H NMR spectra of $19A$. The selenophene protons show near 0.03 ppm concluding tilt of the middle selenophene rings. The thiophene β protons (**b** and **c**) show at 8.9 ppm and 9.2ppm as two doublets respectively. The pyrrole β -CH protons resonate as a single signal at 8.2 ppm. The *meso* mesityl -CH protons resonate at 7.2 ppm and methyl protons are in the required region.

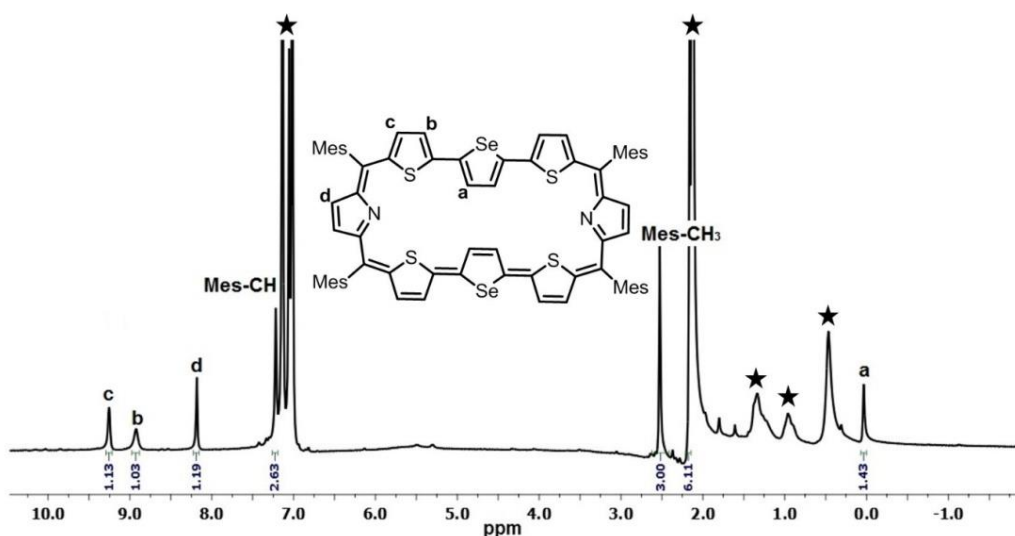


Figure 5.24: ^1H NMR spectrum of **19** in Toluene- D_8 at 298K.

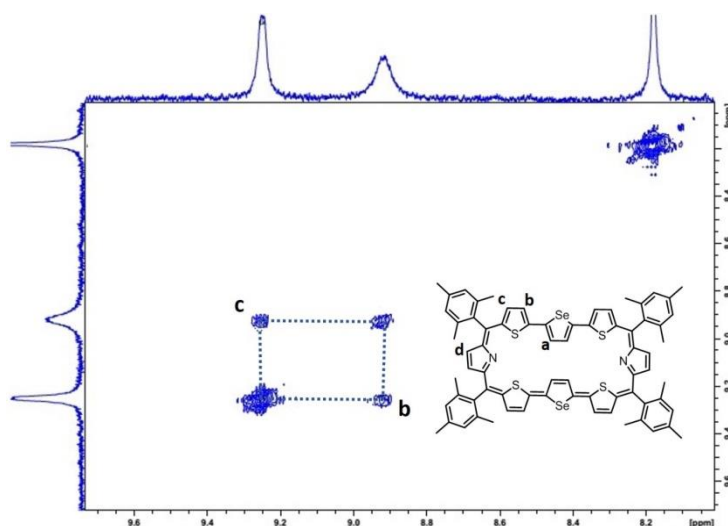


Figure 5.25: ^1H - ^1H COSY spectrum of **19** at 213K in Toluene- D_8 .

Addition of proton to pyrrole nitrogens in **19** shows a large upfield and downfield shift of protons owing to the nature of the rings (Figure 5.26 and 5.27). The inverted selenophene β -CH protons experience a significant shielding of 4.00 ppm and appear at -4.04 ppm, suggesting that the selenophene rings come into the plane exposing the β -CH protons to the ring current of macrocycle upon protonation. The thiophene ring β -CH protons (**b** and **c**) experience deshielding (2.0 ppm for 'c' protons and 1.1 ppm

for 'b' protons) and appeared at 10.28 ppm and 10.93 ppm respectively. The pyrrole NH protons appear as a broad signal at -4.59 ppm suggesting the aromatic nature of the macrocycle.

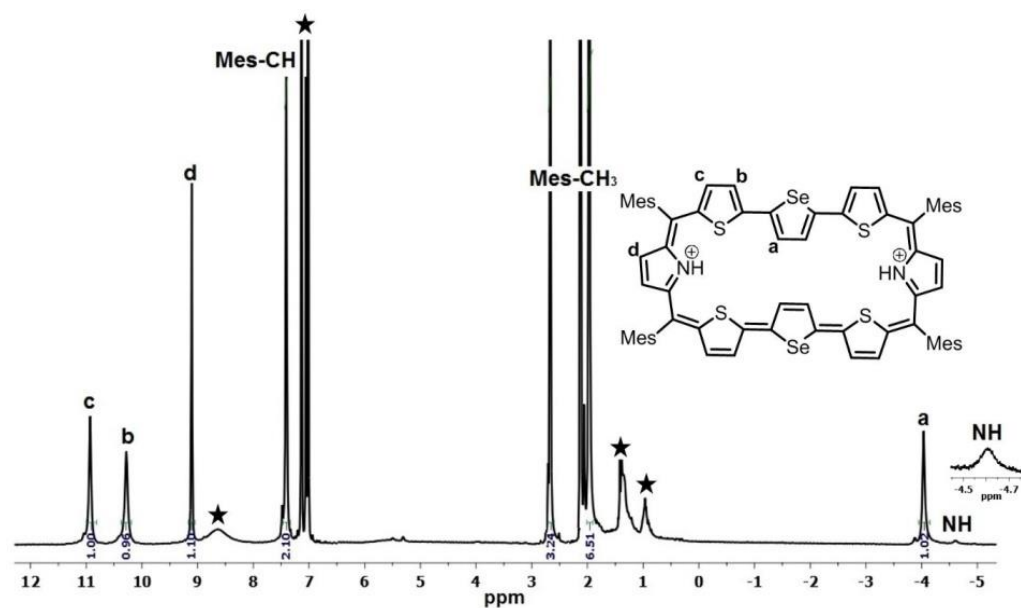


Figure 5.26: ^1H NMR spectrum of 19.2H^+ in Toluene- D_8 at 298K

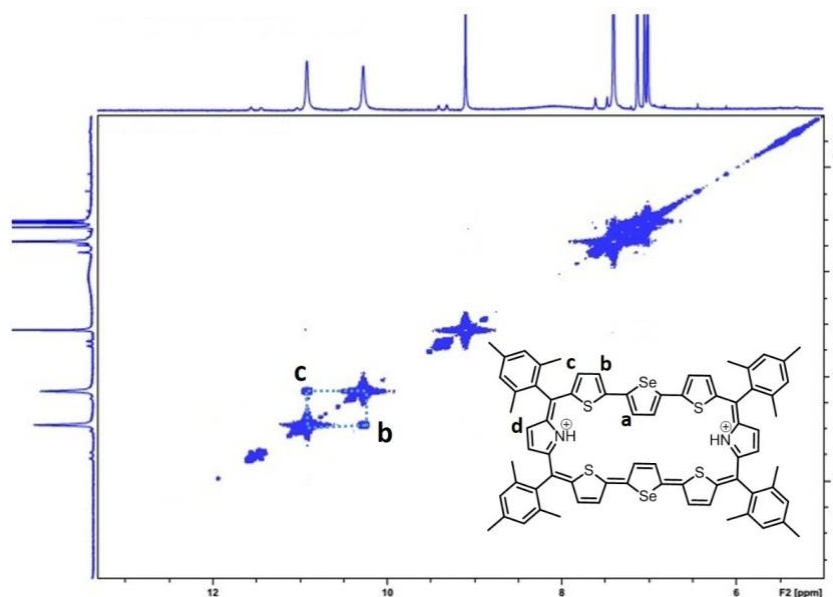


Figure 5.27: ^1H - ^1H COSY spectrum of 19.2H^+ at 213K in Toluene- D_8 .

5.3.2.3 Difference in Chemical shifts ($\Delta\delta$)

The difference in chemical shifts of most deshielded and most shielded ring protons (represented by $\Delta\delta$) for various octaphyrin isomers listed in Table 5.1 gives some insight into the aromaticity of the macrocycles. The results are as follows; (i) **A** isomers have lower aromatic character relative to **B** isomer ($\Delta\delta= 8.97$ vs 12.11); (ii) Protonated derivatives exhibit significantly larger $\Delta\delta$ values relative to freebase forms. The chemical shifts of inverted rings β -CH protons depend on the orientation of inverted ring relative to the mean macrocyclic plane. In **A** isomer, the centrally inverted heterocyclic rings are not completely planar due to which these protons experience only partial ring current. The terminally inverted rings in the **B** isomer, are oriented in the plane of the macrocycle and hence these protons are more shielded relative to **A** isomer protons accounting for larger $\Delta\delta$ values. On protonation of pyrrole nitrogens, the inverted rings come into plane of the macrocycle and the β -CH protons are completely exposed to ring current of the macrocycle which results in larger shielding of these protons. Hence, the protonated derivatives show larger aromaticity.

Table 5.1: $\Delta\delta$ values of Octaphyrin Isomers

Octaphyrin Isomer	$\Delta\delta$ (ppm)	Octaphyrin Isomer	$\Delta\delta$ (ppm)
16A	9.73	18A	9.06
16B	12.11	18B	11.25
16B.2H⁺	15.98	18A.2H⁺	17.36
		18B.2H⁺	18.14
17A	8.97		
17B	11.12	19A	9.21
17B.2H⁺	15.15	19A.2H⁺	15.52

5.3.2.4 Single Crystal X-ray analysis

The proposed structures of octaphyrin isomers were confirmed through single crystal X-ray analysis. The single crystal **16**, obtained by slow diffusion of CH₂Cl₂ solution in *n*-hexane crystalizes in monoclinic crystal lattice with *P2₁/n* space group.³² (Figure 5.28a and Table 5.2). As reflected in ¹H NMR spectral analysis, both the isomers with the same empirical formula exist in the crystal lattice. Both the molecules contain two terthiophene units connected with two pyrrole units via *meso* carbon bridges. The only difference is in inversion of one of the thiophene rings in the terthiophene units. The middle thiophene is inverted in **16A** whereas in **16B**, one of the terminal ring is inverted. The difference in dihedral angle between the two planes (C5, C10, C5' and C10' vs C45, C50, C45' and C50') is 38.84° (Figure 5.28b). As reflected from the Δδ values (9.73 vs 12.11) in table-2.1, the terminally inverted thiophene rings (**16B**) are deviated by 16.27°, whereas the middle inverted thiophene rings are deviated by 21.23° (**16A**) confirms that the terminal rings are moving towards to plane and experiencing an effective ring current as compared to middle thiophene rings. The maximum deviation of middle thiophene ring is reflected in the steric repulsion between the inner core hydrogen atoms (H39...H38'). The *meso* aryl rings in **16** are almost perpendicular to the mean plane of the macrocycle (For **16A** 79.89°, 83.03°, 79.89°, 83.03° and for **16B** 86.37°, 81.10°, 86.37°, 81.10°) as observed in other *meso*-aryl expanded porphyrinoids.³³ The crystal analyses of **16** revealed three different intermolecular hydrogen bonding interactions between (i) π-clouds of inner thiophene (S2') of **16B** and C43-H43 of **16A**, (ii) π-clouds of *meso*-mesityl unit of **16A** and C17'-H17' of **16B** and (iii) π-clouds of *meso*-mesityl unit of **16B** and C71-H71B of **16A** with bond distances and angles of S2'(π)...C43-H43, Mes(π)...C17'-

H17' and Mes(π)...C71-H71B are 2.83Å & 136.14° and 2.71Å & 137.01° and 3.15Å & 150.91° respectively (Figure 5.28).

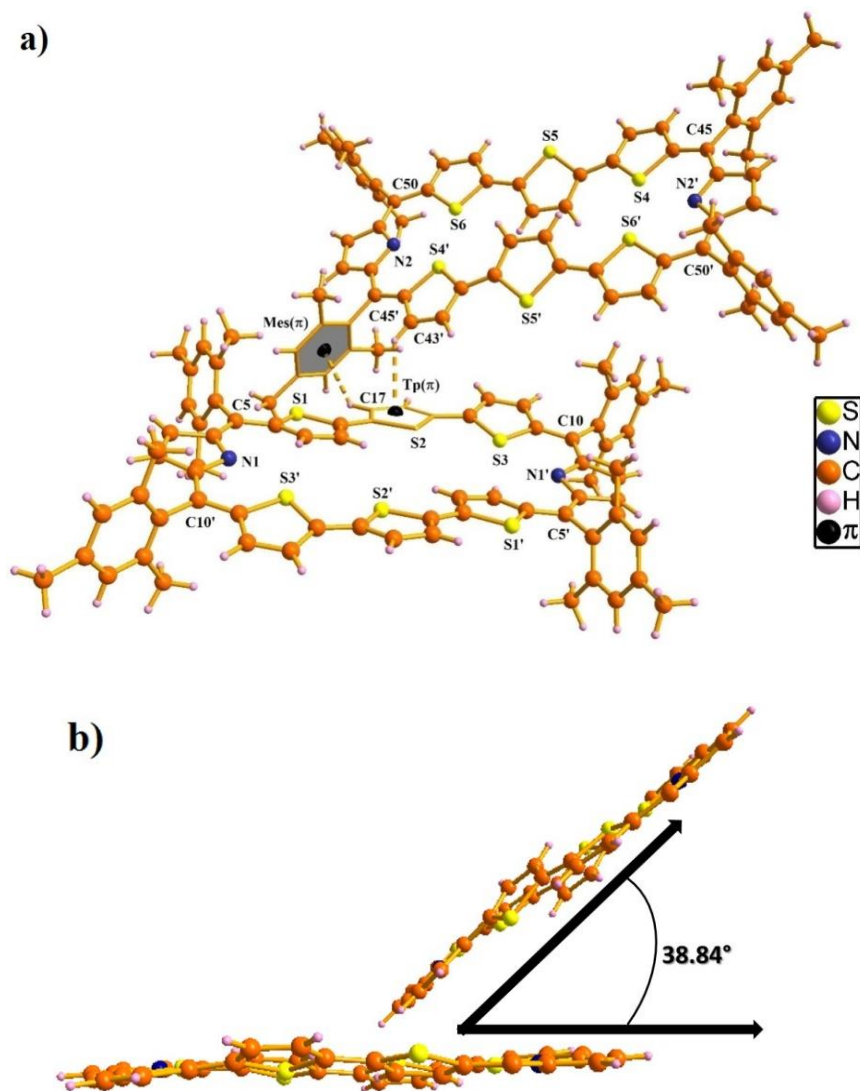


Figure 5.28: X-ray structure of **16**. a) Top view and b) Side view (The *meso* mesityl substituents are omitted).

The exclusively stabilized **16B**.2H⁺ isomer upon protonation was unambiguously confirmed by single crystal X-ray analysis shown in Figure 5.29 and Table 5.2. The molecule crystallizes in triclinic lattice with *P*-1 space group.³¹ Two perchlorate anions (O1/O1') are in intermolecular hydrogen bonding interaction with the protonated imine NH (N1-H1/ N1'-H1') with a bond distance and angle of N1-

H1...O1/ N1'-H1'...O1' is 2.33Å and 118.41° respectively. These N-H...O bond length and bond angles compare well with previously reported octaphyrin-TFA complex.³⁴ The end thiophene components (S1/S1') is slightly deviated (12.99°) from mean molecular plane (C5, C10, C5', C10') and maintain the planarity as observed in freebase form of **16**. The deviation is lower as compared to **16B** (16.27°) proves the higher aromatic ring current in the terminal thiophene unit of protonated form over freebase, as reflected from the higher $\Delta\delta$ value (15.98 vs 12.11) in (Table 5.1).

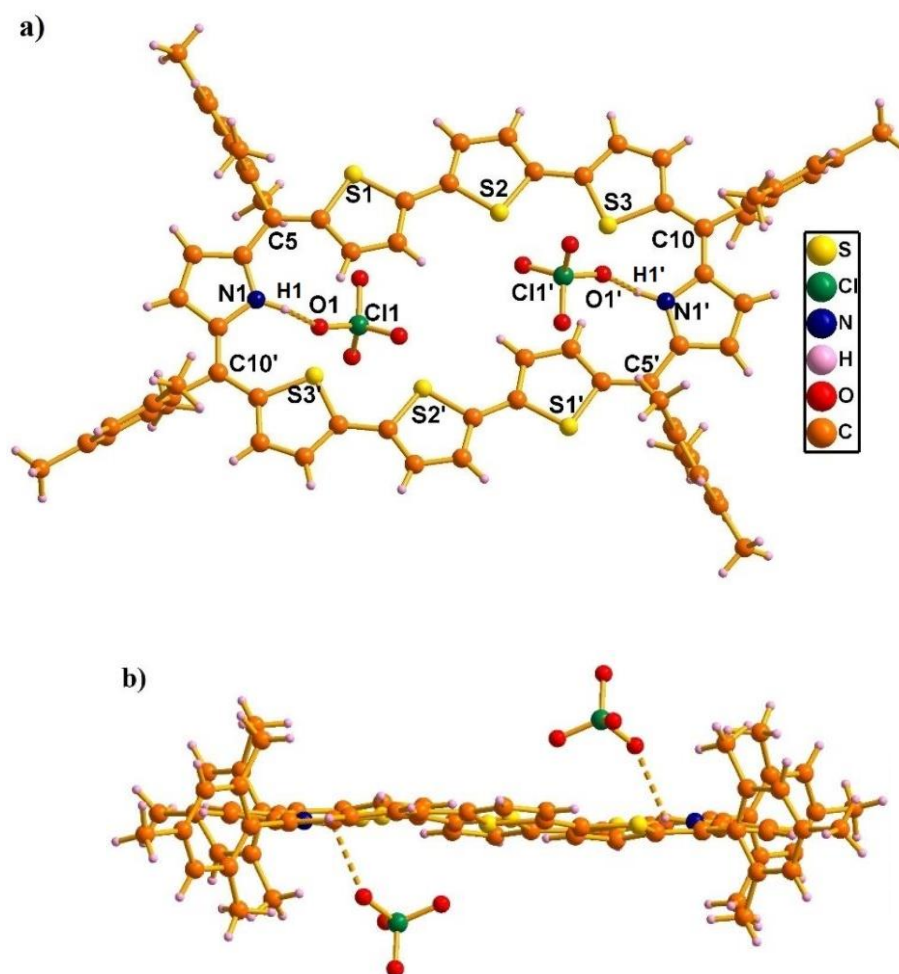


Figure 5.29: Single crystal X-ray structure a) Top view and b) Side view of **16B**.2H⁺(2ClO₄⁻).

Table 5.2: Crystallographic data for **16** and **16.2H⁺**.

	16	16.2H⁺	
		100K	100K
<i>T</i> , K	100 K	100K	100K
Formula	C72H60N2S6	C72H62N2S6Cl2O8	C72H62N2S7O4
Formula weight	1145.58	1455.97	1351.60
Color	brown	green	Golden brown
Crystal lattice	monoclinic	triclinic	monoclinic
Space group	<i>P</i> 2 ₁ /n	<i>P</i> -1	<i>P</i> 2 ₁ /c
<i>a</i> , (Å)	19.747(6)	14.477(3)	18.466(9)
<i>b</i> , (Å)	15.812(6)	17.107(3)	27.362(14)
<i>c</i> , (Å)	22.766(7)	24.756(5)	16.312(8)
α , deg	90	81.890(12)	90
β , deg	92.329(10)	79.104(12)	100.556(3)
γ , deg	90	76.504(12)	90
<i>V</i> , Å ³	7103(4)	5823.8(19)	8103.2(7)
Radiation λ , (Å)	Mo K α (0.7107)	Mo K α (0.7107)	Mo K α (0.7107)
<i>Z</i>	4	2	4
d _{calc} , g•cm ⁻³	1.071	1.245	1.108
μ , mm ⁻¹	0.231	0.300	0.263
<i>F</i> (000)	2408	2282.0	2829
No. of unique reflns	13018	21219	17352
No. of params. refined	733	1352	824
GOF on <i>F</i> ²	0.906	0.949	1.149
<i>R</i> 1 [^{>} 2 σ (<i>I</i>)]	0.0794	0.0791	0.1460
<i>R</i> 1 (all data)	0.1900	0.1622	0.4382
w <i>R</i> 2 (all data)	0.1790	0.2061	0.4783

Octaphyrin **19** crystallizes in monoclinic crystal lattice with *P*2₁/*c* space group (Figure 5.30 and Table 5.3). As observed in **16**, two molecules of **19** are present in single unit cell, however both are identical isomers in which only middle selenophene ring is inverted. The terminally inverted isomer **B** was not formed in the reaction. The

difference in dihedral angle between the two molecular planes (C7, C12, C7', C12' vs C7'', C12'', C7''', C12''') is 21.41° . The middle selenophene unit in **19A** is tilted by around 20.10° from the mean macrocyclic plane, whereas, the rest thiophene and pyrrolic rings are more or less planar with the mean molecular plane. The marginal difference in deviation (20.10° vs 21.23°) of the middle selenophene unit over middle thiophene unit (**16A**), adopts similar trend as observed in $\Delta\delta$ values (9.21 vs 9.73) shown in Table 5.1. Like **16A**, here also the repulsion between the inverted selenophene β -hydrogens (H1...H18) is responsible for maximum deviation. The *meso* mesityl groups are nearly perpendicular with the mean macrocyclic plane (78.30° , 76.37° , 78.30° and 76.37°). The structural analysis of **19A** revealed two weak intermolecular hydrogen bonding interactions between the two molecules, i) Mes(π)...C4'-H4' and ii) Mes(π)...C44'''-H44''' with bond distances and angles were i) 3.30\AA and 132.35° and ii) 3.19\AA and 123.57° respectively.

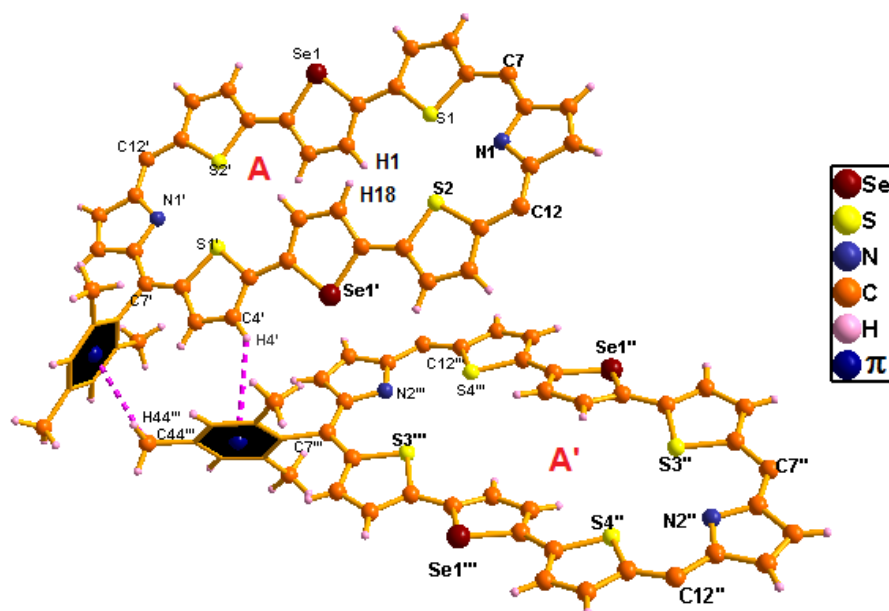


Figure 5.30: Single crystal X-ray structure of **19A** (Front View). (The *meso* mesityl substituents are omitted for clarity)

The single crystal X-ray structure of **19A.2H⁺** is shown in Figure 5.31 and Table 5.3. The crystal was grown by slow evaporation of toluene in methanol at room temperature. The compound crystallizes in triclinic crystal lattice with P-1 space group. The structural analysis reveals that the middle selenophene rings of 2,5-di(thiophen-2-yl)selenophene are inverted as in the freebase form. The inverted selenophene units are deviated by 17.92° from the mean macrocyclic plane (C7, C12, C7', C12') due to the steric repulsion between the β-CH protons (H1...H18) of the inverted selenophene moieties. The deviation in **19A.2H⁺** is 3.48° less as compared to its freebase **19A** further confirms 4 ppm upfield shift of the inverted β-CH protons of **19A.2H⁺** as revealed in ¹H NMR spectroscopy. As reflected in **19A** the remaining heterocyclic rings are nearly coplanar (9.96° and 14.55°), whereas, the *meso* mesityl substituents are nearly perpendicular (63.50°, 77.99°, 63.50° and 77.99°) to the mean macrocyclic plane. The two perchlorate anions are located above and below the plane of the macrocycle with intermolecular hydrogen bonding interaction with the protonated imine NH's (N1-H1 / N1'-H1') with distance and angle of N1-H1...O1/ N1'-H1'...O1' is 2.54Å and 107.83° respectively.

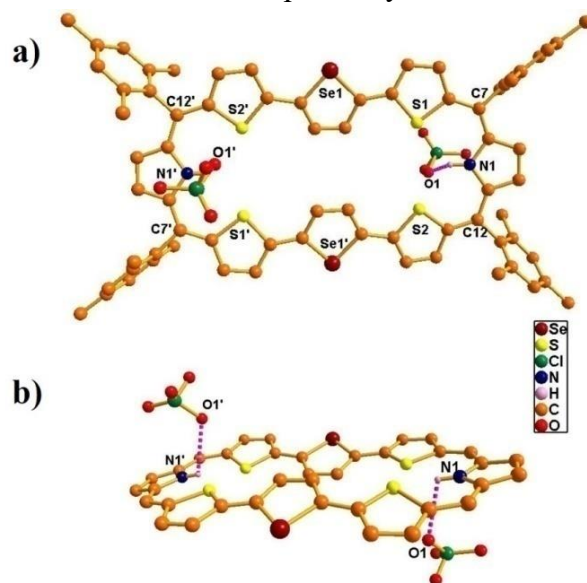


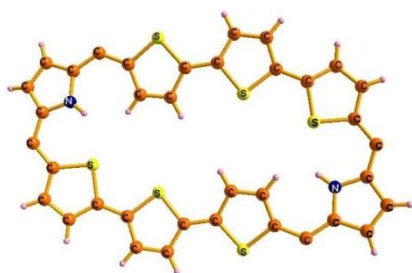
Figure 5.31: Single crystal X-ray structure a) Top view and b) Side view of **19A.2H⁺(2ClO₄⁻)**.

Table 5.3: Crystallographic data for **19A** and **19A.2H⁺**

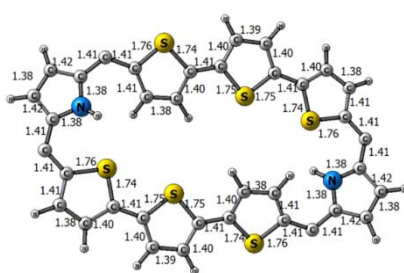
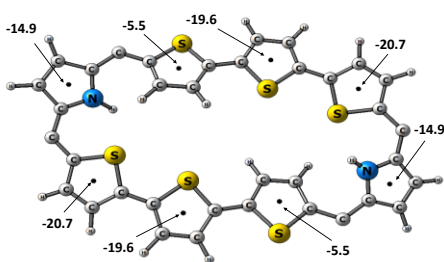
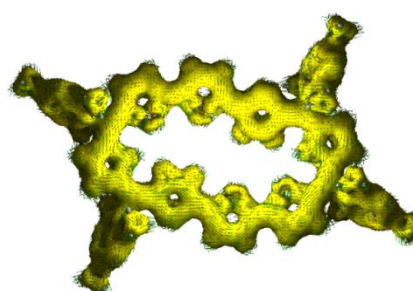
	19A	19A.2H⁺
<i>T</i> , K	100 K	113 K
Formula	C ₇₂ H ₆₀ N ₂ S ₄ Se ₂	C ₇₂ H ₆₂ Cl ₂ N ₂ O ₁₂ S ₄ Se ₂
Formula weight	1239.38	1539.74
Color and Habit	Dark brown	Golden
Crystal system	monoclinic lattice	triclinic
Space group	<i>P</i> 2 ₁ / <i>c</i>	<i>P</i> -1
<i>a</i> , Å	22.7958(4)	14.4054(5)
<i>b</i> , Å	11.8670(2)	18.9004(7)
<i>c</i> , Å	29.0481(4)	19.3632(6)
<i>α</i> , deg	90	107.869(3)
<i>β</i> , deg	93.89(10)	107.260(3)
<i>γ</i> , deg	90	105.339(3)
<i>V</i> , Å ³	7839.9(2)	4409.8(3)
Radiation (<i>λ</i> , Å)	CuKα (<i>λ</i> = 1.54184)	CuKα (<i>λ</i> = 1.54184)
<i>Z</i>	4	2
d _{calc} , g•cm ⁻³	1.050	1.160
<i>μ</i> , mm ⁻¹	2.436	3.180
<i>F</i> (000)	2552.0	1574.0
No. of unique reflns	56327	60529
No. of params. refined	14125	18011
GOF on <i>F</i> ²	1.056	1.609
<i>R</i> 1 [<i>I</i> > 2σ(<i>I</i>)]	0.1062	0.1639
<i>R</i> 1 (all data)	0.1207	0.2028
<i>wR</i> 2 (all data)	0.3029	0.4114

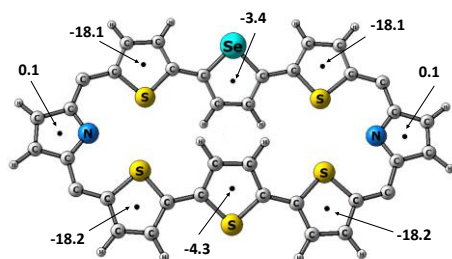
5.3.2.5 NICS(0) Calculation and ACID Plots

The NICS values calculation for core octaphyrins and the individual heterocyclic rings for all (**16**, **18** and **19**) in freebase and protonation forms (Chart 5.1, 5.2, 5.3, 5.4, 5.5).³¹ It is observed in all the cases that the NICS(0) value for the pyrrole rings in the freebase form is 0.1 ppm, inverted heterocyclic rings are from -3.3 ppm to -4.4 ppm, whereas the normal heterocyclic rings are between -18.1 ppm and -25.8 ppm, respectively and with overall NICS values are from -9.95 ppm to -12.04 ppm suggests the aromatic character in the freebase form. Upon protonation, the pyrrole rings are with higher NICS(0) value as compared to free base (-13.4 ppm to -15.2 ppm), whereas there is a nominal increase in the inverted heterocyclic rings (-4.2 ppm to -5.6 ppm) and marginal shift in the normal heterocyclic rings (-17.5 ppm to -20.6 ppm) with overall increase in NICS values of -13.66 ppm to -15.18 ppm reveals the protonated forms are more aromatic than the free base form, justifying the conclusion drawn from ¹H NMR chemical shift data. For example, the NICS(0) value of **16B** and **16B.2H⁺** are shown in and found to be -11.4 ppm in **16B** and -15.17 ppm in **16B.2H⁺**, justifying that protonation enhances the aromatic character as compared to free base form. Furthermore, the anisotropy induced current density plots (AICD plots) calculated on to isosurface value 0.026 clearly suggests diatropic ring current in the Octaphyrin owing to clockwise orientation of current density vectors.

16B.2H⁺

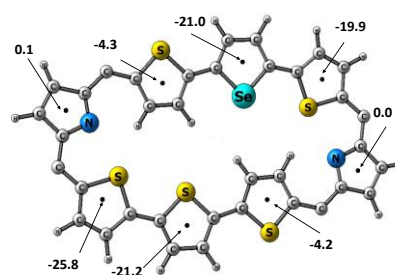
X-ray structure

16B.2H⁺M06L/6-31G** level optimized
geometryNICS(0) values at M06L/6-31G**
levelACID Plot - the current density
vectors plotted on to isosurface
of value 0.026**Chart 5.2:** X-ray structure, Optimized geometry, NICS(0) values and ACID plots for **16B.2H⁺**.

18A

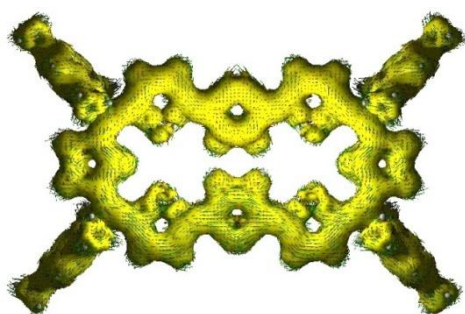
NICS(0) values at M06L/6-31G**

level

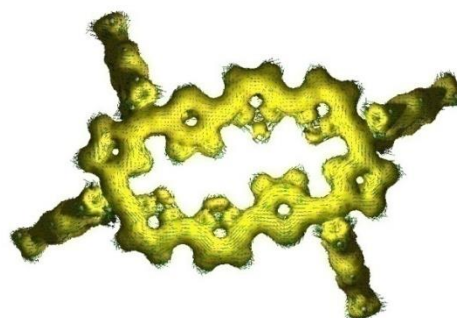
18B

NICS(0) values at M06L/6-31G**

level

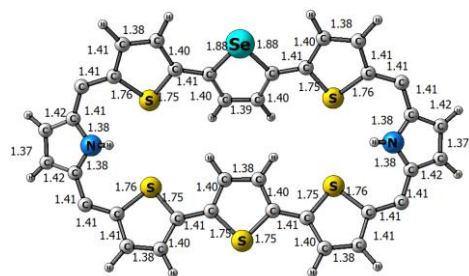


ACID Plot - the current density
vectors plotted on to isosurface of
value 0.026



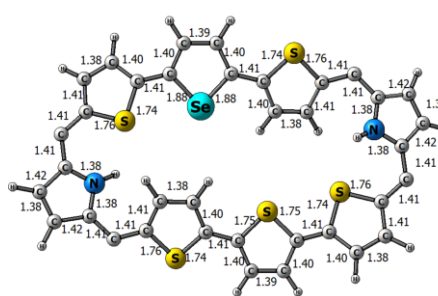
ACID Plot - the current density
vectors plotted on to isosurface of
value 0.026

Chart 5.3: Optimized geometry, NICS (0) values and ACID plots for **18A**, **18B**.**18A.2H⁺****18B.2H⁺**



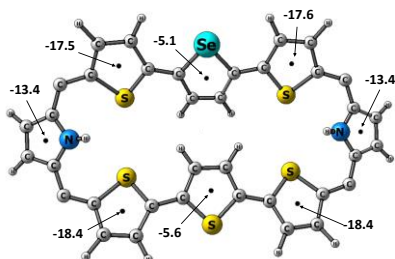
M06L/6-31G** level optimized

geometry

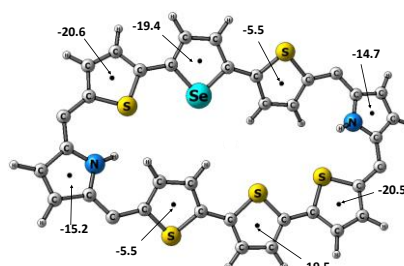


M06L/6-31G** level optimized

geometry



NICS(0) values at M06L/6-31G** level



NICS(0) values at M06L/6-31G**

level

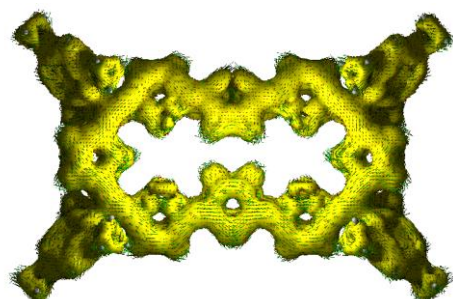
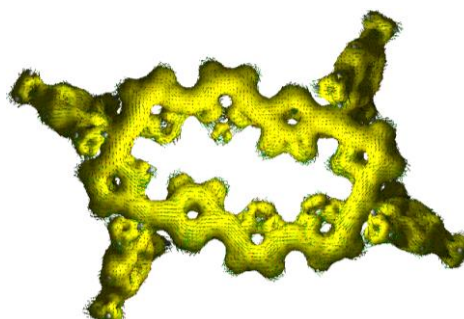
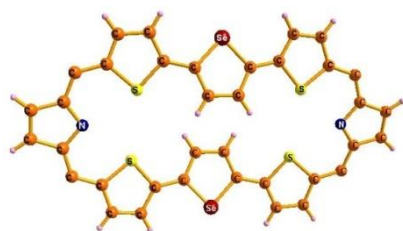
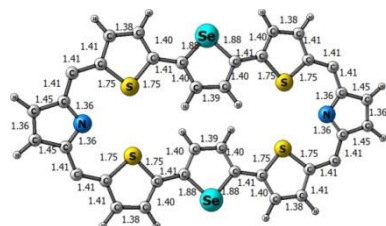
ACID Plot - the current density vectors
plotted on to isosurface of value 0.026ACID Plot - the current density vectors
plotted on to isosurface of value 0.026

Chart 5.4: Optimized geometry, NICS (0) values and ACID plots for **18A.2H⁺** and **18B.2H⁺**

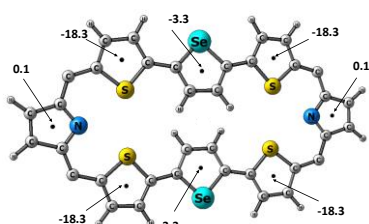
19A

X-ray structure



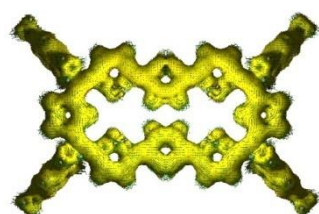
M06L/6-31G** level optimized

geometry



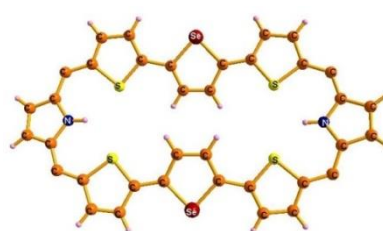
NICS(0) values at M06L/6-31G**

level

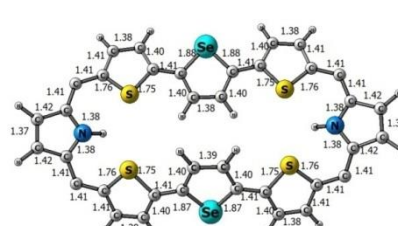


ACID Plot - the current density

vectors plotted on to isosurface of
value 0.026

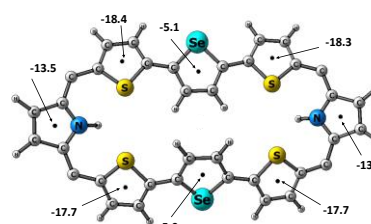
19A.2H⁺

X-ray structure



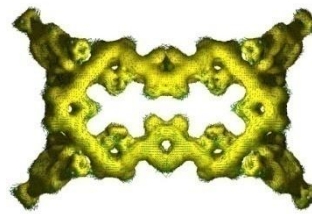
M06L/6-31G** level optimized

geometry



NICS(0) values at M06L/6-31G**

level



ACID Plot - the current density

vectors plotted on to isosurface of
value 0.026

Chart 5.5: X-ray structure, Optimized geometry, NICS (0) values and ACID plots for **19A** and **19A.2H⁺**

5.3.2.6 DFT Calculations

The exclusive formation of a particular isomer relative to other, suggests a small energy difference between the isomers. Any small external perturbation can alter this difference in energy and favour one isomer over the other. Keeping this in mind, we have calculated single point energies on the optimized structures of isomers in freebase and protonated forms using M06L/CC-pVTZ//M06L/6-31G** level of theory. Table 5.4 summarizes the energies calculated. For example, the table shows **16A** is more stable than **16B** by 2 Kcal/mol. However, **16B.2H⁺** is found to be more stable than **16A.2H⁺** by 0.5 Kcal/mol. Further the protonation is found to have more stabilizing effect on **16B.2H⁺** relative to **16A.2H⁺** due to increased aromaticity. In addition, our calculation does not take into account the effect of counter anion and crystal packing forces. Taken together these observations explain the stabilization of **16B.2H⁺** relative to **16A.2H⁺**. In the case of **18**, **18A** is more stable by 3.4 Kcal/mol relative to **18B**. Upon protonation, these energy difference between the two isomers remain same and protonation effects are similar in both **A** and **B** isomers, explaining the formation of both isomers **18A.2H⁺** and **18B.2H⁺** upon protonation. In case of **19**, our calculations showed **19A** is more stable than **19B** by 4.8 Kcal/mol, supporting the formation of only isomer **19A**. Even in the protonated state **19A.2H⁺** is found to more stable than **19B.2H⁺** by 5.9 Kcal/mol, justifying the formation of **19A.2H⁺** upon protonation.

Table 5.4: Total energy in a.u. and relative energy (E_{rel}) of ‘B’ configuration with respect to ‘A’ in kcal/mol.

Macrocycle	M06L/CC- pVTZ//M06L/6- 31G**(a.u.)	E_{rel} (Kcal/m)
16A	-5279.089075	0.0
16B	-5279.085954	2.0
18A	-7282.397194	0.0
18B	-7282.391794	3.4
19A	-9285.705583	0.0
*19B	-9285.697999	4.8
*16A.2H⁺	-5279.873635	0.0
16B.2H⁺	-5279.874464	-0.5
19A.2H⁺	-7283.185147	0.0
18B.2H⁺	-7283.179498	3.5
19A.2H⁺	-9286.494571	0.0
*19B.2H⁺	-9286.485212	5.9

***16A.2H⁺**, ***19B** and ***19B.2H⁺** were not formed in the reaction. However, for our calculation purpose, we have energy minimized optimized structures of ***16A.2H⁺**, ***19B** and ***19B.2H⁺**.

5.3.2.7 Electronic spectral analysis

The electronic absorption spectra of **16**, **17**, **18** and **19** were recorded in CH₂Cl₂ solution. In every case, a splitted B band between 600-650 nm and a Q-type band from 900-920 nm were seen, showing porphyrinoid aromatic taste of the

molecules. The minor change in absorption intensity on change of solvent (Figure 5.32, 5.33) suggesting no conformational change.

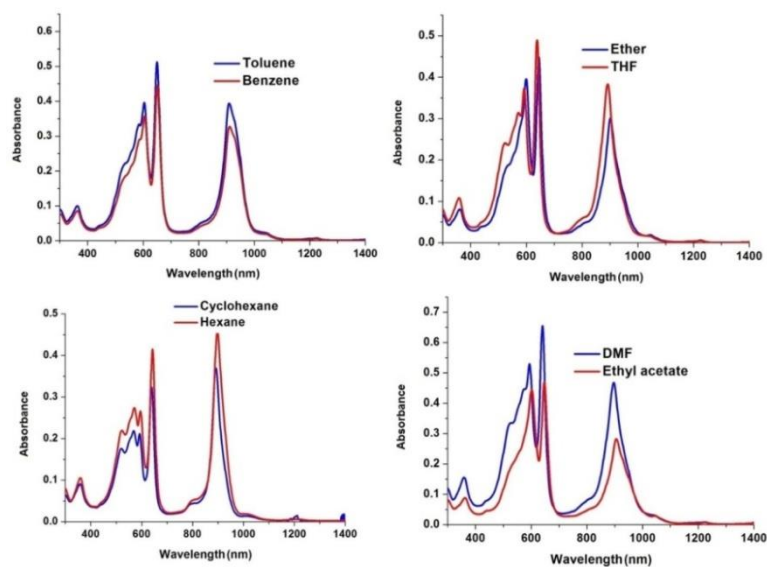


Figure 5.32: Electronic absorption spectra of **16** in various solvents.

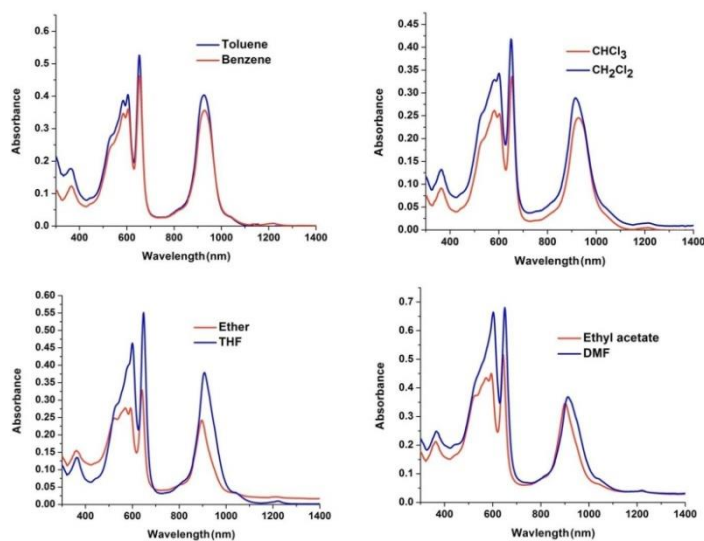


Figure 5.33: Electronic absorption spectra of **17** in various solvents.

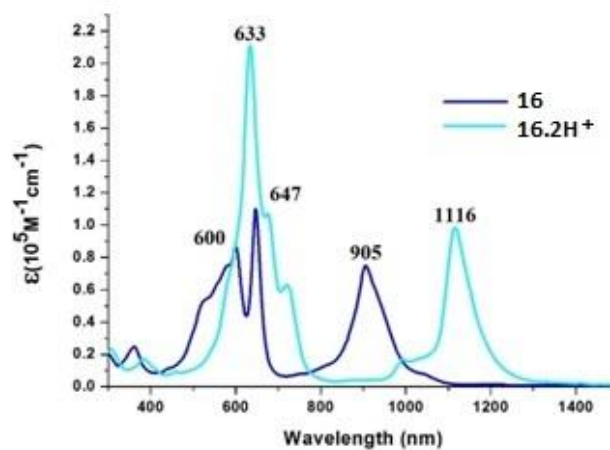


Fig. 5.34: Electronic absorption Spectra of **16** and **16.2H⁺** in CH₂Cl₂.

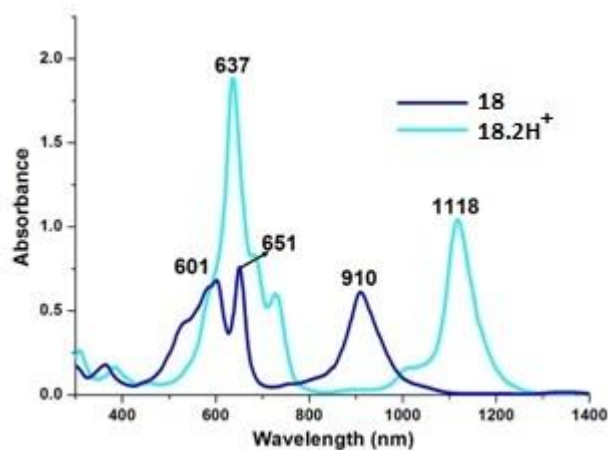


Fig. 5.35: Electronic absorption Spectra of **18** and **18.2H⁺** in CH₂Cl₂.

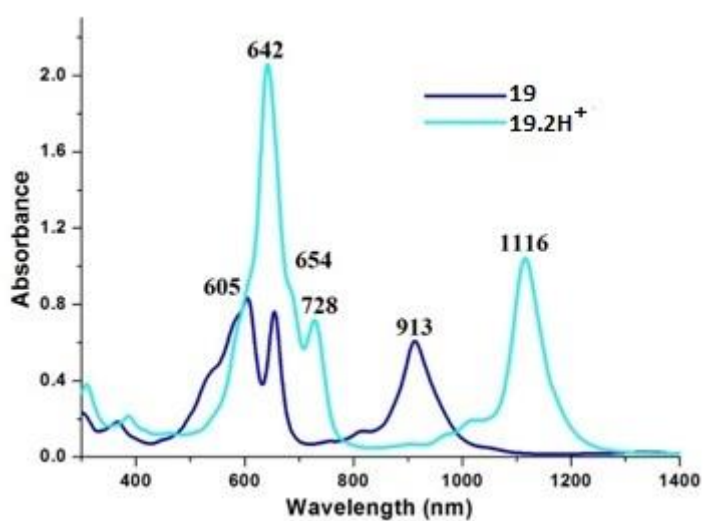


Fig. 5.36: Electronic absorption Spectra of **19** and **19.2H⁺** in CH₂Cl₂.

Upon protonation of pyrrolic nitrogens with dilute solution of TFA in CH_2Cl_2 , the Soret like band is moderately red shifted and Q-like band experience a red shift of >200 nm with two fold increase in Soret type band intensity. A representative absorption spectra of **16** shown in Figure 5.34 exhibit Soret like band at 600 nm ($\epsilon = 8.65 \times 10^4 \text{ dm}^3\text{mol}^{-1}\text{cm}^{-1}$) and 647 nm ($\epsilon = 1.10 \times 10^5 \text{ dm}^3\text{mol}^{-1}\text{cm}^{-1}$) and a broad Q-like band at 905 nm ($\epsilon = 7.45 \times 10^4 \text{ dm}^3\text{mol}^{-1}\text{cm}^{-1}$). Protonation leads to red shift of Soret type band to 633 nm ($\epsilon = 2.10 \times 10^5 \text{ dm}^3\text{mol}^{-1}\text{cm}^{-1}$) with double fold increment in ϵ values and the Q-like band is at 1116 nm ($\epsilon = 9.8 \times 10^4 \text{ dm}^3\text{mol}^{-1}\text{cm}^{-1}$). These changes upon protonation are typical of *meso*-aryl expanded porphyrins.³⁰ Upon careful addition of dilute solution of Trifluoroacetic acid in CH_2Cl_2 seems to extinguish absorption followed by shift of the absorption bands with arrival of isobestic points suggesting the binding of TFA anion to the macrocycle. The binding constant evaluated is of the order of 10^3 M^{-1} suggesting a moderate binding. The similar absorption spectral trends were observed in **18** and **19** (Figure 5.35-5.36).

5.4 Conclusion

In conclusion, syntheses spectral and structural characterization of four 34π core modified octaphyrins has been described. Spectral and X-ray structural studies indicate that octaphyrins exhibit rotational isomers and the structure of the isomer depends on the nature of the hetero atom present in the core of the macrocycle. The octaphyrins are aromatic both in freebase and protonated forms. In the protonated forms, counter anion (ClO_4^-) bind to the macrocycle through N-H...O hydrogen bonding interaction and anions are found above and below the macrocyclic plane. The NICS(0) values and AICD plots satisfactorily explains the aromaticity and the presence of diatropic ring current in both

freebase and protonated forms. DFT calculations support the exclusive formation of particular isomer upon protonation in terms of stabilization energies. Further studies on their excited state properties and nonlinear optical behaviour by two photon absorption technique are in progress to exploit their diverse chemistry.

5.5 Experimental Procedure

5.5.1 Synthesis of 16

A mixture of 5,5''-bis(mesityl(1H-pyrrol-2-yl)methyl)-2,2':5',2''-terthiophene (200 mg, 0.31mmol) (**21**) and [2,2':5',2''-terthiophene]-5,5''-diylbis(mesitylmethanol) (169 mg, 0.31 mmol) (**20a**) were dissolved in 200 ml of dry CH₂Cl₂ and the mixture solution was stir for 15 min. TFA (24 μ l, 0.31 mmol) resulting solution was added and stirred for 1h. The pathway of the reaction was observed by TLC. DDQ (212 mg, 0.93 mmol) to the reacting solution was stirred for more 1h. The solvent was dried. The residual was purified by basic alumina following silica gel (100-200 mesh) purification. The dark blue color eluted with CH₂Cl₂/*n*-hexane (55:45, v/v) and was octaphyrin (**16**) in 12% yield. Recrystallization with CH₂Cl₂/CH₃OH gave bronze color crystalline product.

Compound 16: ¹H NMR (400 MHz, Toluene-d₈) δ (in ppm) = 9.85 (d, 1H), 9.83 (d, 1H), 9.76 (d, 1H), 9.21 (s, 5H), 8.60 (s, 1H), 8.58 (d, 1H), 8.49 (d, 1H), 8.06 (s, 4H), 7.39 (s, 2H), 7.25 (s, 2H), 7.16 (s, 8H), 2.60 (s, 3H), 2.53 (s, 3H), 2.46 (s, 12H), 2.34 (s, 6H), 2.16 (s, 6H), 2.12 (s, 12H), 0.37 (s, 3H), -1.26 (s, 1H); **16.2H⁺** : ¹H NMR (400 MHz, Toluene-d₈) δ (in ppm) = 11.28 (d, 1H), 11.16 (d, 1H), 11.07 (d, 1H), 10.47 (d, 1H), 9.34 (d, 1H), 9.29 (d, 1H), 7.61 (s, 2H), 7.45 (s, 2H), 2.75 (s, 3H), 2.67 (s, 3H), 2.59 (s, 2H), 2.31 (s, 6H), 2.01 (s, 4H), -2.76 (s, 1H, NH), -4.29 (d, 1H), -4.70 (d, 1H).

16: UV/Vis (CH₂Cl₂): λ_{\max} in nm (ϵ in dm³mol⁻¹cm⁻¹) = 600 (8.65×10⁴), 647 (1.10×10⁵), 905 (7.45×10⁴); **16**·2H⁺: (TFA/CH₂Cl₂): λ_{\max} in nm (ϵ in dm³mol⁻¹cm⁻¹) = 633 (2.10×10⁵), 1116 (9.80×10⁴).

5.5.2 Synthesis of **17**

5,5''-Bis(mesityl(1H-pyrrol-2-yl)methyl)-2,2':5',2''-terthiophene (200 mg, 0.34 mmol) (**21**), [2,2':5',2''-terthiophene]-5,5''-diylbis(tolylmethanol) (185 mg, 0.34 mmol) (**20b**) and Trifluoroacetic acid (26 μ l, 0.34 mmol) was taken in 200 ml of dry CH₂Cl₂ in same synthetic procedure as shown in **16**. DDQ (232 mg, 1.02 mmol) for oxidation was added, the residue went under purification by basic alumina followed by silica gel (100-200 mesh) column chromatography. The blue colour band with CH₂Cl₂/*n*-hexane (58:42, v/v) and identified as octaphyrin (**17**) in 10% yield.

Compound 17: ¹H NMR (400 MHz, Toluene-d₈) δ (in ppm) = 9.88-9.80 (m, 3H), 9.31 (s, 2H), 9.21 (s, 2H), 8.74 (d, 1H), 8.63 (d, 1H), 8.53 (s, 1H), 8.34 (d, 1H), 8.27 (s, 2H), 8.13 (s, 3H), 7.88 (s, 4H), 7.59 (d, 2H), 7.44 (d, 3H), 7.34 (s, 4H), 7.24 (s, 4H), 2.54 (s, 6H), 2.45 (s, 6H), 2.22 (s, 12H), 2.13 (s, 25H), 0.48 (m, 4H), -1.10 (d, 1H), -1.24 (d, 1H). **17**·2H⁺: ¹H NMR (400 MHz, Toluene-d₈) δ (in ppm) = 11.06-10.83 (m, 5H), 10.61 (s, 1H), 10.26 (d, 1H), 10.12 (d, 1H), 9.19 (d, 2H) 9.16 (d, 1H), 9.09 (d, 2H), 8.99 (d, 2H), 8.88 (d, 2H), 8.69 (d, 1H), 8.59 (d, 1H), 8.44 (d, 1H), 7.88 (d, 2H), 7.76 (d, 2H), 7.63 (s, 1H), 7.59 (s, 2H), 7.44 (s, 2H), 7.34 (s, 1H), 2.73 (s, 3H), 2.67 (s, 6H), 2.63 (s, 3H), 2.30 (s, 6H), 2.03 (s, 6H), -1.12 (s, 1H, NH), -3.12 (d, 1H), -3.27 (s, 1H, NH), -3.73 (d, 1H), -3.86 (d, 1H), -4.09 (d, 1H). **17:** UV/Vis (CH₂Cl₂): λ_{\max} in nm (ϵ in dm³mol⁻¹cm⁻¹) = 602 (8.58×10⁴), 650 (1.03×10⁵), 917 (7.32×10⁴); **17**·2H⁺ (TFA/CH₂Cl₂): λ_{\max} in nm (ϵ in dm³mol⁻¹cm⁻¹) = 634 (2.07×10⁵), 1153 (8.95×10⁴).

5.5.3 Synthesis of 18

5,5''-bis(mesityl(1H-pyrrol-2-yl)methyl)-2,2':5',2''-terthiophene (200 mg, 0.31mmol) (**21**), (5,5'-(selenophene-2,5-diyl)bis(thiophene-5,2-diyl))bis(mesitylmethanol) (184 mg, 0.30mmol) (**22**) and TFA (24 μ l, 0.31mmol) under same condition as shown in **17** in 200 ml of dry CH₂Cl₂. DDQ (213 mg, 0.93mmol) addition for oxidation was done and remaining was treated by basic alumina further by silica gel (100-200 mesh) column. The dark blue colour band with CH₂Cl₂/*n*-hexane (58:42, v/v) is Octaphyrin (**18**) in 9% yield.

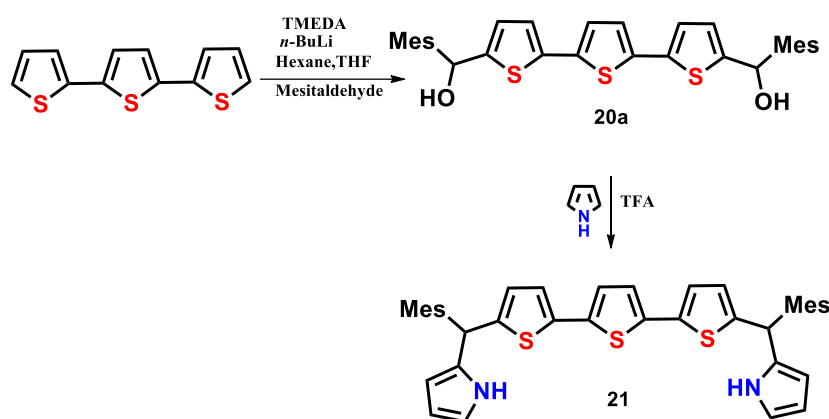
Compound 18: ¹H NMR (400 MHz, Toluene-d₈) δ (in ppm) = 10.03 (d, 1H), 9.93 (d, 1H), 9.81 (d, 2H), 9.71 (d, 2H), 9.20 (d, 2H), 9.06 (d, 2H), 8.78-8.73 (m, 4H), 8.56 (d, 1H), 8.48 (d, 2H), 8.42 (d, 1H), 8.08 (d, 2H), 8.02 (d, 2H), 7.37 (s, 4H), 7.23 (s, 4H), 7.15 (s, 8H), 2.58 (s, 3H), 2.52 (s, 3H), 2.45 (s, 12H), 2.32 (s, 6H), 2.11 (s, 12H), 0.49 (s, 3H), 0.14 (s, 3H), -1.01 (s, 1H), -1.22 (s, 1H); **18.2H⁺** : ¹H NMR (400 MHz, Toluene-d₈) δ (in ppm) = 11.60 (d, 1H), 11.47-11.45 (m, 2H), 11.29 (d, 1H), 11.19 (d, 1H), 11.03 (d, 1H), 10.82-10.80 (m, 4H), 10.47 (d, 1H), 10.37 (d, 1H), 10.16-10.13 (m, 4H), 9.40 (d, 1H), 9.35 (d, 1H), 9.30-9.28 (m, 2H), 9.02 (d, 2H), 8.99 (d, 1H), 7.62 (s, 2H), 7.60 (s, 2H), 7.46 (s, 4H), 7.37 (s, 8H), 2.76 (s, 6H), 2.68 (s, 3H), 2.63 (s, 12H), 2.25 (s, 6H), 2.07 (s, 12H), 2.00 (s, 6H), -3.35 (s, 4H), -4.02 (s, 4H), -4.13 (d, 1H), -4.36 (d, 1H), -4.73 (d, 1H), -4.92 (d, 1H), -6.54 (NH, br). **18:** UV/Vis (CH₂Cl₂): λ_{\max} in nm (ϵ in dm³mol⁻¹cm⁻¹) = 601 (8.54 \times 10⁴), 651 (9.48 \times 10⁴), 910 (7.65 \times 10⁴); **18.2H⁺** (TFA/CH₂Cl₂): λ_{\max} in nm (ϵ in dm³mol⁻¹cm⁻¹) = 637 (2.35 \times 10⁵), 1118 (1.30 \times 10⁵).

5.5.4 Synthesis of 19

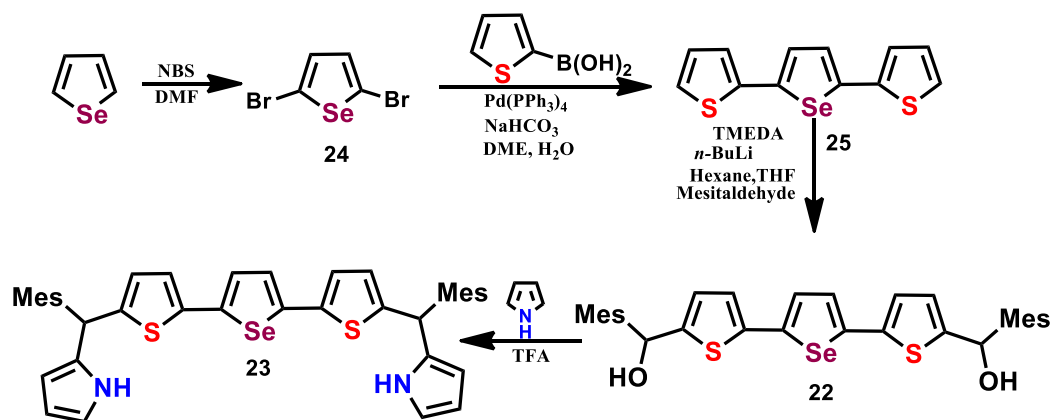
2,5-bis(5-(mesityl(1H-pyrrol-2-yl)methyl)thiophen-2-yl)selenophene (200mg, 0.29mmol) (**23**), diol (171 mg, 0.29mmol) (**22**) and TFA (22 μ l, 0.29mmol) under similar condition as mentioned in **18** in 200 ml of dry CH₂Cl₂. DDQ (165 mg, 0.80 mmol) was added for oxidation, the residual was treated by basic alumina following silica gel (100-200 mesh) column. The band eluted with CH₂Cl₂/*n*-hexane (52:48, v/v) and identified as Octaphyrin (**19**) in 10% yield.

Compound 19: ¹H NMR (400 MHz, Toluene-d₈) δ (in ppm) = 9.25 (d, 4H), 8.91 (d, 4H), 8.18 (s, 4H), 7.22 (s, 8H), 2.52 (s, 12H), 2.16 (s, 24H), 2.12 (s, 12H), 0.037 (s, 3H); **19**·2H⁺: ¹H NMR (400 MHz, Toluene-d₈) δ (in ppm) = 10.93 (d, 4H), 10.28 (d, 4H), 9.11 (s, 4H), 7.41 (s, 8H), 2.67 (s, 12H), 1.97 (s, 24H), -4.04 (s, 4H), -4.59 (NH, br). **19**: UV/Vis (CH₂Cl₂): λ_{max} in nm (ϵ in dm³mol⁻¹cm⁻¹) = 605 (8.48 \times 10⁴), 654 (7.74 \times 10⁴), 913 (6.18 \times 10⁴); **19**·2H⁺ (TFA/CH₂Cl₂): λ_{max} in nm (ϵ in dm³mol⁻¹cm⁻¹) = 642 (2.09 \times 10⁵), 1116 (1.24 \times 10⁵).

5.5.5 Precursor syntheses



Scheme 5.6: Precursor Synthesis.



Scheme 5.7: Precursor Synthesis.

5.5.5.1 Synthesis of **20a**

Terthiophene (1 g, 4 mmol), N,N,N'N'-tetramethylethylene diamine (1.8 ml, 12 mmol), *n*-butyllithium (7.8 ml, 1.6 M in hexane, 12 mmol) and mesitaldehyde (1.07 ml, 12 mmol) in 15 ml dry THF. The product was purified by silica gel (100-200 mesh) column chromatography. Pale yellow color band eluted with ethyl acetate/hexane (23:77, V/V) considered as desired diol **5,5'**-bis(mesitylhydroxymethyl)-2,2':5,2''-terthiophene (**20a**) with yield 64%. **20b** was made under similar synthetic scheme.

^1H NMR (400 MHz, CDCl_3 , 298K): δ (ppm): 6.98 (s, 2H), 6.95 (d, 2H), 6.88 (s, 4H), 6.54 (d, 2H); 6.41 (s, 2H); 2.35 (s, 12H); 2.30 (s, 6H).

5.5.5.2 Synthesis of **21**

To a solution of **20a** (0.5 g, 0.92 mmol) in pyrrole (2.6 ml, 36 mmol), TFA (0.007 ml, 0.09 mmol) was added and stirred for 40 minutes under nitrogen atmosphere. The crude product was extracted and then purified by silica gel (100-200 mesh) column chromatography. The light yellow color compound was eluted with ethyl acetate/hexane (9:91) identified as desired compound **5,18-dimesityl-24,25,26-trithiapentapyrrane (21)** with 91% yield.

^1H NMR (400 MHz, CDCl_3 , 298K): δ (ppm): 7.80 (br, 2H), 6.98 (d, $J= 4.3\text{Hz}$, 2H), 6.94 (s, 2H), 6.88 (s, 4H), 6.76 (m, $J= 4.3\text{ Hz}$, 2H), 6.68 (d, $J= 3.2\text{ Hz}$, 2H), 6.19 (m, $J= 3.2\text{ Hz}$, 2H), 6.11 (d, $J= 3.2\text{ Hz}$, 2H), 6.04 (s, 2H), 2.29 (s, 2H), 2.15 (s, 12H).

5.5.5.3 Synthesis of **22**

2,5-di(thiophene-2-yl)selenophene (1 g, 3.3 mmol), N,N,N'N' -tetramethylethylenediamine (1.2 ml, 8.4 mmol), *n*-butyllithium (7.2 ml, 1.6 M in hexane, 10 mmol) and mesitaldehyde (0.78 ml, 10 mmol) in 15 ml dry THF. The product was purified by silica gel (100-200 mesh) column chromatography. Pale yellow color band eluted with ethyl acetate/hexane (23:77, V/V) considered as desired diol (5,5'-(selenophene-2,5-diyl)bis(thiophene-5,2-diyl))bis(mesitylmethanol) (**22**) with yield 51%.

^1H NMR (400 MHz, CDCl_3 , 298K): δ (ppm): 7.10 (s, 2H), 6.98 (d, 2H), 6.89 (s, 4H), 6.55 (d, 2H), 6.41 (s, 2H), 2.35 (s, 12H), 2.30 (s, 6H).

5.5.5.4 Synthesis of **23**

To a solution of **22** (1 g, 1.6 mmol) in pyrrole (4.7 ml, 67 mmol), TFA (0.013 ml, 0.16 mmol) was added and stirred for 40 minutes under nitrogen atmosphere. The crude product was extracted and then purified by silica gel (100-200 mesh) column chromatography. The light yellow color compound was eluted with ethyl acetate/hexane (9:91) identified as desired compound 2,5-bis(5-(mesityl(1H-pyrrol-2-yl)methyl)thiophen-2-yl)selenophene (**23**) with 89% yield.

^1H NMR (400 MHz, CDCl_3 , 298K): δ (ppm): 7.81 (br, 2H), 6.99 (d, $J= 4.3\text{Hz}$, 2H), 6.9 (s, 2H), 6.89 (s, 4H), 6.78 (m, $J= 4.3\text{ Hz}$, 2H), 6.69 (d, $J= 3.2\text{ Hz}$, 2H), 6.21 (m, $J= 3.2\text{ Hz}$, 2H), 6.13 (d, $J= 3.2\text{ Hz}$, 2H), 6.05 (s, 2H), 2.29 (s, 2H), 2.15 (s, 12H).

5.5.5.5 Synthesis of 24

To the suspension of selenophene (2 g 15.2 mmol) in DMF excess N-bromosuccinimide (13.51 g, 76.3 mmol) was added and to mixture and stirred entire 12h in ambient temperature. The crude mixture was collected with CH₂Cl₂. The organic layer was cleaned with saturated NaHCO₃ and brine solution. The residue was precipitated in ethanol and filtered to give white solid 2,5-dibromoselenophene (**24**) with yield of 85%.

¹H NMR (400 MHz, CDCl₃, 298K): δ (ppm): 7.45 (s, 2H).

5.5.5.6 Synthesis of 25

2,5-dibromoselenophene (1 gm, 3.4 mmol) and 2-thiophene boronic acid (1.1 gm, 8.6 mmol) was added in 3:1 (V/V) DME and water solvents mixture under nitrogen atmosphere. Then NaHCO₃ (1.50 gm, 17 mmol) was added in the reaction mixture. The solution was further purged with nitrogen for about 15 min and then Pd(PPh₃)₄ (0.39 gm, 0.34 mmol) was added under nitrogen atmosphere. The reaction was allowed to stir for 8 h then work up was performed, dried by Na₂SO₄ and purified by column chromatography using silica gel (100-200 mesh) in hexane and ethyl acetate (92:8). The compound was further recrystallized from CH₂Cl₂/n-hexane to afford white solid 2,5-di(thiophen-2-yl)selenophene (**25**) in 71% Yield.

¹H NMR (400 MHz, CDCl₃, 298K): δ (ppm): 7.68 (d, 2H), 7.56 (s, 2H), 7.45(d, 2H), 7.17 (m, 2H).

5.6 References

1. N. Shivran, S. C. Gadekar, V. G. Anand, *Chem. Asian J.* **2017**, *12*, 6-20.
(b) T. Sarma, G. Kim, S. Sen, W.-Y. Cha, Z. Duan, M. D. Moore, V. M. Lynch, Z. Zhang, D. Kim, J. L. Sessler, *J. Am. Chem. Soc.* **2018**, *140*, 12111-12119. (c) S.-i. Ishida, J. Kim, D. Shimizu, D. Kim, A. Osuka, *Angew. Chem. Int. Ed.* **2018**, *57*, 5876-5880. (d) N. Sprutta, L. Latos-Grażyński, *Chem. Eur. J.* **2001**, *7*, 5099-5112. (e) D. Seidel, V. Lynch, J. L. Sessler, *Angew. Chem. Int. Ed.* **2002**, *41*, 1422-1425.
2. E. Vogel, M. Bröring, J. Fink, D. Rosen, H. Schmickler, J. Lex, K. W. K. Chan, Y.-D. Wu, D. A. Plattner, M. Nendel, K. N. Houk, *Angew. Chem. Int. Ed. Engl.* **1995**, *34*, 2511-2514.
3. K. Mitsuno, T. Yoshino, I. Gupta, S. Mori, S. Karasawa, M. Ishida, H. Furuta, *Angew. Chem. Int. Ed.* **2017**, *56*, 14252-14256.
4. V. G. Anand, S. K. Pushpan, S. Venkatraman, A. Dey, T. K. Chandrashekar, B. S. Joshi, R. Roy, W. Teng, K. R. Senge, *J. Am. Chem. Soc.* **2001**, *123*, 8620-8621.
5. J. S. Reddy, S. Mandal, V. G. Anand, *Org. Lett.* **2006**, *8*, 5541-5543.
6. H. Rath, J. Sankar, V. Prabhuraja, T. K. Chandrashekar, B. S. Joshi, R. Roy, *Chem. Commun.* **2005**, 3343-3345.
7. V. G. Anand, S. Saito, S. Shimizu, A. Osuka, *Angew. Chem. Int. Ed.* **2005**, *44*, 7244-7248.
8. G. Karthik, W.-Y. Cha, A. Ghosh, T. Kim, A. Srinivasan, D. Kim, T. K. Chandrashekar, *Chem. Asian J.* **2016**, *11*, 1447-1453.
9. E. Vogel, M. Köcher, H. Schmickler, J. Lex, *Angew. Chem. Int. Ed. Engl.* **1986**, *25*, 257-259.

-
10. J. L. Sessler, E. A. Brucker, S. J. Weghorn, M. Kisters, M. Schäfer, J. Lex, E. Vogel, *Angew. Chem. Int. Ed. Engl.* **1994**, *33*, 2308-2312.
11. E. Vogel, M. Bröring, S. J. Weghorn, P. Scholz, R. Deponte, J. Lex, H. Schmickler, K. Schaffner, S. E. Braslavsky, M. Müller, S. Pörting, C. J. Fowler, J. L. Sessler, *Angew. Chem. Int. Ed. Engl.* **1997**, *36*, 1651-1654.
12. (a) H. Furuta, T. Asano, T. Ogawa, *J. Am. Chem. Soc.* **1994**, *116*, 767-768. (b) P. J. Chmielewski, L. Latos-Grażyński, K. Rachlewicz, T. Głowiak, *Angew. Chem., Int. Ed. Engl.* **1994**, *33*, 779-781.
13. V. V. Roznyatovskiy, C.-H. Lee, J. L. Sessler, *Chem. Soc. Rev.* **2013**, *42*, 1921-2204.
14. T. Chatterjee, A. Srinivasan, M. Ravikanth, T. K. Chandrashekar, *Chem. Rev.* **2017**, *117*, 3329-3376.
15. T. Sharma, P. K. Panda, *Chem. Rev.* **2017**, *117*, 2785-2838.
16. (a) K. Rachlewicz, N. Sprutta, P. J. Chmielewski, L. Latos-Grażyński, *J. Chem. Soc., Perkin Trans. 2.* **1998**, 969-976. (b) S. J. Narayanan, B. Sridevi, T. K. Chandrashekar, U. Englisch, K. Ruhlandt-Senge, *Inorg. Chem.* **2001**, *40*, 1637-1645.
17. S. K. Pushpan, A. Srinivasan, V. G. Anand, S. Venkatraman, T. K. Chandrashekar, B. S. Joshi, R. Roy, H. Furuta, *J. Am. Chem. Soc.* **2001**, *123*, 5138-5139.
18. L. Simkhovich, S. Rosenberg, Z. Gross, *Tetrahedron Lett.* **2001**, *42*, 4929-4931.
19. I. Gupta, A. Srinivasan, T. Morimoto, M. Toganoh, H. Furuta, *Angew. Chem. Int. Ed.* **2008**, *47*, 4563-4567.
-

-
20. S. Gokulnath, K. Yamaguchi, M. Toganoh, S. Mori, H. Uno, H. Furuta, *Angew. Chem. Int. Ed.* **2011**, *50*, 2302-2306.
21. A. Srinivasan, T. Ishizuka, A. Osuka, H. Furuta, *J. Am. Chem. Soc.* **2003**, *125*, 878-879.
22. Y.-S. Xie, K. Yamaguchi, M. Toganoh, H. Uno, M. Suzuki, S. Mori, S. Saito, A. Osuka, H. Furuta, *Angew. Chem. Int. Ed.* **2009**, *48*, 5496-5499.
23. V. G. Anand, S. K. Pushpan, S. Venkatraman, S. J. Narayanan, A. Dey, T. K. Chandrashekar, R. Roy, B. S. Joshi, S. Deepa, G. N. Sastry, *J. Org. Chem.* **2002**, *67*, 6309-6319.
24. K. Zhang, J. Zhang, X. Li, R. Guo, H. Ågren, Z. Ou, M. Ishida, H. Furuta, Y. Xie, *Org. Lett.* **2015**, *17*, 4806-4809.
25. R. Misra, T. K. Chandrashekar, *Acc. Chem. Res.* **2008**, *41*, 265-279.
26. (a) A. Chaudhary, A. Srinivasan, T. K. Chandrashekar, *The Handbook of Porphyrin Science*, K. M. Kadish, K. M. Smith, R. Guilard, World scientific Ltd, **2014**, *32*, 271-366. (b) J.-Y. Shin, K. S. Kim, M.-C. Yoon, J. M. Lim, Z. S. Yoon, A. Osuka, D. Kim, *Chem. Soc. Rev.* **2010**, *39*, 2751-2767. (c) J. M. Lim, Z. S. Yoon, J.-Y. Shin, K. S. Kim, M.-C. Yoon, D. Kim, *Chem. Commun.* **2008**, 261-273. (d) R. Kumar, R. Misra, T. K. Chandrashekar, A. Nag, D. Goswami, E. Suresh, C. H. Suresh, *Eur. J. Org. Chem.* **2007**, 4552-4562. (e) H. Rath, J. Sankar, V. Prabhuraja, T. K. Chandrashekar, A. Nag, D. Goswami, *J. Am. Chem. Soc.* **2005**, *127*, 11608-11609.
27. W.-Y. Cha, T. Kim, A. Ghosh, Z. Zhang, X.-S. Ke, R. Ali, V. M. Lynch, J. Jung, W. Kim, S. Lee, S. Fukuzumi, J. S. Park, J. L. Sessler, T. K. Chandrashekar, D. Kim, *Nat. Chem.* **2017**, *9*, 1243-1248.
-

28. H. Rath, V. Prabhuraja, T. K. Chandrashekar, A. Nag, D. Goswami, B. S. Joshi, *Org. Lett.* **2006**, *8*, 2325-2328.
29. S. Kumar, M. Ravikanth, *J. Org. Chem.* **2017**, *82*, 12359-12365.
30. R. Kumar, R. Misra, T. K. Chandrashekar, E. Suresh, *Chem. Commun.* **2007**, 43-45.
31. T. K. Chandrashekar, V. Prabhuraja, S. Gokulnath, R. Sabarinathan, A. Srinivasan, *Chem. Commun.* **2010**, *46*, 5915-5917.
32. V. G. Anand, S. Venkatraman, H. Rath, T. K. Chandrashekar, W. Teng, K. Ruhlandt-Senge, *Chem. Eur. J.* **2003**, *9*, 2282-2290.

CHAPTER 6

Core-modified 48π and 42π decaphyrins: syntheses, properties and structures

6.1	Introduction	168
6.2	Objective	170
6.3	Results and Discussion	171
6.3.1	Synthesis	171
6.3.2	Spectral characterisation	173
6.3.2.1	Mass spectrometric analysis	173
6.3.2.2	NMR Analysis	175
6.3.2.3	Single crystal X-ray analysis	181
6.3.2.4	DFT Calculations	188
6.3.2.5	Electronic spectral analyses	191
6.4	Conclusions	193
6.5	Experimental Procedure	194
6.5.1	Synthetic procedure of 10	194
6.5.2	Synthetic procedure of 12	195
6.5.3	Precursor Syntheses	196
6.5.3.1	Synthesis of 14	197
6.5.3.2	Synthesis of 7	197
6.6	References	198

6.1 Introduction

Expanded porphyrins¹ by virtue of their diverse applications such as nonlinear optical materials,² sensitizers for PDT,³ models for Hückel,⁴ Möbius⁵ and Baird type⁶ aromaticity, radiation therapy enhancers³ and contrast agent in MRI⁷ have attracted attention of researchers working in the areas of material science,⁸ chemistry⁹ and biology.¹⁰ Expanded porphyrins containing up to eight pyrrole/heterocyclic rings connected through *meso* carbon bridges are well documented in literature.¹¹⁻¹⁴ However, studies on higher analogues containing ten or more heterocyclic rings in conjugations are only limited owing to synthetic difficulties, conformational flexibilities and stability. Early synthesis of few higher analogues include Sessler's 40π turcasarin **1**¹⁵ and its di-oxa analogues **2**,¹⁶ (Figure 6.1) Setsune's 48π dodecaphyrin and 64π helical hexadecaphyrin,¹⁷ Osuka's helical 56π dodecaphyrin,¹⁸ ring size selective syntheses of expanded porphyrins and a 42π core-modified decaphyrin.¹⁹

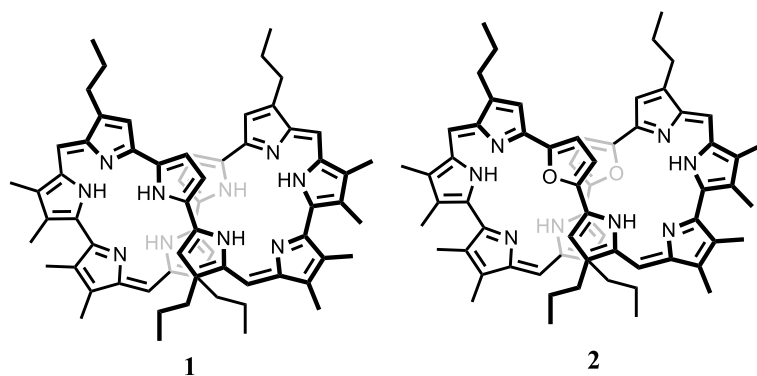


Figure 6.1: Structures of Turcasarin **1** and its di-oxa complex **2**.

These reports were confined only to develop the synthetic methods and their characterizations. Osuka and coworkers were the first to report studies on chemistry of decaphyrins.²⁰ They used an internal bridge containing 1,4-phenylene and 2,5-thienylene inside decaphyrin core **3**^{21a, 21b} to avoid figure-eight conformation (Figure

6.2). This attachment not only resulted in restoration of effective 46π electronic conjugation but also restores diatropic ring current. Later, they reported reductive metalation of 44π decaphyrin with Pd(II) which gave 46π Hückel aromatic Pd(II) complex.²² This complex on oxidation with DDQ gave Hückel antiaromatic 44π decaphyrin Pd(II) complex. Further, they reported a stable organic π radical containing Zn(II)-Cu(I)-Zn(II) decaphyrin complex in 2015.²³ This complex was found to be fairly stable despite its radical nature and did not show any intermolecular magnetic interaction due to extensive delocalization. Furthermore, Osuka and coworkers reported 46π decaphyrin **4**. The structure of **4** contains two segments; a semi helical tripyrrolic subunit and a near planar dipyrromethane subunit.^{24a} Later the same group synthesized a series of expanded porphyrins including a 44π decaphyrin by an acid catalyzed reaction of *meso* pentafluoro substituted dipyrromethane with aldehyde.^{24b}

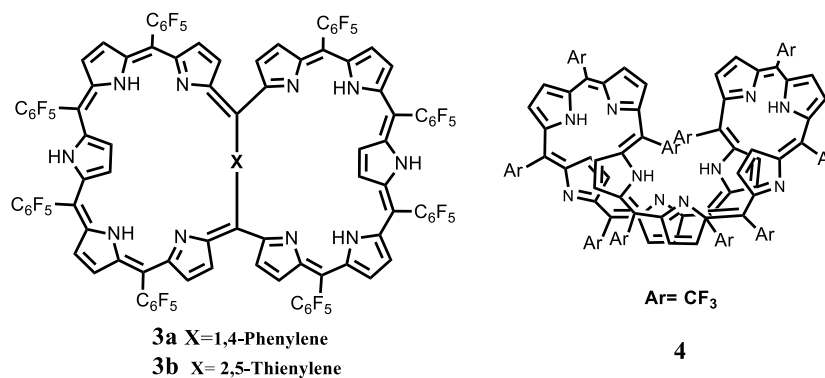


Figure 6.2: Structure of decaphyrin **3** and **4**.

More recently Okujima and Kobayashi reported synthesis of a decaphyrin without any *meso* bridges which shows a red shifted intense L-band at 1982 nm.²⁵ In 2018, Ravikanth and coworkers described synthesis of dibenziddecaphyrins **5**²⁶ and their bis-BF₂ complexes which exhibits figure-eight conformation (Figure 6.3).

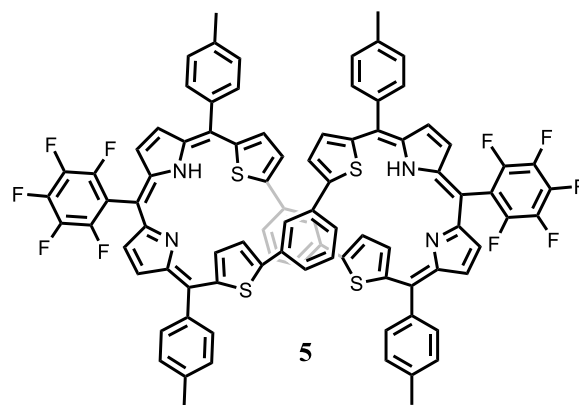


Figure 6.3: Structure of dibenziddecaphyrin **5**.

6.2 Objective

From the above literature survey, it is well understood that decaphyrins exist as figure-eight conformation because of its high degree of flexibilities due to large numbers of meso carbon bridges. In order to avoid the twist, researchers have introduced two different approaches, 1) bridging between the two oppositely oriented meso carbon atoms and 2) reduction of number of meso carbon bridge. Here in this chapter I introduced two different decaphyrin analogues, i) 48π decaphyrin **10** which contains twelve meso carbon bridges and ii) 42π decaphyrin **12** with only four meso carbons Shown in Figure 6.4. The 48π decaphyrin reporting here is the largest decaphyrin reporting till date. Freebase nonaromatic 48π decaphyrin transform into a Hückel antiaromatic decaphyrin upon protonation. Whereas, after reduction of meso carbons bridge the 42π decaphyrin remains twisted conformation due to the macrocyclic rigidity. Therefore the main objective of this chapter is to synthesize highly flexible and rigid decaphyrin analogues and check their aromaticity and structural diversity triggered by protonation.

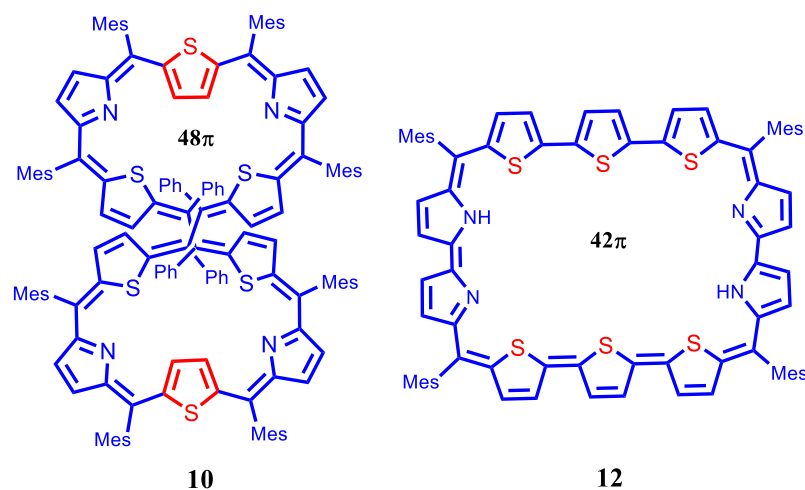
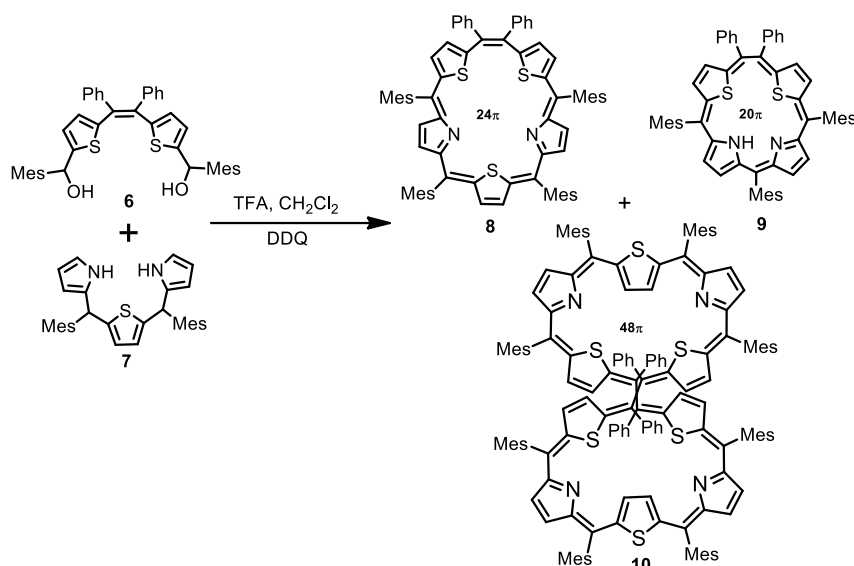


Figure 6.4: Structures of decaphyrins **10** and **12**.

6.3 Results and Discussion

6.3.1 Syntheses

Recently, we reported synthesis of a stable 24π pentaphyrin **8**²⁷ by [3+2] Mac-Donald type condensation of **7** and **6** under acid catalyzed condition in CH_2Cl_2 . In addition to the expected formation of **8**, homoporphyrin **9** was also isolated Scheme 6.1. During the optimization of this reaction, we noticed formation of trace amount decaphyrin **10** when acid concentration was slightly increased in the reaction. When this reaction was probed further using different acid concentrations shown in Table 6.1, we found that the product distribution was altered. For example, use of one equiv. of trifluoroacetic acid (TFA), resulted in formation of **8** and **9** as reported. Reduction of TFA concentration to 0.5 equiv. results in exclusive formation of **8** in about 10% yield in addition to linear chain polymeric products. Increase of TFA concentration to 1.5 equiv. resulted in formation of **8** (10%) and decaphyrin **10** (2%). The yield of 48π decaphyrin **10** increased upon further increase in TFA concentration to 3 equiv. and 10.0 equiv. of TFA resulted in formation of both **8** and **10** in 8% yield.



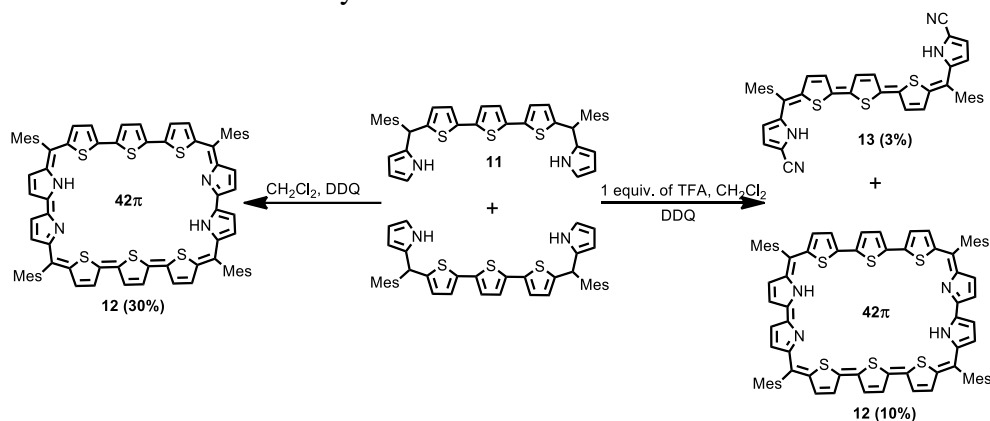
Scheme 6.1: Formation of **8**, **9** and Decaphyrin **10**

Table 6.1: Formation of **8**, **9** and **10** with different concentration of TFA

TFA (Equivalent)	8	Yield(%)	
		9	10
0.5	10	-	-
1.0	10	8	-
1.5	10	-	2
3.0	8	-	6
10.0	8	-	8

We wanted to study the effect of introducing molecular rigidity by reducing the number of *meso* carbons linking the heterocyclic rings on the conformation and properties of the decaphyrin. Keeping this in mind, the 42π decaphyrin **12** was synthesized by oxidative coupling reaction of **11**¹⁹ using 1 equiv. of TFA in CH₂Cl₂ followed by oxidation with 2,3-dichloro-5,6-dicyano-1,4-benzoquinone (DDQ). Furthermore, we noticed formation of **13** where terminal pyrrole rings of **11** have undergone cyanation. Such cyanation reaction of aryl boronic acids with DDQ using Cu-triflate as Lewis acid is reported in literature where DDQ is the source of

cyanide.³¹ When the oxidative coupling reaction was performed in absence of TFA, exclusively decaphyrin **12** was formed in 30% yield shown in Scheme 6.2. Instead of DDQ, we also tried *p*-chloranil for oxidation. The oxidative coupling reaction in presence of 1.0 equiv. of TFA followed by chloranil oxidation gave **12** in 8% yield. However, the yield of **12** was increased significantly to 30% when the reaction was performed without acid catalyst.



Scheme 6.2: Synthesis of Cyano complex **13** and decaphyrin **12**

6.3.2 Spectral Characterization

6.3.2.1 Mass Spectroscopic analysis

The exact composition of **10** was confirmed through mass spectral analysis (m/z , 2154.8571 for **10**) shown in Figure. 6.5. The composition of **13** and **12** were confirmed by HRMS mass spectrometric analysis (m/z , 689.1857 for **13** and m/z , 1277.3817 for **12**) shown in Figure 6.6 and 6.7.

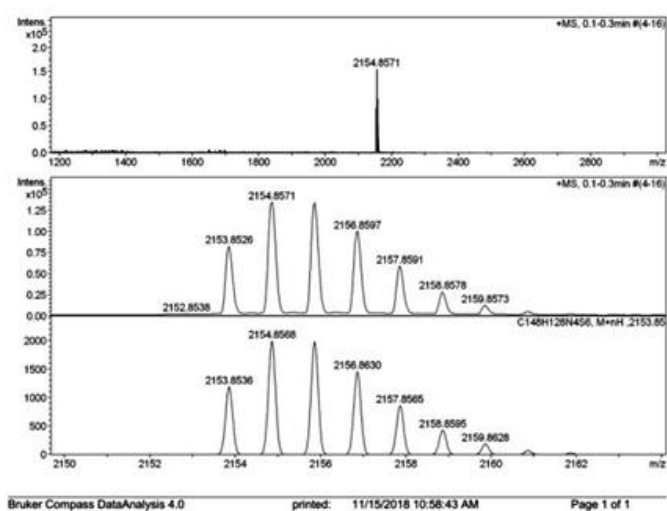


Figure 6.5: HRMS of decaphyrin 10.

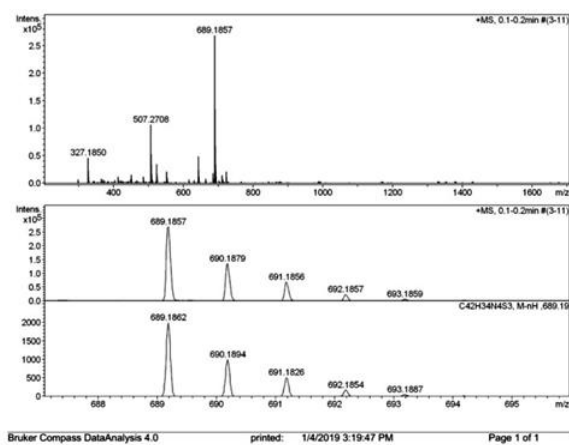


Figure 6.6: HRMS of cyano complex 13.

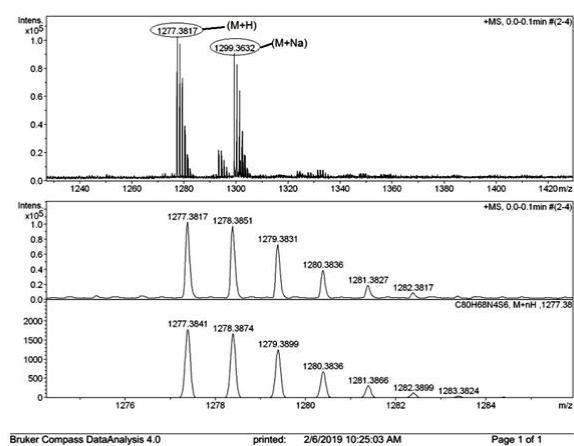


Figure 6.7: HRMS of decaphyrin 12.

6.3.2.2 NMR analysis

The proposed solution structure of decaphyrin **10** was based on ^1H and 2D NMR studies shown in Figure 6.8 and. Specifically, the ^1H NMR spectrum of **10** exhibits a sharp singlet at 8.65 ppm assignable to the β -CH protons of (a) inverted thiophene rings. The pyrrole β -CH protons (b, c) and normal thiophene β -CH protons (d, e) resonate in the region 5.54 - 6.49 ppm while the *meso* phenyl ring protons resonate in the region 7.16 - 7.81 ppm. The *meso* mesityl -CH protons appear between 6.83 -7.10 ppm. All these assignments were confirmed through ^1H - ^1H COSY experiments shown in Figure 6.9. These chemical shift values clearly suggest the nonaromatic nature of **10** in its freebase form. Temperature variation (298K to 193 K) did not show any significant changes in the chemical shifts suggesting the conformational stability of **10** shown in Figure 6.10.

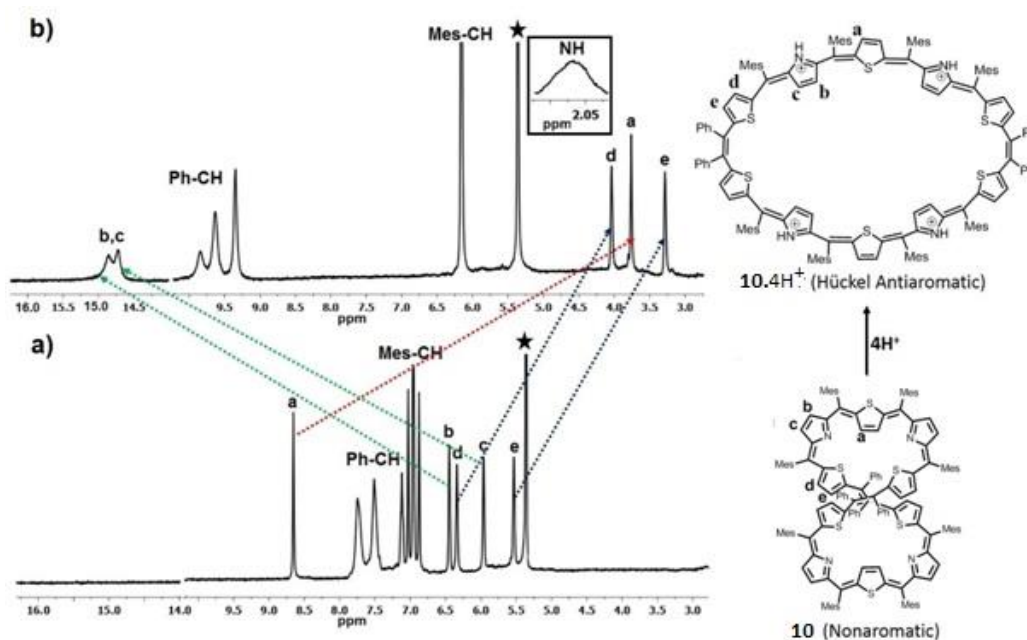


Figure 6.8: ^1H NMR Spectra (a) **10** (298K) and (b) **10.4H⁺** (298K) in CD_2Cl_2 .

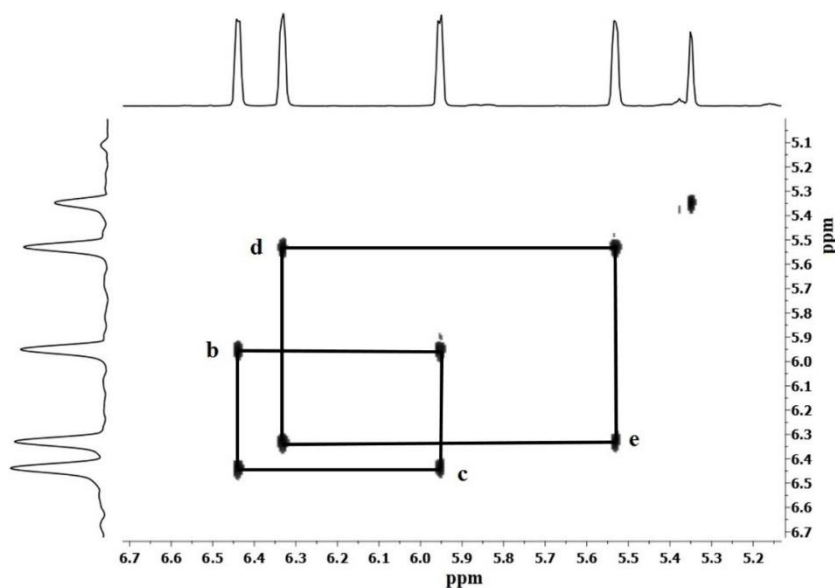


Figure 6.9: ^1H - ^1H COSY spectrum of **10** with correlation in pyrrole and thiophene rings as part of the ethene bridge.

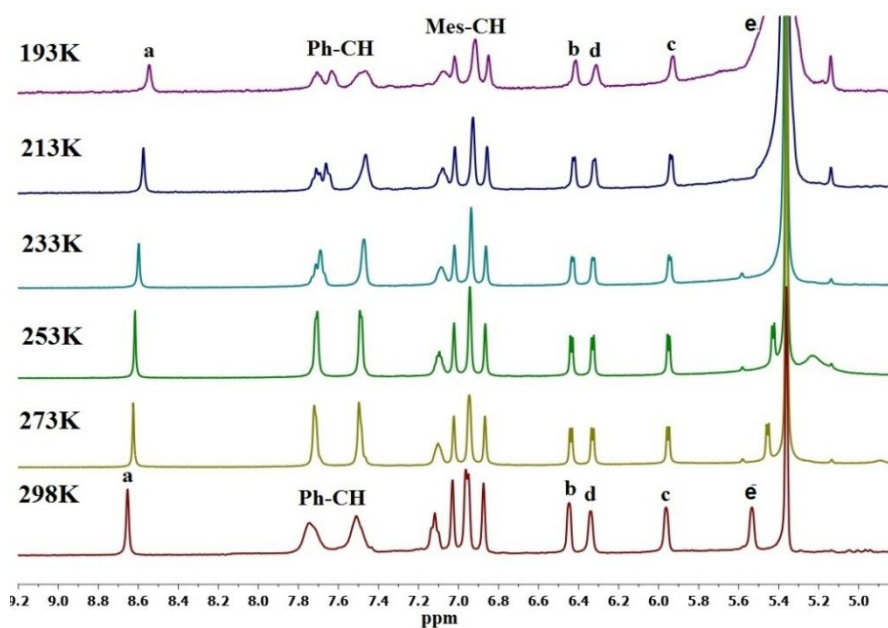


Figure 6.10: Low temperature ^1H NMR spectrum of **10** in CD_2Cl_2 (Aromatic region).

However, significant changes were observed upon protonation of **10**. Specifically, the chemical shifts of pyrrole rings and the β -CH protons (b, c) experience a large deshielding of 8.5 ppm relative to freebase form shown in Figure 6.8b. The central thiophene rings which were inverted in the freebase form comes back to the normal position²⁸ and these protons (a) experience a shielding of 4.9 ppm relative to freebase

form. The normal thiophene ring protons (d, e) also experience a shielding of 2 ppm. The β -CH protons of pyrrole, thiophene unit of tripyrrane moiety and thiophene unit of ethene moieties were resonated at 14.86 and 14.72 (b, c), 3.76 (a) and 4.03 and 3.28 (d, e) ppm respectively. These assignments are confirmed by ^1H - ^1H COSY and 2D NOESY experiments shown in Figure 6.11 and 6.12. The pyrrole NH protons appear as a broad signal at 2.06 ppm and this assignment was confirmed by D_2O exchange experiments. The *meso* phenyl ring protons are also deshielded by 2 ppm. The large deshielding of the β -CH protons of inverted pyrrole rings and shielding of the β -CH protons of thiophene rings upon protonation shown in Figure 6.13 clearly suggests existence of paratropic ring current due to the restoration of π -electronic conjugation. This can happen only when the figure-eight conformation of freebase form change over to an open planar conformation. The appearance of outer pyrrole NH protons at 2.0 ppm also justifies such a conclusion.

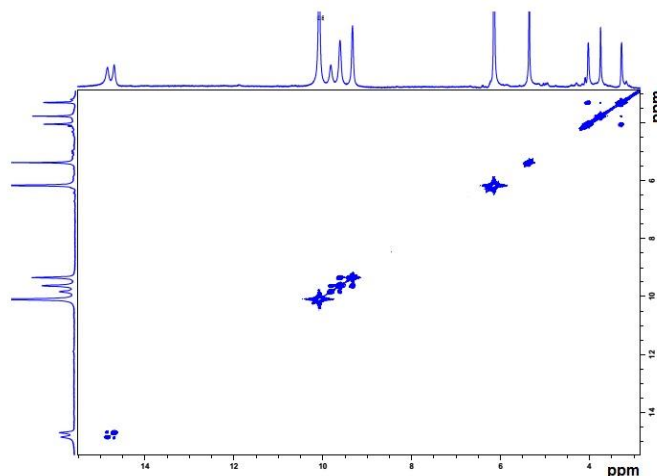


Figure 6.11: ^1H - ^1H COSY spectrum of 10.4H^+ with correlation in pyrrole and thiophene rings as part of the ethene bridge.

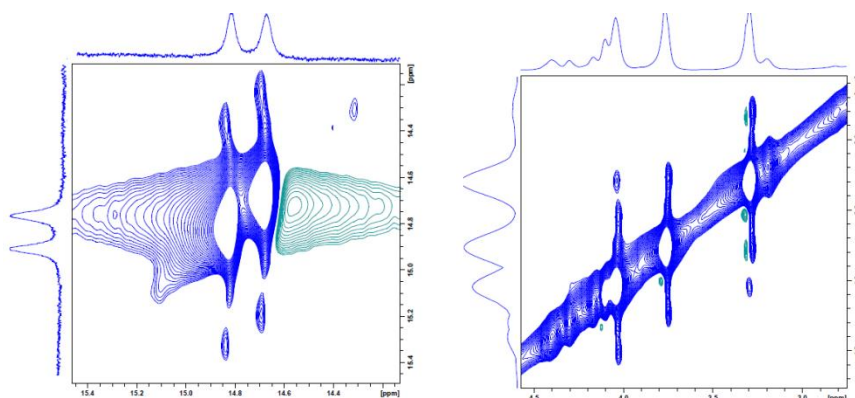


Figure 6.12: 2D NMR NOESY spectrum of 10.4H^+ in CD_2Cl_2 .

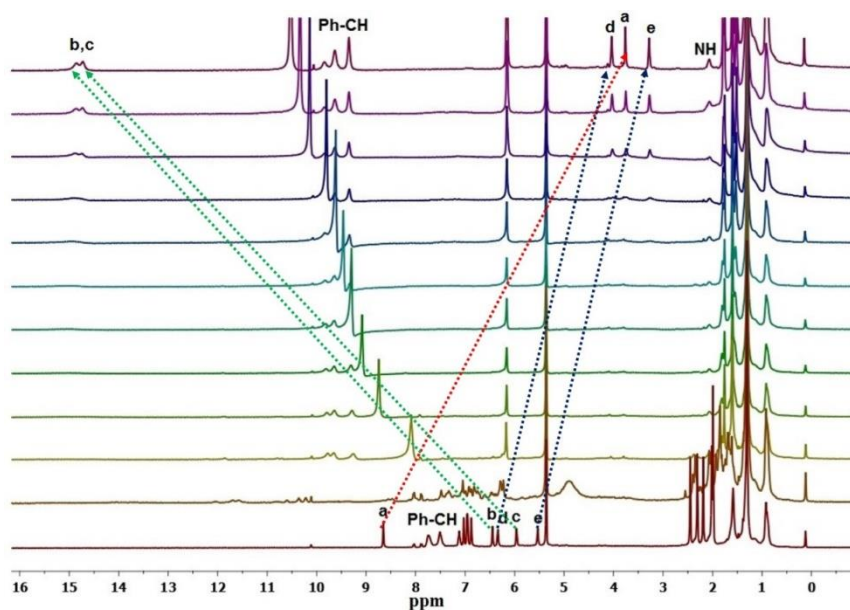


Figure 6.13: Titration spectrum of 10.4H^+ in CD_2Cl_2 .

The ^1H NMR of **12** was simple to interpret due to its symmetric nature. The ring inversion was neither observed in freebase form nor in protonated state. The β -CH protons of two terminal thiophene rings of terthiophene units (b, c) resonate as a doublet at 6.85 and 7.17 ppm while the central thiophene rings β -CH protons (a) observed at 7.4 ppm as a sharp singlet. The pyrrole β -CH protons of pentapyrrane unit (d, e) resonate at 6.6 ppm and the NH protons appear at 8.16 ppm. These chemical shift values clearly indicate the nonaromatic nature of **12**. Upon protonation small deshielding of various protons (Figure 6.14-6.16) were observed and the chemical

shift values suggest that **12** remains nonaromatic (Figure 6.17). The rigid nature of **12** does not permit a conformational change observed for **10** and hence **12** remains nonaromatic. **13** also are fully characterized using absorption spectra, ^1H NMR (Figure 6.18 and 6.19) where the NH proton resonated at 7.7 ppm and all other β -CH protons resonated individually between 6.7 to 7.6 ppm.

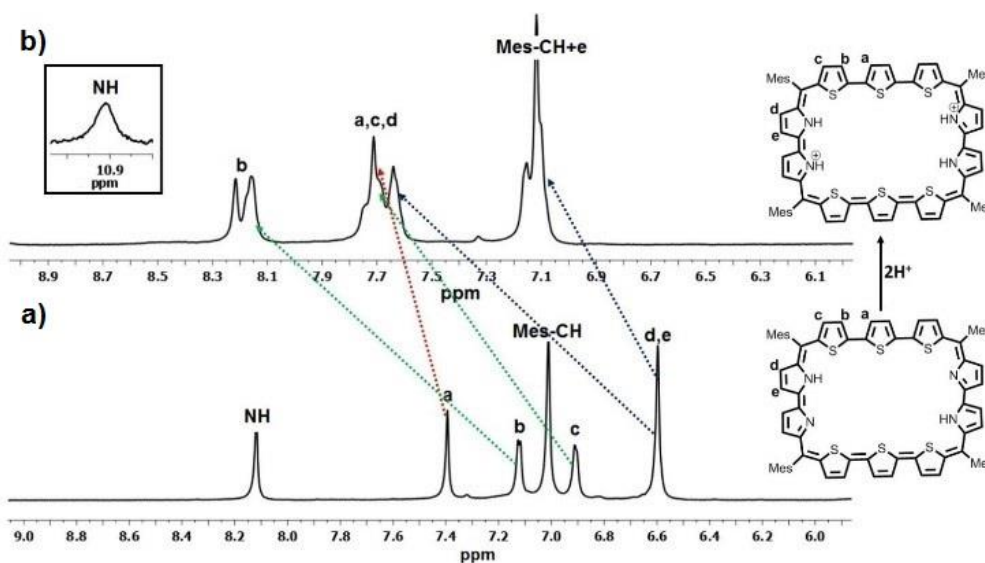


Figure 6.14: ^1H NMR Spectrum; (a) **12** (298K) and (b) **12.2H⁺** (298K) in CD_2Cl_2 .

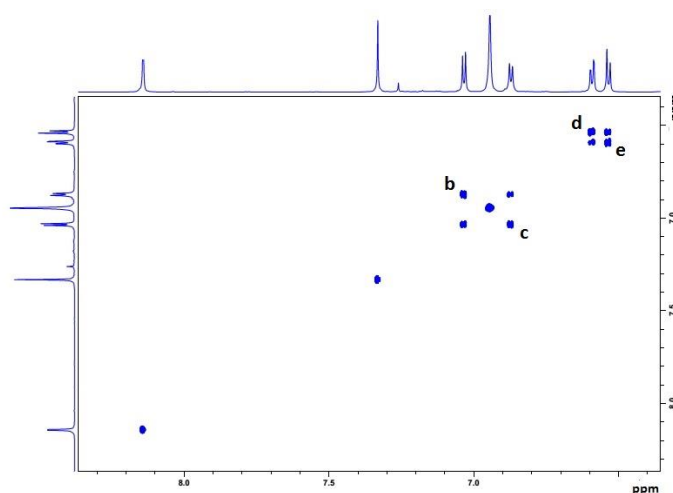


Figure 6.15: ^1H - ^1H COSY spectrum of **12** with correlation in pyrrole and thiophene rings.

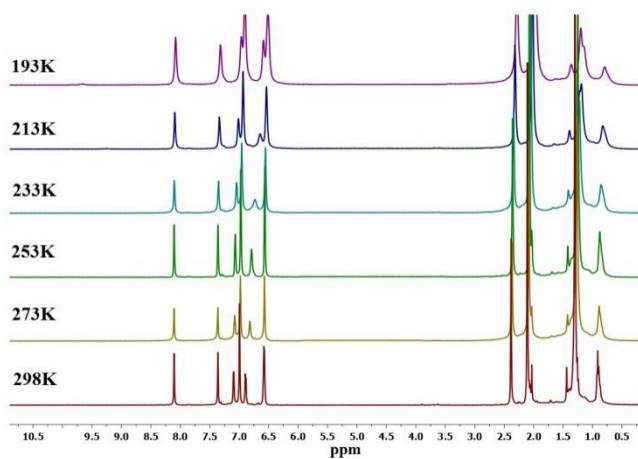


Figure 6.16: Low temperature ^1H NMR spectrum of **12** in CD_2Cl_2 (Full).

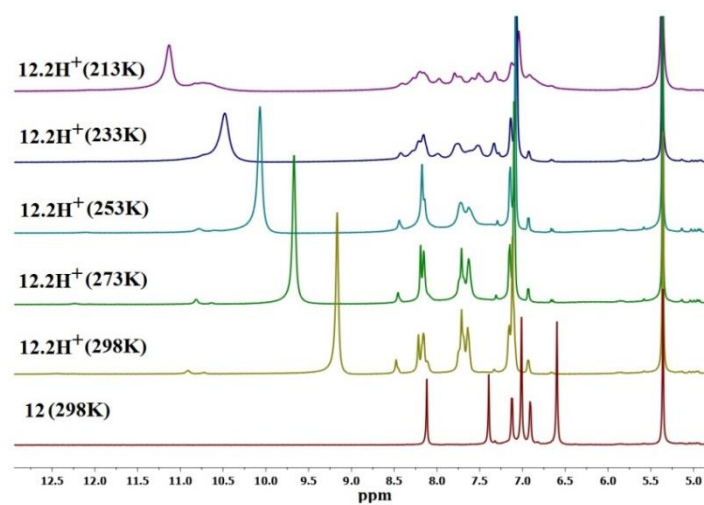


Figure 6.17: Low temperature ^1H NMR spectrum of 12.2H^+ in CD_2Cl_2 (Full).

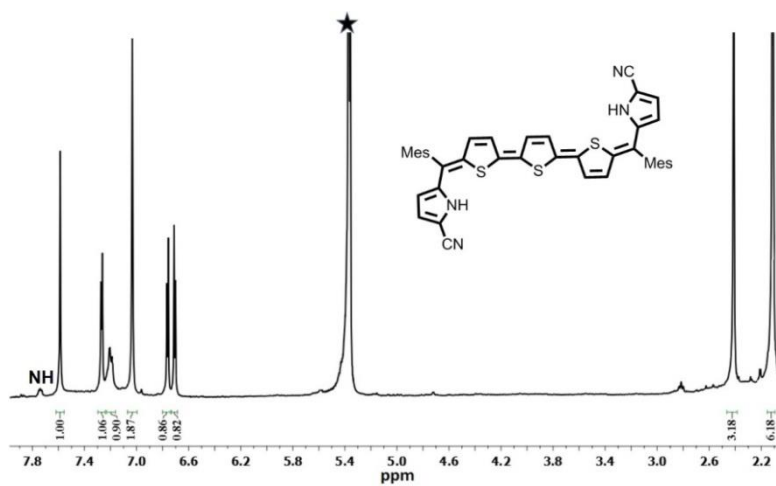


Figure 6.18: ^1H NMR spectrum of **13** in CD_2Cl_2 .

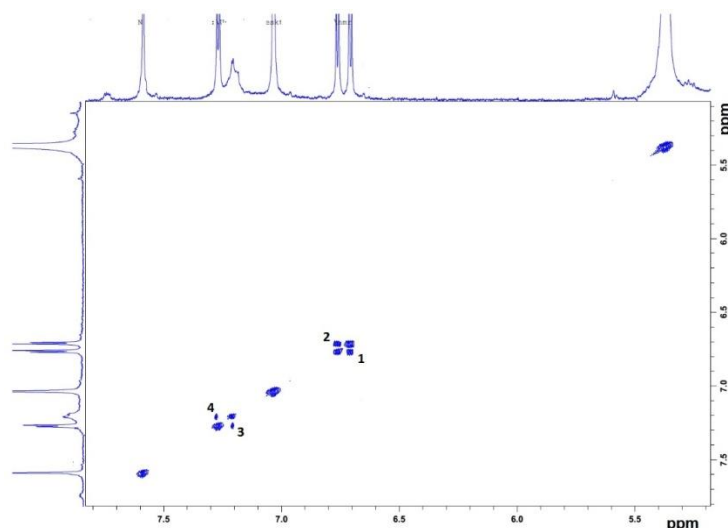


Figure 6.19: ^1H - ^1H COSY spectrum of **13** with correlation in pyrrole and thiophene rings.

6.3.2.3 Single Crystal X-ray analysis

The structure of **10** in solid state was determined by single crystal X-ray structure Figure 6.2 and Table 6.2. The single crystal of **10** was grown by slow diffusion of dichloromethane in *n*-heptane at 4°C and crystallizes in hexagonal crystal lattice with space group of $P6_222$. The structural elucidation reveals that two units of thiophene tripyrrane and 1,2-diphenyl-1,2-dithienyl ethene moieties are linked with each other through four *meso* carbon bridges. Overall, twelve flexible *meso* carbon atoms are bridging between ten heterocyclic units, results in figure-eight conformation of the macrocycle. The thiophene units of the tripyrrane moieties are inverted whereas the other heterocyclic rings are pointed towards the macrocyclic core. The two 1,2-diphenyl-1,2-dithienyl ethene moieties are nearly planar to each other. In spite of figure-eight conformation, the macrocycle is highly symmetric in nature, which is also reflected in its ^1H NMR spectral analysis. The inverted thiophene ring is deviated by 8.3° whereas the thiophene unit of the ethene moiety and pyrrolic units are deviated by 29.4° and 21.6° from the mean macrocyclic plane ($C7\ C2\ C2'\ C7'\ C7''\ C2''\ C2''' C7'''$). The *meso* mesityl groups are tilted by 80.3°, whereas the *meso* phenyl

rings on the ethene bridge are deviated by 63.7° from the mean macrocyclic plane. The crystal analysis of decaphyrin revealed three different types of hydrogen bonding interactions responsible for self-assembled dimer, one dimensional and two dimensional arrays; i) Thio(π)...C48-H48, ii) S2...H73-C73 and iii) S1...H55-C55 with bond distances and angles are 2.87\AA & 124.2° (i), 2.88\AA & 152.5° (ii) and 2.76 & 159.8° (iii) respectively (Figure 6.21-6.23).

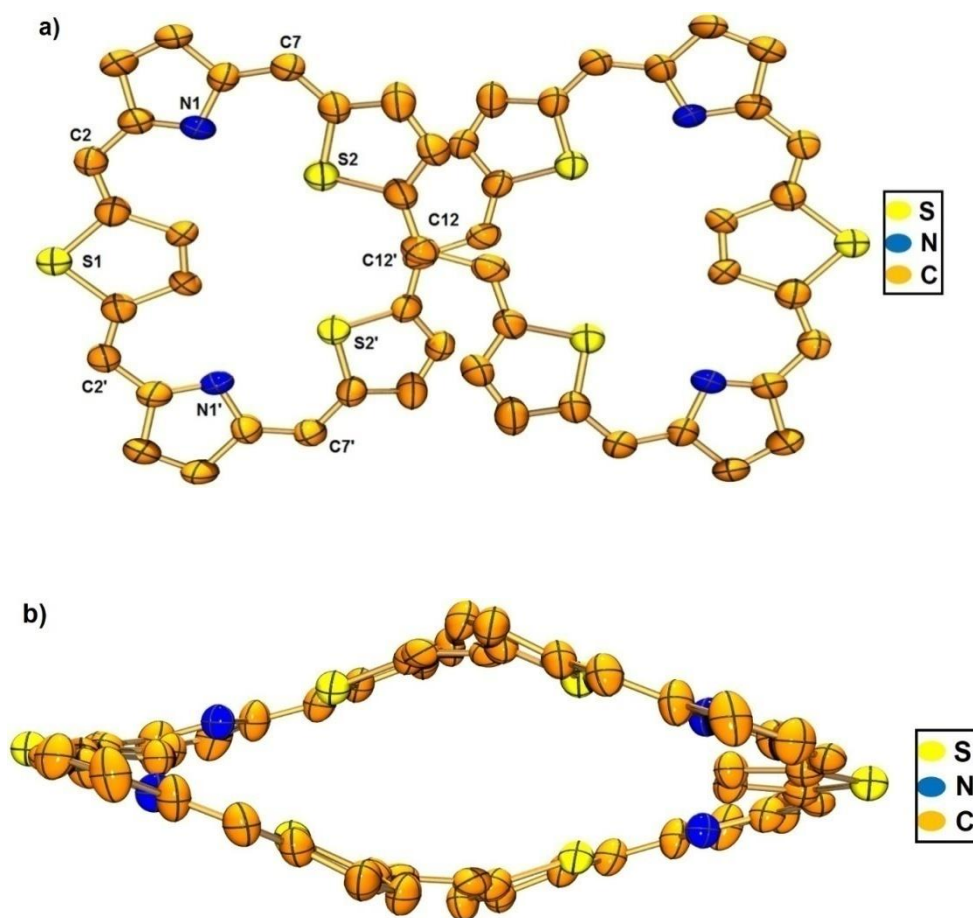


Figure 6.20: Crystal structure of **10** (a) Top view and (b) side view (*Meso* substituents and hydrogen atoms are omitted for clarity). Thermal ellipsoids are drawn at 50% probability.

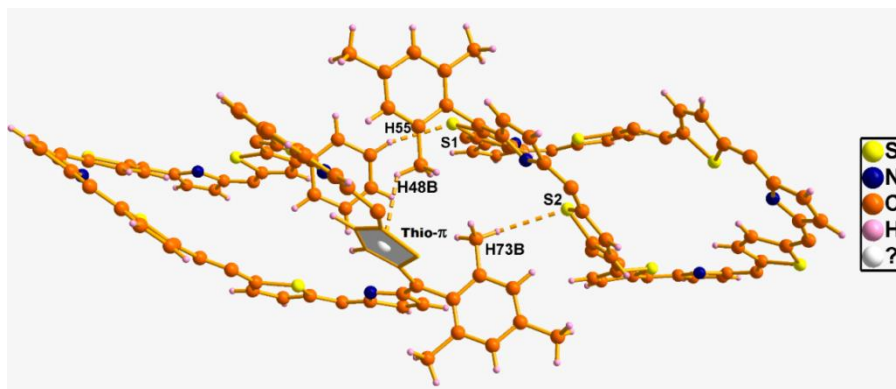


Figure 6.21: Self-assembled dimer of **10** (a) The CH... π interaction generated between thiophene π electron cloud and C48-H48 (b) Intermolecular molecular hydrogen bonding between (i) S2...H73-C73 and (ii) S1...H55-C55.

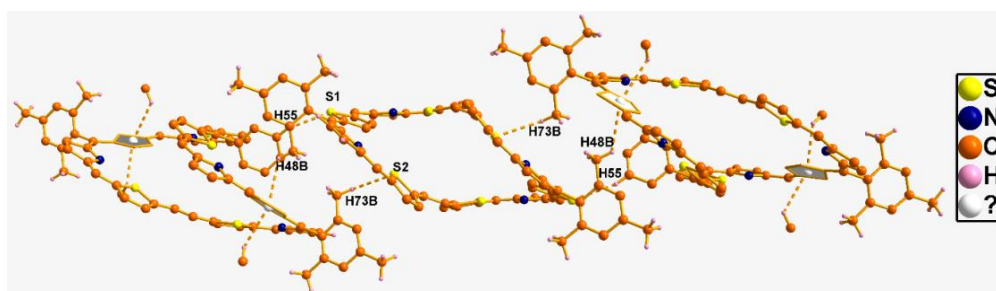


Figure 6.22: One dimensional array structure of **10**.

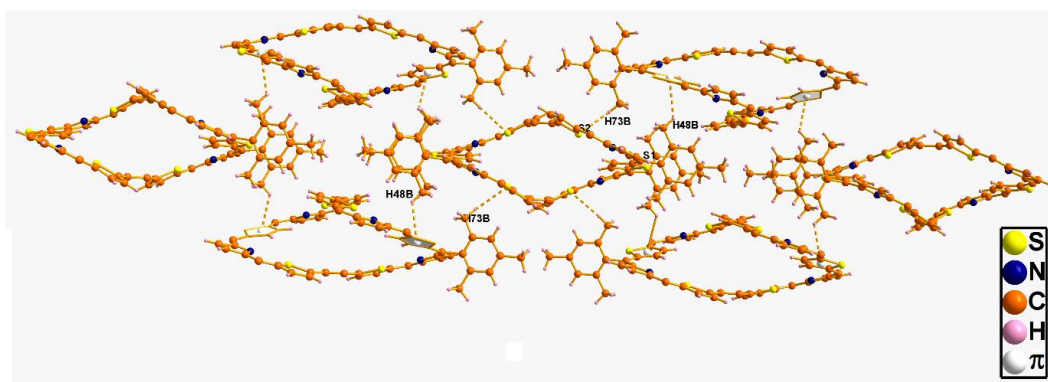


Figure 6.23: Two dimensional arrays of **10**.

Table 6.2: Crystal data for **10**

Identification code	tkc_Decaphyrin_Final
Empirical formula	C ₁₄₈ H ₁₂₈ N ₄ S ₆
Formula weight	2154.9
Temperature/K	100.0
Crystal system	hexagonal
Space group	<i>P</i> 6 ₂ 22
<i>a</i> /Å	28.8585(6)
<i>b</i> /Å	28.8585(6)
<i>c</i> /Å	37.6170(4)
α /°	90
β /°	90
γ /°	120
Volume/Å ³	27130.8(12)
<i>Z</i>	6
ρ_{calc} /cm ³	0.791
μ /mm ⁻¹	0.971
<i>F</i> (000)	6840.0
Crystal size/mm ³	0.2 × 0.15 × 0.12
Radiation	CuK α (λ = 1.54184)
2 θ range for data collection/°	5.88 to 154.814
Index ranges	-31 ≤ <i>h</i> ≤ 31, -17 ≤ <i>k</i> ≤ 18, -46 ≤ <i>l</i> ≤ 46
Reflections collected	18453
Independent reflections	18452 [<i>R</i> _{int} = 0.0000, <i>R</i> _{sigma} = 0.0636]
Data/restraints/parameters	18452/0/725
Goodness-of-fit on <i>F</i> ²	0.911
Final <i>R</i> indexes [<i>I</i> >= 2 σ (<i>I</i>)]	<i>R</i> ₁ = 0.0421, <i>wR</i> ₂ = 0.0947
Final <i>R</i> indexes [all data]	<i>R</i> ₁ = 0.0697, <i>wR</i> ₂ = 0.1041
Largest diff. peak/hole / e Å ⁻³	0.18/-0.15
Flack parameter	0.037(8)

The unusual formation of cyano-pentapyrene **13** was unambiguously confirmed by single crystal X-ray analysis (Figure 6.24 and Table 6.3). **13** was crystallized in triclinic crystal lattice with *P*-1 space group. The structural elucidation reveals that the pyrrole rings and the terminal thiophene units of the terthiophene moiety are oppositely oriented with each other. The two cyanide groups are at the α -carbon atoms of the pyrrolic moiety which gives an evidence that DDQ is acting as the cyanide source. All the heterocyclic rings are exactly planar with the mean plane. The structural analysis revealed that there are two different types of hydrogen bonding interactions; (i) intramolecular hydrogen bonding interaction between sulphur atoms of terminal thiophene moieties with pyrrolic NH units (N2-H2...S1 is 2.29Å & 127.5° and N1-H1...S3 is 2.07Å & 134.6°) and (ii) two inter-molecular hydrogen bonding interaction between nitrogen atoms of the cyanide group with the *meso* mesityl group and π -cloud of pyrrolic moiety with the *meso* mesityl group (C40-H40...N3 is 2.71Å & 149.4° and Py(π)...H42-C42 is 3.03Å & 169.2°). These intermolecular hydrogen bonding interactions generate self assembled dimer and one dimensional array (Figure 6.25-6.26)

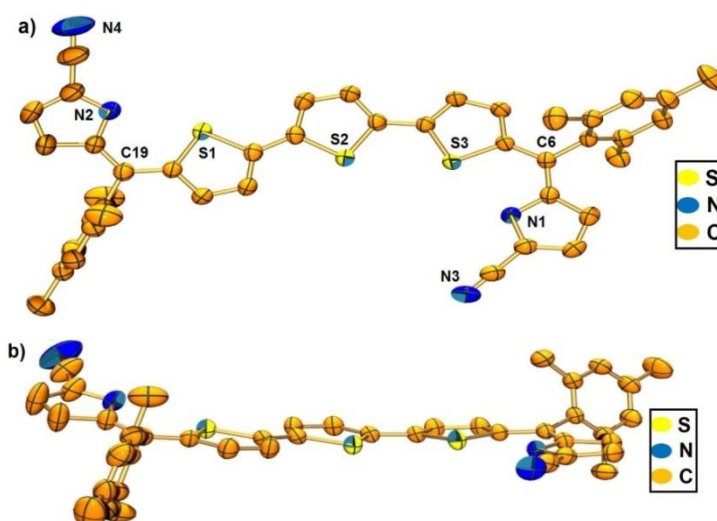


Figure 6.24: Crystal structure of **13** (a) Top view and (b) side view (Hydrogen atoms are omitted for clarity). Thermal ellipsoids are drawn at 50% probability.

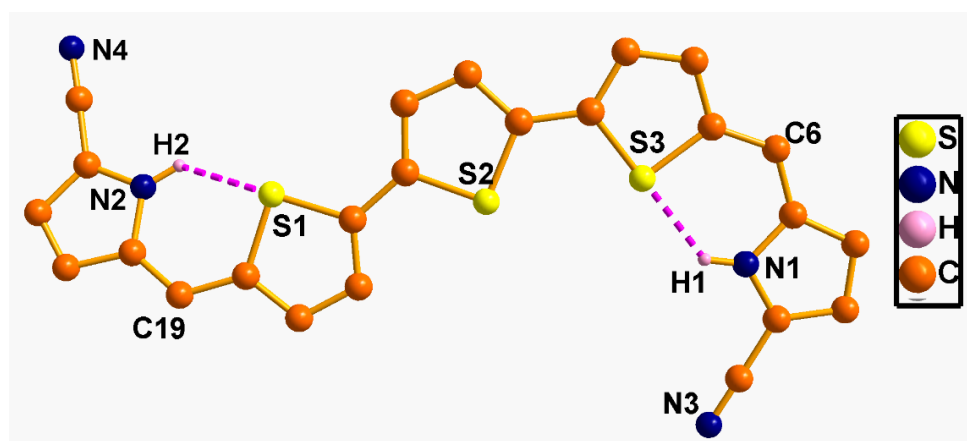


Figure 6.25: Intermolecular hydrogen bonding in **13** (C40-H40...N3 with a distance 2.71Å and angle 149.41°).

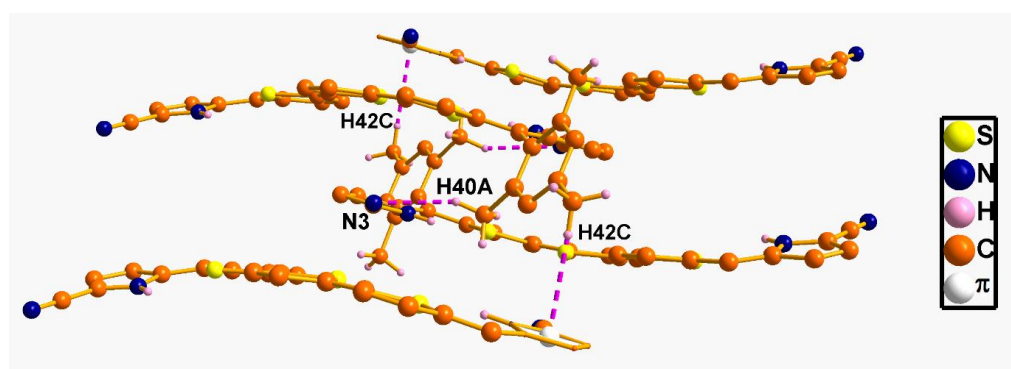


Figure 6.26: Two dimensional array of **13** (a) Intermolecular hydrogen bonding (C40-H40...N3 with a distance 2.71Å and angle 149.41°) (b) π ...H interaction between Py(π)...C42-H42.

Table 6.3: Crystal data for **13**

Crystal data and structure refinement for TKC_CYANO_TPM.	
Identification code	TKC_CYANO_TPM
Empirical formula	C ₄₂ H ₃₄ N ₄ S ₃
Formula weight	690
Temperature/K	293(2)
Crystal system	triclinic
Space group	<i>P</i> -1
<i>a</i> /Å	8.69725(17)
<i>b</i> /Å	10.9283(2)
<i>c</i> /Å	20.5323(5)
α /°	84.0758(17)
β /°	88.6243(18)
γ /°	67.6514(18)
Volume/Å ³	1795.05(7)
<i>Z</i>	2
ρ_{calc} /cm ³	1.278
μ /mm ⁻¹	2.162
<i>F</i> (000)	724.0
Crystal size/mm ³	0.18 × 0.16 × 0.14
Radiation	CuK α (λ = 1.54184)
2 θ range for data collection/°	8.66 to 136.49
Index ranges	-10 ≤ <i>h</i> ≤ 10, -10 ≤ <i>k</i> ≤ 13, -24 ≤ <i>l</i> ≤ 24
Reflections collected	25727
Independent reflections	6570 [<i>R</i> _{int} = 0.0934, <i>R</i> _{sigma} = 0.0607]
Data/restraints/parameters	6570/0/448
Goodness-of-fit on <i>F</i> ²	1.092
Final <i>R</i> indexes [<i>I</i> ≥ 2 σ (<i>I</i>)]	<i>R</i> ₁ = 0.0779, <i>wR</i> ₂ = 0.2323
Final <i>R</i> indexes [all data]	<i>R</i> ₁ = 0.0852, <i>wR</i> ₂ = 0.2367
Largest diff. peak/hole / e Å ⁻³	0.59/-0.53

6.3.2.4 DFT Calculations

The changeover from figure-eight conformation to open planar conformation upon protonation of **10**. Calculated structure of both **10** and **10.4H⁺** shown in Figure 6.28 at M062X/6-31G** level of DFT were done. The calculated structure of **10** clearly is comparable to the single crystal X-ray structure and the protonated structure **10.4H⁺** clearly indicates the open conformation with four pyrrole rings undergoing inversion justifying ¹H NMR observations. The optimized structure of **10.4H⁺** is found to be energetically more stable by 16.7 Kcal/mole relative to the calculated optimized figure eight conformation accounting for the stability of open conformation upon protonation in Figure 6.29. The HOMA value^{29b,29c} of (-0.32) and NICS value of (+1.7) ppm clearly suggest the antiaromatic nature of **10.4H⁺**. Bond length parameters in Å for **10** and **10.4H⁺** are also shown in Figure 6.27.

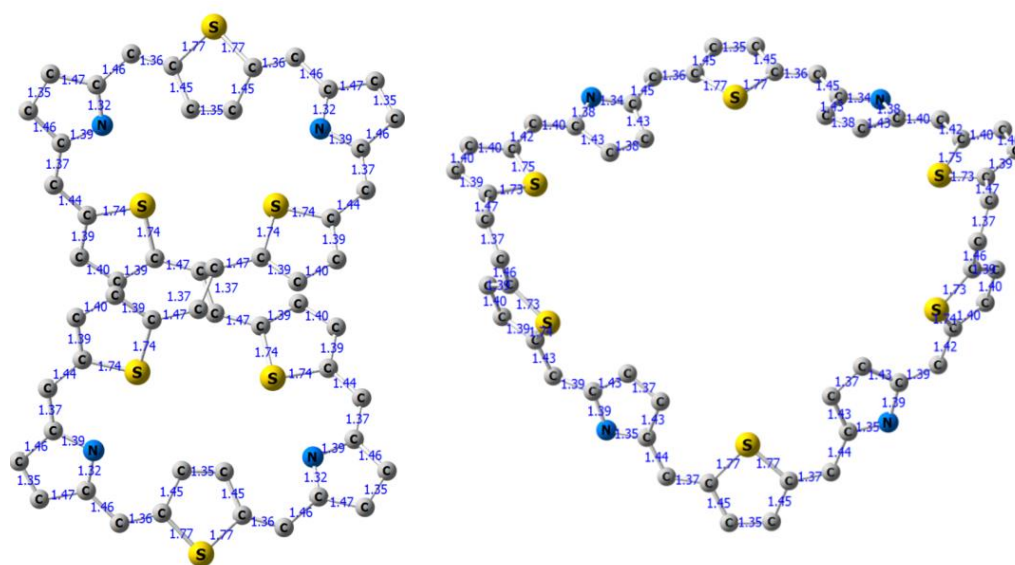


Figure 6.27: Optimized structure of **10** and **10.4H⁺** at M062X/6-31G** level of DFT with Bond length parameters. Mesityl groups and hydrogen atoms are omitted for clarity.

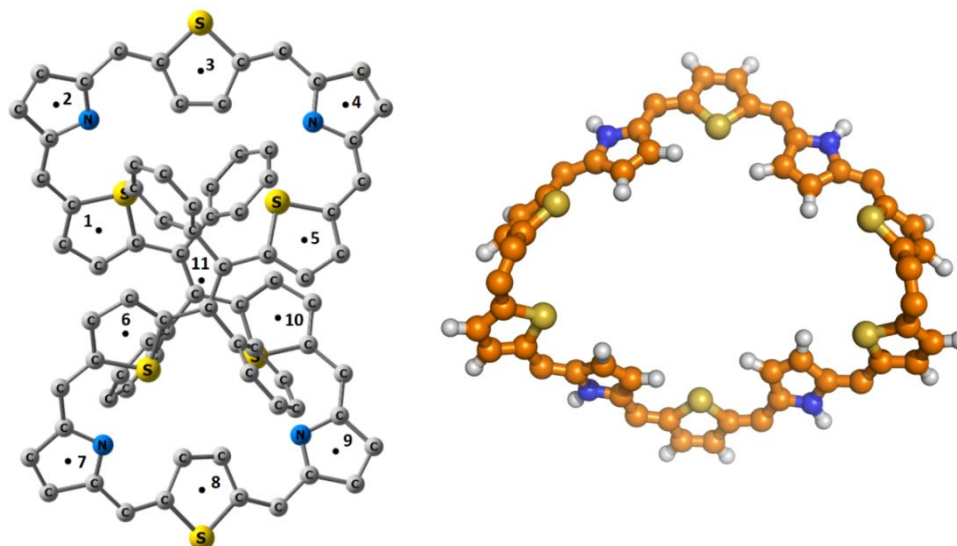


Figure 6.28: Optimized structure of **10** and **10.4H⁺** without meso groups at M062X/6-31G** level of DFT.

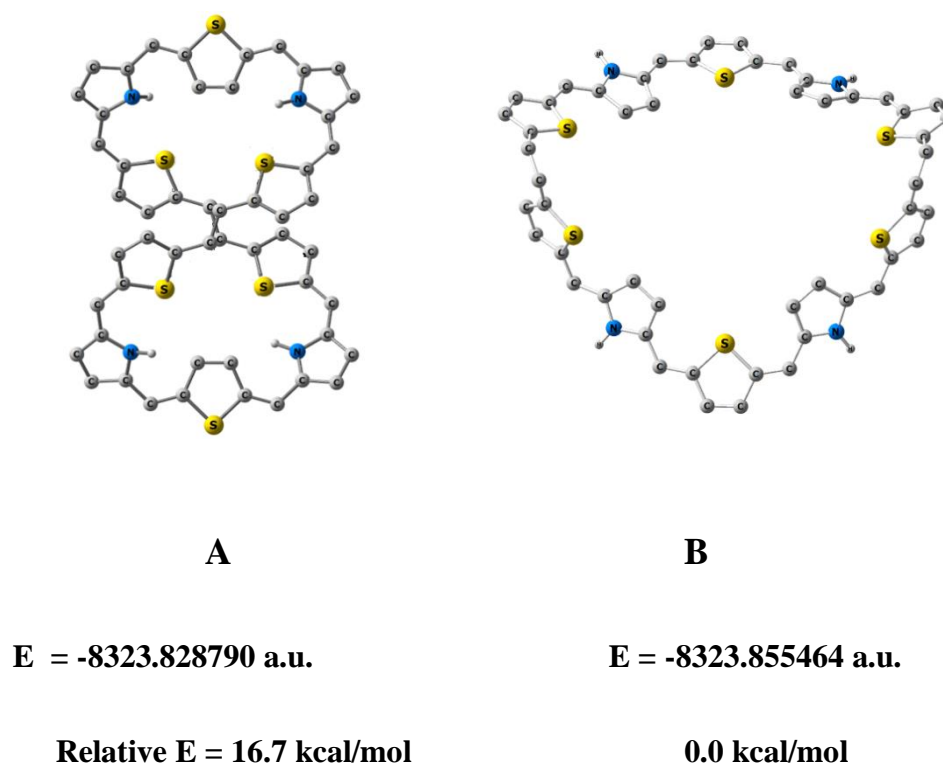


Figure 6.29: Energy and relative energy of the two configurations of **10.4H⁺** at M062X/6-31G** level of DFT. Mesityl groups, phenyl groups and the H atoms are omitted for clarity.

The rigid nature of **12** does not permit a conformational change observed for **10** and hence **12** remains nonaromatic. Energy optimization studies suggest a figure-eight conformation for **12** and **12.2H⁺** shown in Figure 6.30. Bond length parameters in Å for **12** and **12.4H⁺** are also shown in Figure 6.31.

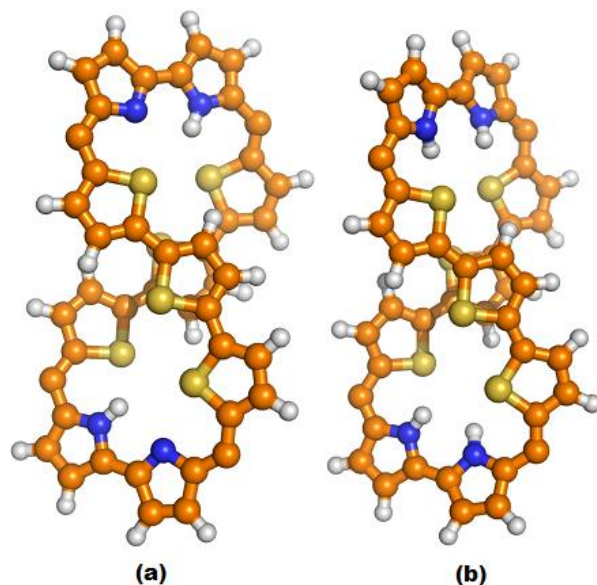


Figure 6.30: Optimized structure of (a) **12** and (b) **12.2H⁺** at M062X/6-31G** level of DFT (mesityl groups are omitted for clarity).

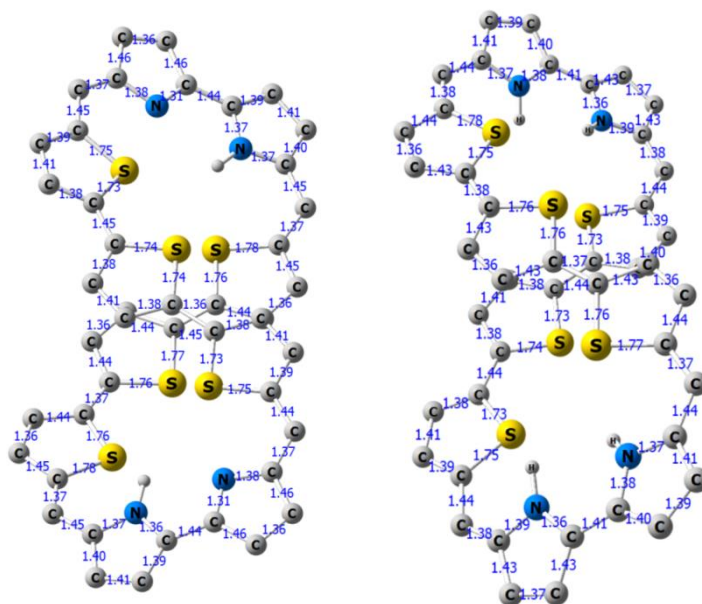


Figure 6.31: Optimized structure of (a) **12** and (b) **12.2H⁺** at M062X/6-31G** level of DFT (mesityl groups are omitted for clarity).

6.3.2.5 Electronic spectral analyses

The nonaromatic nature of **10** in freebase form is also reflected in the UV-Vis spectrum where broad absorption at 468 nm ($\epsilon = 2.5 \times 10^4$), 634 nm ($\epsilon = 3.6 \times 10^4$) and a shoulder at 736 nm ($\epsilon = 1.2 \times 10^4$) were observed in CH_2Cl_2 (Figure 6.32). Stepwise protonation of **10** was followed by a titration of dilute solution of TFA in CH_2Cl_2 by UV-Visible spectrum (Figure 6.33) for example, for $\mathbf{10.1H^+}$, the band shifts to 773 nm but the bands still remain broad. For $\mathbf{10.2H^+}$, bands are observed at 773 and 840 nm. Here also bands are broad. $\mathbf{10.3H^+}$ and $\mathbf{10.4H^+}$ exhibit sharper bands with increased intensity and larger molar extinction coefficients. The sharpening of absorption bands and increase in molar absorptivity suggest changes in the structure upon protonation.

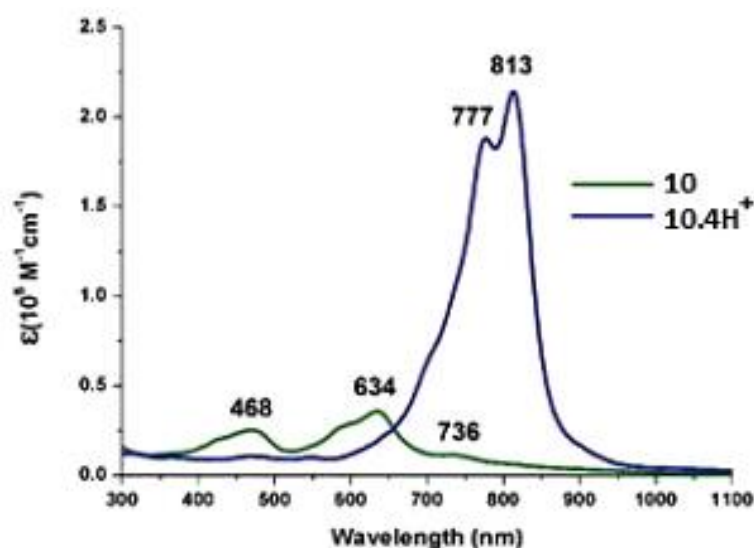


Figure 6.32: Absorption spectra of decaphyrin **10** and $\mathbf{10.4H^+}$ in CH_2Cl_2 .

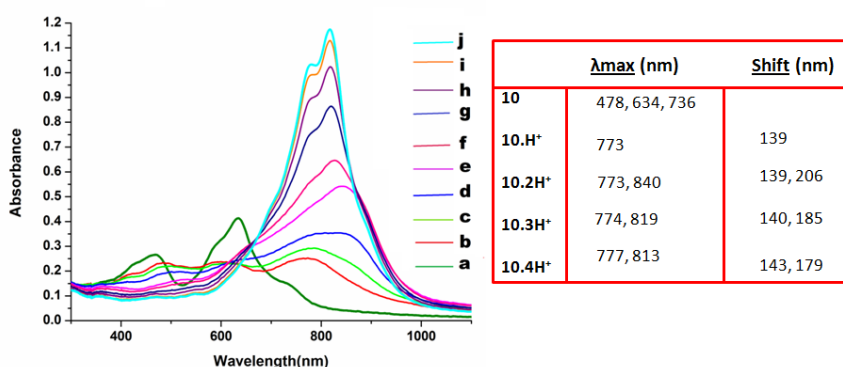


Figure 6.33: Titration with dilute solution of TFA in CH_2Cl_2 on decaphyrin **10** with concentration 1.39×10^{-5} M. The concentration of TFA used are a) 0 M, b) 6.5×10^{-6} M, c) 1.3×10^{-5} M, c) 2.6×10^{-5} M, e) 3.9×10^{-5} M, f) 5.2×10^{-5} M, g) 7.8×10^{-5} M, h) 1.04×10^{-4} M, i) 1.3×10^{-4} M and j) 1.56×10^{-4} M.

12 also exhibits a broad absorption band at 535 nm ($\epsilon = 5.4 \times 10^4$) (Figure 6.34) which is red shifted to 703 nm ($\epsilon = 1.20 \times 10^5$) upon diprotonation. Here also the first and second protonation stages were identified by the titration of a dilute solution of TFA in CH_2Cl_2 . Protonation results in a gradual redshift of the absorption to 661 nm **12.H⁺** and 703 nm **12.2H⁺**. However the bands remain relatively broad (Figure 6.35). The larger redshifts observed for the absorption bands of **10** after protonation (777 nm, 803 nm relative to **12** 703 nm reflect in 48π vs. 42π electronic circuits and the increase in their ϵ -value reflects the antiaromatic vs. Nonaromatic characteristics.

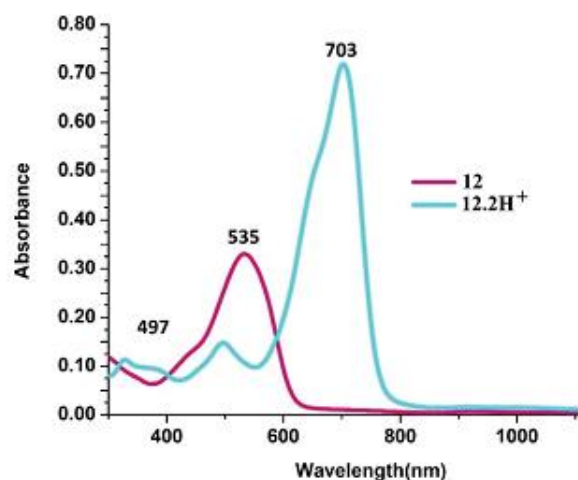


Figure 6.34: Absorption spectra of decaphyrin **12** and **12.2H⁺** in CH_2Cl_2 .

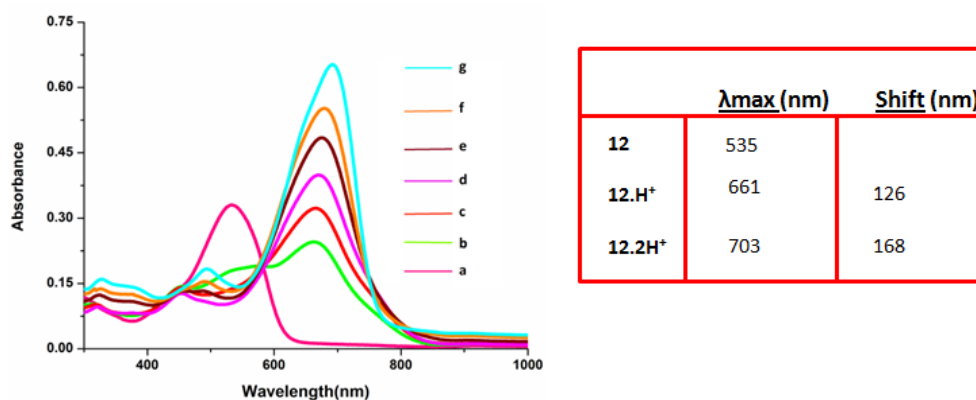


Figure 6.35: Titration with dilute solution of TFA in CH_2Cl_2 on decaphyrin **12** with concentration 7.83×10^{-7} M. The concentration of TFA used are a) 0 M, b) 1.3×10^{-7} M, c) 3.9×10^{-7} M, d) 7.8×10^{-7} M, e) 1.1×10^{-6} M, f) 1.5×10^{-6} and g) 1.9×10^{-6} M.

6.4 Conclusions

In conclusion, synthesis and characterization of two decaphyrins **10** and **12** containing 48π and 42π electrons are described. The compound **10** adopts figure-eight conformation with nonaromatic characteristics and changes to an open conformation with 48π Hückel antiaromatic features upon simple protonation. The flexible nature of the macrocycle allows such a structural change. However, the drastic reduction in the number of *meso* carbon links from twelve to four restricts any structural change in **12** and maintains nonaromatic characteristics both in freebase and protonated form. It is interesting to note that the protonated form of **10** is an ideal candidate for testing Baird's rule according to which **10.4H⁺** should exhibit aromatic property in the lowest excited triplet state. Further studies are in progress to exploit the photochemistry of **10.4H⁺** in the excited state.

6.5 Experimental Procedure

6.5.1 Synthesis of **10**:

A mixture of precursors 5,10-dimesityl-16-thia-tripyrane (**7**) (150 mg, 0.31 mmol) and 5,5'-bis(mesitylhydroxymethyl)-1,2-diphenyl-1,2-di(thiophene-2-yl)ethene (**6**) (200 mg, 0.31 mmol) were dissolved in dry CH₂Cl₂ under nitrogen atmosphere for 10 min. Excess trifluoroacetic acid was added and the resultant mixture was stirred for 1 h under N₂ atmosphere. 2,3-Dichloro-5,6-dicyano-*p*-benzoquinone (DDQ) (213 mg, 0.93 mmol) were added and the resultant mixture was stirred in open air for another 1h. Progress of the reaction was monitored through TLC. Solvent was evaporated under vacuum. Residue was purified through basic alumina followed by silica gel (100-200 mesh) column chromatography. The first moving green band was eluted with CH₂Cl₂/*n*-Hexane (20:80, V/V) and identified as pentaphyrin (**8**). The second dark greenish band eluted with CH₂Cl₂/*n*-Hexane (30:70, V/V) turned out to be decaphyrin (**10**) with 8% yield. After evaporation, decaphyrin (**10**) gave bronze color solid (30 mg). mp > 300 °C.

¹H NMR (400 MHz, CD₂Cl₂, 298K): δ (in ppm) = 8.65 (s, 2H), 7.81 (d, 4H, *J*=2.8), 7.48 (d, 4H, *J*=2.8), 7.16 (t, 2H, *J*=3.6), 7.10 (s, 2H), 6.92 (s, 2H), 6.91 (s, 2H), 6.83 (s, 2H), 6.49 (d, 2H, *J*=4.2), 6.30 (d, 2H, *J*=3.8), 5.92 (d, 2H, *J*=4.2), 5.54 (d, 2H, *J*=3.8), 2.41 (s, 6H), 2.27 (s, 6H), 2.14 (s, 6H), 1.97 (s, 6H), 1.95 (s, 12H). **10**·4H⁺: ¹H NMR (400 MHz, CD₂Cl₂) δ (in ppm) = 14.86 (d, 2H), 14.72 (d, 2H), 9.84 (t, 2H), 9.63 (d, 4H), 9.35 (d, 4H), 6.16 (s, 8H), 4.03 (d, 2H), 3.76 (s, 2H), 3.28 (d, 2H), 2.06 (br, NH), 1.78 (s, 6H), 1.76 (s, 6H), 1.59 (s, 12H), 1.52 (s, 12H). ¹³C NMR (100 MHz, CD₂Cl₂, 298K): δ (in ppm) = 166.7, 157.0, 154.4, 151.7, 142.6, 140.1, 139.5, 138.7, 137.4, 136.8, 136.4, 135.5, 134.8, 134.2, 133.9, 129.1, 128.4, 128.2, 128.1, 127.8, 31.7, 29.7, 22.7, 20.1, 19.9, 15.5. **10**: UV/Vis (CH₂Cl₂): λ_{max} in nm (ε in dm³mol⁻¹

$^1\text{cm}^{-1}$) = 468 (2.34×10^4), 634 (3.6×10^4), 735 (9.88×10^3); $\mathbf{10} \cdot 4\text{H}^+$ (TFA/ CH_2Cl_2): λ_{max} in nm (ϵ in $\text{dm}^3\text{mol}^{-1}\text{cm}^{-1}$) = 777 (1.27×10^5), 813 (1.48×10^5). HRMS (ESI-TOF) m/z : $[\text{M} + \text{H}]^+$ calcd. for $\text{C}_{148}\text{H}_{128}\text{N}_4\text{S}_6$, 2154.8568; found 2154.8571.

6.5.2 Synthesis of **12**:

Method-I (With TFA):

5,5''-Bis(mesityl(1H-pyrrol-2-yl)methyl)-2,2':5',2''-terthiophene (**11**) (150 mg, 0.31 mmol) was dissolved in dry CH_2Cl_2 under nitrogen atmosphere for 10 min. Trifluoroacetic acid (24 μl , 0.31 mmol) was added and the resultant mixture was stirred for 1h under N_2 atmosphere. 2,3-Dichloro-5,6-dicyano-*p*-benzoquinone (DDQ) (213 mg, 0.93 mmol) was added and the resultant mixture was stirred in open air for another 1h. Progress of the reaction was monitored through TLC. Solvent was evaporated under vacuum. Residue was purified through basic alumina followed by silica gel (100-200 mesh) column chromatography. The first moving bluish band was eluted with $\text{CH}_2\text{Cl}_2/n$ -Hexane (35:65, V/V) and identified as cyano-pentapyrrane (**13**) with 3% yield. The second dark reddish band was eluted with $\text{CH}_2\text{Cl}_2/n$ -Hexane (80:20, V/V) and identified as decaphyrin (**12**) with 10% yield (18 mg). After evaporation it gave bronze color solid.

Method-II (Without TFA):

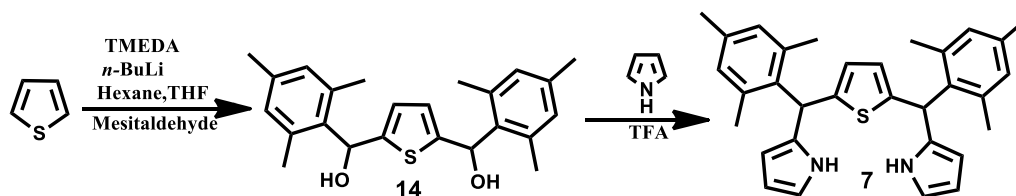
5,5''-Bis(mesityl(1H-pyrrol-2-yl)methyl)-2,2':5',2''-terthiophene (**11**) (150 mg, 0.31 mmol) was dissolved in dry CH_2Cl_2 . 2,3-Dichloro-5,6-dicyano-*p*-benzoquinone (DDQ) (426 mg, 1.86 mmol) was added and the resultant mixture was stirred in open air for another 30 mins. Progress of the reaction was monitored through TLC. Solvent was evaporated under vacuum. Residue was purified through basic alumina column chromatography followed by silica gel (100-200 mesh) column chromatography. The major dark reddish band was eluted with $\text{CH}_2\text{Cl}_2/n$ -Hexane (80:20, V/V) and

identified as decaphyrin (**12**) with 30% yield (48 mg). After evaporation it gave bronze color solid. mp > 280 °C.

^1H NMR (400 MHz, CD_2Cl_2 , 298K): δ (in ppm) = 8.16 (br, NH), 7.40 (s, 1H), 7.17 (d, 1H), 7.01 (s, 2H), 6.85 (d, 1H), 6.6-6.58 (m, 2H), 2.40 (s, 3H), 2.12 (s, 6H). **12** $\cdot 2\text{H}^+$: ^1H NMR (400 MHz, CD_2Cl_2) δ (in ppm) = 10.91 (br, NH), 8.20 (d, 1H), 7.74-7.64 (m, 3H), 7.15 (d, 1H) 7.12 (s, 2H), 2.42 (s, 3H), 2.07 (s, 6H). ^{13}C NMR (100 MHz, CD_2Cl_2 , 298K): δ (in ppm) = 161.5, 152.2, 147.8, 143.0, 139.6, 138.0, 137.5, 136.5, 135.9, 134.1, 134.0, 127.9, 127.5, 126.1, 123.9, 29.7, 20.8, 19.6. **12**: UV/Vis (CH_2Cl_2): λ_{max} in nm (ϵ in $\text{dm}^3\text{mol}^{-1}\text{cm}^{-1}$) = 535 (5.4×10^4); **12** $\cdot 2\text{H}^+$ (TFA/ CH_2Cl_2): λ_{max} in nm (ϵ in $\text{dm}^3\text{mol}^{-1}\text{cm}^{-1}$) = 497 (2.52×10^4), 703 (1.20×10^5); HRMS (ESI-TOF) m/z: $[\text{M} + n\text{H}]^+$ calcd. for $\text{C}_{80}\text{H}_{68}\text{N}_4\text{S}_6$, 1277.3841; found 1277.3817.

13: ^1H NMR (400 MHz, CD_2Cl_2 , 298K): δ (in ppm) = 7.75 (br, NH), 7.58 (s, 2H), 7.27 (d, 2H), 7.21 (d, 2H), 7.05 (s, 4H), 6.78 (d, 2H), 6.70 (d, 2H), 2.41 (s, 6H), 2.11 (s, 12H); ^{13}C NMR (100 MHz, CDCl_3 , 298K): δ (in ppm) = 182.4, 173.7, 138.5, 137.4, 137.3, 133.5, 133.2, 128.7, 127.9, 124.8, 20.9, 20.8, 19.7, 19.6, 19.0. **13**: UV/Vis (CH_2Cl_2): λ_{max} in nm (ϵ in $\text{dm}^3\text{mol}^{-1}\text{cm}^{-1}$) = 620 (3.6×10^4); **13** $\cdot 2\text{H}^+$ (TFA/ CH_2Cl_2): λ_{max} in nm (ϵ in $\text{dm}^3\text{mol}^{-1}\text{cm}^{-1}$) = 710 (4.78×10^4), 780 (1.17×10^5). HRMS (ESI-TOF) m/z: $[\text{M} - \text{H}]^+$ calcd. for $\text{C}_{42}\text{H}_{33}\text{N}_4\text{S}_3$, 689.1862; found 689.1857.

6.5.3 Precursor Syntheses:



Scheme 6.3: Precursor Synthesis.

6.5.3.1 Synthesis of **14**

To a solution of N,N,N',N'-tetramethylethylene diamine (8.05 ml, 53.5 mmol) in dry hexane (160 ml), *n*-butyllithium (35.67 ml, 1.6 M in hexane, 53.5 mmol) was added followed by thiophene (1.43 ml, 17.8 mmol) under nitrogen atmosphere. The reaction mixture was stirred for 1h and later refluxed for another 1h. The reaction mixture was then allowed to attain room temperature. Mesitaldehyde (6.56 ml, 44.57 mmol) in dry THF (25 ml) was added dropwise to the ice cooled condition. The resultant solution was stirred at ambient temperature overnight. The reaction was quenched with 100 ml saturated NH₄Cl solution and extracted with diethyl ether. Organic layer was washed with brine solution and dried over anhydrous Na₂SO₄. After evaporation of the solvent, the crude product was purified by silica gel (100-200 mesh) column chromatography. The diol 2,5-Bis(mesitylhydroxymethyl)thiophene (**14**) was eluted with ethyl acetate/hexane (20:80, V/V) and obtained as pale yellow color solid. Yield: 4.1 g, 56%.

¹H NMR (400 MHz, CDCl₃, 298K): δ (ppm): 6.82 (s, 4H), 6.39 (s, 2H), 6.36 (s, 2H), 2.29 (s, 12H), 2.25 (s, 6H), 1.65 (br, 2H).

6.5.3.2 Synthesis of **7**

Diol (**14**) (1 g, 2.63 mmol), pyrrole (7.3 ml, 105.28 mmol) were mixed. To this mixture, TFA (0.06 ml, 0.79 mmol) was added and the resulting mixture was stirred in dark condition for 30 min in room temperature. After completion of reaction, 100 ml of CH₂Cl₂ was added in open air condition and the mixture was neutralized with 100 ml of 0.1 M NaOH solution. Organic layer was separated, twice washed with water and dried over anhydrous Na₂SO₄. The solvent and excess pyrrole was removed by vacuum. The light yellow color compound was eluted with ethyl acetate/hexane

(3:97, V/V) identified as 5,10-dimesityl-16-thiatripyrrane (**7**) Yield: 0.78 g, 90% .
Precursors **6**, **11** are shown in the previous chapters.

¹H NMR (400 MHz, CDCl₃, 298K): δ (ppm): 7.85 (br, 2H), 6.85 (s, 2H), 6.65 (d, *J*=3.8 Hz, 2H), 6.62 (s, 2H), 6.16 (d, *J*=3.8 Hz, 2H), 6.03 (d, *J*=3.8 Hz, 4H), 5.99 (s, 2H), 2.27 (s, 6H), 2.12 (s, 12H).

6.6 References

1. S. Saito, A. Osuka, *Angew. Chem. Int. Ed.* **2011**, *50*, 4342-4373; (b) J. L. Sessler, D. Seidel, *Angew. Chem. Int. Ed.* **2003**, *42*, 5134-5175; (c) M. Stępień, N. Sprutta, L. Latos-Grażyński, *Angew. Chem. Int. Ed.* **2011**, *50*, 4288-4340; (d) A. Osuka, S. Saito, *Chem. Commun.* **2011**, *47*, 4330-4339; (e) T. Tanaka, A. Osuka, *Chem. Rev.* **2017**, *117*, 2584-2640. (f) N. Shivran, S. C. Gadekar, V. G. Anand, *Chem. Asian. J.* **2017**, *12*, 6-20.
2. (a) A. Chaudhary, A. Srinivasan, T. K. Chandrashekar, *The Handbook of Porphyrin Science*, Kadish, K. M.; Smith, K. M.; R. Guilard, World scientific Ltd, **2014**, *32*, 271-366; (b) J.-Y. Shin, K. S. Kim, M. -C. Yoon, J. M. Lim, Z. S. Yoon, A. Osuka, D. Kim, *Chem. Soc. Rev.* **2010**, *39*, 2751-2767; (c) J. M. Lim, Z. S. Yoon, J. -Y. Shin, K. S. Kim, M. -C. Yoon, D. Kim, *Chem. Commun.* **2009**, 261-273; (d) M. O. Senge, M. Fazekas, E. G. A. Notaras, W. J. Blau, M. Zawadzka, O. B. Locos, E. M. Ni Mhuircheartaigh, *Adv. Mater.* **2007**, *19*, 2737-2774.
3. (a) B. Marydasan, B. Madhuri, S. Cherukommu, J. Jose, M. Viji, S. C. Karunakaran, T. K. Chandrashekar, K. S. Rao, C. M. Rao, D. Ramaiah, *J. Med. Chem.* **2018**, *61*, 5009-5019; (b) T. Wang, D. Zhu, G. Liu, W. Tao, W. Cao, L. Zhang, L. Wang, H. Chen, L. Mei, L. Huang, X. Zeng, *RSC*

-
- Adv.* **2015**, *5*, 50617-50627; (c) J. Tian, L. Ding, H. -J. Xu, Z. Shen, H. Ju, L. Jia, L. Bao, J. -S. Yu, *J. Am. Chem. Soc.* **2013**, *135*, 18850-18858.
4. (a) Y. M. Sung, J. Oh, W. -Y. Cha, W. Kim, J. M. Lim, M. -C. Yoon, D. Kim, *Chem. Rev.* **2017**, *117*, 2257-2312; b) M. Ménand, M. Sollogoub, B. Boitrel, S. Le Gac, *Angew. Chem. Int. Ed.* **2016**, *55*, 297-301; (c) A. Rana, S. Lee, D. Kim, P. K. Panda, *Chem. Eur. J.* **2015**, *21*, 12129-12135; (d) I. T. Ho, Z. Zhang, M. Ishida, V. M. Lynch, W.-Y. Y. Cha, M. Sung, D. Kim, J. L. Sessler, *J. Am. Chem. Soc.* **2014**, *136*, 4281-4286; e) H. Gopee, X. Kong, Z. He, I. Chambrier, D. L. Hughes, G. J. Tizzard, S. J. Coles, A. N. Cammidge, *J. Org. Chem.* **2013**, *78*, 9505-9511.
5. (a) A. Ghosh, A. Chaudhary, A. Srinivasan, C. H. Suresh T. K. Chandrashekar, *Chem. Eur. J.* **2016**, *22*, 3942-3946; (b) K. Möbius, M. Plato, G. Klihm, C. Laurich, A. Savitsky, W. Lubitz, B. Szyszko, M. Stępień, L. Latos-Grażyński, *Phys. Chem. Chem. Phys.* **2015**, *17*, 6644-6652; (c) K. Naoda, H. Mori, J. Oh, K. H. Park, D. Kim, A. Osuka, *J. Org. Chem.*, **2015**, *80*, 11726-11733; (d) S. Saito, J. -Y. Shin, J. M. Lim, K. S. Kim, D. Kim, A. Osuka, *Angew. Chem. Int. Ed.* **2008**, *47*, 9657-9660; (e) M. Stępień, L. Latos-Grażyński, N. Sprutta, P. Chwalisz, L. Szterenberga, *Angew. Chem. Int. Ed.* **2007**, *46*, 7869-7873; (f) D. Ajami, O. Oeckler, A. Simon, R. Herges, *Nature*, **2003**, *426*, 819-821.
6. (a) N. C. Baird, *J. Am. Chem. Soc.* **1972**, *94*, 4941-4948; (b) Y. M. Sung, M. -C. Yoon, J. M. Lim, H. Rath, K. Naoda, A. Osuka, D. Kim, *Nat. Chem.* **2015**, *7*, 418-422; (c) W.-Y. Cha, T. Kim, A. Ghosh, Z. Zhang, X. -S. Ke, R. Ali, V. M. Lynch, J. Jung, W. Kim, S. Lee, S. Fukuzumi, J. S. Park, J. L. Sessler, T. K. Chandrashekar, D. Kim, *Nat. Chem.* **2017**, *9*, 1243-1248.
-

-
7. H.-J. Yoon, T. G. Lim, J. -H. Kim, Y. M. Cho, Y. S. Kim, U. S. Chung, J. H. Kim, B. W. Choi, W. -G. Koh, W. -D. Jang, *Biomacromol.* **2014**, *15*, 1382-1389.
8. (a) T. Stuyver, M. Perrin, P. Geerlings, F. De Proft, M. Alonso, *J. Am. Chem. Soc.* **2018**, *140*, 1313-1326; (b) Z. Tian, S. Dai, D.-e. Jiang, *ACS Appl. Mater. Interfaces*, **2015**, *7*, 13073-13079; (c) C. Zhang, P. Chen, H. Dong, Y. Zhen, M. Liu, W. Hu, *Adv. Mater.* **2015**, *27*, 5379-5387; (d) M. S. R. Bobe, M. Al Kobaisi, S. V. Bhosale, *Chem. Open.* **2015**, *4*, 516-522.
9. (a) B. M. Rambo, J. L. Sessler, *Chem. Eur. J.* **2011**, *17*, 4946-4959; (b) J. L. Sessler, S. Camiolo, P. A. Gale, *Coord. Chem. Rev.* **2003**, *240*, 17-55; (c) H. Kido, J. -Y. Shin, H. Shinokubo, *Angew. Chem. Int. Ed.* **2013**, *52*, 13727-13730; (d) L. K. Blusch, O. Mitevski, V. Martin-Diaconescu, K. Pröpper, S. DeBeer, S. Dechert, F. Meyer, *Inorg. Chem.* **2014**, *53*, 7876-7885.
10. (a) N. Sheng, S. Zong, W. Cao, J. Jiang, Z. Wang, Y. Cui, *ACS Appl. Mater. Interfaces*, **2015**, *7*, 19718-19725; (b) R. Chandra, M. Tiwari, P. Kaur, M. Sharma, R. Jain, S. Das, *Indian journal of clinical biochemistry : IJCB*, **2000**, *15*, 183-199.
11. I. Gupta, A. Srinivasan, T. Morimoto, M. Toganoh, H. Furuta, *Angew. Chem. Int. Ed.* **2008**, *47*, 4563-4567.
12. M. Suzuki, R. Taniguchi, A. Osuka, *Chem. Commun.* **2004**, 2682-2683.
13. G. Karthik, A. Srinivasan, C. H. Suresh, T. K. Chandrashekar, *Chem. Commun.* **2014**, *50*, 12127-12130.
14. K. Mitsuno, T. Yoshino, I. Gupta, S. Mori, S. Karasawa, M. Ishida, H. Furuta, *Angew. Chem. Int. Ed.* **2017**, *56*, 14252-14256.
-

-
15. J. L. Sessler, S. J. Weghorn, V. Lynch, M. R. Johnson, *Angew. Chem. Int. Ed. Engl.* **1994**, *33*, 1509-1512.
16. J. L. Sessler, D. Seidel, A. Gebauer, V. Lynch, K. A. Abboud, *J. Heterocycl. Chem.* **2001**, *38*, 1419-1424.
17. J. -i. Setsune, Y. Katakami, N. Iizuna, *J. Am. Chem. Soc.* **1999**, *121*, 8957-8958.
18. (a) T. Soya, W. Kim, D. Kim, A. Osuka, *Chem. Eur. J.* **2015**, *21*, 8341-8346; (b) T. Soya, H. Mori, A. Osuka, *Angew. Chem. Int. Ed.* **2018**, *57*, 15882-15886; (c) S. Shimizu, W. -S. Cho, J. L. Sessler, H. Shinokubo, A. Osuka, *Chem. Eur. J.* **2008**, *14*, 2668-2678.
19. H. Rath, V. Prabhuraja, T. K. Chandrashekar, A. Nag, D. Goswami, B. S. Joshi, *Org. Lett.* **2006**, *8*, 2325-2328.
20. (a) R. Taniguchi, S. Shimizu, M. Suzuki, J. -Y. Shin, H. Furuta, A. Osuka, *Tetrahedron Lett.* **2003**, *44*, 2505-2507; (b) S. Shimizu, N. Aratani, A. Osuka, *Chem. Eur. J.* **2006**, *12*, 4909-4918; (c) Y. Tanaka, J. -Y. Shin, A. Osuka, *Eur. J. Org. Chem.* **2008**, 1341-1349.
21. (a) V. G. Anand, S. Saito, S. Shimizu, A. Osuka, *Angew. Chem. Int. Ed.* **2005**, *44*, 7244-7248; (b) T. Soya, H. Mori, Y. Hong, Y. Koo, D. Kim, A. Osuka, *Angew. Chem. Int. Ed.* **2017**, *56*, 3232-3236.
22. T. Yoneda, Y. M. Sung, J. M. Lim, D. Kim, A. Osuka, *Angew. Chem. Int. Ed.* **2014**, *53*, 13169-13173.
23. Y. Tanaka, T. Yoneda, K. Furukawa, T. Koide, H. Mori, T. Tanaka, H. Shinokubo, A. Osuka, *Angew. Chem. Int. Ed.* **2015**, *54*, 10908-10911.
24. (a) S. Shimizu, N. Aratani, A. Osuka, *Chem. Eur. J.* **2006**, *12*, 4909-4918; (b) Y. Tanaka, J. -Y. Shin, A. Osuka, *Eur. J. Org. Chem.* **2008**, 1341-1349.
-

-
25. T. Okujima, C. Ando, S. Agrawal, H. Matsumoto, S. Mori, K. Ohara, I. Hisaki, T. Nakae, M. Takase, H. Uno, N. Kobayashi, *J. Am. Chem. Soc.* **2016**, *138*, 7540-7543.
26. S. Kumar, K. G. Thorat, M. Ravikanth, *J. Org. Chem.* **2018**, *83*, 14277-14285.
27. A. Ghosh, S. Dash, A. Srinivasan, M. S. R. Sahu, C. H. Suresh, T. K. Chandrashekar, *Chem. Eur. J.* **2018**, *24*, 17997-18002.
28. R. Myśluborski, K. Hurej, M. Pawlicki, L. Latos-Grażyński, *Angew. Chem. Int. Ed.* **2018**, *57*, 16866-16870.
29. G. Karthik, J. M. Lim, A. Srinivasan, C. H. Suresh, D. Kim, T. K. Chandrashekar, *Chem. Eur. J.* **2013**, *19*, 17011-17020; (b) R. Nozawa, H. Tanaka, W. -Y. Cha, Y. Hong, I. Hisaki, S. Shimizu, J. -Y. Shin, T. Kowalczyk, S. Irye, D. Kim, H. Shinokubo, *Nat. Commun.* **2016**, *7*, 13620, DOI: 10.1038/ncomms13620; (c) J. Dominikowska, M. Palusiak, *Struct Chem.* **2012**, *23*, 1173-1183.
30. (a) L. Zhai, R. Shukla, S. H. Wadumethrige, R. Rathore, *J. Org. Chem.* **2010**, *75*, 4748-4760; (b) Q. Ouyang, K-Q. Yan, Y-Z. Zhu, C-H. Zhang, J-Z. Liu, C. Chen, J-Y. Zheng, *Org. Lett.* **2012**, *14*, 2746-2749.
31. G. Zhang, S. Chen, H. Fei, J. Cheng, F. Chen, *Synlett*, **2012**, *23*, 2247-2250.

SUMMARY

Porphyrins are tetra pyrrolic macrocycle with 18π electrons in their conjugated pathway and follows Hückel aromatic character. By increasing an atom or meso carbon in the inner core leads to expanded porphyrinoids. The $[4n+2]\pi$ rule of Hückel is very well understood and there are lot of examples of organic molecules exhibiting Hückel Aromaticity. However, understanding of Möbius $[4n]\pi$ aromaticity are still at their infancy and there are only limited examples obeying Möbius rule using expanded porphyrins as models are discussed. Furthermore, the transformation of a nonaromatic to Hückel aromatic or Möbius topology or a Hückel antiaromatic topology under an external trigger will also be discussed. This thesis highlights syntheses, conformation, and aromaticity switch in expanded porphyrin analogues. The first chapter describes the literature survey of expanded porphyrinoids analogues. The second chapter deals with Core-Modified Homoporphyrins and its Phenyl bridged derivatives. 1,2-diphenyl-1,2-dithienyl ethene embedded 30π and 28π core-modified Hexaphyrins; its syntheses and protonation triggered Hückel and Möbius aromatic transformations are discussed in third chapter. The fourth chapter outlines the synthesis of dithienothiophene fused 30π Heptaphyrin and 34π Octaphyrins. The fifth chapter reports on two Non-identical Octaphyrin twins; syntheses, structural isomers and properties are shown. The sixth chapter demonstrates the syntheses of rigid and flexible Core-modified Decaphyrins and protonation triggered nonaromatic to antiaromatic transformation in flexible 48π decaphyrin.

Conclusion chapter

The entire thesis is engrossed on syntheses of a range of core-modified expanded porphyrins, like homoporphyrins, hexaphyrins, heptaphyrins, octaphyrins and decaphyrins and probe their properties in terms of conformational changes, structural diversity, Hückel-Möbius aromatic switch-over and electronic structure to understand the optical properties.

This thesis is comprised of six chapters. Chapter one describes Evolution of core-modified expanded Porphyrins and their molecular topology. The chemistry of expanded porphyrin and its electronic properties are well known in the literature; however expanded porphyrin exhibits various structures, and aromaticity which is less known. and facile interconversion of aromaticity through modifications is possible through modulators. The second chapter deals with Core-modified homoporphyrins and its *p*-phenylene bridged derivatives, where we discussed the synthesis of smallest core-modified expanded porphyrin and synthesized its *p*-phenylene bridged dimer. In third chapter, we reported the 1,2-diphenyl-1,2-dithienyl ethene embedded 30π and 28π core-modified hexaphyrins; syntheses and protonation triggered Hückel and Möbius aromatic transformations where protonation was used as a source of modulation for aromatic switchover. The fourth chapter reports dithienothiophene fused 30π heptaphyrin and 34π octaphyrins its syntheses, characterization and spectral Properties where both the heptaphyrin and octaphyrin were highly planar in nature and flipping of such a huge fused group is unprecedented in literature. The fifth chapter reports two non-identical octaphyrin twins in a single unit cell. The syntheses, structural isomers and properties have been shown in this chapter and transformation from non-identical twins to identical twins on changing the middle heterocyclic unit in the macrocycle. In the last chapter In conclusion, rigid and flexible core-modified decaphyrins; syntheses and protonation triggered nonaromatic to antiaromatic

transformation in flexible 48π decaphyrin aromaticity switching which attracts the porphyrin chemist to explore this field in future.

SUMMARY

Porphyrins are tetra pyrrolic macrocycle with 18π electrons in their conjugated pathway and follows Hückel aromatic character. By increasing an atom or meso carbon in the inner core leads to expanded porphyrinoids. The $[4n+2]\pi$ rule of Hückel is very well understood and there are lot of examples of organic molecules exhibiting Hückel Aromaticity. However, understanding of Möbius $[4n]\pi$ aromaticity are still at their infancy and there are only limited examples obeying Möbius rule using expanded porphyrins as models are discussed. Furthermore, the transformation of a nonaromatic to Hückel aromatic or Möbius topology or a Hückel antiaromatic topology under an external trigger will also be discussed. This thesis highlights syntheses, conformation, and aromaticity switch in expanded porphyrin analogues. The first chapter describes the literature survey of expanded porphyrinoids analogues. The second chapter deals with Core-Modified Homoporphyrins and its Phenyl bridged derivatives. 1,2-diphenyl-1,2-dithienyl ethene embedded 30π and 28π core-modified Hexaphyrins; its syntheses and protonation triggered Hückel and Möbius aromatic transformations are discussed in third chapter. The fourth chapter outlines the synthesis of dithienothiophene fused 30π Heptaphyrin and 34π Octaphyrins. The fifth chapter reports on two Non-identical Octaphyrin twins; syntheses, structural isomers and properties are shown. The sixth chapter demonstrates the syntheses of rigid and flexible Core-modified Decaphyrins and protonation triggered nonaromatic to antiaromatic transformation in flexible 48π decaphyrin.



राष्ट्रीय विज्ञान शिक्षा एवं अनुसंधान संस्थान, भुवनेश्वर
(परमाणु उर्जा विभाग, भारत सरकार का एक स्वायत्त संस्थान)
NATIONAL INSTITUTE OF SCIENCE EDUCATION AND RESEARCH, BHUBANESWAR
(An autonomous Institution under Department of Atomic Energy, Govt. of India)

CERTIFICATE BY THE GUIDE

This is to certify that **Ms. Syamasrit Dash** bearing HBNI Enrolment No.: **CHEM11201604031** has incorporated all the suggestions, corrections and comments received from the thesis examiners & Guide, in the final thesis. Furthermore, the suggestions, corrections and comments received from the members of the viva-voce board during the viva-voce examination held on **30.12.2020** have also been incorporated in the final PhD thesis which is submitted to the Academic Office, NISER.

Prof. T. K. Chandrashekar

Signature & Name of the PhD Guide

Date: 30.12.2020

Prof. A. Srinivasan

Signature & Name of the PhD Co-Guide

Date: 30.12.2020

Thesis Highlight

Name of the Student: Syamasrit Dash

Name of the CI/OCC: NISER

Enrolment No.: CHEM11201604031

1. Thesis Title: Expanded Porphyrins: Ideal Models to Probe Conformational topology, Möbius and Hückel Aromaticity
2. Discipline: **Chemical Science**
3. Sub-Area of Discipline: **Inorganic Chemistry**

Date of viva voce: 30.12.2020.

Porphyrins are naturally occurring tetrapyrrolic macrocycles which are termed as “Pigments of Life”. The tetrapyrrolic moiety consists of two amine and two imine nitrogens connected by four methine/*meso* carbon bridges and the inner core contains 16 atoms in the macrocyclic framework with 18π conjugated electrons exhibiting aromatic features.

Several modifications such as; replacement of one or more pyrrole rings by other heterocyclic ring such as thiophene and selenophene and new isomers of porphyrins have been done to exploit their rich chemistry as well as their diverse functional applications. This thesis is predominantly engrossed on syntheses of a range of core-modified expanded porphyrins, like *homoporphyrins*, *hexaphyrins*, *heptaphyrins*, *octaphyrins* and *decaphyrins* and probe their properties in terms of conformational changes, structural diversity, Hückel-Möbius aromatic switch-over and electronic structure to understand the optical, electrochemical, photochemical and excited state properties. The initial part of the thesis is mainly focused synthesis of smallest core-modified expanded porphyrin and synthesized its *p*-phenylene bridged dimer and in the second part, 30π and 28π core-modified hexaphyrins; syntheses and protonation triggered Hückel and Möbius aromatic transformations where perchlorate and trifluoroacetic acid are source of is aromatic switchover. The third part contains dithienothiophene fused 30π heptaphyrin and 34π octaphyrins its syntheses, characterization and spectral Properties.

The fifth part reports two non-identical octaphyrin twins in a single unit cell. The syntheses, structural isomers and properties have been shown in this chapter and transformation from non-identical twins to identical twins on changing the middle heterocyclic unit in the macrocycle. In the last part of the thesis, rigid and flexible core-modified decaphyrins; syntheses and protonation triggered nonaromatic to antiaromatic transformation of largest decaphyrin reported in literature (Figure 1).

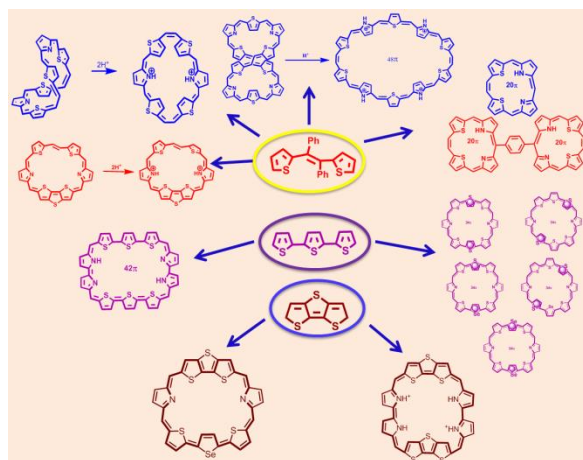


Figure 1. Representative examples of expanded porphyrin analogues highlighted in the thesis.

Overall, the thesis describes the synthesis of several expanded porphyrinoids and probe their properties in terms of conformational changes, structural diversity, Hückel-Möbius aromatic switch-over and electronic structure to understand the optical properties.